LBNL-49593

ERNEST ORLANDO LAWRENCE
BERKELEY NATIONAL LABORATORY

Experimental Cross Sections for Reactions of Heavy Ions and ^{208}Pb, ^{209}Bi, ^{238}U, and ^{248}Cm Targets

Joshua B. Patin

Nuclear Science Division

May 2002

Ph.D. Thesis

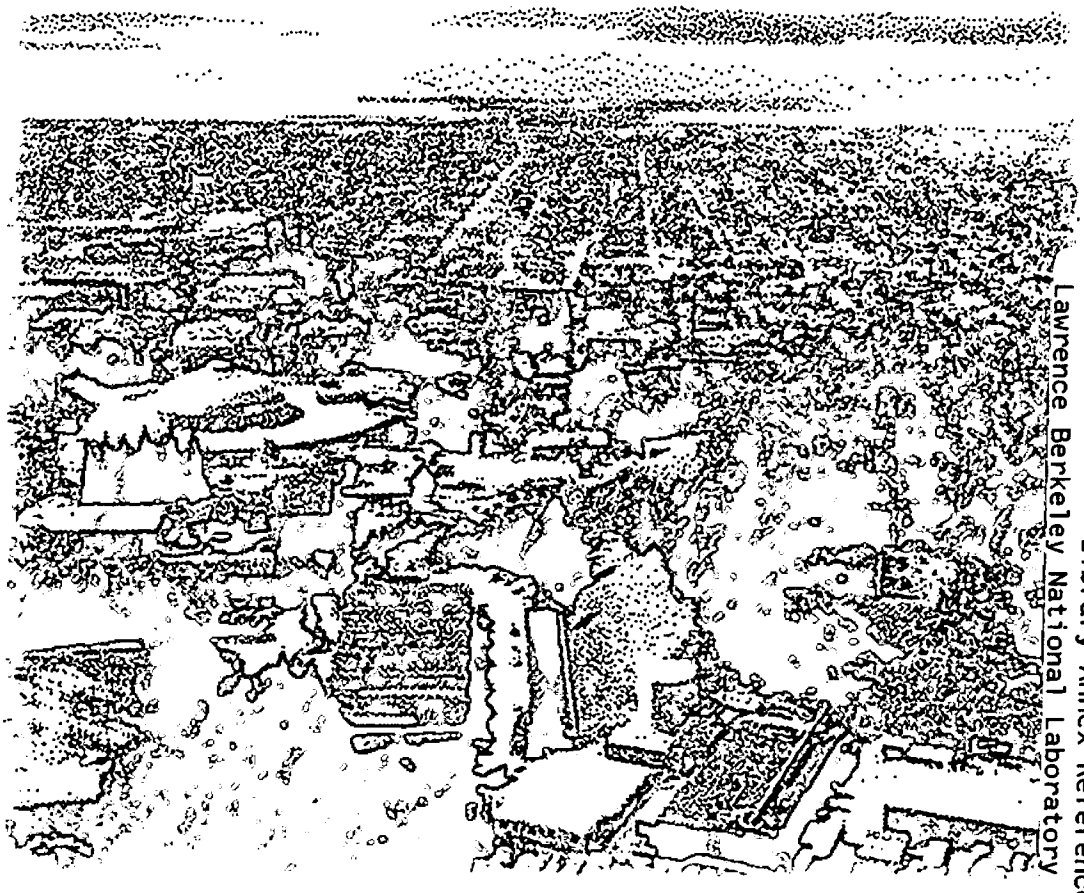

DISCLAIMER

LBNL-49593

Experimental Cross Sections for Reactions of Heavy Ions and ^{208}Pb, ^{209}Bi, ^{238}U, and ^{248}Cm Targets

Joshua B. Patin
Ph.D. Thesis

Department of Chemistry
University of California, Berkeley

and

Nuclear Science Division
Ernest Orlando Lawrence Berkeley National Laboratory
University of California
Berkeley, CA 94720

May 2002

This work was supported by the Director, Office of Science, Office of High Energy and Nuclear Physics, Division of Nuclear Physics, of the U.S. Department of Energy under Contract No. DE-AC03-76SF00098.

Experimental Cross Sections for Reactions of Heavy Ions and ^{208}Pb, ^{209}Bi, ^{238}U, and ^{248}Cm Targets

by

Joshua Barnes Patin

Abstract

Experimental Cross Sections for Reactions of Heavy Ions and ^{208}Pb, ^{209}Bi, ^{238}U, and ^{248}Cm Targets

by

Joshua Barnes Patin

Doctor of Philosophy in Chemistry

University of California, Berkeley

Professor Darleane C. Hoffman, Chair

The study of the reactions between heavy ions and ^{208}Pb, ^{209}Bi, ^{238}U, and ^{248}Cm targets was performed to look at the differences between the cross sections of hot and cold fusion reactions. Experimental cross sections were compared with predictions from statistical computer codes to evaluate the effectiveness of the computer code in predicting production cross sections.

Hot fusion reactions were studied with the MG system, catcher foil techniques and the Berkeley Gas-filled Separator (BGS). 3n- and 4n-exit channel production cross sections were obtained for the $^{238}U(^{18}O,xn)^{256-x}Fm$, $^{238}U(^{22}Ne,xn)^{260-x}No$, and $^{248}Cm(^{15}N,xn)^{263-x}Lr$ reactions and are similar to previous experimental results. The experimental cross sections were accurately modeled by the predictions of the HIVAP code using the Reisdorf and Schädel parameters and are consistent with the existing systematics of 4n exit channel reaction products.

Cold fusion reactions were examined using the BGS. The $^{208}Pb(^{48}Ca,xn)^{256-x}No$, $^{208}Pb(^{50}Ti,xn)^{258-x}Rf$, $^{208}Pb(^{51}V,xn)^{259-x}Db$, $^{209}Bi(^{50}Ti,xn)^{259-x}Db$, and $^{209}Bi(^{51}V,xn)^{260-x}Sg$

reactions were studied. The experimental production cross sections are in agreement with the results observed in previous experiments. It was necessary to slightly alter the Reisdorf and Schädel parameters for use in the HIVAP code in order to more accurately model the experimental data. The cold fusion experimental results are in agreement with current 1n- and 2n-exit channel systematics.

Dedication

This dissertation is dedicated to my mom and dad. Without your constant love, support, and guidance, none of this would have ever been possible. I love you both!

Table of Contents

List of Figures

List of Tables

Acknowledgments

I would like to start by thanking my advisor Darleane. Her guidance has led me to take pride in all my work, to question everything I do, and to never give up searching for the answers.

I would also like to thank Ken Gregorich. Without his help and willingness to answer all of my questions, day after day, I would still not understand how to calculate anything, work the BGS, or enjoy the pleasure that is Fry's.

I would like to thank Diana Lee and Victor Ninov for all of their experimental help. Diana's help was extremely important in understanding all of the aqueous chemistry that was performed, and Victor's help with GOOSY was vital to the completion of this thesis.

I would like to extend gratitude to the operators of the 88-Inch Cyclotron for without their talents, my experiments would have gone nowhere.

Many multitudes of thanks go to former Hoffman graduate students Dawn Shaughnessy, Dan Strellis, Phil Wilk, Eric Sylwester, and Mike Lane for their humor, their help, their friendship, the sports talk on Mondays, General Tso's chicken, and for welcoming me into the group and making it a comfortable place for me to begin my work.

Thanks to more recent groupmates Peter Zielinski and Cody Folden and the rest of the Springfield Isotopes for helping me with our Chemistry Department softball league perfect 10-0 season!

Thanks to past and present group members for help with experiments and making my life easier: Jeb Adams, Chris McGrath, Ralf Sudowe, Carola Laue, and Uwe Kirbach.

I'd like to thank Robert Eichler and Andreas Türler for their friendship and hospitality during my excursions to Switzerland.

I would like to thank Mr. Simon for if you can't have fun in chemistry class, what use is their in studying it. Thank you for letting me blow things up, tweak the conditions and then blow things up again. Learning from you that chemistry was fun, exciting, and rewarding began this journey for me. I would like to thank my advisors in college, Prof. Crim for instilling in me an unbelievable fascination and enthusiasm for all that is chemistry and Prof. Woods for telling me I had what it took to go to Berkeley in the first place.

More personally, I'd like to thank Steve and Otto for always being the best of friends. Their visits (Steve and the Jack in the Box at 2AM, Otto and the Rose Bowls and Jerry Rice's fumble) were appreciated much more then they'll ever know and to settle things for once and all, I am the RIA! I'd like to thank Sladek for always being available when I was home, and I would like to thank Earl for those two New Year's vacations in Southern California and Cake on the drives down there. Finally, I'd like to thank Paul for always being the one who could make me laugh when I needed it the most. The five of them are my boys and always will be!

I would gratefully like to thank my sister for always listening and being the best sister a brother could ever ask for. She's so special to me and I wish nothing but the best for her in everything she does.

I would also like to thank Trevor. His youthfulness, joy, energy, and always insightful questions have kept me motivated these last two years and focused on one of the most important things to me, my new family.

Finally, to my fiancé and best friend, Shannon. You are the light of my life. You have made these last two years the best in my life, and I am eternally grateful. Thank you for always helping me stay focused on my goals, for keeping me on track these last few months and for being the wonderfully beautiful person that you are. I will always be right there and I will always love you.

1 Introduction

1.1 Discovery of the transuranium elements

Chemistry has played an important role in the discovery and positive identification of new artificial elements since the production and identification of neptunium and plutonium in 1940-41. In 1872, Mendeleev furthered the progress for the search of new elements with his formulation of the periodic table. This helped give insight on where to look for new elements, and how these new elements might behave chemically. In the 1930's, technical advances and the invention of the cyclotron by E. O. Lawrence, opened up a new era in element discovery.

The first elements heavier than uranium, neptunium (Z = 93) and plutonium (Z = 94), were produced and identified in 1940 and 1941. The discoveries involved the irradiation of uranium by neutrons and deuterium ions and identification through chemistry. Neptunium was discovered by E. M. McMillian in the neutron activation of uranium [McM1940] in which a single neutron was added to a ^{238}U nucleus, producing ^{239}U which then beta-decayed to neptunium.

$$^{238}_{92}U\left(^{1}_{0}n,\gamma\right)^{239}_{92}U \xrightarrow[23.5\,\mathrm{min}]{\beta^-} {}^{239}_{93}Np \tag{1.1}$$

Plutonium was discovered not long afterward through the interaction of deuterium with uranium [Sea1946]. Neptunium was the reaction product which then beta-decayed to plutonium.

$$^{238}_{92}U\left(^{2}_{1}H,2\,^{1}_{0}n\right)^{238}_{93}Np \xrightarrow[2.12d]{\beta^-} {}^{238}_{94}Pu \tag{1.2}$$

Americium (Z = 95) and curium (Z = 96) were the next two heavy elements to be discovered. Initial experiments to chemically separate and identify them as homologues

of iridium and platinum were unsuccessful until Glenn T. Seaborg proposed a new actinide series similar to the lanthanide series [Sea1945]. Curium was identified first through the irradiation of a long-lived isotope of plutonium with alpha-particles [Sea1945].

$$^{239}_{94}Pu\left(^{4}_{2}He,^{1}_{0}n\right)^{242}_{96}Cm \tag{1.3}$$

Chemical separation as the trivalent species later confirmed the production of the new element. Americium was later identified in the multiple neutron capture of the same long-lived plutonium isotope [Ghi1950].

$$^{239}_{94}Pu\left(2\,^{1}_{0}n,\gamma\right)^{241}_{94}Pu \xrightarrow[14.4y]{\beta^-} {}^{241}_{95}Am \tag{1.4}$$

Seaborg formally proposed the actinide concept in the discovery letter for curium, supported by the separation of curium and americium in the trivalent oxidation state and with it a new periodic table [Sea1945]. This postulation was extremely important to the discovery of new heavier elements. Seaborg's proposal paved the way for chemical identification of the heavier elements by predicting that the actinides behaved chemically similarly to their homologue lanthanides. The lanthanide series filled the inner 4f shell, while the actinides fill the 5f shell [Hff1999]. Based on this concept, new heavy elements would fill the actinide row up to element 103. These new actinides were predicted to all exhibit stable 3+ oxidation states, except for element 102, which was predicted to have a stable 2+ oxidation state like its homologue ytterbium. Chemical separations used at the time involved changing the oxidation state of the species of interest while not changing the oxidation states of the impurities, and then extracting the species of interest effectively separating it from the impurities. With the majority of

these new actinides exhibiting a stable 3+ oxidation state, new chemical separation techniques were needed.

With the actinide concept in mind, work began on the discovery of still heavier elements. The technology of the time was limited to light ion beams, so heavier target material needed to be produced in significant quantities to produce a target suitable for irradiations. In 1949, berkelium was discovered through the irradiation of americium with helium ions [Tho1950a].

$$^{241}_{95}Am\left(^{4}_{2}He, 2\,^{1}_{0}n\right)^{243}_{97}Bk \tag{1.5}$$

Positive identification of these new activities as isotopes of new elements required new chemical separation techniques. Elution from ion-exchange resin columns with different elutants was performed to separate species with similar oxidation states. These new techniques were used in the positive identification of berkelium and californium.

Californium was produced in 1950 through the irradiation of curium with helium ions [Tho1950b].

$$^{242}_{96}Cm\left(^{4}_{2}He, \,^{1}_{0}n\right)^{245}_{98}Cf \tag{1.6}$$

Chemical separations of californium from the other actinides produced in this reaction were critical to its discovery. A cation exchange column technique was used to elute californium before the similar trivalent actinides berkelium and curium [Tho1950b].

The discovery of elements 99 and 100 did not occur through the use of accelerated projectiles and a target. Great effort was given at the time to use the heaviest and most neutron-rich targets available. However, short target material half-lives, difficulty in the production of significant quantities of target material, and the limited

number of beam options slowed the continuing search for these two new elements. Einsteinium and fermium, elements 99 and 100 were discovered in the debris from the "Mike" thermonuclear device tested in the South Pacific on November 1, 1952 [Ghi1955a]. Early chemical separations from the "Mike" test debris identified the heaviest known isotopes of plutonium, ^{246}Pu and ^{244}Pu. This provided evidence that the ^{238}U used in the "Mike" test had captured at least eight neutrons forming ^{246}U which then decayed to ^{246}Pu via successive beta decay. This led the researchers to speculate that more neutrons might have been captured and maybe heavier elements could be detected from the multiple beta-decays that followed the multiple neutron captures. This indeed proved to be true as an intensive search for elements 99 and 100 by researchers at the Radiation Laboratory in Berkeley, Argonne National Laboratory in Illinois, and the Los Alamos Scientific Laboratory verified the multiple neutron capture of ^{238}U. These researchers performed the first chemical separation and isolation of elements 99 and 100 from debris recovered from the "Mike" test. Chemical separation techniques similar to those used to discover curium, berkelium and californium were used. Elution from cation exchange resins showed einsteinium and fermium in their predicted positions.

Names for the previous elements were all proposed by their discoverers soon after they were identified as being new elements. In 1997, the International Union of Pure and Applied Chemistry (IUPAC) assigned credit for discovery and approved the names of elements 101-109. The elements name and symbol can be found in Table 1.1 [Iup1997].

Table 1.1: IUPAC approved names and symbols for elements 101-109 [Iup1997].

Element	Name	Symbol
101	mendelevium	Md
102	nobelium	No
103	lawrencium	Lr
104	rutherfordium	Rf
105	dubnium (hahnium*)	Db (Ha*)
106	seaborgium	Sg
107	bohrium	Bh
108	hassium	Hs
109	meitnerium	Mt

*Hahnium and the symbol "Ha" appeared in the literature for chemical studies of element 105 prior to 1997.

In 1955, mendelevium was discovered in the bombardment of einsteinium atoms by helium ions. Enough ^{253}Es had been separated to form a target, which was then irradiated by helium ions [Ghi1955b].

$$^{253}_{99}Es\left(^{4}_{2}He, ^{1}_{0}n\right)^{256}101 \tag{1.7}$$

This experiment was important because mendelevium was the first heavy element produced and identified using atom-at-a-time techniques which became important in future experiments. It would also incorporate a new technique to simplify the chemical analysis. The new technique used a catcher foil placed directly behind the target to collect the recoiling products as they left the target. This too would become important in future research. It was also the last experiment performed using light ion beams ($Z \leq 2$, $A \leq 4$). Beams heavier than helium were required to produce the elements with $Z > 101$.

Nobelium, element 102 was erroneously reported discovered in 1957. Irradiations were performed in the cyclotron at the Nobel Institute in Stockholm, Sweden. Curium targets were irradiated by carbon ions at various energies. It was believed that the following reactions were observed [Fie1957],

$$^{244}_{96}Cm\left(^{13}_{6}C, 6\,^{1}_{0}n\right)^{251}102 \tag{1.8}$$

$$^{244}_{96}Cm\left(^{13}_{6}C, 4\,^{1}_{0}n\right)^{253}102 \tag{1.9}$$

Chemical separations were performed to isolate nobelium from the other reaction products. Separations were performed under the assumption that nobelium behaved similarly to mendelevium, fermium and einsteinium, exhibiting a stable 3+ oxidation state in aqueous solution. This was later proven incorrect when nobelium was shown to

exhibit a stable 2+ oxidation state in aqueous solution [Mal1968]. Soon afterwards, additional experiments to find nobelium were performed in Berkeley. Ghiorso and coworkers performed similar experiments with carbon on curium [Ghi1958].

$$^{246}_{96}Cm\left(^{12}_{6}C, 4\,^{1}_{0}n\right)^{254}102 \tag{1.10}$$

Researchers at Berkeley identified nobelium through the chemical identification of its alpha-decay daughter ^{250}Fm and separately through the direct counting of ^{252}No collected in a catcher foil [Hff1998]. Work was also performed at the same time at Dubna using plutonium targets [Fle1958].

$$^{239}_{94}Pu\left(^{16}_{8}O, xn\right)^{255-x}102 \tag{1.11}$$

Through the efforts of researchers in Berkeley and in Dubna, the discovery of nobelium was possible. A more through discussion of the events of the discoveries of nobelium and the rest of the heavy elements can be found in [Sea1990] and [Hff1998, Hff2000]. This was the first of the discovery experiments that used a beam heavier than helium. Four neutrons were evaporated in this reaction because of the large excitation energy of the resulting compound nucleus.

Lawrencium, element 103, and the last of the actinides, was discovered in 1961. Californium targets were bombarded by intense beams of accelerated boron ions to produce various isotopes of lawrencium [Ghi1961].

$$^{249-252}_{98}Cf\left(^{10,11}_{5}B, 4\,^{1}_{0}n\right)^{255-259}103 \tag{1.12}$$

Lawrencium was detected by collecting the activity from the reaction on a tape which was moved between a series of alpha-particle detectors [Sea1990]. Various isotopes

were observed by examining the resulting spectra of alpha-particle energies. From the information gathered, the most probable isotope produced was found to be ^{257}Lr. It is the product resulting from the emission of three, four and five neutrons from the fusion of ^{10}B with $^{250\text{-}252}$Cf, respectively, and four, five and six neutrons from the fusion of ^{11}B with $^{250\text{-}252}$Cf, respectively [Ghi1961]. This behavior is consistent with the reactions that produce large amounts (~ 40 MeV) of excitation energy in the compound nucleus. Such reactions that produce compound nuclei from reactions of ions with actinide targets are called "hot fusion" reactions. Increased excitation energy leads to a smaller probability of surviving from fission due to increased neutron evaporation steps required to remove the excess energy. With the fission probability significantly higher than neutron emission probability at each step, the total fission survivability probability is small. Hot fusion reactions have higher compound nucleus fusion probabilities though as incident projectile energies are well above the interaction barrier.

Enhanced physical detection techniques [Ghi1967a, Ghi1967b] and enhanced beam accelerators (HILAC and SuperHILAC) were used to discover the transactinide elements 104, 105 and 106. The californium target so successfully used to produce lawrencium was used again with various beams to produce the new heavy elements 104, 105, and 106, later named rutherfordium, dubnium and seaborgium [Iup1997]. Rutherfordium was produced in the hot fusion reaction of carbon ions with californium [Ghi1969].

$$^{249}_{98}Cf\left(^{12}_{6}C, 4\,^{1}_{0}n\right)^{257}104 \qquad (1.13)$$

Dubnium was produced a short time later in the reaction of californium with nitrogen ions [Ghi1970].

$$^{249}_{98}Cf\left(^{15}_{7}N,4\,^{1}_{0}n\right)^{260}105 \tag{1.14}$$

Seaborgium was produced in the reaction of californium with oxygen ions [Ghi1974].

$$^{249}_{98}Cf\left(^{18}_{8}O,4\,^{1}_{0}n\right)^{263}106 \tag{1.15}$$

The highlights of the discoveries of elements 104-106 as well as additional discovery claims can be found in Seaborg and Hoffman [Sea1990, Hff1998, Hff2000]. All of these experiments used physical means to verify the discovery of the new elements. The most reliable physical method was to observe the alpha decay of the isotopes produced and link them to the alpha decay of previously known isotopes. This method was used for the discovery of rutherfordium, dubnium and seaborgium. For example, ^{263}Sg was linked genetically to ^{259}Rf which was genetically linked to ^{255}No. Detection systems were designed to provide optimum conditions for detecting these genetic relationships. The chemical properties of these transactinide elements were predicted to be similar to their d-block homologues. Chemical separations to test these ideas were not performed until production rates were increased and chemical separation techniques became more sophisticated. Various production methods were also examined in the hope of producing isotopes of these heavy elements with long enough half-lives to perform chemistry. The first chemistry experiments on rutherfordium [Zva1969], dubnium [Zva1970] and seaborgium [Shä1997] were performed in 1969, 1970 and 1997, respectively.

After the discovery of seaborgium, it would again be sometime before the discovery of a new heavy element. Extremely low production rates, small cross sections,

and limited beam currents all contributed to the difficulty in producing new elements. All of the approaches to this point involved the use of actinide targets to produce the heavy elements. In 1975, Oganessian and co-workers [Oga1975] postulated that through the use of lead and bismuth targets and beams with Z ~ 20, compound nuclei could be created with smaller excitation energies which would increase the survivability of the evaporation residues from fission. This new reaction was called a "cold fusion" reaction, as the compound nucleus was "colder" than those produced in hot fusion reactions. The cold fusion reactions targets ^{208}Pb and ^{209}Bi have binding energies (^{208}Pb: 1636 MeV, ^{209}Bi: 1640 MeV), that are 150 MeV – 200 MeV smaller than the binding energies of hot fusion targets like ^{238}U (1802 MeV) and ^{249}Cf (1863 MeV). In addition the compound nucleus Q-value is approximately 100 MeV smaller for cold fusion reactions than hot fusion reactions. For example, the Q-value for ^{258}Rf, the compound nucleus from the ^{208}Pb + ^{50}Ti reaction is –169 MeV, whereas the Q-value for ^{262}Rf, the compound nucleus from the ^{238}U + ^{24}Mg reaction is –69 MeV. These two factors lead to smaller compound nucleus excitation energies in cold fusion reactions.

In 1981, element 107 was produced in the cold fusion reaction of bismuth with chromium ions [Mün1981].

$$^{209}_{83}Bi\left(^{54}_{24}Cr, ^{1}_{0}n\right)^{262}107 \qquad (1.16)$$

This was the first cold fusion reaction used in the discovery of a new heavy element. The evaporation of only one neutron is characteristic of smaller excitation energies in the compound nucleus. This discovery would not have been possible without the construction of the UNILAC accelerator and SHIP (Separator for Heavy Ion reaction

Products) velocity filter [Mün1979] under the direction of Armbruster at GSI in Darmstadt.

Following the successful discovery of bohrium, elements 108 and 109 were quickly discovered in 1982-84 [Mün1984a, Mün1987, Mün1982, Mün1984b] using cold fusion reactions of heavy ions with ^{208}Pb or ^{209}Bi targets.

$$^{208}_{82}Pb\left(^{58}_{26}Fe, ^{1}_{0}n\right)^{265}108 \tag{1.17}$$

$$^{209}_{83}Bi\left(^{58}_{26}Fe, ^{1}_{0}n\right)^{266}109 \tag{1.18}$$

Elements 110 – 112 were not discovered by the GSI team until nearly ten years later after improvements were made in the efficiency and detection system of SHIP and the use of more intense beams [Hof1995a, Hof1995b, Hof1996].

$$^{208}_{82}Pb\left(^{62}_{28}Ni, ^{1}_{0}n\right)^{269}110 \tag{1.19}$$

$$^{209}_{83}Bi\left(^{64}_{28}Ni, ^{1}_{0}n\right)^{272}111 \tag{1.20}$$

$$^{208}_{82}Pb\left(^{70}_{30}Zn, ^{1}_{0}n\right)^{277}112 \tag{1.21}$$

The reactions producing elements 111 and 112 have not yet been confirmed outside of GSI [Hof2001]. Additional information on the discoveries of elements 107 through 110 can be found in [Sea1990] and of elements 107 through 112 in [Hff1998, Hff2000].

The problem with using cold fusion reactions to extend the discovery to heavier elements ($Z > 112$) resides in the fact that production cross sections for the best reactions are approximately 1 picobarn (10^{-36} cm^2). The current sensitivity of detection equipment is approximately 1 picobarn as well. It can be seen that the best reactions to produce

these heavy elements have cross sections that decrease rapidly with Z, and increasingly better sensitivities are required.

To create the superheavy elements (Z > 112), detection equipment needs to be improved, beam currents need to be increased, or a completely different route needs to be investigated. The possibility of using actinide targets with the same heavy ion beams used in cold fusion reactions to produce elements heavier than 112 was discussed as early as 1981 [Oga1981]. Reactions of actinide targets and intense ^{48}Ca beams produce compound nucleus Q-values similar to the compound nucleus Q-values of the cold fusion reactions, leading to slightly larger compound nucleus excitation energies.

As a result of better equipment and increased detection sensitivity as well as the ability to produce rather intense ^{48}Ca beams, elements 114 and 116 were reported produced. In 1999, element 114 was reported in the reaction of ^{48}Ca ions with neutron-rich plutonium targets [Oga1999a, Oga2000a].

$$^{244}_{94}Pu\left(^{48}_{20}Ca, 4\,^{1}_{0}n\right)^{288}114 \tag{1.22}$$

Built upon the success of the reactions of ^{48}Ca on plutonium and uranium reported for the production of neutron-rich element 112 isotopes [Oga1999b], high intensity ^{48}Ca beams were used to irradiate ^{248}Cm targets to produce element 116 [Oga2000b].

$$^{248}_{96}Cm\left(^{48}_{20}Ca, 4\,^{1}_{0}n\right)^{292}116 \tag{1.23}$$

Only five atoms of element 114 [Oga2001a, Oga2000a, Oga1999a] and one atom of element 116 [Oga2000b] have been produced and these experiments have not been confirmed. The expectation of the emission of four neutrons is consistent with compound

nucleus excitation energies between 30 and 40 MeV and the classification of these reactions as hot fusion reactions.

The search for still heavier elements will continue to use both cold and hot fusion reactions. Advanced beam development will lead to higher intensity beams which will require innovative target designs to dissipate the heat produced. Separation devices will be improved to detect activity faster and more accurately than before. Aside from the instrumentation aspect of the search, it is also important to understand the physical reasons for the success of these individual reaction paths, cold- and hot fusion, and when to use one type of reaction over another.

1.2 Cold and hot fusion

The initial predictions on cold fusion reactions [Oga1975] was based on a simple compound nucleus excitation energy calculation. The calculation showed a minimum excitation energy (E^*_{min}) in the compound nucleus formed in reactions of projectiles with masses around 45. The calculation is based on finding the excitation energy of the compound nucleus at the interaction barrier (B_{int}). The interaction barrier in this calculation is a Coulomb potential barrier (V_{coul}).

$$E^*_{\min} = B_{\text{int}} + Q, \tag{1.24}$$

$$B_{\text{int}} = V_{coul} \tag{1.25}$$

$$V_{coul} = \frac{Z_1 Z_2 e^2}{r_e\left(A_1^{\frac{1}{3}} + A_2^{\frac{1}{3}}\right)} \tag{1.26}$$

$$Q = \left(M_1 + M_2 - M_{CN}\right)c^2 \tag{1.27}$$

The effective interaction radius (r_e) was taken as 1.45 fm and the nuclear masses were taken from Myers and Swiatecki [Mye1966]. Using this simple calculation and various projectile and target combinations for the production of fermium and rutherfordium, Oganessian and co-workers produced the graph seen in Figure 1.1. It is easy to notice from Figure 1.1 that the minimum of this curve appears around a projectile mass of 45. This meant that ion beams like ^{40}Ar and ^{48}Ca with ^{208}Pb and ^{209}Bi targets might be more effective in forming the heavy elements than actinide target reactions with lighter ions. This can be seen in Figure 1.2.

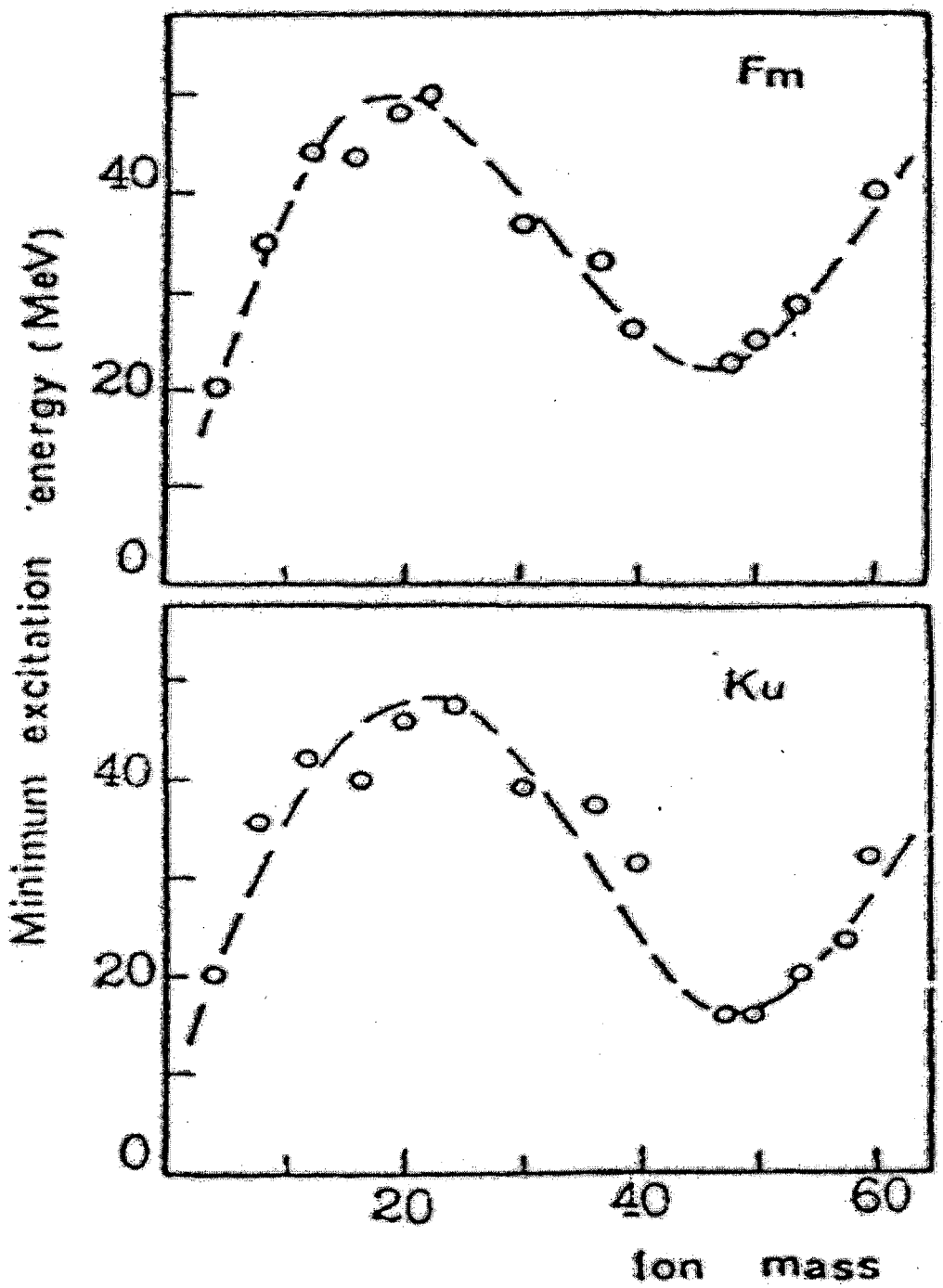

Figure 1.1: Graphs of projectile (ion) mass versus E^*_{min} for various projectile-target reactions leading to ^{248}Fm and ^{258}Rf (denoted Ku). The dashed curves are drawn through the calculated E^*_{min} values shown by the points [Oga1975].

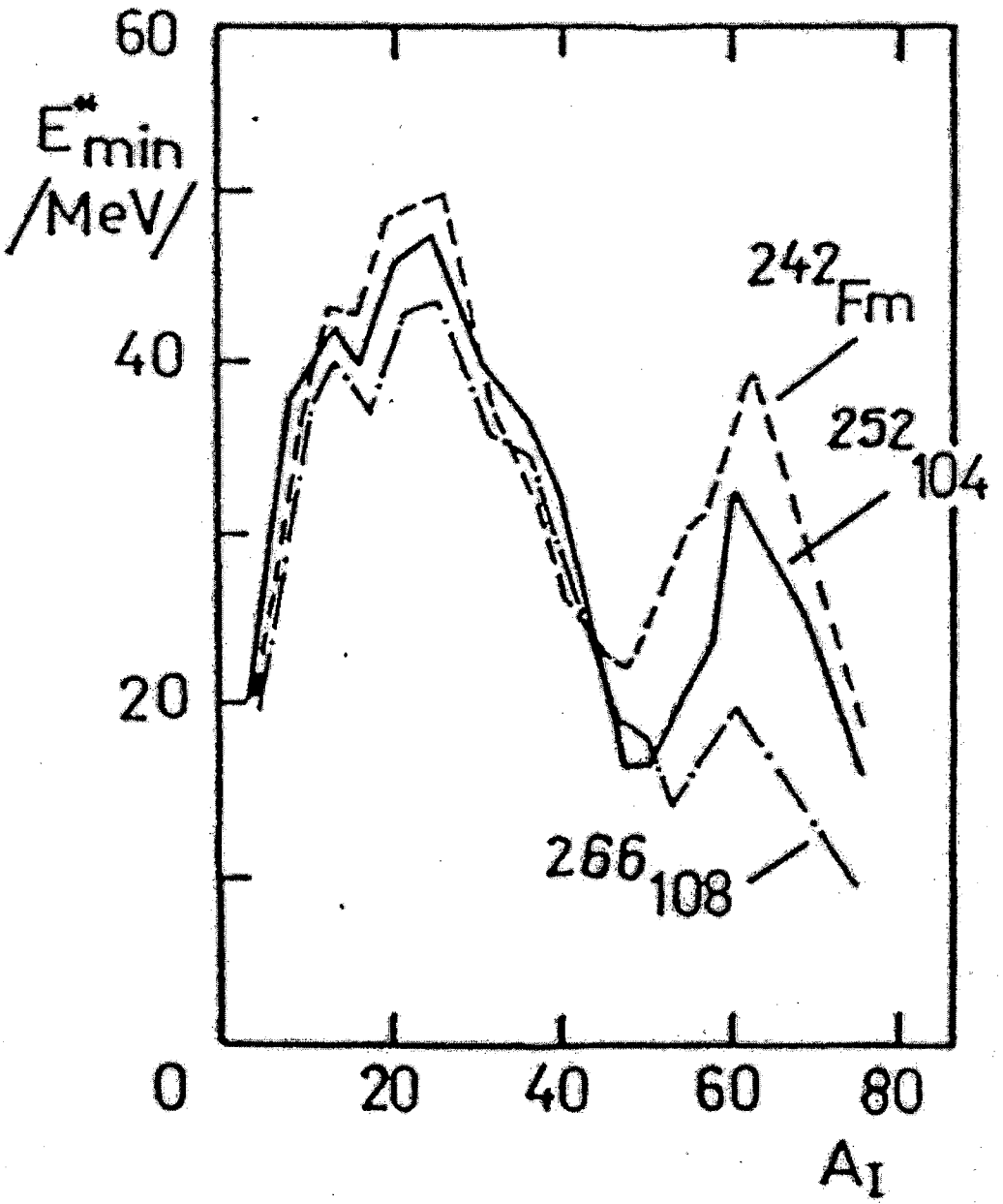

Figure 1.2: The minimum excitation energy versus the projectile mass A_I for different target-projectile combinations leading to ^{242}Fm, ^{252}Rf and ^{266}Hs compound nuclei [Oga1981].

One can see from Figure 1.2 that the trend continues for even heavier elements like hassium (element 108). The minimum in these curves does shift to higher masses with the production of the heavier elements, meaning that the corresponding target is centered around lead. This postulate led to the discovery of elements $107 \leq Z \leq 112$ by researchers at GSI in Darmstadt using their velocity filter SHIP [Mün1979]. Table 1.2 illustrates the E^*_{min} values for the confirmed discovery reactions from mendelevium through element 110 and reported discovery reactions for elements 111, 112, 114 and 116.

Table 1.2 shows that the minimum excitation for the discovery of elements 101 through 106 remained constant around 40 MeV. Hot fusion experiments to produce elements heavier than seaborgium were difficult due to lower fusion probabilities. Lower fusion probabilities combined with constant high fission competition in the exit channel reduced the production cross sections for hot fusion reactions. The use of cold fusion reactions helped solve the decreasing production cross section problem. Smaller compound nucleus excitation energies meant reduced fission competition in the exit channel and higher production cross sections. Only small gains were made as decreases in the fusion probability for cold fusion reactions continued the decline of production cross sections. Figure 1.3 illustrates the decrease in cross section of various 1n-exit channels for cold fusion reactions for elements 102 – 113 [Hof2000].

Table 1.2: Projectile, target and compound nucleus Z and A for the discovery reactions for elements 101 –110 and reported reactions for elements 111,112,114, and 116 and calculated E^*_{min} values. Z_p, Z_t, and Z_{CN} refer to the atomic number of the projectile, target, and compound nucleus. A_p, A_t, and A_{CN} refer to the atomic mass number of the projectile, target, and compound nucleus.

Z_p	A_p	Z_t	A_t	Z_{CN}	A_{CN}	E^*_{min} (MeV)[a]
2	4	99	253	101	257	17.48
6	12	96	244	102	256	37.72
5	10	98	251	103	261	44.46
6	13	98	249	104	262	38.45
7	15	98	249	105	264	38.63
8	18	98	249	106	267	40.19
24	54	83	209	107	263	14.31
26	58	82	208	108	266	11.49
26	58	83	209	109	267	10.83
28	62	82	208	110	270	8.05
28	64	83	209	111	273	4.13
30	70	82	208	112	277	-0.78
20	48	94	244	114	292	19.11
20	48	96	248	116	296	18.14

[a] An r_e value of 1.45 fm and masses from [Lir1976, Lir2001] were used.

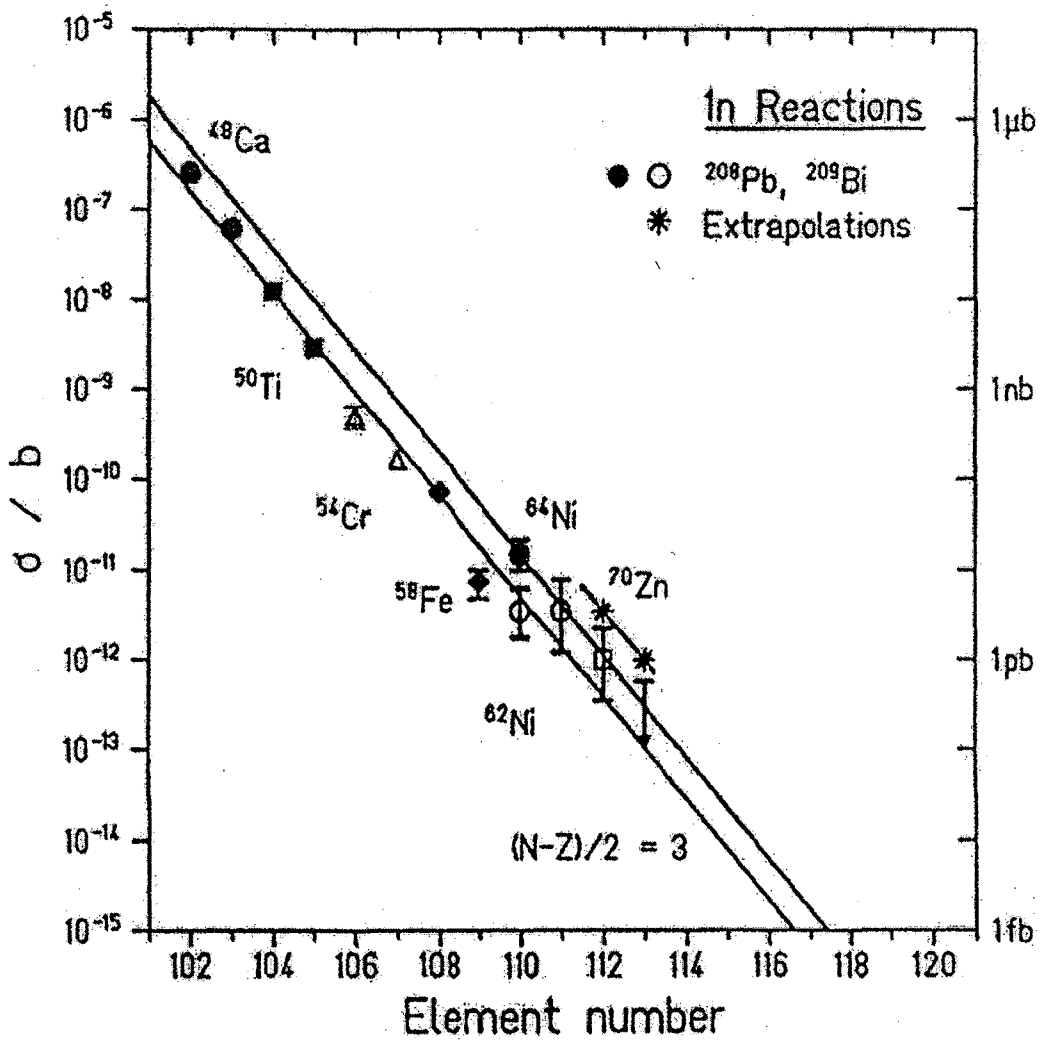

Figure 1.3: 1n-exit channel cross sections for elements 102-113 from cold fusion reactions of various projectiles with lead and bismuth targets [Hof2000].

The deciding factor in choosing between hot and cold fusion reactions is the desired end product. Currently hot fusion reactions using ^{48}Ca projectiles and actinide targets appear to be the route to the superheavy elements because of the neutron-rich character of the heavy element isotopes produced. Cold fusion reactions with ^{208}Pb and ^{209}Bi targets are preferred for the study of the neutron-deficient transactinide isotopes.

One advantage to using hot fusion reactions is the ability to form compound nuclei that are neutron-rich and have longer half-lives. Trial calculations have predicted a doubly deformed shell around Z = 108 and N = 162 [Pat1989, Pat1991]. Hot fusion reactions are a possible reaction mechanism for the formation of such neutron-rich nuclides. A second advantage to using the hot fusion mechanism is the enhanced probability of fusion of the projectile-target system [Oga1994]. The highest production cross sections in hot fusion reactions occur in the 4n- and 5n- exit channels which are located well above the projectile-target interaction barrier. The disadvantages to hot fusion reactions are all due to the large amount of excess excitation energy in the compound nucleus. The higher excitation energy destabilizes the compound nucleus by eliminating the shell effects present in the de-excited evaporation residues [Fle1976]. Numerous neutron evaporation steps are required to evaporate this excess excitation energy leading to an enhanced fission probability, and therefore lower production cross sections.

The main advantage of using cold fusion reactions is the enhanced survivability to fission during compound nucleus de-excitation. With smaller compound nucleus excitation energies, less neutron evaporation steps are required leading to a smaller fission probability. This smaller probability to fission is also related to the fact that the

smaller excitation energy does not tend to eliminate the shell effects. The remaining shell effects add stability to the compound nucleus reducing the chance of fission [Oga1994]. Additionally, fusion of more symmetrical projectile-target combinations leads to cooler compound nuclei [Arm1985]. Another advantage to the cold fusion reaction mechanism is the ability of these reactions to produce neutron-deficient nuclei. This gives access to the study of the decay properties and lifetimes of nuclei away from areas of spherical and deformed stability. Cold fusion reactions, however, do not produce neutron-rich nuclei, and therefore cannot form the neutron-rich superheavy elements. For example, a cold fusion reaction to form rutherfordium, $^{208}Pb + {}^{50}Ti$, forms the compound nucleus, ^{258}Rf, with only 154 neutrons whereas a hot fusion reaction to form rutherfordium, $^{238}U + {}^{26}Mg$, forms the compound nucleus, ^{264}Rf, with 160 neutrons.

The following three figures illustrate the decrease in cross sections for hot and cold fusion reactions as a function of increasing atomic number. Figure 1.4 compares ^{208}Pb and ^{209}Bi cold fusion reactions with ^{238}U and ^{244}Pu target based hot fusion reactions [Oga2001b]. Figure 1.5 displays additional hot and cold fusion cross sections as well as some reported experimental work on the production cross sections of elements with $Z > 112$ [Mün2001]. Finally, Figure 1.6 illustrates for a variety of reactions, the maximum cross section recorded for a given element from fermium through 116 produced in either hot and cold fusion reactions [Ghi1961, Oga1975, Mün1982, Mün1984, Hof1995a, Hof1995b, Hof1996, Oga1999a, Oga2000a, Shi1986, Sik1968, Gäg1989, Nit1981, Heβ1997, Kra1992, Heβ2001a, Gre1994, Mün1985, Wil2000, Mün1989, Tür2001, Hof1998, Hof2001, Oga1999b, Laz1996, Moo2001].

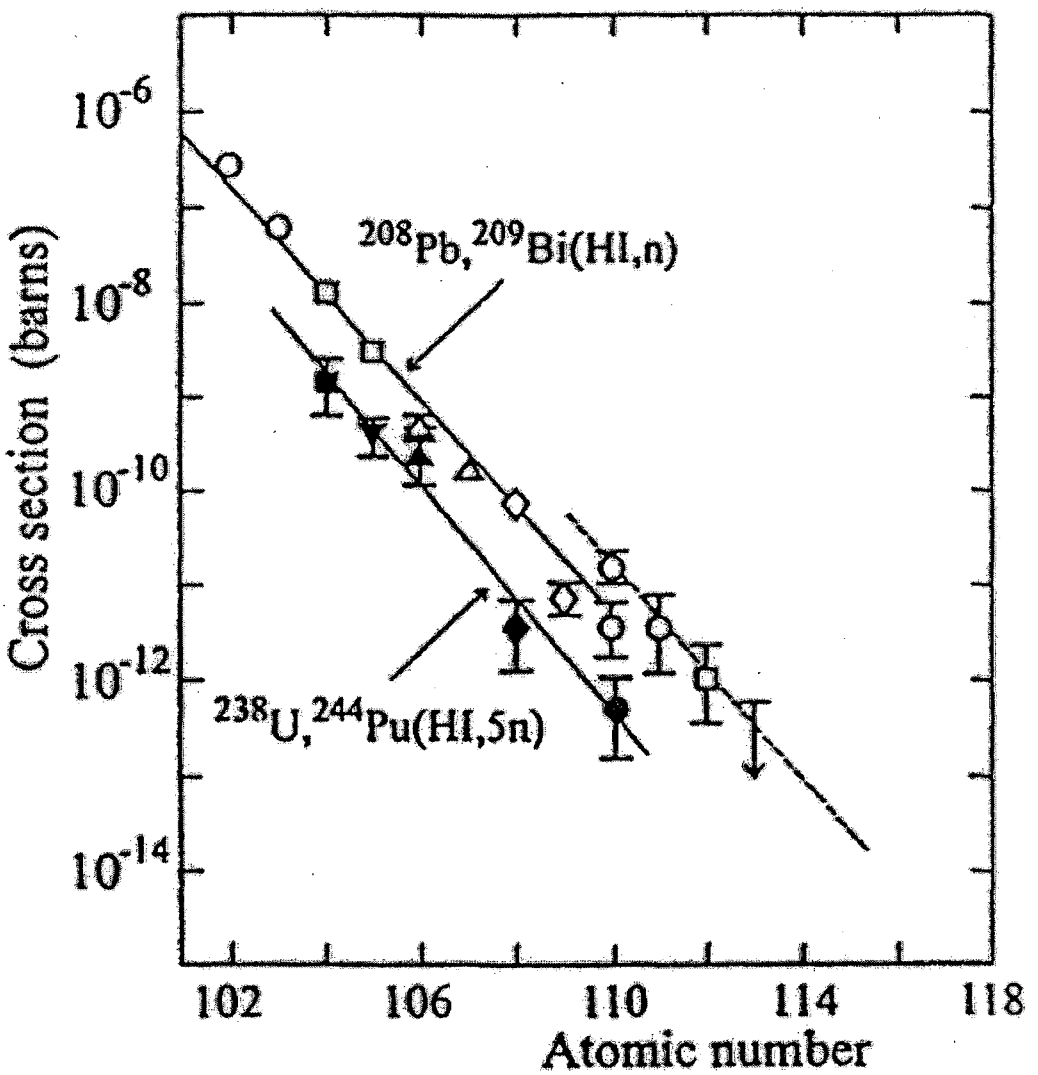

Figure 1.4: Production cross section versus atomic number for various cold and hot fusion reactions [Oga2001b]. HI denotes heavy ion projectile.

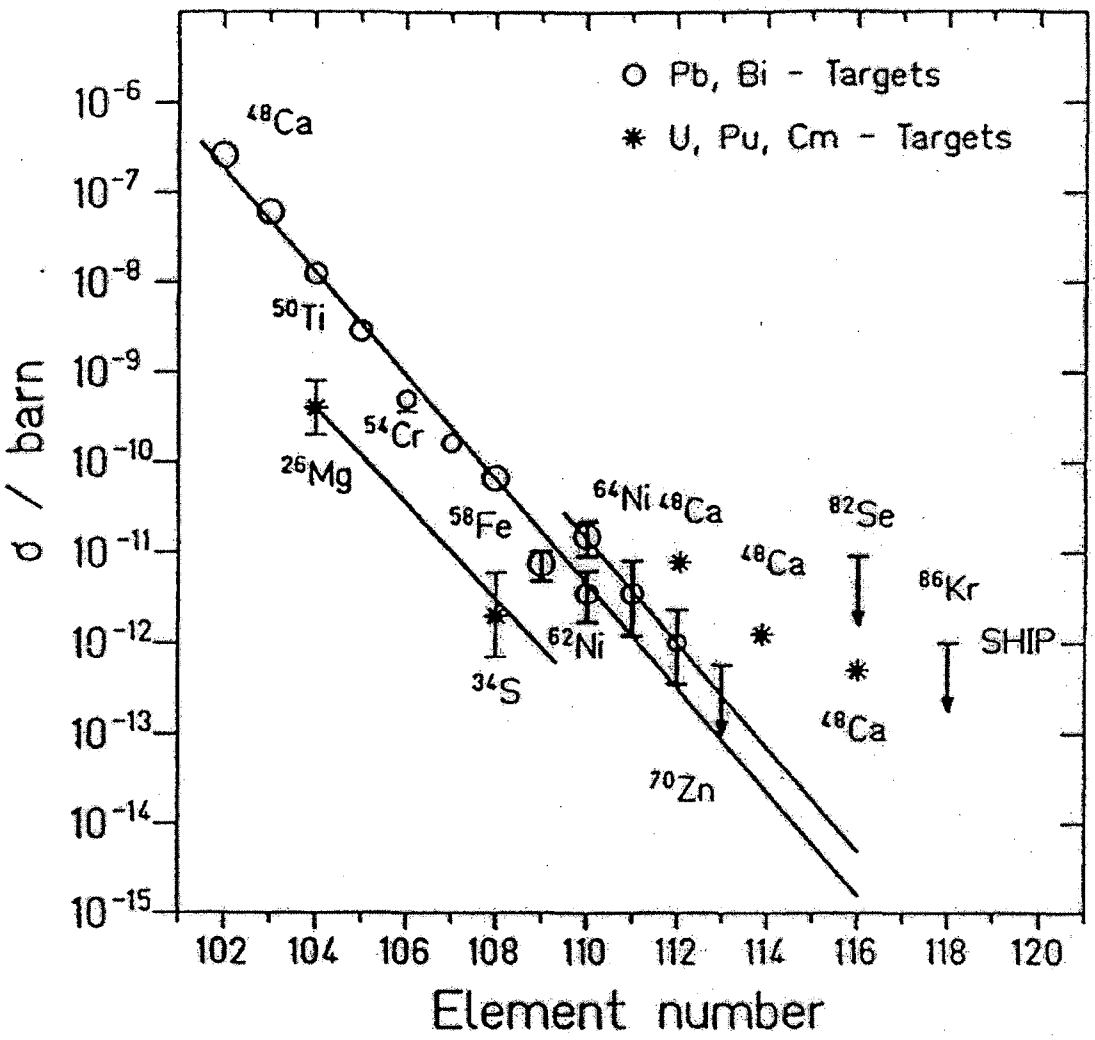

Figure 1.5: Cross section versus increasing element number for cold fusion reactions with lead and bismuth targets and hot fusion reactions with uranium, plutonium and curium targets. Recent work on elements $Z \geq 116$ is also included. Adapted from [Mün2001].

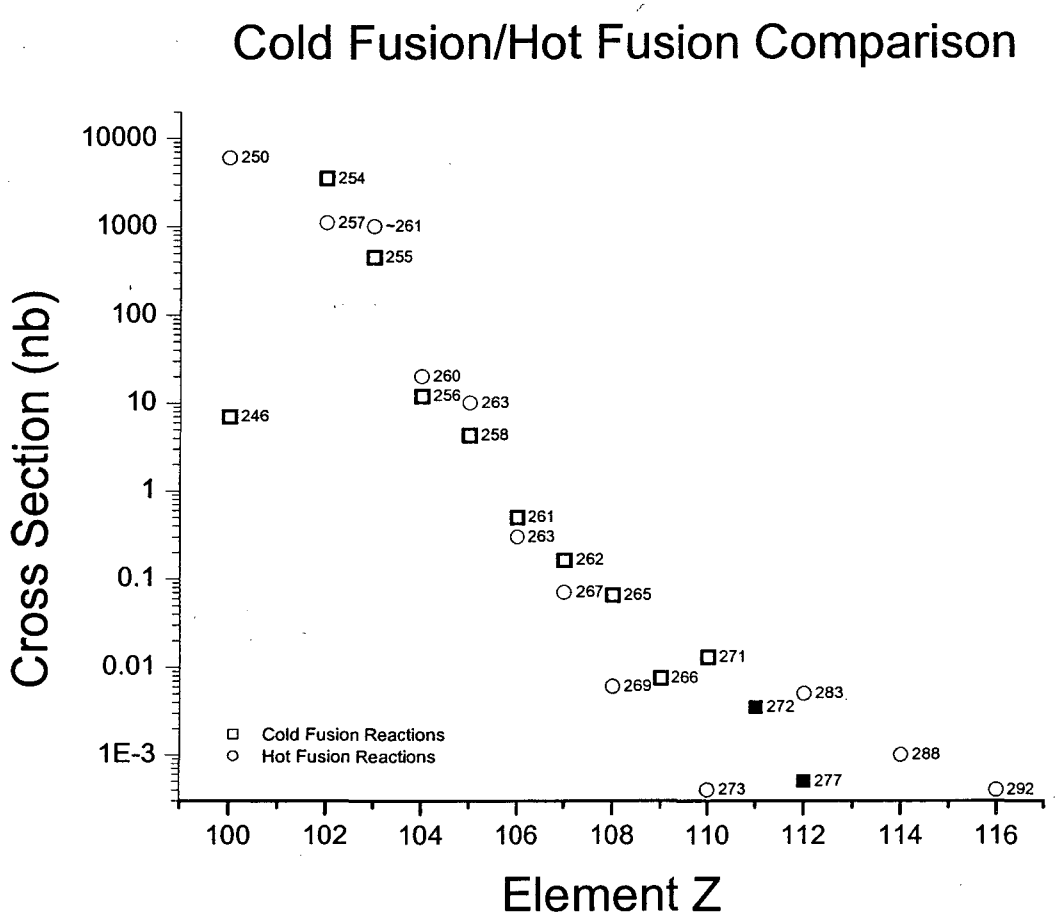

Figure 1.6: Cross section versus Z. The maximum cross section for a given reaction (cold/hot fusion) is shown. Hot fusion in circles and cold fusion in squares. Open symbols represent confirmed reactions while solid symbols represent unconfirmed reactions. The mass number for the isotope produced is given to the left or right of each symbol [Ghi1961, Oga1975, Mün1982, Mün1984, Hof1995a, Hof1995b, Hof1996, Oga1999a, Oga2000a, Shi1986, Sik1968, Gäg1989, Nit1981, Heβ1997, Kra1992, Heβ2001a, Gre1994, Mün1985, Wil2000, Mün1989, Tür2001, Hof1998, Hof2001, Oga1999b, Laz1996, Moo2001].

From Figure 1.6 it can be seen that the hot fusion reactions do indeed produce nuclei that are more neutron-rich. Hot fusion reactions also produce evaporation residues with higher cross sections for the elements $Z \leq 105$ and $Z \geq 112$. The lone exception is the production of nobelium using the cold fusion of doubly magic ^{48}Ca and ^{208}Pb.

The study of hot and cold fusion reactions can be extremely enlightening in terms of the production routes to the heavy elements. The importance of understanding hot and cold fusion does not end with the heavy elements. Understanding which method is preferred over the other for a given region of nuclides can facilitate the study of a particular area of the chart of nuclides in greater detail. By examining particular reactions and making subtle changes in the choice of target and projectile combinations, a greater understanding of the structure of the nuclei in the region of the heaviest elements can be developed.

1.3 Scope

In this dissertation, experimental investigations of both hot and cold fusion reactions are described. Three hot fusion reactions will be examined: $^{248}Cm(^{15}N,xn)^{263-x}Lr$, $^{238}U(^{18}O,4n)^{252}Fm$, and $^{238}U(^{22}Ne,xn)^{260-x}No$. The 3n- and/or 4n-exit channel was studied in each experiment. Five cold fusion experiments are examined: $^{208}Pb(^{48}Ca,xn)^{256-x}No$, $^{208}Pb(^{50}Ti,xn)^{258-x}Rf$, $^{208}Pb(^{51}V,2n)^{257}Db$, $^{209}Bi(^{50}Ti,xn)^{259-x}Db$, and $^{209}Bi(^{51}V,2n)^{258}Sg$. A review of three of the various computer codes available for the prediction of production cross sections are reviewed. An examination of the results from various hot and cold fusion experiments is presented and compared with literature values. The relevance of these experiments to the development of a better understanding of hot and cold fusion excitation functions is discussed. The importance of projectile odd-even effects and target odd-even effects in the production cross sections of neutron deficient nuclides is discussed. The relevance of computer codes in calculating cross sections, and how these codes can help in understanding the physics behind the production of nuclides of the heaviest elements is pointed out.

2 Evaporation codes

2.1 JORPLE and SPIT

Cross sections are important to the study of hot and cold fusion reactions. A cross section is defined as a measure of the probability or likelihood that a specific reaction will occur. Different reactions leading to the same isotope will have different cross sections. These cross sections can be compared to evaluate the best mechanism for the synthesis of that particular isotope. Cross sections are measured in units of area called barns (b) where one barn is equal to 10^{-24} cm^2.

Heavy element experimental cross section measurements are performed on isotopes that have small (< 1 millibarn) cross sections. This means that the amount of time required for the experiment can be quite long, and therefore expensive in terms of equipment costs and beam time. Knowing the expected cross section can greatly reduce the amount of time spent on an experiment by helping determine what experimental energies should be tested and for how long.

The foundations of the JORPLE code are based in the estimations of the production cross sections for heavy element reactions [Sik1966]. The computer code was written in 1970 [Alo1970, Alo1974]. This code provides a general prediction of the cross sections that could be expected from a variety of heavy element reactions.

The interaction potential for the JORPLE code is based on a sum of individual potentials [Ilj1982], a Coulomb term like Equation 1.26, a rotational term, and a nuclear term. The nuclear part of the equation resembles the Woods-Saxon potential but is partially modified [Alo1974] by adding in terms dependant on the orientation angles of the nuclear deformation axis with respect to the incident beam direction. The total fusion

probability in the JORPLE code is solely based on the barrier penetration probability, which is calculated using the Hill and Wheeler approximation [Hil1953].

The de-excitation of the compound nucleus is performed using the Jackson model to calculate neutron evaporation probabilities [Sik1968a, Sik1968b]. The values for the (Γ_n/Γ_f) values are calculated according to Sikkeland and co-workers [Sik1968a],

$$\log\left(\frac{\Gamma_n}{\Gamma_f}\right) = -0.276Z + \begin{cases} 5.46 + 0.140N, N \leq 153 \\ 19.23 + 0.050N, N \geq 153 \end{cases} \quad (2.1)$$

where Z and N refer to the atomic number and neutron number of the compound nucleus.

By combining the effects of all of the partial angular momentum waves through the interaction barrier, and adding in the barrier penetration factor with a compound nucleus de-excitation factor, the JORPLE code is a simple calculation that gives relatively good production cross section estimations.

The SPIT code is a modification of the JORPLE code developed to increase the accuracy of cross section predictions [Wil1988]. Modifications were made to the original code by changing the interaction potential in the attempt to make the estimations better reflect the existing experimental data.

The SPIT code differs from the JORPLE code in using a different Coulomb potential as well as a different nuclear potential. The rotation part of the interaction potential is kept the same as in the JORPLE code. The Coulomb potential is taken from Bondorf, Sobel and Sperber [Bon1974]. The nuclear part of the interaction potential is based on the Bass proximity potential [Bas1977].

Taking the new nuclear and Coulomb parts to the interaction potential, the first step in the SPIT code is the determination of the barrier energy. From here, using the same calculations as in the JORPLE code, the barrier penetration factor and the compound nucleus cross section are calculated. From there, the neutron evaporation probability and neutron width to fission width ratio are calculated and multiplied together with the compound nucleus cross section to give the production cross section for a given energy and number of neutrons evaporated.

Using these modified Coulomb and nuclear potentials leads to enhanced accuracy in predicting production cross sections for the heavy elements. The SPIT and JORPLE codes and their ability to predict production cross sections for heavy ion projectile actinide target reactions have been reviewed in [Hay1988, Moo1990]. In most cases for reactions involving projectiles equal to or lighter than oxygen, the SPIT code can reproduce the experimental cross section within an order of magnitude or two. Heavier projectile beams lead to larger discrepancies. As new reaction mechanisms were developed to study heavier element systems, a new cross section prediction code was needed to predict the cross sections for these new reactions.

2.2 HIVAP

The HIVAP code was produced in the attempt to predict production cross sections for a variety of different reactions. One of the failures of earlier codes like JORPLE and SPIT is their tendency to be useful for only a given region of the Chart of Nuclides, like the heaviest elements. Their approach is based on the black box model of compound nucleus formation and therefore the production cross sections that these codes produced are often off by orders of magnitude in cross section. Further, JORPLE and SPIT are small parameter codes, meaning the only input is the projectile and target atomic number and atomic mass. Inevitably, more parameters would enhance a code's ability to accurately predict production cross sections. As the search for heavier elements moved to the cold fusion reaction mechanism, a different production cross section code was needed.

The HIVAP code is a modification of an earlier code that examined the de-excitation of highly excited nuclei [Gro1967]. This code, named GROGI, is based on looking at nuclei that have large excitation energies and large angular momentum values. It incorporates the statistical de-excitation of the excited compound nucleus through neutron, gamma-ray and charged particle emission. HIVAP is an improvement of the GROGI code through the incorporation of fission into the de-excitation step as well as the incorporation of new insights into level density calculations, interaction barriers, ground-state masses and shell-effects and fission barriers. One of the advantages of the HIVAP code is the use of multiple independent sources for the determination of the many parameters involved in the calculation of the production cross sections [Ver1984].

The HIVAP code is a modular code that can be used in a multitude of situations. Because of this, a detailed list of the parameters used must be kept in order to distinguish the results of one parameter set from another. The multiple parameters used in the HIVAP code can be adapted to a specific section of the Chart of Nuclides to make cross section predictions for a small region more accurate than the earlier more global codes JORPLE and SPIT.

An overview of the calculations in the HIVAP code used in this dissertation is as follows. Most of the following conditions for HIVAP were set according to calculations done by Reisdorf and Schädel, fitting HIVAP results to actinide target based experimental data [Rei1992]. Compound nucleus formation is considered as separate from the de-excitation step. Fusion occurs when the projectile-target system passes the interaction barrier which is calculated using the Bass interaction potential [Bas1977]. Below the barrier, a WKB (Wentzel-Kramer-Brillouin) approximation is made to estimate barrier penetration. The fusion barrier in HIVAP is considered to be fluctuating using a Gaussian parameter with a user-defined standard deviation. Corrections in the entrance channel are also made for extra push and extra-extra push effects [Swi1982]. The de-excitation of the excited compound nuclei is calculated using the following sources: liquid drop masses [Mye1966], level density calculations [Rei1981], level density ratios [Tök1981], and fission barriers [Coh1974]. The standard set of parameters used from this description of the HIVAP code will be referred to as the Reisdorf and Schädel parameters and are given in Table 2.1.

Table 2.1: Reisdorf and Schädel Parameter set for the HIVAP code [Rei1992].

Variable	Description	Value
LEVELPAR	Scale parameter for the level density	1.153
AF / AN	Level density ratio parameter value	1
BARFAC	Scale parameter for the fission barrier	1
EDAMP	Shell effect damping energy (MeV)	18.0
DELT	Nuclear pairing correction energy (MeV)	11.0
V0	Initial value of the nuclear potential (MeV)	70.0
R0	Nuclear radius parameter (fm)	1.12
D	Fuzziness in the nuclear radius parameter (fm)	0.75
Q2	Nuclear quadrupole moment (fm^2)	1050
CRED	Scale parameter for the interaction barrier	1.0
SIGR0	Fluctuation of the interaction barrier (% of R0)	3.0
CUTOFF	Integration limits in (SIGR0) for barrier fluctuations	5.0
XTH	Extra push theory threshold fissility parameter	0.7
APUSH	Slope coefficient from extra push theory	18.0
FPUSH	Angular momentum coefficient from extra push theory	0.75

Additional parameters from the Reisdorf and Schädel parameter set can be seen in the dissertation of Dressler [Dre1999]. Another invaluable source of information regarding the description of the calculation loop and the various parameters and their associated meanings is a guidebook written by Reisdorf [Rei1990].

With the numerous independent variables that can be changed and altered to suit the needs of the experiment, the HIVAP code is definitely not a general global code for predicting production cross sections. The HIVAP code is much more effective at predicting cross sections when the individual parameters are tailored to a specific type of reaction or particular region of the Chart of Nuclides. The aforementioned Reisdorf and Schädel parameters will be used by HIVAP in this dissertation to compare with the experimentally obtained production cross sections. By using codes such as HIVAP to accurately predict production cross sections, information regarding the physical properties of the transactinide nuclei will be obtained.

3 Experimental procedures

As hot- and cold fusion reactions are both used to produce isotopes of the heaviest elements, so are there different experimental procedures used to produce, separate and detect these heavy element isotopes. Three different experimental procedures were used to produce the heavy element isotopes studied for this dissertation.

For each of these individual experimental procedures there are five basic components: the accelerator, the target chamber and targets, the transportation/ separation/collection systems, the detector system and the data acquisition system.

The first of the five basic components is the accelerator. The 88-Inch Cyclotron at Lawrence Berkeley National Lab provided all of the heavy ion beams used in the three experimental procedures. The 88-Inch Cyclotron is a sector focused cyclotron that is capable of providing intense beams of a multitude of ions from protons through uranium. The intense beams are produced in advanced electron-cyclotron resonance (ECR) ion sources created and developed at Lawrence Berkeley National Lab. The beams produced by the cyclotron are controlled, directed and maintained by the experienced staff of the 88-Inch Cyclotron.

Two of the experimental procedures involved stationary targets. The compound nucleus recoils from the projectile-target reactions for the first of these experimental procedures were transported to our rotating wheel system known as the Merry-Go-Round (MG) [Hff1980]. The MG system is important in the study of the heavier elements as the length of time between production and detection is extremely short, however, without any chemical separation, the presence of any interfering activity would mask the activity of interest making positive identification difficult. These negatives are balanced by the

positive aspect that the techniques can be used in reactions where highly active actinide targets are required. Only one experiment was performed using this procedure: $^{248}Cm(^{15}N,xn)^{263-x}Lr$.

The compound nucleus recoils from the second stationary target experimental procedure were collected on gold catcher foils located directly behind the standing target. The success of the catcher foil technique lies in the ability to effectively chemically separate the activity of interest from the gold foil and the rest of the reaction products. The duration of the chemistry separation is also extremely important, as longer chemical separations lead to the inability to study short lived isotopes. Only one experiment was performed using this procedure: $^{238}U(^{18}O,4n)^{252}Fm$.

If non-active or only slightly active targets can be used, a faster and more efficient experimental procedure can be used, the Berkeley Gas-filled Separator (BGS) [Nin1999]. Six separate experiments ($^{238}U(^{22}Ne,xn)^{260-x}No$, $^{208}Pb(^{48}Ca,xn)^{256-x}No$, $^{208}Pb(^{50}Ti,xn)^{258-x}Rf$, $^{208}Pb(^{51}V,2n)^{257}Db$, $^{209}Bi(^{50}Ti,xn)^{259-x}Db$, and $^{209}Bi(^{51}V,2n)^{258}Sg$) were performed using this third experimental procedure involving a rotating target wheel system and the BGS physical separation apparatus.

3.1 MG system

The $^{248}Cm(^{15}N,3n)^{260}Lr$ reaction was studied using the Merry-Go-Round (MG) rotating wheel collection and detection apparatus. The target system used a 2.63 mg/cm^2 beryllium vacuum window, 0.3 mg/cm^2 nitrogen as a cooling gas, and a 2.58 mg/cm^2 beryllium target backing. The 0.873 mg/cm^2 curium target (96% ^{248}Cm, 4% ^{246}Cm) contained approximately 0.84 mg/cm^2 ^{248}Cm as the oxide $^{248}Cm_2O_3$. Because of the short range of the ^{15}N projectiles in curium, the effective thickness of the curium target was only 0.368 mg/cm^2. The uncertainty in the target thickness was estimated to be 0.010 mg/cm^2. The ^{248}Cm had been electroplated [Aum1974, Mül1975] onto the beryllium target backing in a circle 6-mm in diameter. After the compound nucleus reaction, the recoiling products were thermalized in 1 atm of helium gas inside the target chamber. There they were attached to KCl aerosols in a helium gas-jet and transported via a 7-meter 1.4-mm i.d. capillary at a flow rate of 1.8 STP liters/min at a pressure of 5.0 PSIG (pounds per square inch gauge) to the MG collection site. A schematic illustration of the target chamber can be seen in Figure 3.1. The activity-laden aerosols were deposited on polypropylene foils (40 – 60 μg/cm^2 thick) held in eighty collection positions located around the periphery of the 51.0-cm diameter fiberglass wheel. The polypropylene foils containing the activity were stepped between six opposing pairs of PIPS (Passivated Implanted Planar Silicon) detectors. Figure 3.2 shows a schematic diagram of the MG collection wheel inside a vacuum chamber.

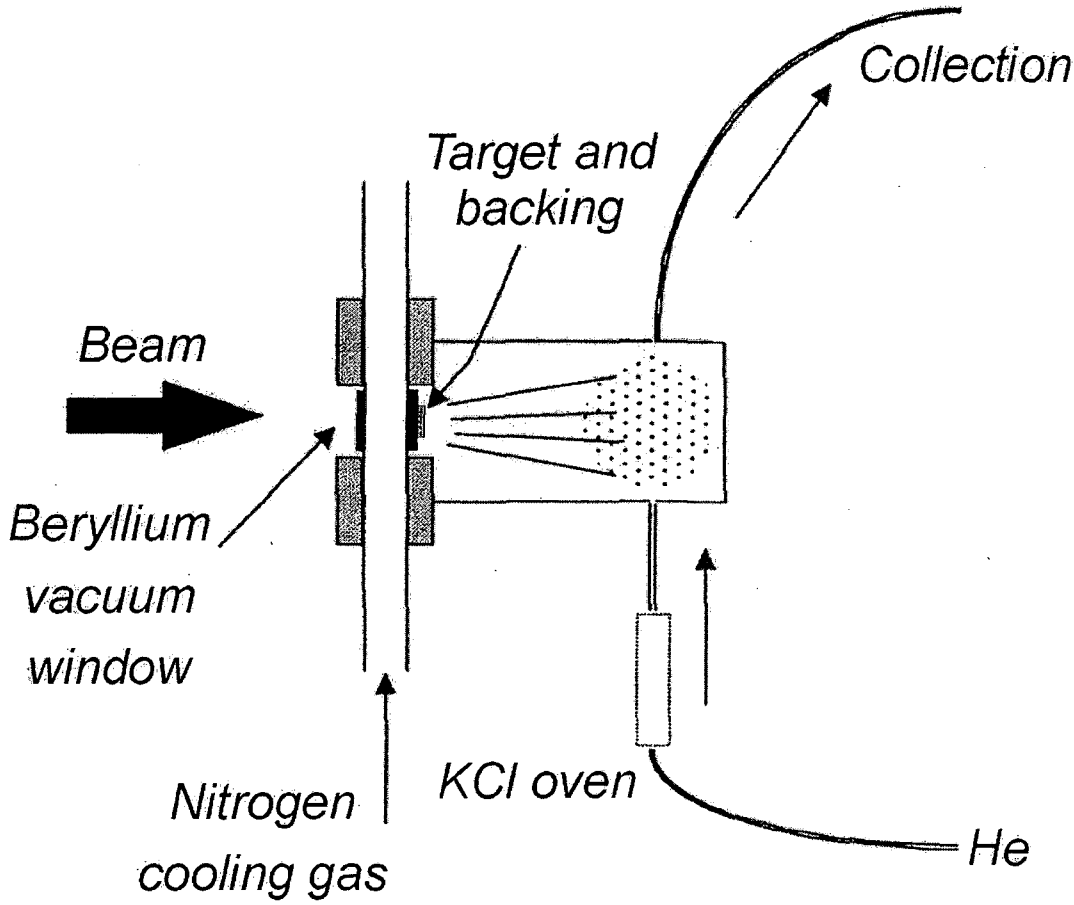

Figure 3.1: Target chamber used in the MG experiment. Recoiling products are thermalized and attached to KCl aerosols in a helium gas-jet for transport to the collection site.

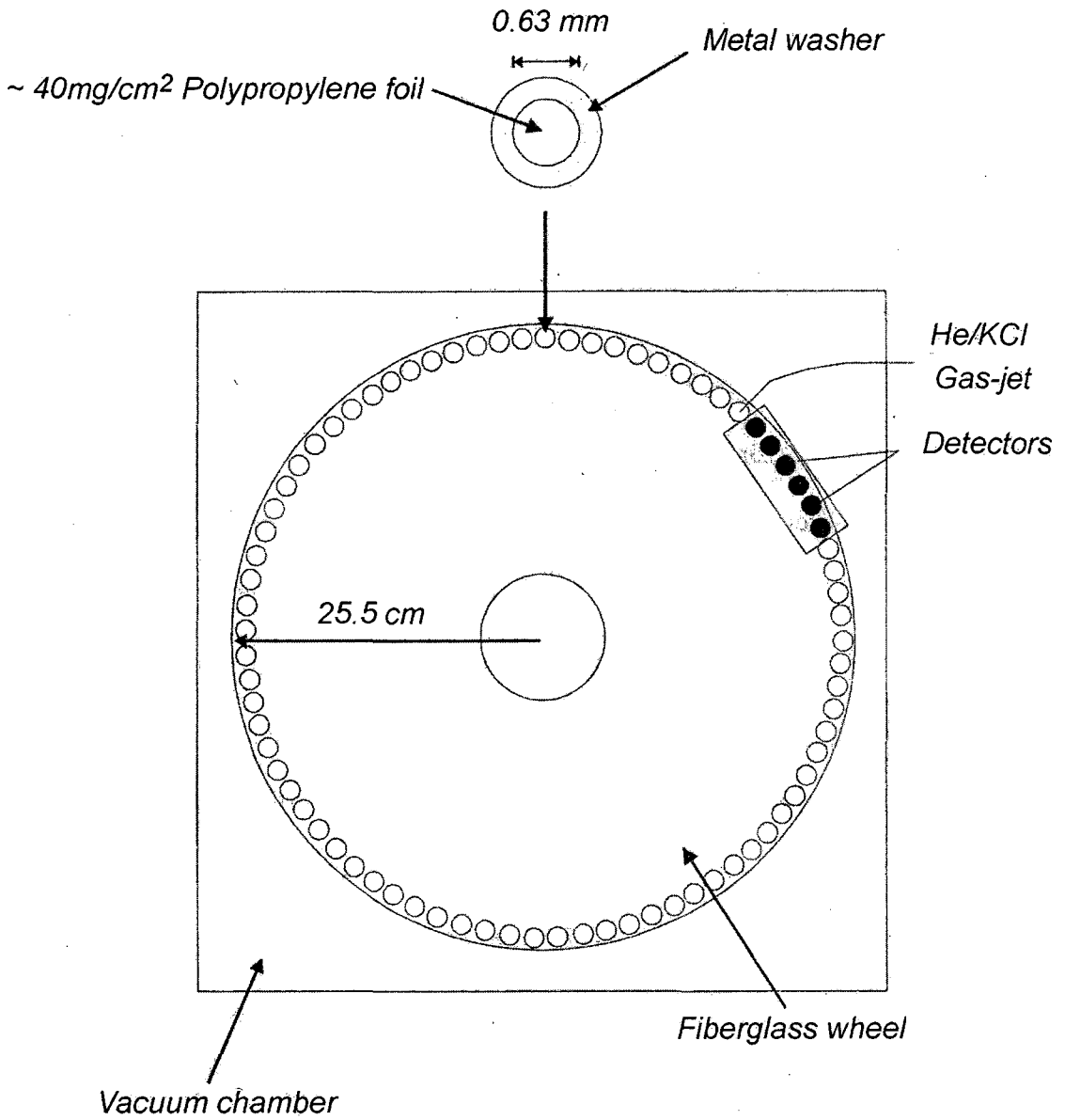

Figure 3.2: View of the Merry-Go-Round rotating wheel collection and detection system. The activity laden KCl aerosols are deposited on one of eighty polypropylene foils located on the periphery of the wheel that is rotated clockwise through the six pairs of detectors, above and below the wheel.

Detectors both below and above the polypropylene foil allowed for coincidence measurements and better efficiency for detecting α-particles. The experimental resolution (FWHM) of the first top detectors was determined to be 45 ± 5 keV by examining the ^{213}Fr (E_α = 6.7750(17) MeV) peak in the first top detector. The experimental resolution for the remaining top detectors was then assumed to be 45 ± 5 keV as well. Experimental resolution for the bottom detectors was approximately 100 keV due to energy degradation in the polypropylene foil [Sha2000]. Transport time from the target to the first polypropylene foil was determined to be 1.0 ± 0.3 s [Lan1998]. A gas-jet and deposition efficiency of 50 ± 20% was determined by comparing on-line and off-line measurements of ^{254}Fm (E_α = 7.192(2) MeV, $t_{½}$ = 3.240 ± 0.002 h) produced via transfer reactions with the ^{248}Cm target. Measurements were also made of the 4n-out product ^{259}Lr (E_α = 8.450(20) MeV, $t_{½} = 6.3\ ^{+0.5}_{-0.4}$ s) to check the accuracy of the gas-jet and deposition efficiency measurement. With a larger cross section and a shorter half-life, several short measurements were made to observe ^{259}Lr and confirm 50 ± 20% as the gas-jet and deposition efficiency. The specific details of this measurement are located in Section 4.1. The time between successive wheel movements, or stepping time, was chosen to be two minutes. This allowed for a total detection time of twelve minutes, or four half-lives of ^{260}Lr (E_α = 8.030(20) MeV, $t_{½}$ = 180 ± 30 s). The collection of data was suspended for the first two seconds for the first detector pair to eliminate the detection of the short-lived activities. The uncertainties in the stepping time, collection time, and delayed start counting time were all assumed to 1 millisecond. Given a source-to-detector distance of two millimeters and an active detector area of 100 mm^2, a

geometric detector efficiency for a point source of 33% was calculated. The uncertainty in the detector efficiency was assumed to be 2%. New fiberglass wheels with clean polypropylene foils were used every two to three hours to eliminate build up of long-lived activities. The PIPS detectors were calibrated using activity from a ^{228}Th source. The ^{228}Th source produces ^{212}Bi (E_α = 6.062(1) MeV) and ^{212}Po (E_α = 8.78437(7) MeV) activity. The decay data from the 12 detectors, 6 top and 6 bottom, were recorded by the CHAOS [Rat1991] data acquisition software in a list mode that included the detector number, channel, and time for each alpha particle detected. Detection with the six pairs of silicon detectors allowed construction of decay curves for half-life analysis. The CHAOS program generated histogram files used for α-spectrum analysis, α-α correlation analysis and decay-curve analysis.

The production cross sections for the MG experiment were calculated with Equation 3.1,

$$\sigma = \frac{R}{N_t I} \tag{3.1}$$

where R equals the rate that the species of interest is produced, N_t equals the number of target nuclei per unit area, and I equals the rate of the incoming beam particles. This equation was corrected for the MG experiment by accounting for the various decay and growth times (t_{trans}, t_{start}, t_{col}, and t_{count}), efficiencies (Eff_{gj} and Eff_{det}) and branching ratios (BR):

$$\sigma = \frac{N_{events}\lambda}{N_t I_a \left(e^{-\lambda t_{trans}}\right)\left(e^{-\lambda t_{start}}\right)\left(1-e^{-\lambda t_{col}}\right)\left(1-e^{-\lambda t_{count}}\right) Eff_{gj} Eff_{det} N_{expt} BR} \tag{3.2}$$

where N_{events} is the number of events detected in N_{expt} number of similar experiments. λ is the decay constant for the particular isotope of interest.

3.2 Catcher foil experiment

The $^{238}U + ^{18}O$ reaction was studied using the catcher foil technique. The target system used a 1.8 mg/cm^2 HAVAR vacuum window, 0.3 mg/cm^2 nitrogen as a cooling gas, 2.35 mg/cm^2 beryllium used as a target backing and a 0.540 mg/cm^2 ^{238}U target. Correcting for the range of the oxygen ions in uranium, the effective thickness of the uranium target was 0.318 ± 0.010 mg/cm^2.

The $^{nat}U_3O_8$ target was electrodeposited in a manner similar to the curium target used in the MG experiment in Section 3.1. Natural uranium (99.28% ^{238}U and 0.71% ^{235}U) as uranylnitrate hexahydrate ($UO_2(NO_3)_2 \cdot 6H_2O$) was dissolved in concentrated HCl. The uranium was purified by passing the HCl solution through a Dowex AG1-X8 (200-400 mesh) anion exchange column to sorb the uranium, allowing most impurities to pass through the column. The uranium was eluted from the column with 0.1M HCl and collected. A 10-µl aliquot of the purified uranium solution was evaporated on a platinum disk and counted using alpha spectroscopy to determine the amount of uranium activity per volume of solution. 2077 counts of ^{238}U ($t_{½} = (4.468 \pm 0.003) \times 10^9$ y) were detected in 10 minutes at a detector efficiency of 20% resulting in 17.3 disintegrations of ^{238}U per second or 1.44 mg of ^{238}U per 10 µl aliquot. A uranium isopropanol stock solution was made for use in electroplating [Sha2000]. A solution was prepared in which 20 µl of uranium isopropanol solution contained 28.8 µg of ^{238}U which equaled a thickness of about 0.100 mg/cm^2 with a target diameter of 6 mm. The 2.35 mg/cm^2 beryllium target backing was placed in the bottom of the electroplating cell. 20 µl of uranium isopropanol stock solution and 1 ml of isopropanol were placed in the cell. The UO_2^{2+} ions in the

solution were deposited on the beryllium cathode when a 600 V voltage was applied to the anode. The electrodeposition was continued for 45 minutes, the isopropanol solution was removed and the resulting uranium on the beryllium target backing were baked in an oven at 400-500°C for 30 minutes to convert the uranium to the oxide (U_3O_8) form. The thickness of each of the target layers was measured via alpha spectroscopy. The target was placed in a small vacuum chamber under a silicon surface barrier detector at 20 ± 2% efficiency. After counting the target overnight, the target thickness was determined from the measured ^{238}U α-activity. A total of seven layers were added to the target by repeating the above process until the target reached a thickness of 0.540 mg/cm^2. The effective target thickness was 0.318 ± 0.010 mg/cm^2.

The compound nucleus recoils from this reaction were collected in a 4.69 mg/cm^2 thick gold catcher foil located five millimeters behind the target in the target chamber. At this thickness, the gold catcher foil collected everything recoiling from the target. The uranium target was irradiated for about 8 hours at each of the energies. The gold foils were carefully removed from the target chamber and then underwent chemical separation. An illustration of the target chamber used in this experiment is shown in Figure 3.3.

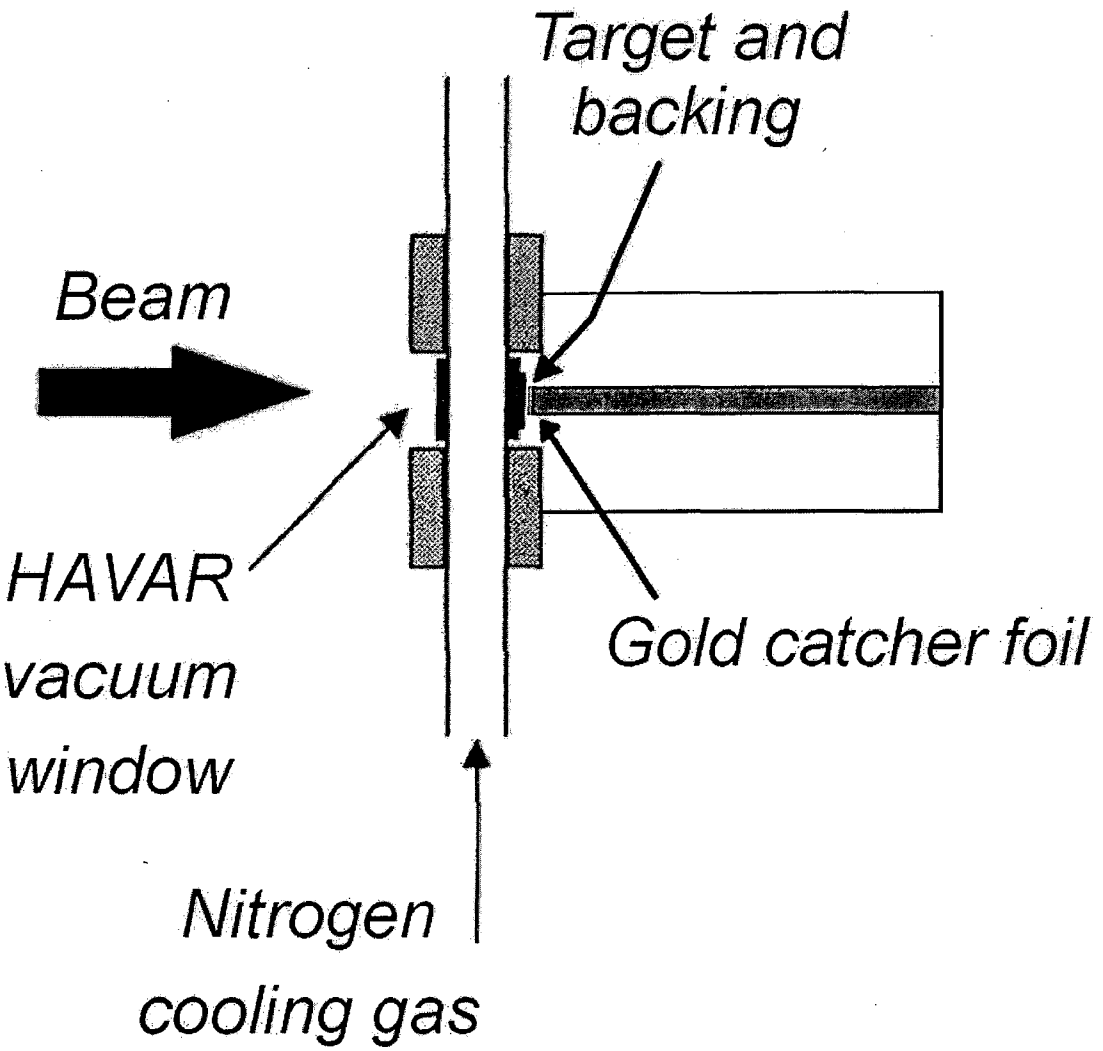

Figure 3.3: Target chamber used in catcher foil experiment. System for the transportation of activity-laden KCl aerosols from Figure 3.1 has been removed and replaced with a gold catcher foil placed directly behind the target.

The first step in the chemical separation was the separation of the trivalent actinides from the gold foil and other reaction products. A flow chart for the chemical separation procedure can be found in Figure 3.4. The highly active gold foil was placed in a test tube containing ^{241}Am (E_α = 5.48556(12) MeV, $t_{½}$ = 432.2 ± 0.7 y) tracer and dissolved in 3 drops of concentrated HCl and one drop of concentrated HNO_3. After dissolution, the solution of trivalent actinides was transferred to a Dowex AG1-X8 (200-400 mesh) anion exchange column. The gold and unwanted reaction products were sorbed on the column in concentrated HCl while the trivalent activities passed through. The trivalent actinide solution was dried, taken up in 0.5 M HCl, and transferred to a pre-treated Dowex 50W-X4 (200 mesh) cation exchange column. The trivalent fermium activity was separated from the other trivalent activities by elution with 0.5M ammonium alpha-hydroxyisobutyrate (α-HIB) solution at a pH of 3.38 [Cho1956a, Cho1956b, Smi1956]. The fermium fraction eluted from the column in the first 20 drops (4 free column volumes) ahead of the lighter trivalent actinides. Individual drops from the cation column were collected two at a time onto platinum disks. The appropriate platinum disks corresponding to the fermium fraction were transferred to one platinum disk, evaporated to dryness and flamed to fix the activity to the platinum. The ^{241}Am tracer was then eluted from the column using 0.5M α-HIB at a pH of 3.72, collected and counted using alpha spectroscopy to determine the chemical separation efficiency. The chemical efficiency was determined to be 90 ± 10% for the combined anion column and cation column separation. The chemical separation efficiency for the anion column chemistry alone was 95 ± 5%.

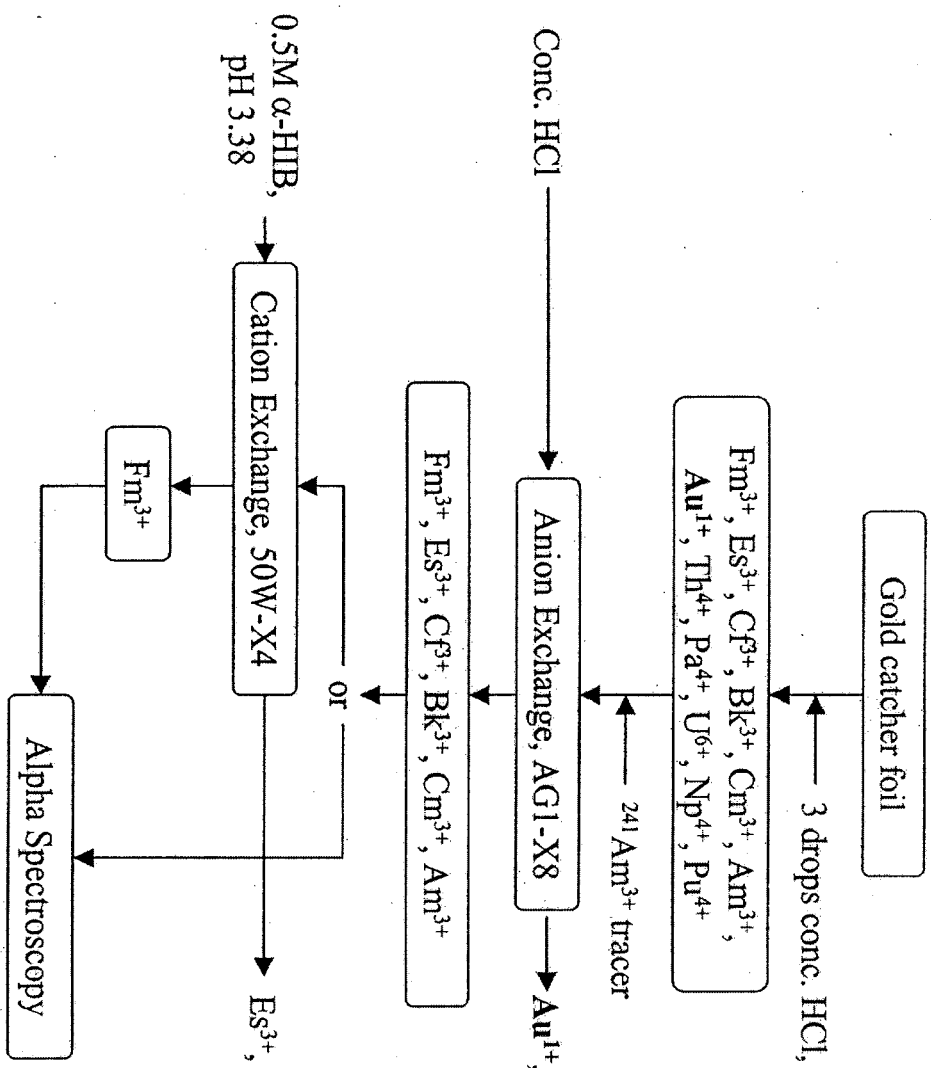

Figure 3.4: Flow chart for the chemical separation of ^{252}Fm from the gold catcher foil and other unwanted reaction products.

The platinum disk with the fermium fraction was then counted by alpha spectroscopy to observe the decay of fermium. The detector efficiency was 30 ± 2%. Alpha spectra were collected continuously every 3 hours for the first 3 days, then continuously every day for the next seven days. Finally, spectra were obtained continuously every 3 days for the final 20 days. These times correspond to the half-lives of ^{252}Fm ($t_{½}$ = 25.39 ± 0.05 h) and ^{253}Fm ($t_{½}$ = 3.00 ± 0.12 d), the 4n- and 3n- exit channel products. The detectors used in these experiments were calibrated using a three peak standard containing ^{241}Am, ^{244}Cm (E_{α} = 5.80482(5) MeV), and ^{252}Cf (E_{α} = 6.11824(4) MeV). Checks of the calibration were performed during the experiment using activity produced in the experiment. From these individual spectra, decay curves were obtained to determine the initial activity and half-life of ^{252}Fm. Histogram files were obtained for both experiments using a simple multi-channel analyzer computer card and software from the detector manufacturer. The anion column separation from the gold foil and other reaction products was done for all of the experiments studied. The cation column separation was only performed for the 94.9 MeV experiment.

Cross sections for the catcher foil experiment were measured using the initial activity (A_b) obtained from decay curve fitting and Equation 3.3 which was based on Equation 3.1 corrected for growth and delay times (t_{irr} and t_{start}), efficiencies (Eff_{sep} and Eff_{det}), and branching ratio (BR).

$$\sigma = \frac{A_b}{N_t I_a \left(1 - e^{-\lambda t_{irr}}\right)\left(e^{-\lambda t_{start}}\right) Eff_{sep} Eff_{det} BR} \tag{3.3}$$

3.3 Berkeley Gas-filled Separator experiments

Six experiments were performed with the BGS: $^{208}Pb(^{51}V,2n)^{257}Db$, $^{208}Pb(^{48}Ca,xn)^{256-x}No$, $^{209}Bi(^{50}Ti,xn)^{258-x}Db$, $^{208}Pb(^{50}Ti,xn)^{258-x}Rf$, $^{238}U(^{22}Ne,xn)^{260-x}No$, and $^{209}Bi(^{51}V,2n)^{258}Sg$. A general description of the BGS experimental procedure follows [Nin1999]. A schematic diagram of the BGS can be found in Figure 3.5.

Accelerated projectiles passed through a carbon vacuum window that separated the vacuum of the cyclotron and the beam line from the BGS. The beam then passed through a centimeter of helium before hitting the target backing and then the target. The targets in BGS experiments were located on a rotating wheel. Rotating targets were used in these reactions so beam currents larger than those used for normal stationary target reactions could be used. Increased beam currents lead to larger production rates for the activities of interest. By rotating the targets, the heat associated with an intense beam can be spread over several targets instead of one stationary target. Table 3.1 contains the carbon vacuum window thicknesses, carbon target backing thicknesses, target thicknesses, and He pressures in the BGS for the six experiments listed in the order they were performed.

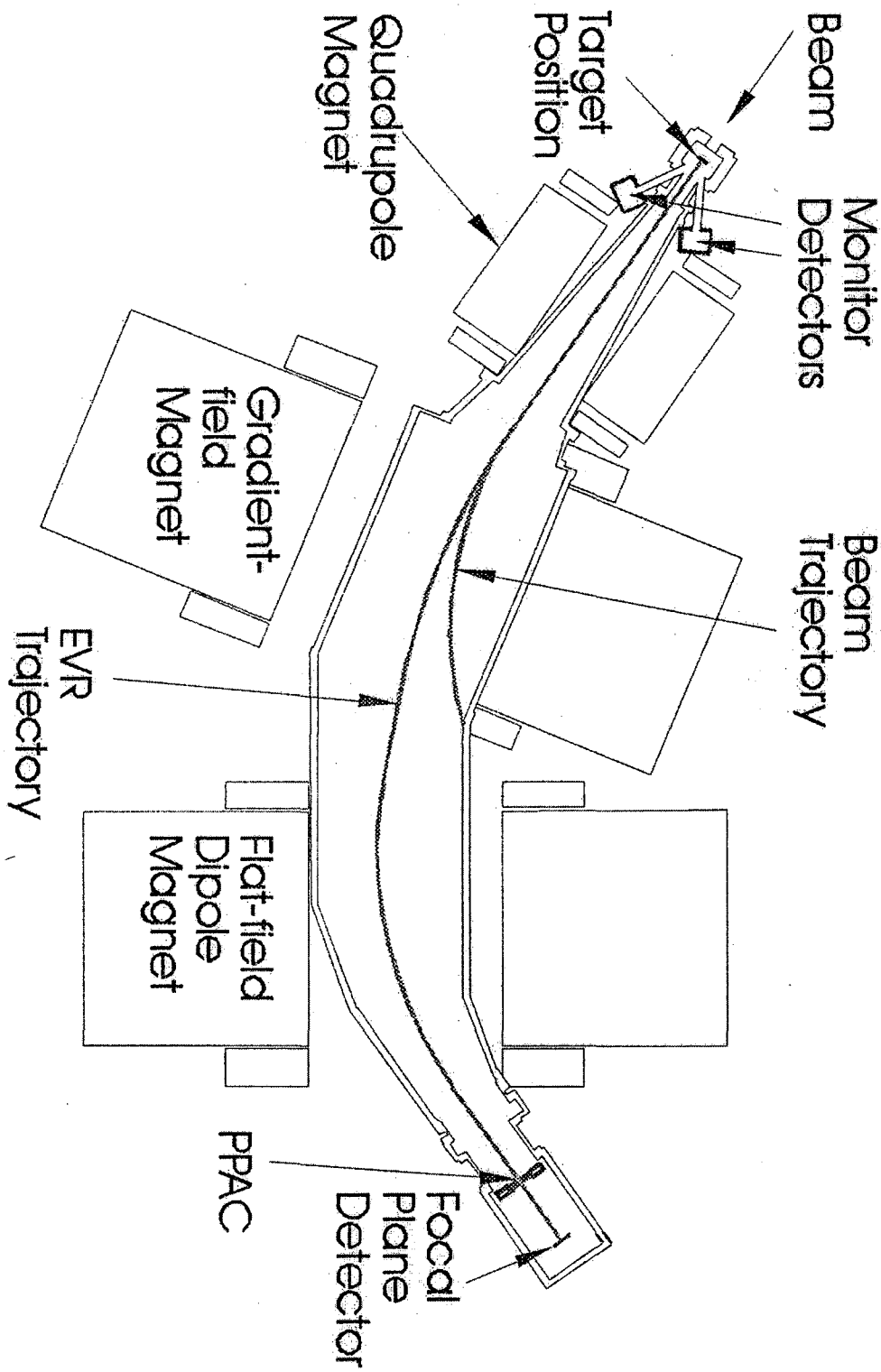

Figure 3.5: Schematic of the BGS showing the target chamber, quadrupole magnet, two dipole magnets and detection chamber. Evaporation residues travel a distance of 460 cm between the target and the PPAC detector.

Table 3.1: BGS reaction specifics. For each reaction, the thickness of the carbon window, carbon backing and target, as well as helium pressure in the BGS is listed. The uncertainty in the target thicknesses were assumed to be 10 $\mu g/cm^2$.

Reaction	Thickness ($\mu g/cm^2$) Carbon Window	Carbon Backing	Target	He Pressure (Torr)
$^{208}Pb(^{51}V,2n)^{257}Db$	50	35	500	1.000
$^{208}Pb(^{48}Ca,xn)^{256-x}No$	50	35	453	0.742
$^{209}Bi(^{50}Ti,1n)^{258}Db$	52	40	390	0.785
$^{208}Pb(^{50}Ti,xn)^{258-x}Rf$	50	35	460	1.000
$^{209}Bi(^{50}Ti,xn)^{259-x}Db$	46	29	400	1.000
$^{208}Pb(^{48}Ca,xn)^{256-x}No$	48	35	460	0.787
$^{238}U(^{22}Ne,xn)^{260-x}No$	46	46	160.5	0.501
$^{209}Bi(^{51}V,2n)^{258}Sg$	46	26	400	0.712

The ^{208}Pb, ^{209}Bi, and ^{238}U target wheels were produced either at the Gesellschaft für Schwerionenforschung (GSI) in Darmstadt, Germany or at the Thin Foil Lab at Lawrence Berkeley National Laboratory. Thin carbon target backings were created first and transferred to one of nine target frames. The target frames were banana shaped and measured 105 mm from end to end and 12 mm wide. ^{208}Pb, ^{209}Bi, or ^{238}U was then evaporated onto the carbon backing producing targets that were uniform in thickness throughout the target wheel.

Beam, transfer products, and compound nucleus evaporation residues (EVRs) from the associated projectile/target reactions traversed the helium gas-filled chamber between the magnets. Rutherford-scattered beam projectiles were used to monitor the amount of beam delivered to the target. Two small p-i-n diode detectors, located 292 ± 1 mm from the target, at an angle $\pm 27.0 \pm 0.1°$ from the beam axis, covered by a collimator with a radius of 0.52 ± 0.01 mm, were used to detect the Rutherford scattered beam (see Figure 3.6). The integrated spectra from these detectors was used with the known equations for Rutherford scattering (Equations 3.10 – 3.12) to determine the total beam dose. The scattered beam, transfer products, and the EVRs traveled 460 centimeters through a vertically focusing quadrupole magnet, a gradient field dipole magnet, and a flat field dipole magnet. The quadrupole magnet focused all of the beam, transfers, and EVRs into a rough horizontal plane. The gradient dipole magnet continued the horizontal focusing and began the separation of the beam, transfers and EVRs according to their average charge state and momentum. The flat field magnet then completed the separation.

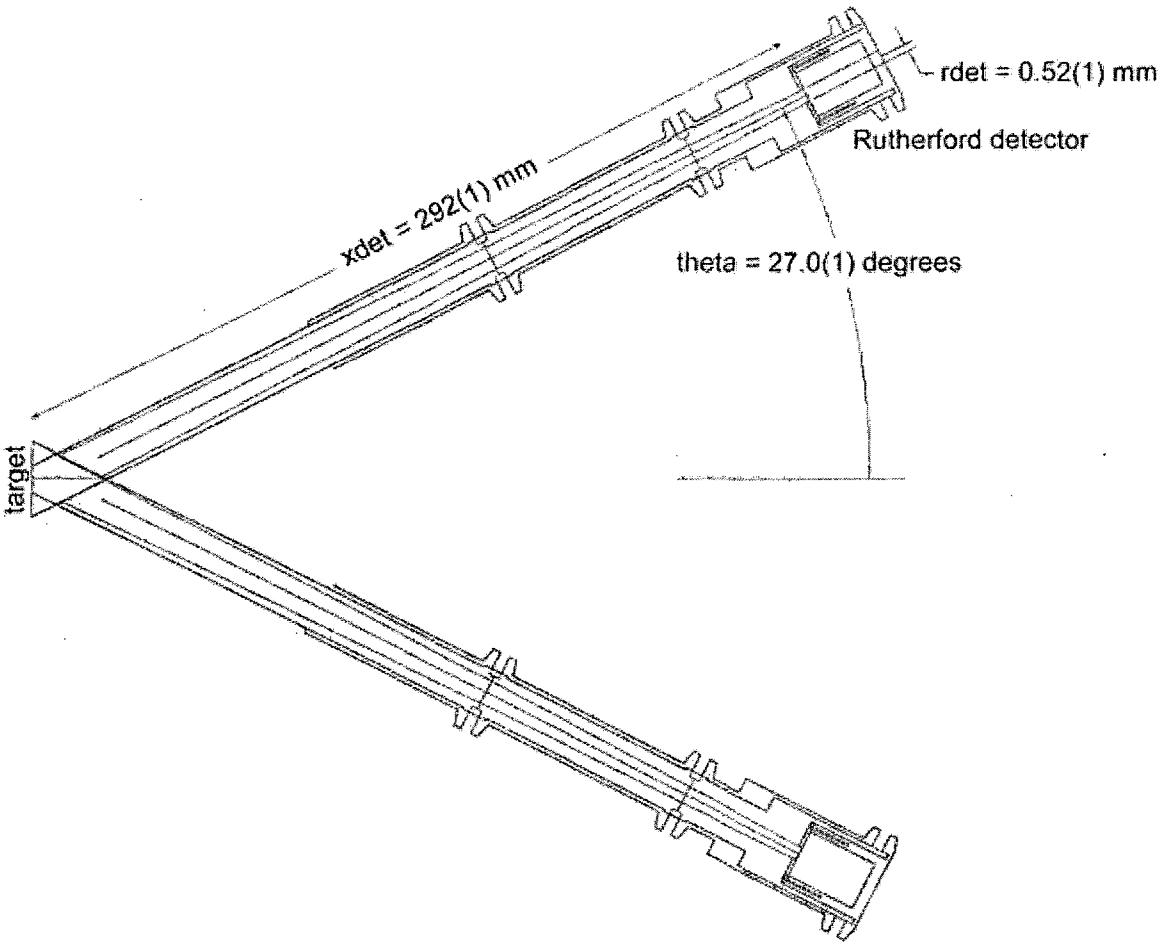

Figure 3.6: Drawing of the Rutherford detector setup showing the target and Rutherford detector positions, distance between the target and Rutherford detector (xdet), the angle between the Rutherford detectors and the beam axis (theta, θ), and the radius of the collimator that covers the Rutherford detectors (rdet). The uncertainties in the last digit of xdet, rdet and theta are listed in parenthesis.

Separation in a gas-filled magnetic separator is dependent on the magnetic field, the velocity and mass of the particle, and its average charge state. Charged particles in a magnetic field feel a force equal to the product of the particle's charge (q), the particle's velocity (v), the magnetic field (B) present, and the sine of the angle (θ) between the velocity and magnetic field vectors.

$$F_B = qvB\sin(\theta) \tag{3.4}$$

This force is equal to the centrifugal force felt by a particle moving in a circle,

$$F_c = \frac{mv^2}{r} \tag{3.5}$$

where m is the mass of the particle and r is the radius of the circle the particle is moving around. Setting these two equations equal to each other and solving for the magnetic rigidity, which is the product of the magnetic field and the radius of curvature for the particle in the magnetic field, gives Equation 3.6.

$$B\rho = \frac{mv}{q} \tag{3.6}$$

The average charge state of the particle moving through a dilute gas can be approximated using the following equation [Bet1972],

$$\overline{q} = Z\left\{1 - C_1 \exp\left[-C_2\left(\frac{v}{v_o}\right)Z^{-\frac{2}{3}}\right]\right\} \tag{3.7}$$

where Z is the atomic number of the particle and C_1 and C_2 are constants determined from fits to experimental data. In dilute helium gas [Ghi1988], C_1 and C_2 were

determined to be 1.04 and 0.91 respectively. The Bohr velocity (v_o) in Equation 3.7 is equal to,

$$v_o = \frac{e^2}{2\varepsilon h} \tag{3.8}$$

where e is the elementary charge constant, ε is the permittivity of vacuum and h is Planck's constant. The mass and velocity of Equation 3.6 can be found easily from the kinetics of the observed reaction. Therefore, the beam, transfer products and EVRs can be separated based on their differences in magnetic rigidity in the dilute helium gas.

After separation from the transfer products and beam, the EVRs continued to the detection chamber. The total transit time in the BGS between the target and detector is on the order of 1 μs. Once inside the detection chamber, they passed through a parallel plate avalanche counter (PPAC) before striking the focal plane silicon strip detector. The PPAC was used to provide a time of flight signal. This signal was used to discriminate between events that originated in the focal plane detector and those that originated from EVRs implanted in the detector. The 116-mm wide by 58-mm tall silicon strip detector, 300 μm thick PIPS detector was divided into 32 vertical strips that recorded energy, time and position, through resistive readout from both the top and bottom of each strip, for each event that hit the detector. The focal plane detector was located towards the back end of the detection chamber, centered between the top, bottom, left and right sides of the detection chamber. The focal plane alpha detection efficiency was 50 ± 2% and spontaneous fission detection efficiency was 100 ± 2%.

Either a microcomputer called the CVC (CAMAC to VSB Computer) running in a CAMAC (Computer Aided Measurement And Control) crate or the microcomputer RIO2 running in a VME (VERSA Module Eurocard) crate along with the data acquisition software called MBS [Ess2000] were used to collect the data into events and then send it either for storage on tape or for online analysis. The CVC was used for several of the experiments and the RIO2 was used for the rest of the experiments. The RIO2 offered faster data collection and transfer rates than the CVC. A Digital Equipment VAX workstation running the VMS operating system and the data analysis software GOOSY [Ess1987] was used to perform online and offline analysis of the data. For each event over 250 pieces of data or words (see Table 3.2) were recorded. GOOSY analysis routines were written in the PL1 programming language to analyze the data event by event. GOOSY analysis codes were also used to analyze the data from tape after the experiment was completed. The analysis routines were written to produce EVR, alpha, fission, time, position, Rutherford, and PPAC detector spectra as well as EVR-alpha, EVR-fission, and alpha-alpha correlation lists. From these analysis programs, detailed information could be gathered about a particular isotope's decay energies, half-life, activity and eventually production cross section. An example of a GOOSY analysis code can be found in Appendix A.

Table 3.2: Event word list for the $^{209}Bi(^{51}V,2n)^{258}Sg$ experiment.

Word Parameter	Description
1-2	microsecond scaler chopper
3-4	microsecond scaler since start acquisition
5-6	millisecond scaler since start acquisition
7-8	second scaler since start acquisition
9-10	minute scaler since start acquisition
11-12	microsecond scaler since @start
13-14	millisecond scaler since @start
15-16	second scaler since @start
17-18	minute scaler since @start
19-20	number of beam pulses
21-22	number of beam dumps
23-24	scaled number of beam dumps
25-26	Rutherford east scaler
27-28	Rutherford west scaler
29	user bit 0,1
30	error location
31	error type
32-63	energy low focal plane detector strips 1-32
64-95	energy high focal plane detector strips 1-32
96-127	position low top focal plane detector strips 1-32
128-159	position high top focal plane detector strips 1-32
160-191	position low bottom focal plane detector strips 1-32
192-223	position high bottom focal plane detector strips 1-32
224-239	energy low backward detector strips 1-16
240-255	energy high backward detector strips 1-16
256-259	individual PPAC signals
260	PPAC time to amplitude converter signal
261-267	- empty -
268	energy low sodium iodide detector
269	energy high sodium iodide detector
270	energy Rutherford east detector
271	energy Rutherford west detector
272-279	energy low punch through detector strips 1-8

Production cross sections for the BGS reactions were calculated using a different method than what has been described in Sections 3.1 and 3.2. The BGS technique for calculating the production cross section is based on a ratio of the number of events observed (N_{events}) to the number of Rutherford events ($N_{rutherfords}$) observed, multiplied by the Rutherford scattering cross section ($\sigma_{Rutherford}$):

$$\sigma = \frac{N_{events}}{N_{Rutherfords}} \sigma_{Rutherford} \tag{3.9}$$

The number of events observed and the number of Rutherford-scattered events observed can be found in the experimental data. $\sigma_{Rutherford}$ involves the calculation of the Rutherford scattering differential cross section and then multiplying by the solid angle subtended by the Rutherford detector. The lab frame Rutherford scattering differential cross section equation is found in Equation 3.10 [Seg1977],

$$\frac{\partial\sigma}{\partial\omega_{lab}} = \left(\frac{e^2 Z_p Z_t}{2Ebeam_{lab}}\right)^2 \sin^{-4}(\theta_{lab}) \frac{\left[\cos(\theta_{lab}) + \left[1 - \left(\frac{A_p}{A_t}\right)^2 \sin^2(\theta_{lab})\right]^{\frac{1}{2}}\right]^2}{\left[1 - \left(\frac{A_p}{A_t}\right)^2 \sin^2(\theta_{lab})\right]^{\frac{1}{2}}} \tag{3.10}$$

where Z_p and Z_t are the atomic numbers of the projectile and target and A_p and A_t are the atomic mass numbers of the projectile and target. The angle and beam energy are in the lab frame and are determined in the experiment. The solid angle can be determined from the following equation,

$$\partial\omega_{lab} = \pi\left(\frac{r\,\mathrm{det}}{x\,\mathrm{det}}\right)^2 \tag{3.11}$$

where rdet is the radius of the detector and xdet is the distance from the detector face to the target (see Figure 3.6). The product of Equation 3.10 and 3.11 gives rise to $\sigma_{Rutherford}$.

$$\sigma_{Rutherford} = \frac{\partial\sigma}{\partial\omega_{lab}}\,\partial\omega_{lab} \tag{3.12}$$

Add in efficiencies (Eff_{bgs}, Eff_{det} and Eff_{det2}) and the branching ratio (BR) to arrive at the final result for the BGS cross section calculation method.

$$\sigma = \frac{N_{events}\sigma_{Rutherford}}{N_{rutherfords}Eff_{bgs}Eff_{\mathrm{det}}Eff_{\mathrm{det}\,2}BR} \tag{3.13}$$

4 Experimental results

Table 4.1 contains the half-lives, branching ratios and primary α-decay energies for the isotopes studied in our experiments [Chu1999]. All of the beam energies used in this section are measured in the lab frame. Equation 1.26 with a radius parameter (r_e) of 1.4 fm was used to calculate the Coulomb barriers for the reactions discussed. The Coulomb barriers are all listed in the lab frame. Excitation energies are calculated in the center of mass system. Uncertainties in the center of target beam energies were assumed to be 2 MeV. The uncertainties in the number of counts was determined from the results of MLDS fits, the square root of the number of counts (number of counts > 20), or from the statistics of [Sch1984] (number of counts ≤ 20) assuming a 68% confidence interval. Unless otherwise noted, the errors in the experimental cross sections were a combination of statistical errors in the initial activity or number of counts and the systematic errors of the experiment. In the BGS experiments, the uncertainty in the time of each experiment was assumed to be 5 seconds, and the uncertainty in the number of Rutherford counts was assumed to be the square root in the number of Rutherford counts.

Table 4.1: Summary of the half-lives, branching ratios and primary α-decay energies for the isotopes studied in our experiments [Chu1999]. Approximate uncertainties (~) in the branching ratios were assumed to be 5%.

Isotope	Half-life	Branching Ratios	E_α (MeV)
^{217}At	32.3 ± 0.4 ms	α 99.988 ± 0.004%	7.0699(5)
^{213}Rn	25.0 ± 0.2 ms	α 100%	8.088(8)
^{213}Fr	34.6 ± 0.3 s	α 99.45 ± 0.03%	6.7750(17)
^{214}Ac	8.2 ± 0.2 s	α 89 ± 3%, εc 11 ± 3%	7.214(5)
^{252}Fm	25.39 ± 0.05 h	α 99.9977 ± 0.0002%	7.039(2)
^{252}No	2.30 ± 0.22 s	α 73.1 ± 1.9%, SF 26.9 ± 1.9%	8.415(6)
^{253}No	1.7 ± 0.3 min	α ~80%, εc ~20%	8.010(20)
^{254}No	55 ± 3 s	α 90 ± 4%	8.093(14)
^{255}No	3.1 ± 0.2 min	α 61.4 ± 2.5%, εc 38.6 ± 2.5%	8.121(6)
^{256}No	2.91 ± 0.05 s	α 99.5 ± 0.1%	8.430(20)
^{257}No	25 ± 2 s	α ~100%	8.220(20)
^{253}Lr	$1.3\ ^{+0.6}_{-0.3}$ s	α 98 ± 2%	8.800(20)
^{259}Lr	$6.3\ ^{+0.5}_{-0.4}$ s	α 77 ± 2%, SF 23 ± 2%	8.450(20)
^{260}Lr	180 ± 30 s	α 75 ± 10%, εc 25 ± 10%	8.030(20)
^{256}Rf	6.7 ± 0.2 ms	SF $98\ ^{+2}_{-7}$%	
^{257}Rf	4.7 ± 0.3 s	α 79.6 ± 2.0%, εc 18 ± 2%	8.774(8), 9.013(8)
^{258}Rf	12 ± 2 ms	SF ~87%	
^{257}Db	$1.3\ ^{+0.5}_{-0.3}$ s	α 82 ± 11%, SF 17 ± 11%	8.970(20)
^{258}Db	$4.4\ ^{+0.9}_{-0.6}$ s	α $67\ ^{+5}_{-9}$%, εc $33\ ^{+9}_{-5}$%	9.172(15)
^{258}Sg	~2.9 ms	SF ~100%	

4.1 $^{248}Cm + ^{15}N$

^{260}Lr (E_α = 8.030(20) MeV, $t_{½}$ = 180 ± 30 s) and ^{259}Lr (E_α = 8.450(20) MeV, $t_{½} = 6.3\ ^{+0.5}_{-0.4}$ s) were produced via the $^{248}Cm(^{15}N,xn)^{263-x}Lr$ reaction, where x = 3 or 4. The MG system described in Section 3.1 was used to produce, transport, collect, and detect the ^{260}Lr and ^{259}Lr activity. $^{15}N^{4+}$ out of the cyclotron energies of 92.0 and 94.5 MeV corresponded to energies of 75.9 and 78.8 MeV in the center of the 0.873 mg/cm^2 curium target, which corresponded to excitation energies of 35.2 and 37.9 MeV, respectively. The Coulomb barrier for this reaction was calculated to be 83.8 MeV. Fiberglass wheels with clean polypropylene foils were used for each of the energies and isotopes of interest.

4.1.1 ^{260}Lr

Beam doses of $(1.210 \pm 0.004) \times 10^{17}$ (75.9 MeV) and $(1.715 \pm 0.005) \times 10^{17}$ (78.8 MeV) were accumulated for the two experiments, corresponding to average beam currents of 2.688 ± 0.010 and 2.568 ± 0.008 eμA on target, respectively. There were a total of 240 separate collections at 75.9 MeV and a total of 354 separate collections at 78.8 MeV.

Alpha decays detected by five of the six top detectors for the two experimental energies were summed to produce the spectra in Figures 4.1 and 4.2. The first top detector was not included in these summed α-spectra. Only alpha decays with energies greater than 5.7 MeV were included in these summed spectra to make sure all of the peaks were visible on the same scale. Table 4.2 lists the prominent activities seen in Figures 4.1 and 4.2 with their decay energies, half-lives and possible production routes.

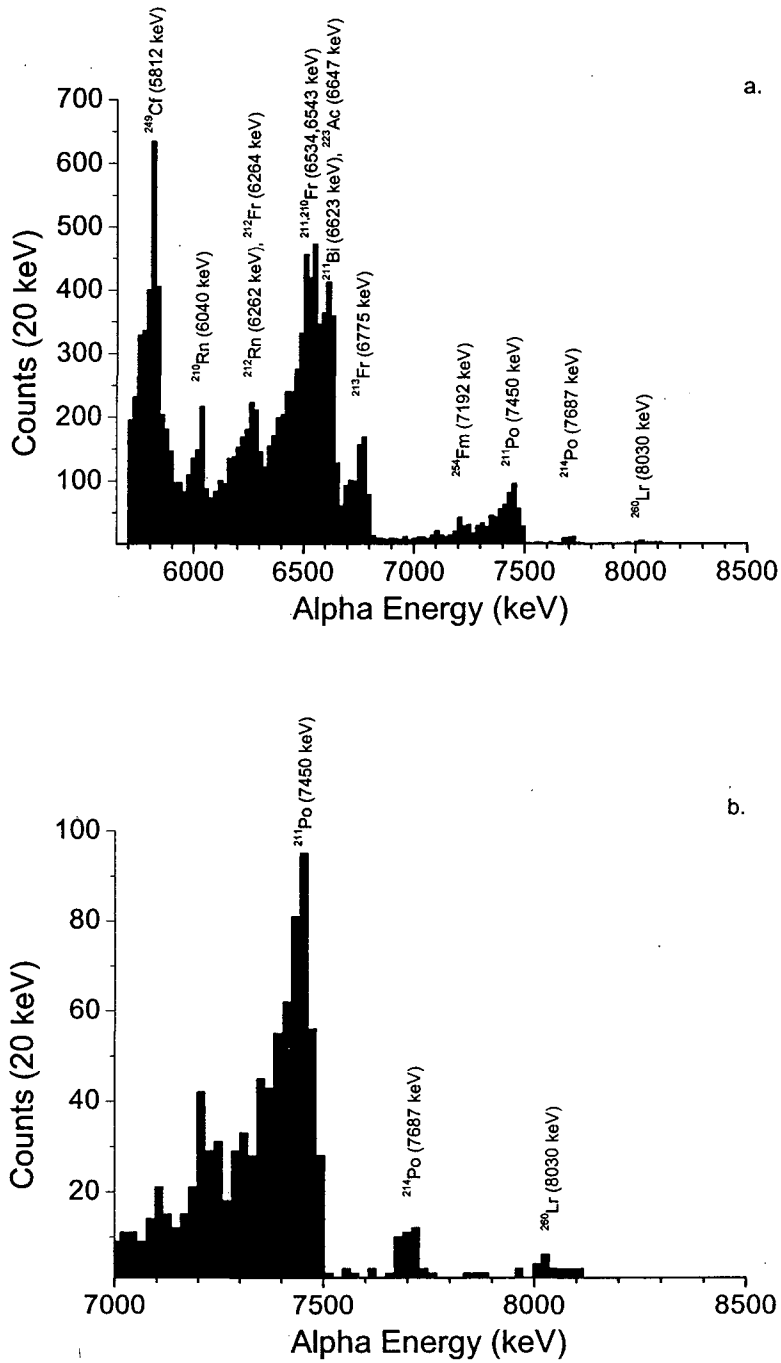

Figure 4.1: Sum spectrum of detectors two top through six top of the MG for the 75.9-MeV $^{248}Cm + ^{15}N$ experiment (a.). Expanded region between 7000 – 8500 keV shown in (b.)

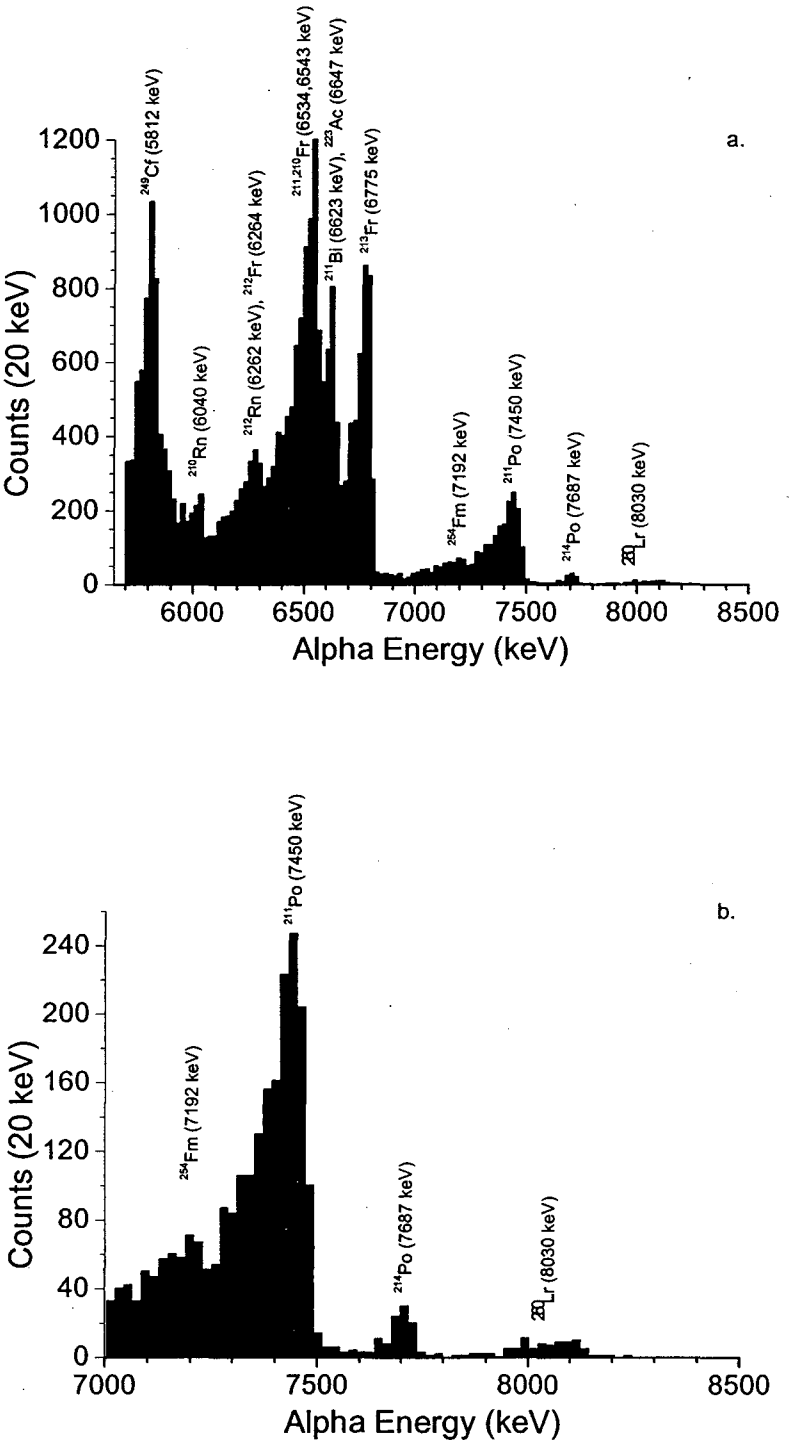

Figure 4.2: Sum spectrum of detectors two top through six top of the MG for the 78.8-MeV $^{248}Cm + ^{15}N$ experiment (a.). Expanded region between 7000 – 8500 keV shown in (b.)

Table 4.2: List of alpha-decay peak assignments for the sum spectra in Figures 4.1 and 4.2. Alpha decay energies and half-lives from [Chu1999].

Isotope	E_α (MeV)	Half-life	Possible Production Route
^{249}Cf	5.8133(10)	351 ± 2 y	present naturally, contamination
^{210}Rn	6.040(2)	2.4 ± 0.1 h	electron capture decay of ^{210}Fr
^{212}Rn	6.262(3)	23.9 ± 1.2 min	electron capture decay of ^{212}Fr
^{212}Fr	6.2619(21)	20.0 ± 0.6 min	^{206}Pb(^{15}N,α5n), ^{207}Pb(^{15}N,α6n), ^{208}Pb(^{15}N,α7n)
^{211}Fr	6.534(5)	3.10 ± 0.02 min	^{204}Pb(^{15}N,α4n), ^{206}Pb(^{15}N,α6n)
^{210}Fr	6.543(5)	3.18 ± 0.06 min	^{204}Pb(^{15}N,α5n), ^{206}Pb(^{15}N,α7n)
^{211}Bi	6.6229(6)	2.14 ± 0.02 min	^{208}Pb(^{15}N,3α), ^{223}Ac → α-decay
^{223}Ac	6.6467(10)	2.10 ± 0.05 min	^{208}Pb(^{15}N,γ)
^{213}Fr	6.7750(17)	34.6 ± 0.3 s	^{208}Pb(^{15}N,α6n), ^{206}Pb(^{15}N,4n)^{217}Ac → ^{213}Fr + α
^{254}Fm	7.192(2)	3.240 ± 0.002 h	^{248}Cm(^{15}N,α5n)^{254}Md → ^{254}Fm, or transfer reaction
^{211}Po	7.4503(5)	0.516 ± 0.003 s	^{208}Pb(α,n), ^{207}Pb(α,γ)
^{214}Po	7.68682(7)	164.3 ± 2.0 μs	present naturally
^{260}Lr	8.030(20)	180 ± 30 s	^{248}Cm(^{15}N,3n)
^{213}Rn	8.090(8)	25.0 ± 0.2 ms	electron capture decay of ^{213}Fr

Most of the isotopes seen in Table 4.2 are the result of compound nucleus reactions between the nitrogen projectiles and trace amounts of lead impurities in the curium target. Although the amounts of lead in the curium target might be small, the cross sections for these reactions are more than an order of magnitude higher than for the production of ^{260}Lr leading to similar production rates.

The search for ^{260}Lr began by examining the individual singles alpha spectra for the two different energy experiments. In particular, the search was aimed at finding a 180-second activity located around 8.0 MeV. A region of the singles spectrum for each of the two experiments was established around 8.030 MeV and integrated in each of the twelve detectors used in the experiment, six on top and six on bottom. The region of interest chosen for these experiments was 7.95 – 8.15 MeV. With an experimental resolution of 45 keV in the top detectors, this region of interest was sufficient to include the decay of ^{260}Lr. Each top/bottom partner integrated region of interest was summed as they both correspond to the same time window. The decay curve values for the two energy experiments can be found in Table 4.3.

Table 4.3: Decay tables for the two reactions showing the number of counts in the region of interest given for each of the two experiments for each set of detectors. The range of time that the samples were between a given set of detectors is noted next to each detector pair.

	Experiment (Region of Interest)	
	75.9 MeV ^{15}N (7.95 - 8.15 MeV)	78.8 MeV ^{15}N (7.95 - 8.15 MeV)
Detector Pair (time, min)	Number of Counts in Region	
1T + 1B (0-2)	89	466
2T + 2B (2-4)	21	77
3T + 3B (4-6)	4	15
4T + 4B (6-8)	6	8
5T + 5B (8-10)	5	6
6T + 6B (10-12)	1	4

This region of interest was extended to 8.15 MeV to include alpha decays from ^{213}Rn (E_α = 8.088(8) MeV, $t_{½}$ = 25.0 ± 0.2 ms), the electron capture decay daughter of ^{213}Fr ($t_{½}$ = 34.6 ± 0.3 s). During the experiment, a secular equilibrium is reached between ^{213}Fr and ^{213}Rn. As a result of the secular equilibrium, the ^{213}Rn activity takes on the half-life of ^{213}Fr. Knowing that this region of interest contained the two activities, the decay curves were then analyzed with a two-component fit using the MLDS method [Gre1991]. The MLDS method is a multicomponent decay curve analysis technique that uses the maximum likelihood technique for decay curves made up of time binned events. Believing the ^{260}Lr was indeed present, the half-life of ^{260}Lr was fixed at 180 seconds in the MLDS fit. The initial activity of the ^{260}Lr was allowed to vary. The half-life and activity of the shorter second component were both allowed to vary. The MLDS program found the best half-life and initial activity for each of the components using the input information given. By integrating the resulting best fit decay curve for the MLDS results, the number of counts corresponding to each component was determined. The results of the MLDS fits to the decay curves in Table 4.3 can be seen in Table 4.4.

Table 4.4: Results of MLDS fits [Gre1991] to the decay curves found in Table 4.3. The errors given are also a result of the MLDS program. The half-life of ^{260}Lr was fixed (^{260}Lr $t_{1/2}$ = 180 ± 30 s, ^{213}Rn,^{213}Fr $t_{1/2}$ = 34.6 ± 0.3 s).

Beam Energy	Isotope	Half-life	Initial Activity	Number of Counts
75.9 MeV	^{260}Lr	180 s	$11\ ^{+3}_{-2}$ min^{-1}	$46\ ^{+11}_{-10}$
	^{213}Rn	$37\ ^{+6}_{-5}$ s	$89\ ^{+14}_{-13}$ min^{-1}	$80\ ^{+13}_{-12}$
78.8 MeV	^{260}Lr	180 s	19 ± 4 min^{-1}	$78\ ^{+18}_{-16}$
	^{213}Rn	$39.8\ ^{+2.0}_{-1.9}$ s	520 ± 30 min^{-1}	500 ± 30

Using the number of counts for ^{260}Lr obtained from the MLDS fit, a 180 ± 30 s half-life, a 66 ± 2% α-particle detection efficiency, and an alpha-decay branching ratio of 75 ± 10%, the production cross section could be calculated using Equation 3.2. ^{260}Lr production cross sections of 2.3 ± 1.2 nb and 2.8 ± 1.4 nb were obtained for the ^{248}Cm(^{15}N,3n)^{260}Lr reaction at excitation energies of 35.2 MeV and 37.9 MeV, respectively. A previous experiment [Esk1971] that produced ^{260}Lr in the ^{248}Cm(^{15}N,3n) reaction reported a production cross section for ^{260}Lr of about 2 nb at an excitation energy of 37.2 MeV. Their cross section value is consistent with our experimental cross sections. An excitation function for the ^{248}Cm(^{15}N,3n) reaction was calculated using HIVAP with the parameters given in Section 2.2. Our experimental results, the results of Eskola et al., and the results of the HIVAP calculation using the parameters of Reisdorf and Schädel are plotted in Figure 4.3.

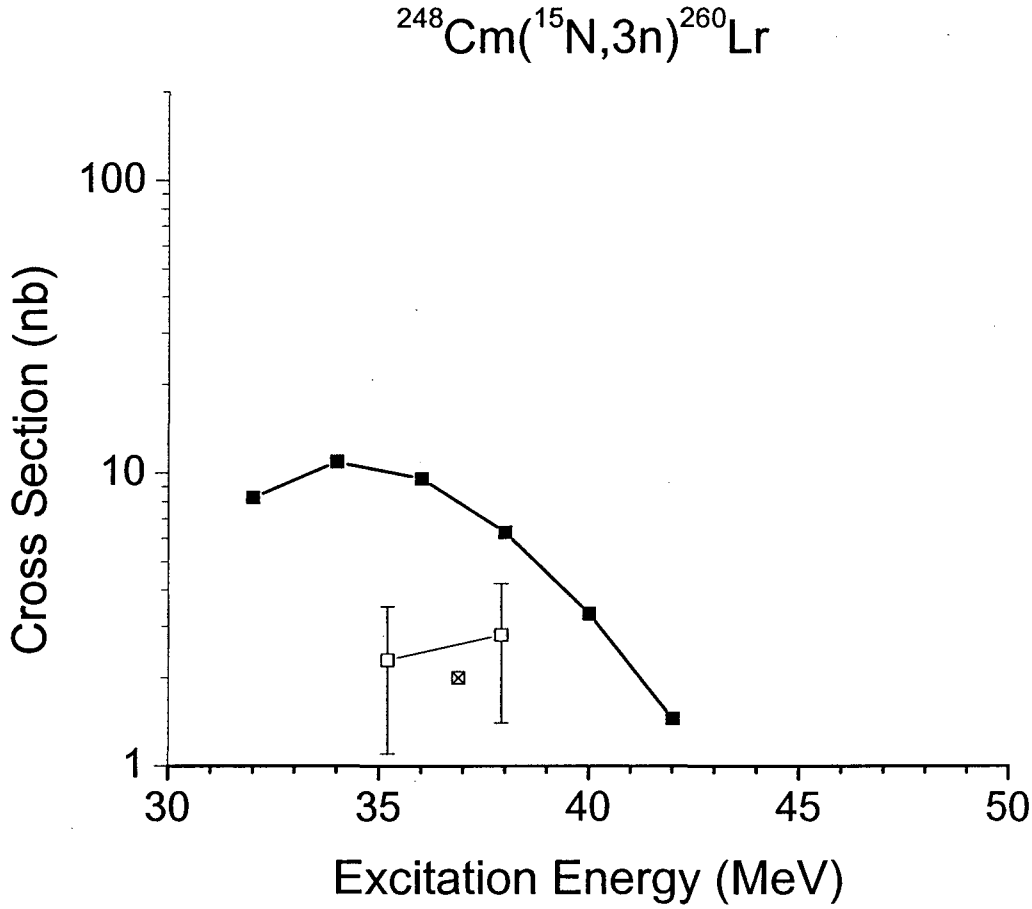

Figure 4.3: Comparison of experimental results and calculated values for the $^{248}Cm(^{15}N,3n)$ reaction. Solid symbols (■) represent the HIVAP code using the Reisdorf and Schädel parameters, open symbols (□) represent the experimental results of this thesis, and the open symbols with an (⊠) through them represent previous experimental results [Esk1971].

4.1.2 ^{259}Lr

Over the course of one hour, a total of 915 separate collections were performed in the 75.9 MeV experiment, and over the course of several hours a total of 4508 separate collections were performed in the 78.8 MeV experiment. The experimental collection time and stepping time for both experimental energy experiments were altered to correspond to the shorter half-life of ^{259}Lr compared to ^{260}Lr. A stepping time of four seconds was used, corresponding to a total time under the detectors of 24 seconds or 4 half-lives of ^{259}Lr. As with the ^{260}Lr experiment, there was a two second dead time window for the collection of data under the first detector. The experiment was run for a total of approximately 1 hour at 75.9 MeV and approximately 5 hours at 78.8 MeV, at an average beam current of 2.80 ± 0.03 eμA and 2.506 ± 0.012 eμA which corresponded to a beam doses of $(0.1594 \pm 0.0016) \times 10^{17}$ and $(0.706 \pm 0.003) \times 10^{17}$, respectively.

The analysis of this experiment was a little more straight forward than the analysis for the ^{260}Lr experiment. Very little activity interfered with the ^{259}Lr activity at 8.450 MeV. The first top and first bottom detector were ignored in response to the large amounts of short-lived activities present in those spectra. Because of its better resolution, the alpha spectrum from the second top detector was integrated around 8.45 MeV and the total number of counts obtained in that integration was used to calculate the production cross section. Because only the alpha-decay recorded from one detector was used, the detector efficiency was only $33 \pm 2\%$. As only the second top detector was used, the time between the end of collection and the beginning of detection and the total collection time was just 4 seconds. The transport time was still 1.0 ± 0.3 s and the gas-jet and deposition efficiency was $50 \pm 20\%$.

The production cross sections at the two energies were calculated assuming an alpha-decay branching ratio of 77 ± 2% and a half-life for ^{259}Lr of 6.3 $^{+0.5}_{-0.4}$ seconds. Only 8 events were detected for the 75.9 MeV experiment and a total of 122 events were detected for the 78.8 MeV experiment, which leads to production cross sections of 27 $^{+17}_{-14}$ nb and 90 ± 40 nb at excitation energies of 35.2 MeV and 37.9 MeV, respectively. This experiment was also previously measured by Eskola, et al. [Esk1971] and compared favorably with the experimental results obtained in this thesis. The experimental point at 37.9 MeV is higher than what might be expected from the Eskola results, but no cross sections were measured around that energy by Eskola. The experimental cross sections do match fairly well with the HIVAP predictions using the Reisdorf and Schädel parameters. The experimental results for ^{259}Lr, the experimental results of Eskola, et al., and the results of the HIVAP code using the Reisdorf and Schädel parameters are shown in Figure 4.4.

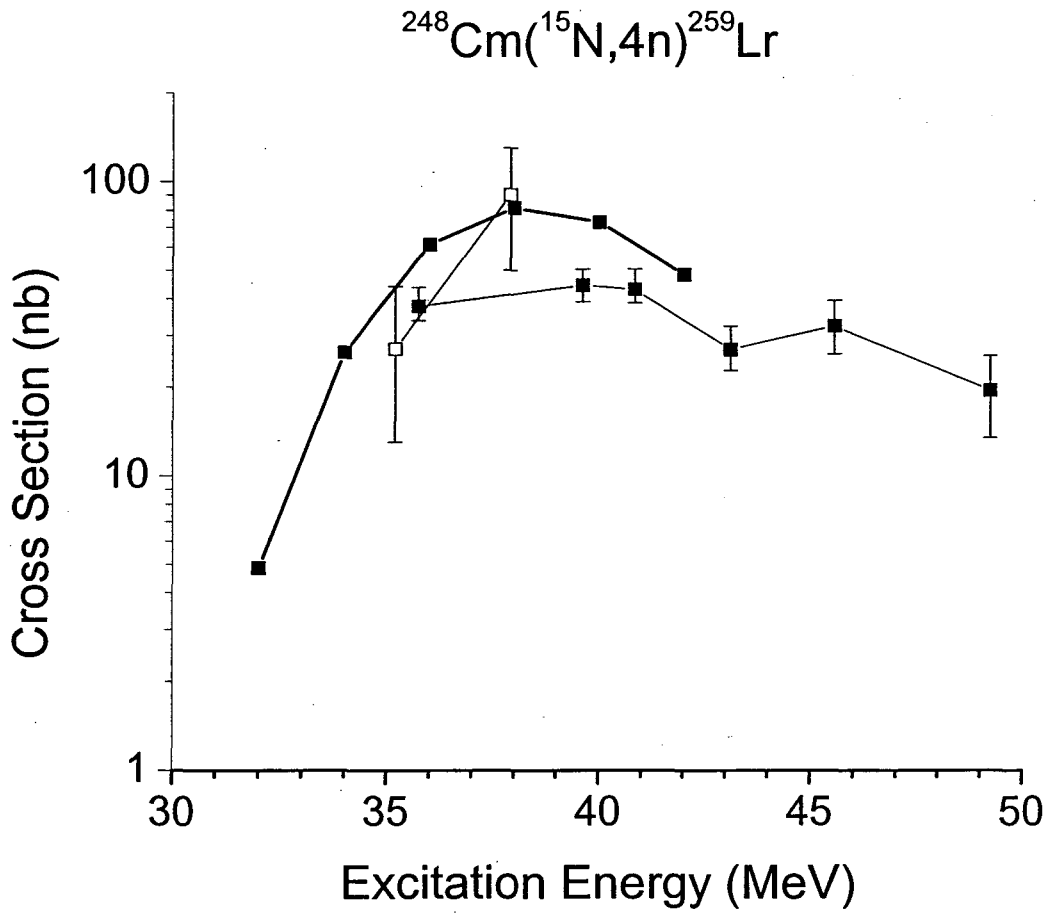

Figure 4.4: Comparison of experimental results and calculated values for the $^{248}Cm(^{15}N,4n)$ reaction. Solid symbols (■) represent the HIVAP code using the Reisdorf and Schädel parameters, open symbols (□) represent the experimental results of this thesis, and the open symbols with an (⊠) through them represent previous experimental results [Esk1971].

4.2 $^{238}U + {}^{18}O \rightarrow {}^{252}Fm + 4n$

^{252}Fm was produced in the $^{238}U(^{18}O,4n)$ reaction at three different energies of $^{18}O^{5+}$. The reactions specifics for the $^{238}U(^{18}O,4n)^{252}Fm$ experiment are located in Table 4.5. The Coulomb barrier for this reaction was 92.3 MeV. After irradiation, the gold foils were then taken and processed chemically to determine the amount of ^{252}Fm produced.

All of the gold foils were processed chemically according to the procedure described in Section 3.2, separating the ^{252}Fm from the gold foil and unwanted non-trivalent species. For the 82.4 MeV experiment and the 99.3 MeV experiment, the fermium fraction was then counted without further processing. The chemical efficiency for these single chemistry experiments was 95 ± 5%. The total time between the end of the irradiations and the beginning of counting for these two experiments was 168 ± 5 minutes and 196 ± 5 minutes respectively. For the 94.9 MeV experiment, the fermium fraction was then processed to separate it from the rest of the trivalent species present. This activity was then counted. The chemical separation efficiency for this experiment was 90 ± 10%. The total time between the end of the irradiation and the beginning of counting for the 94.9 MeV experiment was 525 ± 5 minutes. Background spectra for the three detectors used were obtained over a 21 hour period. The detectors for the 82.4 MeV experiment and 99.3 MeV experiment showed no background counts from 6.3 MeV to 10.0 MeV. The detector used for the 94.9 MeV experiment had a few randomly scattered single events between 6.3 MeV and 10.0 MeV. The detectors used had an energy resolution of 85 ± 15 keV. Figures 4.5, 4.6 and 4.7 are cumulative alpha

decay spectra obtained for the three experiments. Table 4.6 lists the isotopes present, their alpha decay energies, and their half-lives. The alpha spectra for the single chemistry experiments show the presence of additional activity resulting from transfer reactions on the uranium target and lead impurities in the target.

Table 4.5: Reaction specifics for the $^{238}U(^{18}O,4n)^{252}Fm$ experiment. CYC denotes cyclotron energies, COT denotes center of target energies, and E^* denotes excitation energies.

E_{CYC} (MeV)	E_{COT} (MeV)	E^* (MeV)	Current (eμA)	Dose ($\times 10^{16}$)	Time (s)
98.3	82.4	37.7	1.663 ± 0.008	6.00 ± 0.03	28900
109.5	94.9	49.3	1.804 ± 0.008	5.90 ± 0.03	26205
113.5	99.3	53.4	2.397 ± 0.009	9.19 ± 0.03	30700

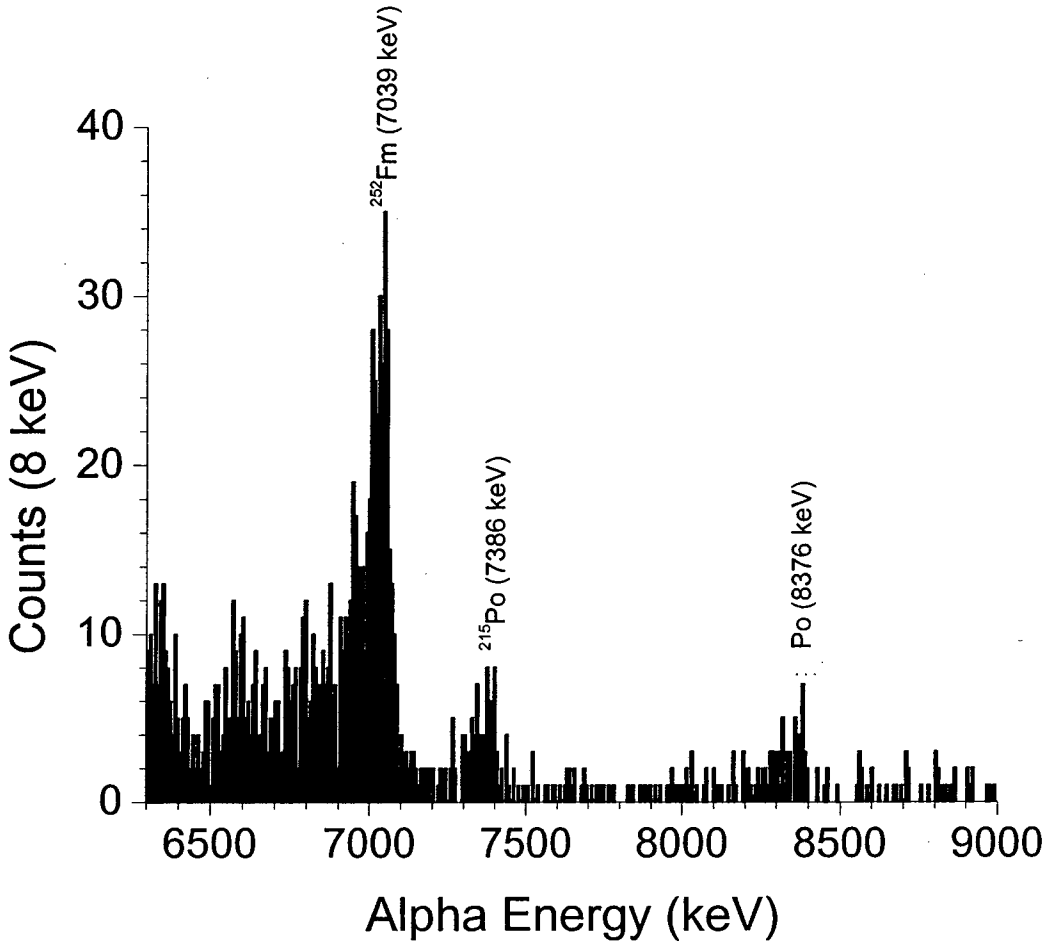

Figure 4.5: Summed alpha spectrum for the 82.4-MeV ^{238}U + ^{18}O experiment.

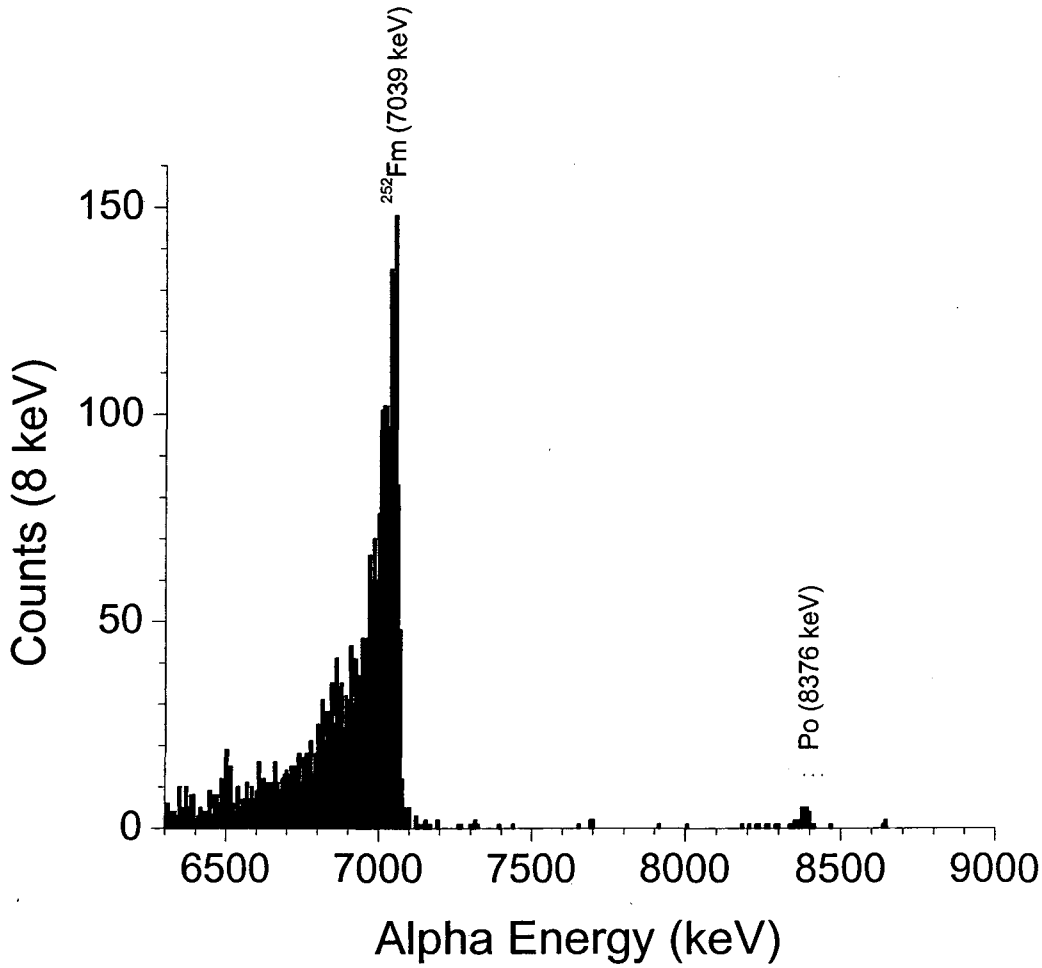

Figure 4.6: Summed alpha spectrum for the 94.9-MeV $^{238}U + ^{18}O$ experiment. Very little activity is present above 7.1 MeV as a result of the α-HIB cation chemistry that was used to separate the fermium from the rest of the trivalent activities and impurities present.

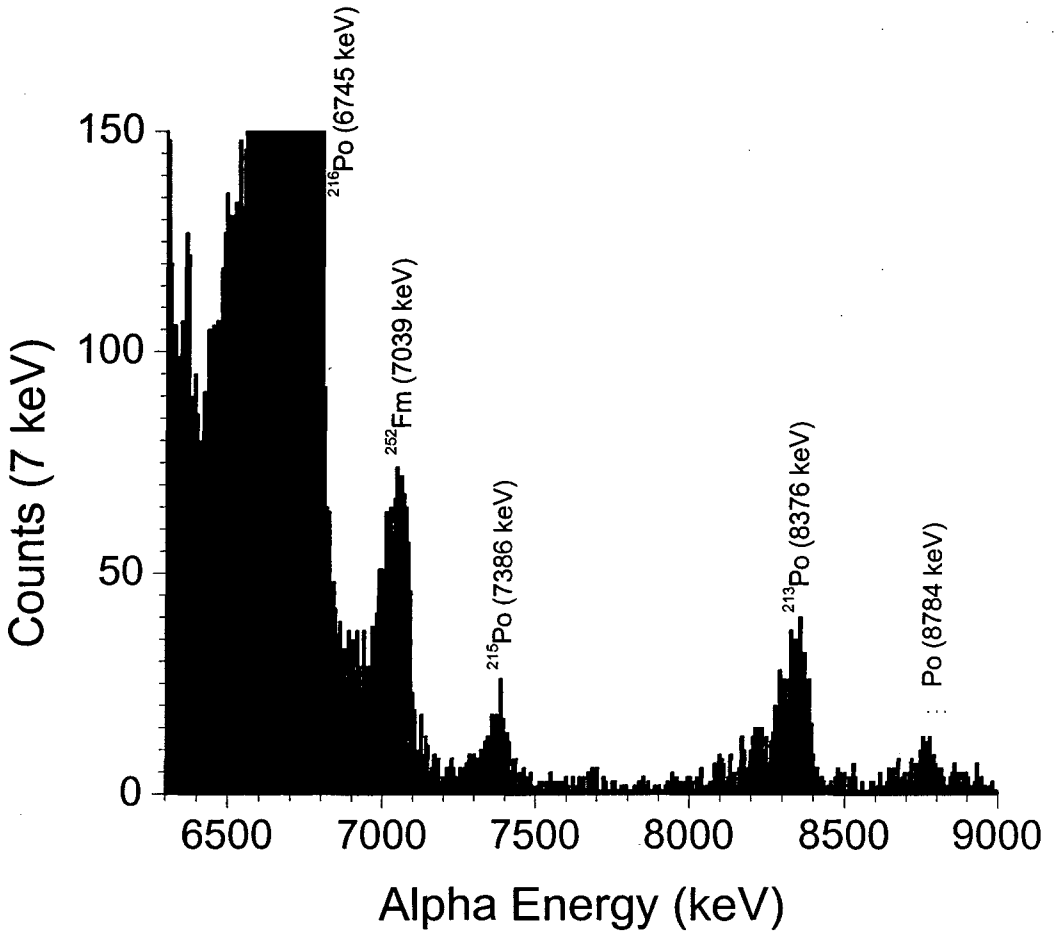

Figure 4.7: Summed alpha spectrum for the 99.3-MeV $^{238}U + ^{18}O$ experiment.

Table 4.6 List of alpha-decay peak assignments for the spectra in Figures 4.5, 4.6 and 4.7. The polonium isotopes result from the decay of long-lived activities produced in transfer reactions with the uranium target and lead impurities in the uranium target. Alpha decay energies and half-lives from [Chu1999].

Isotope	E_α (MeV)	Half-life
^{216}Po	6.7783(5)	0.145 ± 0.002 s
^{252}Fm	7.039(2)	25.39 ± 0.05 h
^{215}Po	7.3862(8)	1.781± 0.004 ms
^{213}Po	8.3759(25)	4.2 ± 0.8 μs
^{212}Po	8.78437(7)	0.299 ± 0.002 μs

As described in Section 3.2, the samples were counted continuously over various time periods to obtain decay curves. The integration of the same region of interest over various time periods produced a decay curve for each energy. The initial activities of the isotopes present in the region of interest were determined from MLDS fits to the decay data. In the search for ^{252}Fm (E_α = 7.039(2) MeV, $t_{½}$ = 25.39 ± 0.05 h), the particular region of interest was approximately between 6.9 and 7.1 MeV. The large search region of interest was due to the poor energy resolution in the detectors (85 ± 15 keV) and alpha particle energy loss in the sample. A time window of 24 hours was chosen to look for the 25.39-hour decay of ^{252}Fm. The results of the integrations of the specific regions of interest for the three different energy experiments are listed in Table 4.6. Because of the differing times that the experiments occurred, not all of the time bins are exactly 24 hours. This factor is considered in MLDS when determining the half-life and initial activity of the ^{252}Fm for each experiment.

A two component fit was used to solve for the decay of ^{252}Fm. The first component would be the 25.39-hour ^{252}Fm and the second component would be a long-lived component due to the decay of ^{217}At (E_α = 7.0669(15) MeV, $t_{½}$ = 32.3 ± 0.4 ms). ^{217}At is present from the decay of the long-lived ^{229}Th which is present naturally and reaches an equilibrium with its longer lived parent and grandparents, giving rise to a much longer half-life than ^{252}Fm. The results of the MLDS fits to the decay curves can be found in Table 4.7. The half-lives and initial activities are the result of the MLDS program. The total number of counts is determined by integrating the MLDS result decay curve over the given counting interval which was 9.53 days (82.4 MeV), 8.75 days (94.9 MeV), and 8.50 days (99.3 MeV).

Table 4.7: Decay tables for the three reactions showing the number of counts in the region of interest given for each of the three experiments. The time window in which the integration of the alpha spectra were integrated is also listed.

Experiment (Region of Interest in MeV)					
82.4 MeV (6.906 – 7.086)		94.9 MeV (6.908– 7.100)		99.3 MeV (6.902 – 7.097)	
Time Window	Number of Counts	Time Window	Number of Counts	Time Window	Number of Counts
0-1 d	163	0-1 d	811	0-1 d	381
1-2 d	90	1-2 d	372	1-1.75 d	177
2-2.83 d	41	2-3 d	196	1.75-2.75 d	101
2.83-3.83 d	22	3-4 d	99	2.75-3.75 d	58
3.83-4.83 d	17	4-5 d	60	3.75-4.75 d	46
4.83-5.83 d	16	5-6 d	36	4.75-5.75 d	23
5.83-6.83 d	3	6-7 d	15	5.75-6.75 d	17
6.83-7.83 d	5	7-8 d	11	6.75-7.75 d	17
7.83-8.83 d	0	8-8.75 d	1	7.75-8.50 d	14
8.83-9.53 d	2				

Table 4.8: Results of MLDS fits to the decay curves found in Table 4.6. The errors given are also a result of the MLDS program (^{252}Fm $t_{½}$ = 25.39 ± 0.05 hr). Both the half-life and initial activities were allowed to fluctuate when performing these fits. Fixing the half-life of ^{252}Fm resulted in differences in the initial activity of only 3%.

Beam Energy	Isotope	Half-life	Initial Activity	Number of Counts
82.4 MeV	^{252}Fm	$27.2\ ^{+1.4}_{-1.3}$ hr	$215\ ^{+14}_{-13}$ d^{-1}	350 ± 20
94.9 MeV	^{252}Fm	$24.6\ ^{+0.6}_{-0.5}$ hr	1080 ± 30 d^{-1}	1590 ± 50
99.3 MeV	^{252}Fm	22.1 ± 0.9 hr	530 ± 30 d^{-1}	710 ± 30

The results of the MLDS fits to the experimental decay curves show half-lives that are in good agreement with the half-life of 25.39 ± 0.05 hours. Assuming a 99.9977 ± 0.0002% alpha decay branch, the initial activities from Table 4.7, and the half-life of ^{252}Fm of 25.39 ± 0.005 hours, production cross sections for the ^{238}U(^{18}O,4n)^{252}Fm reaction were calculated to be 29 ± 3 nb, 180 ± 20 nb, and 47 ± 5 nb at excitation energies of 37.7 MeV, 49.3 MeV and 53.4 MeV, respectively.

This experiment has been performed experimentally once before. Donets et al., reported cross sections of fermium isotopes produced in the same reaction at energies from 80-135 MeV [Don1966]. The experimental cross sections from this thesis are only comparable at the highest energies for the 4n-reaction and are within a factor of two of the results of Donets. The experimental energies from Donets are reported only as energies of the projectiles in the lab frame. These energies were used to calculate the excitation energies for comparison with the experimental results of this thesis and HIVAP. Donets reported a uranium target thickness of approximately 1 mg/cm^2. This would lead to energy differences of up to 1 MeV in excitation energy at the center of the target. The Reisdorf and Schädel parameters were also used in the HIVAP code to predict the excitation function for the 4n-exit channel reaction. The experimental results match with the HIVAP predictions at the two highest energies, but is off considerably at the lowest energy. One possible explanation for the difference in the cross sections could be that the chemistry performed at the lowest energy was incomplete. A correctly performed chemistry would have displayed a larger initial activity and therefore cross section. The experimental results, the results of Donets and the HIVAP predictions are located in Figure 4.8.

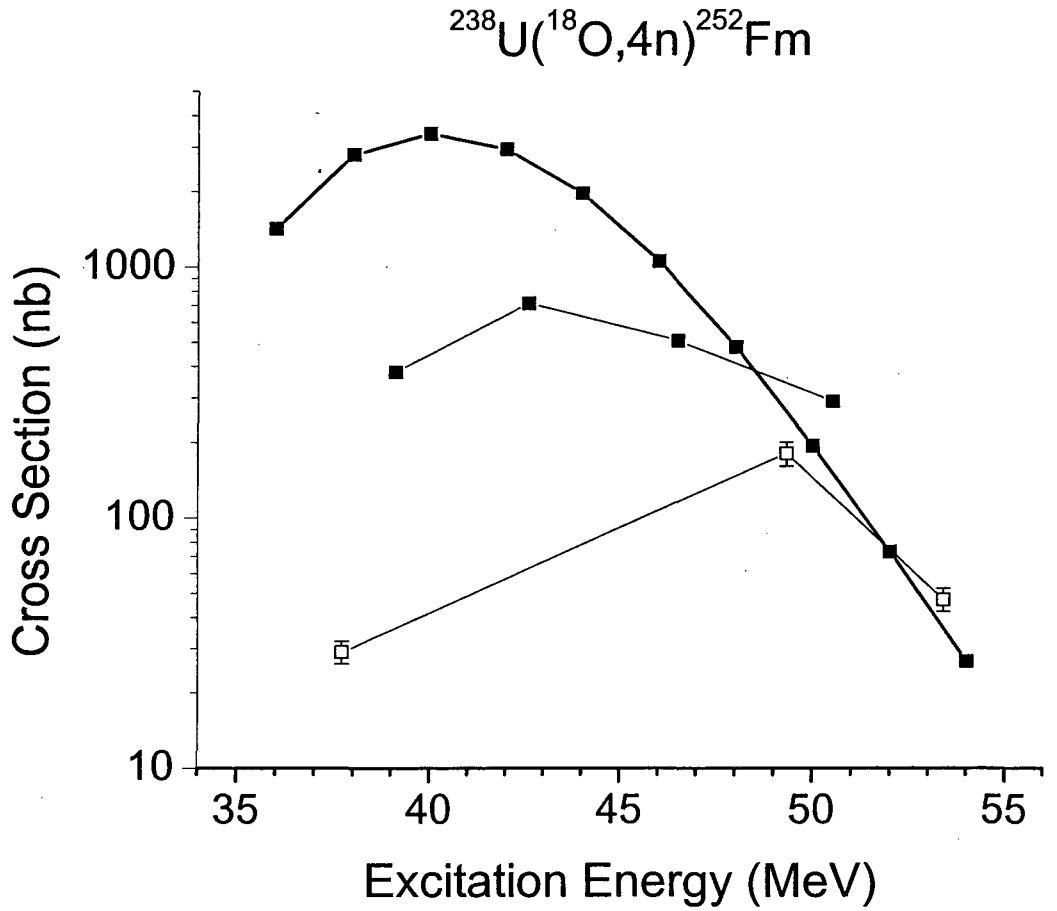

Figure 4.8: Comparison of experimental results and calculated values for the $^{238}U(^{18}O,4n)$ reaction. Solid symbols (■) represent the HIVAP code using the Reisdorf and Schädel parameters, open symbols (□) represent the experimental results of this thesis, and the open symbols with an (⊠) through them represent previous experimental results [Don1966].

4.3 $^{238}U + ^{22}Ne$

^{256}No (E_α = 8.430(20) MeV, $t_{½}$ = 2.91 ± 0.05 s) and ^{257}No (E_α = 8.220(20) MeV, $t_{½}$ = 25 ± 2 s) were produced in the reaction of ^{22}Ne with ^{238}U. The Berkeley Gas-filled Separator (BGS) was used to separate the recoiling evaporation residues from the scattered beam and recoiling transfer products. The reactions specifics for the $^{238}U(^{22}Ne,xn)^{260-x}No$ experiment are located in Table 4.9. The Coulomb barrier for the reaction was 114.9 MeV. To reduce the amount of scattering of beam that occurs with asymmetric reactions like neon on uranium, the pressure of the helium gas that enables the charge exchange collisions possible was lowered to 0.5 Torr for the entire experiment.

The ^{260}No evaporation residues that were created in the hot fusion reaction in the BGS have an average momentum that was small compared with the momenta of evaporation residues resulting from cold fusion reactions. As a result, separation from transfer reaction products was difficult, and the use of a parallel plate avalanche counter (PPAC) to discriminate events that originate in the detector (alpha decay) from those that originate from beam implantations (evaporation residues) was not possible. To counter this deficiency, the beam was chopped in twenty millisecond cycles, ten milliseconds on, and ten milliseconds off. This allowed for the detection of beam events (evaporation residues) from events originating in the detector (alpha decays). Because of the high event rate in the focal plane detector during the ten millisecond beam on phase, the search for alpha events only occurred in the last five milliseconds of the beam off phase.

Table 4.9: Reaction specifics for the $^{238}U(^{22}Ne,xn)^{260-x}No$ experiment. CYC denotes cyclotron energies, COT denotes center of target energies, and E^* denotes excitation energies.

E_{CYC} (MeV)	E_{COT} (MeV)	E^* (MeV)	Current (eμA)	Dose ($\times 10^{16}$)	Rutherfords	Time (s)
106.0	105.2	40.0	0.81 ± 0.07	6.1 ± 0.5	8183920	72298
110.5	109.7	44.2	0.63 ± 0.05	4.0 ± 0.3	4958640	61065
117.0	116.2	50.1	0.91 ± 0.08	4.1 ± 0.3	4505760	42829

The focal plane detector was a surface barrier silicon detector that was segmented into 32 vertical strips. The efficiency of the focal plane detector was 50 ± 2% for alpha particles. Due to the malfunction of one of the vertical strips and the beam area being larger than the focal plane detector, only 90 ± 5% of the evaporation residues were detected. The α-decay calibration of the focal plane detector was performed by examining the α-decay of: ^{198}Po (E_α = 6.1820(22) MeV), ^{197}Po (E_α = 6.281(4) MeV), ^{197m}Po (E_α = 6.3834(24) MeV), and ^{196}Po (E_α = 6.520(3) MeV) from the ^{114}Cd(^{86}Kr,xn)$^{200-x}$Po reaction and ^{204}Rn (E_α = 6.4189(25) MeV), ^{203}Rn (E_α = 6.4992(25) MeV), ^{203m}Rn (E_α = 6.5490(25) MeV), and ^{202}Rn (E_α = 6.6409(25) MeV) from the ^{120}Sn(^{86}Kr,xn)$^{206-x}$Rn reaction.

The separation efficiency was determined through the measurement of ^{214}Ac (E_α = 7.214(5) MeV, $t_{½}$ = 8.2 ± 0.2 s) produced in the ^{197}Au(^{22}Ne,5n) reaction. The first step was to determine the amount of ^{214}Ac produced directly in the reaction. This was accomplished by placing a catcher foil directly behind a standing gold target in the BGS target chamber, collecting the recoiling products and then counting the decays of ^{214}Ac. A 390 μg/cm^2 gold foil was used as the target and irradiated for 60 seconds by 118 MeV ^{22}Ne^{6+} at an average current of 95 enA. The foil was then quickly moved behind a silicon surface barrier detector to detect the activity of ^{214}Ac. The foil was located 1.36 inches from the detector, which had a diameter of 0.84 inches. It was assumed that the activity collected in the foil was in an area small enough to be considered a point source. A point source 1.36 inches from a detector of diameter 0.84 inches would have a geometric detector efficiency of 2 $^{+5}_{-1}$%. The foil was counted for a total of ten minutes in which all

of the ^{214}Ac decayed. The number of decays from ^{214}Ac were counted every 10 seconds to obtain a decay curve. The initial activity and half-life were determined from this decay curve to be 9.8 ± 1.5 s^{-1} and 8.2 ± 0.4 s (Figure 4.9). Next, the production of ^{214}Ac was measured in the focal plane detector. Using the same gold target and at the same energy neon projectiles at an average current of 110 enA, ^{214}Ac was produced and detected in the focal plane detector. Again, the number of decays from ^{214}Ac were counted every 10 seconds. A growth curve was drawn through the data to determine the production rate of ^{214}Ac as measured by the focal plane detector. The efficiency of the focal plane detector was 50 ± 2% for alpha decays. With a 390 μg/cm^2 gold foil, a production rate of 19 ± 3 s^{-1} was determined (Figure 4.10). An additional experiment was performed with a thinner gold target to determine the change in efficiency with a thinner target. ^{22}Ne at an energy of 108 MeV and an average current of 150 enA irradiated a 100 μg/cm^{2}gold target for approximately ten minutes. The number of ^{214}Ac decays was again counted every ten seconds. A curve was drawn through the data establishing the production rate for 100 μg/cm^2 target to be 19 ± 2 s^{-1} (Figure 4.11). Using Equation 4.1, the BGS efficiency was calculated,

$$Eff_{BGS} = \frac{R_{focal}\dfrac{Th_{catcher}}{Th_{focal}}}{\dfrac{Eff_{focal}I_{focal}}{R_{catcher}}} \qquad (4.1)$$

$$\frac{Eff_{catcher}I_{catcher}}{}$$

where R is the initial activity and production rate from above for the catcher foil and focal plane measurements, Eff was the respective detector efficiencies, and I was the

beam current for each experiment. Th is the target thickness used for the particular catcher foil and focal plane detector measurements. The only experiment with the catcher foil involved a target with a thickness of 390 $\mu g/cm^2$. Focal plane measurements were made at both 390 $\mu g/cm^2$ and 100 $\mu g/cm^2$ thicknesses. To accurately calculate the efficiency of the BGS at various target thicknesses, this target thickness factor needed to be included. Using the production rates, beam currents and detector efficiencies from above and Equation 4.1, BGS efficiencies of 8 ± 2% (390 $\mu g/cm^2$) and 21 ± 6% (100 $\mu g/cm^2$) were determined for neon projectiles on gold targets. Computer simulations were run to examine the differences between BGS efficiencies for different target/projectile combinations, target thicknesses and compound nucleus velocities [Gre2002]. Extrapolation between the results of the gold target BGS efficiencies and the results of the computer simulation led to a BGS efficiency of 8 ± 3% for the 160.5 $\mu g/cm^2$ UF_4 targets and the $^{238}U(^{22}Ne,xn)$ reaction.

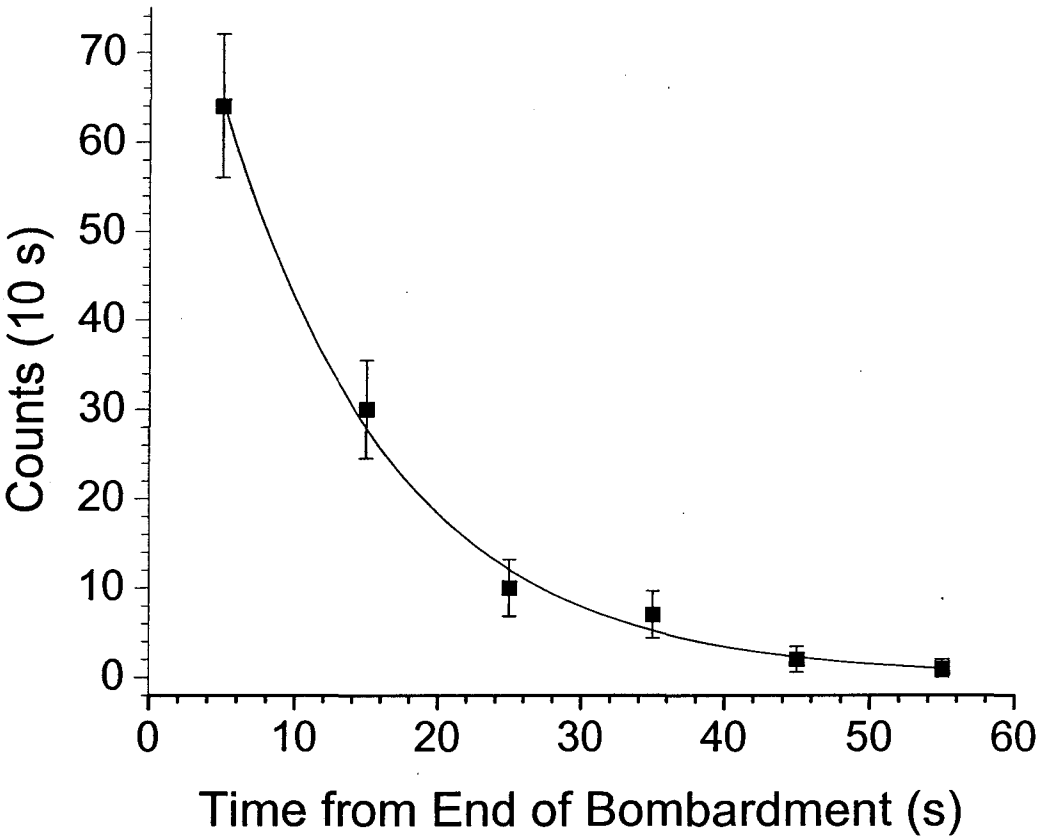

Figure 4.9: Decay data and fit from the catcher foil measurement of ^{214}Ac ($t_{½}$ = 8.2 ± 0.2 s) in the reaction 118 MeV ^{22}Ne + ^{197}Au (390 μg/cm^2). An initial activity of 9.8 ± 1.5 s^{-1} and a half-life of 8.2 ± 0.4 s was determined.

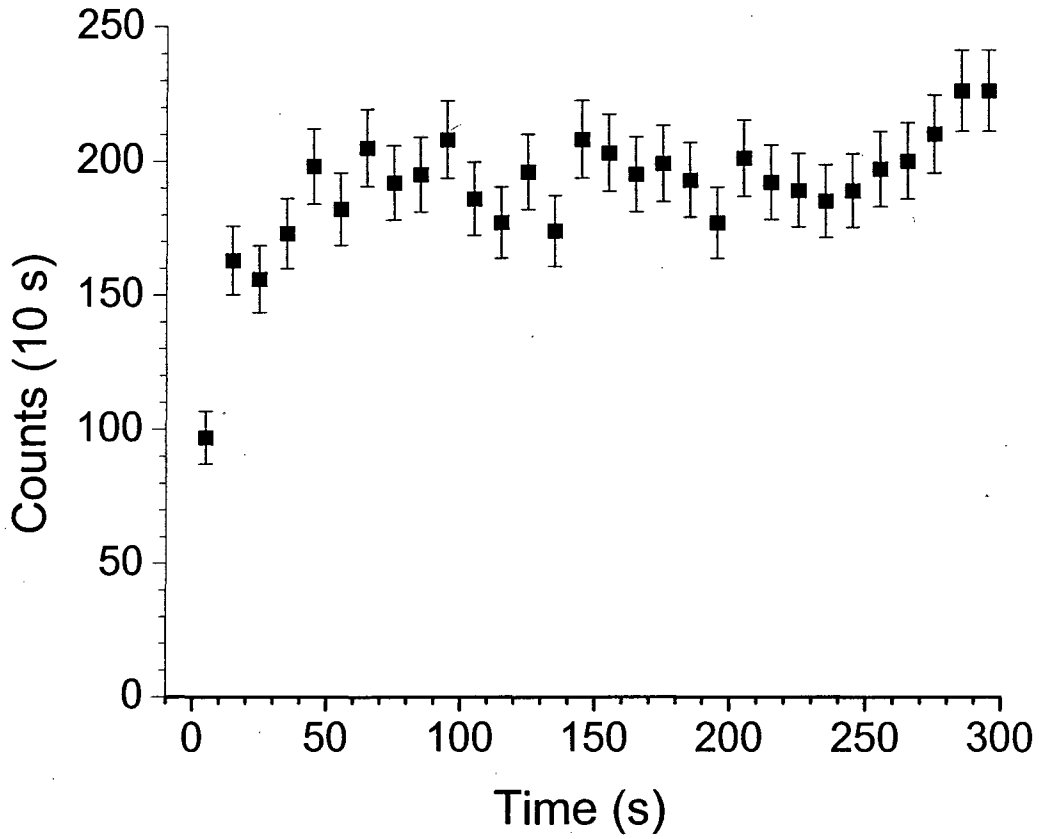

Figure 4.10: Growth data of ^{214}Ac ($t_{½}$ = 8.2 ± 0.2 s) from the reaction of 118 MeV ^{22}Ne + ^{197}Au (390 μg/cm^2). A production rate of 19 ± 3 s^{-1} was determined.

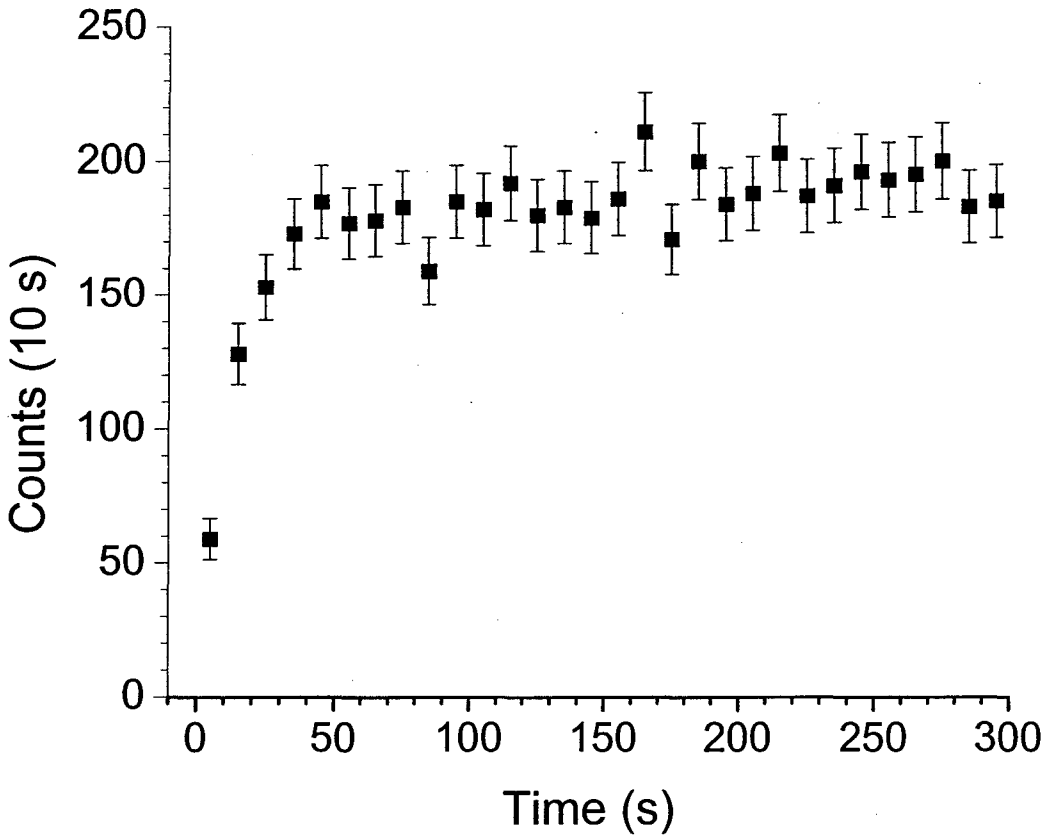

Figure 4.11: Growth data of ^{214}Ac ($t_{½}$ = 8.2 ± 0.2 s) from the reaction of 108 MeV ^{22}Ne + ^{197}Au (100 μg/cm^2). A production rate of 19 ± 2 s^{-1} was determined.

4.3.1 ^{257}No

Analysis of the data obtained in the experiment was performed using the GOOSY data analysis software as described in Section 3.3. Searches were made to look for correlations between evaporation residues and 8.22 MeV, 8.27 MeV and 8.32 MeV alpha particles. After searching though the data with numerous search parameters, no correlations were found. One of the complications was the length of time between a correlated evaporation residue implantation and alpha decay on the order of the half-life of ^{257}No ($t_{½} = 25 \pm 2$ s). With event rates in the focal plane detector around 1000 events per second, the possibility of random correlation was high.

Assuming one correlation would have been seen, a $100 \pm 5\%$ alpha decay branching ratio, and an $8 \pm 3\%$ BGS efficiency, one-event upper limits for the production cross section were calculated for the ^{238}U(^{22}Ne,3n) reaction. Upper limit production cross sections of 4.5 nb, 6.9 nb, and 6.7 nb were calculated at excitation energies of 40.0 MeV, 44.2 MeV, and 50.1 MeV using Equations 3.10 – 3.13. A comparison of these upper limit cross sections and those obtained from the HIVAP code using the Reisdorf and Schädel parameters showed that it was reasonable not to expect any evaporation residue alpha-decay correlations. The predictions of the HIVAP code as well as the experimental upper limit production cross sections are seen in Figure 4.12.

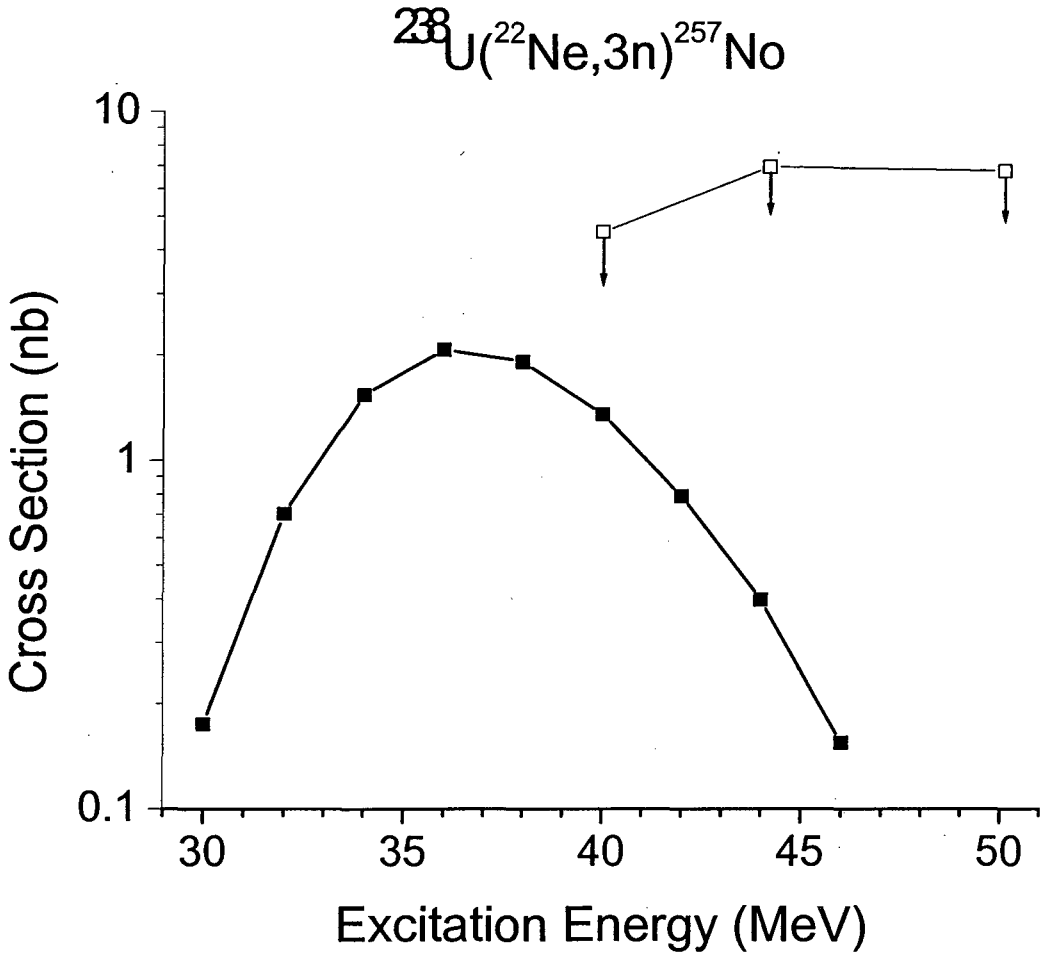

Figure 4.12: Predictions of the HIVAP code using the Reisdorf and Schädel parameters (solid symbols ■) and the experimental upper limit production cross sections (open symbols □) for the $^{238}U(^{22}Ne,3n)^{257}No$ reaction.

4.3.2 ^{256}No

Unlike the search for ^{257}No, the search for ^{256}No was a little more successful. Using a GOOSY analysis code identical to the one in Appendix A, a search was performed to look for correlations between evaporation residue implantations and alpha decay from ^{256}No (E_α = 8.430(20) MeV, $t_{1/2}$ = 2.91 ± 0.05 s). When searching for evaporation residue alpha decay correlations, there were five main search parameters considered: decay time window, position window, evaporation residue energy window, alpha decay energy window and the beam pause/PPAC anti-coincidence window. When searching for ^{256}No the following parameters were set: decay time window (0 - 30 seconds), position window (±20 pixels, ±1.16 mm), evaporation residue energy window (2 – 14 MeV), alpha decay energy (8.35 – 8.50 MeV), and beam pause window (15000 – 20000). The decay time window corresponded to the maximum amount of time allowed between an evaporation residue implantation and alpha decay. The position window corresponded to the maximum distance allowed between the correlated signals in the silicon detector. The energy windows corresponded to the energy of the evaporation residue implantations in the focal plane and the specific alpha decay energy of the isotope of interest. The beam pause window in this correlation search corresponded to the time of the twenty millisecond beam cycle in which alpha decay in the focal plane detector was considered for correlations. In this specific correlation search, only alpha decays that occurred in the last five milliseconds of the beam cycle were considered as possible correlations to evaporation residue implantations.

This correlation search was performed at all three of the experimental energies. A total of 14 correlations were seen at an excitation energy of 40.0 MeV, a total of 8

correlations were seen at an excitation energy of 44.2 MeV, and 1 event was seen at an excitation energy of 50.1 MeV. The times between the evaporation residue implantations and alpha decays were input in a program that created an input file for the MLDS program. Two component fits to the resulting decay input files were made and initial activities and total number of counts were established. The half-life for ^{256}No of 2.9 seconds was fixed in the MLDS program and the second component was set to vary as a long half-life substituting for random events. In addition, all of the correlations were combined into one input file. A 2 component fit to the combined input file was performed with the first component set as a 2.9 second half-life and varied and the second component was set as a long half-life and varied. A half-life of $3.1\ ^{+2.8}_{-1.9}$ seconds resulted giving weight to a successful identification of ^{256}No ($t_{½} = 2.91 \pm 0.05$ s). The results of the MLDS fits to the decay data of ^{256}No at 40.0 MeV and 44.2 MeV as well as the result of the combined decay data can be seen in Table 4.10. Because only one correlation was seen at the highest excitation energy of 50.1 MeV, a one event cross section limit was calculated for the highest excitation energy. As Table 4.10 shows, a long lived component due to random correlations was present, meaning an assignment of one event at 50.1 MeV is not accurate, and therefore only a one event limit was calculated.

Using the number of counts that resulted from the MLDS fits to the correlation data, an alpha decay branching ratio of 99.5 ± 0.1%, and a BGS efficiency of 8 ± 3%, production cross sections were calculated for the ^{238}U(^{22}Ne,4n)^{256}No reaction. Production cross sections of $23\ ^{+20}_{-16}$ nb, $14\ ^{+21}_{-9}$ nb, and ≤ 6.8 nb were calculated at excitation energies of 40.0 MeV, 44.2 MeV, and 50.1 MeV respectively. These results

agree well with the predictions of the HIVAP code using the Reisdorf and Schädel parameters. Donets et al., performed this reaction as well and report cross sections that are similar in magnitude to the experimental cross sections observed in this thesis [Don1966]. Figure 4.13 is a combination of the experimental results of this thesis, the predictions of the HIVAP code and the experimental results of Donets et al.

Table 4.10: Results of MLDS fits to the decay curves from the correlations found in the $^{238}U(^{22}Ne,4n)^{256}No$ reaction. The errors given are a result of the MLDS program. The half-life of ^{256}No ($t_{½} = 2.91 \pm 0.05$ s) was fixed to eliminate the influence of random events.

Excitation Energy	Isotope	Half-life	Initial Activity	Number of Counts
40.0 MeV	^{256}No	2.9 s	$1.1\ ^{+0.9}_{-0.7}\ s^{-1}$	$5\ ^{+4}_{-3}$
44.2 MeV	^{256}No	2.9 s	$0.6\ ^{+0.8}_{-0.2}\ s^{-1}$	$2\ ^{+3}_{-1}$
Combined	^{256}No	$3.1\ ^{+2.8}_{-1.9}$ s		

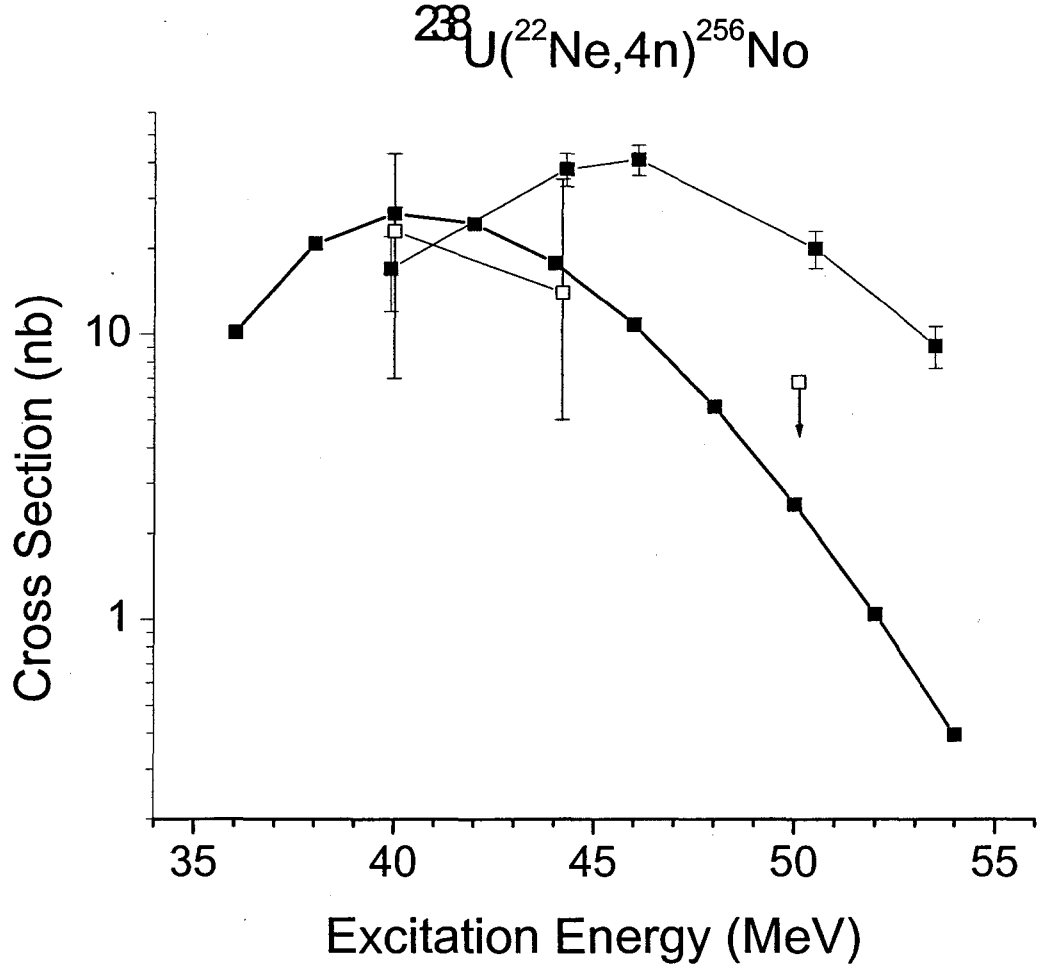

Figure 4.13: Predictions of the HIVAP code using the Reisdorf and Schädel parameters (solid symbols ■), the experimental production cross sections (open symbols □), and results of Donets, et al. [Don1966] (open symbols with an ×) for the $^{238}U(^{22}Ne,4n)^{256}No$ reaction. Upper-limit cross sections denoted with an arrow.

4.4 $^{208}Pb + ^{48}Ca$

^{255}No ($E_\alpha = 8.121(6)$ MeV, $t_{½} = 3.1 \pm 0.2$ min), ^{254}No ($E_\alpha = 8.093(14)$ MeV, $t_{½} = 55 \pm 3$ s), ^{253}No ($E_\alpha = 8.010(20)$ MeV, $t_{½} = 1.7 \pm 0.3$ min), and ^{252}No ($E_\alpha = 8.415(6)$ MeV, $t_{½} = 2.30 \pm 0.22$ s) were all produced in the reaction of ^{48}Ca on ^{208}Pb. $^{48}Ca^{10+}$ energies between 207 MeV and 234 MeV were used in the experiment corresponding to energies at the center of the target from 204 MeV to 231 MeV and excitation energies between 12 MeV and 34 MeV. The Coulomb barrier was 217.1 MeV. The specific energies for each reaction, reaction times, average beam currents, doses, and integrated Rutherford detector counts are listed in Table 4.11.

The efficiency listed in Table 4.11 refers to the percentage of the evaporation residues that made it to the focal plane detector that were actually detected. In each of the experiments, a number of strips of the focal plane detector were not operating correctly, and therefore, an efficiency for the amount of the focal plane detector actually working during each of the reactions was determined. The focal plane detector efficiency was 50 ± 2% for alpha decay and 100 ± 2% for spontaneous fission decay.

Table 4.11: Reaction specifics for the $^{208}Pb(^{48}Ca,xn)^{256-x}No$ experiment. CYC denotes cyclotron energies, COT denotes center of target energies, and E^* denotes excitation energies. Eff denotes the percentage of evaporation residues that were detected by the focal plane detector. The uncertainty in the Eff value was assumed to be 5%.

E_{CYC} (MeV)	E_{COT} (MeV)	E^* (MeV)	Current (eμA)	Dose ($\times 10^{15}$)	Rutherford Counts	Time (s)	Eff
207.5	204.0	12.2	2.13 ± 0.11	24.9 ± 1.3	9303360	18704	80
210.0	206.5	14.2	1.61 ± 0.08	24.1 ± 1.2	8788160	23908	80
211.3	207.8	15.2	2.22 ± 0.11	19.1 ± 1.0	6890880	13812	82
212.5	208.8	16.1	0.220 ± 0.011	1.27 ± 0.06	453303	9230	64
212.5	209.0	16.3	1.66 ± 0.08	34.5 ± 1.8	12306240	33382	85
215.0	211.3	18.1	0.099 ± 0.005	0.43 ± 0.02	150966	7040	64
215.0	211.5	18.3	2.45 ± 0.12	48 ± 2	16835200	31673	87
217.5	213.8	20.2	0.161 ± 0.008	0.142 ± 0.007	48509	1414	64
218.8	215.3	21.4	0.63 ± 0.03	8.8 ± 0.4	2963936	22405	82
220.0	216.3	22.2	0.067 ± 0.003	0.43 ± 0.02	143557	10370	64
222.5	218.8	24.2	0.158 ± 0.008	0.182 ± 0.009	59036	1840	64
225.0	221.4	26.3	0.145 ± 0.007	0.46 ± 0.02	146879	5100	64
234.0	230.6	33.8	1.77 ± 0.09	19.2 ± 1.0	5632320	17384	80

BGS efficiencies for cold fusion reactions were larger than the efficiency for the $^{22}Ne + ^{238}U$ hot fusion reaction mentioned previously. Using Equation 3.6, the magnetic rigidity of compound nuclei and transfer products can be calculated for these two reactions. The magnetic rigidity for the hot fusion reactions was 2.00 Tm (Tesla meters) for the transfer products and 1.85 Tm for the compound nuclei. The difference between these two magnetic rigidities is about 7% and is small when compared to the difference between the rigidities of the cold fusion reaction. In the $^{48}Ca + ^{208}Pb$ reaction, the rigidity of the transfer products was 1.48 Tm and the rigidity of the compound nuclei was 2.12 Tm, equaling a difference of 42%. On this basis alone, a BGS efficiency approximately 5-6 times greater than the BGS efficiency used for the $^{22}Ne + ^{238}U$ would be expected. The actual BGS efficiency was 45 ± 10%.

The experiments were run at helium pressures in the BGS of 0.74 and 0.79 Torr and a PPAC was used in one set of experiments. For the other set of experiments, the beam was pulsed 10 milliseconds on and 10 milliseconds off. Calibrations were performed by examining the products of the $^{165}Ho(^{48}Ca,xn)^{213-x}Fr$ reaction as well as the $^{176}Yb(^{48}Ca,xn)^{224-x}Th$ reaction. The $^{165}Ho(^{48}Ca,xn)^{213-x}Fr$ reaction was run at 203 MeV corresponding to 50 MeV excitation energy, which led to the following products in the focal plane detector used in the calibration: ^{205}At (E_α = 5.902(2) MeV), ^{210}Rn (E_α = 6.040(2) MeV), ^{208}Rn (E_α = 6.1438(21) MeV), $^{211,210}Fr$ (E_α = 6.534(5) MeV, 6.543(5) MeV), and $^{209,208}Fr$ (E_α = 6.646(5) MeV, 6.641(3) MeV). The $^{176}Yb(^{48}Ca,xn)^{224-x}Th$ reaction was also run at 203 MeV corresponding to 40 MeV excitation energy and led to the following alpha decay peaks for use in calibration: ^{213}Rn (E_α = 8.088(8) MeV),

^{221}Th (E_α = 8.472(5) MeV), and ^{215}Ra (E_α = 8.699(4) MeV). This reaction was also run at 220 MeV corresponding to 55 MeV excitation energy. The following peaks from this reaction were used for the calibration: ^{215}Ra and ^{217}Th (E_α = 9.250(10) MeV).

4.4.1 ^{255}No and ^{254}No

Disentangling the decay of ^{255}No and ^{254}No was difficult where the excitation functions for the 1n-exit channel and 2n-exit channel overlapped. Because of the similarities in the decay of ^{255}No and ^{254}No, the search for both was performed at the same time. ^{255}No was seen at excitation energies from 12.1 MeV to 16.2 MeV. ^{254}No was seen at excitation energies from 14.2 MeV to 26.3 MeV. The evaporation residue alpha decay correlation search parameters for ^{255}No and ^{254}No for the first experiment were as follows: time window (0 - 1800 seconds), position window (-20 – 15 pixels, -1.16 – 0.87 mm), evaporation residue energy window (1 – 14 MeV), alpha decay energy window (8.0 – 8.2 MeV), and PPAC window (1000 – 2500). The PPAC was used for four of the energies in which ^{255}No was studied. The second experiment was performed under different conditions and a different set of correlation parameters were used: time window (0-500 seconds), position window (±20 pixels, ±1.16 mm), evaporation residue energy window (4 – 14 MeV), alpha decay energy window (8.0 – 8.2 MeV), and beam pause window (0 – 20000). It is noted that there was no effect on the number of correlations by having a shorter time window, and a smaller evaporation residue window. The event rate in the detector was small enough and the correlation time short enough to allow the use of a large beam pause window.

Figure 4.14 shows the results of the correlation search performed on the data obtained in the 215.3 MeV experiment. The top window (a.) shows all of the alpha decays that fit within the energy window and position window that were correlated to evaporation residues. The evaporation residues that correspond to the correlated alphas are located in the middle window (b.). The difference in position between the two

correlated events is found in the bottom window (c.). These windows help show that there was only one activity of interest in this particular correlation search, ^{254}No, the evaporation residue distribution was fairly large and covers the range between 4 – 10 MeV, and that the difference in position distribution was smaller than the position window used. It also appeared that some random events were present, but were accounted for when the decay curves were fit using a long component in the MLDS fit.

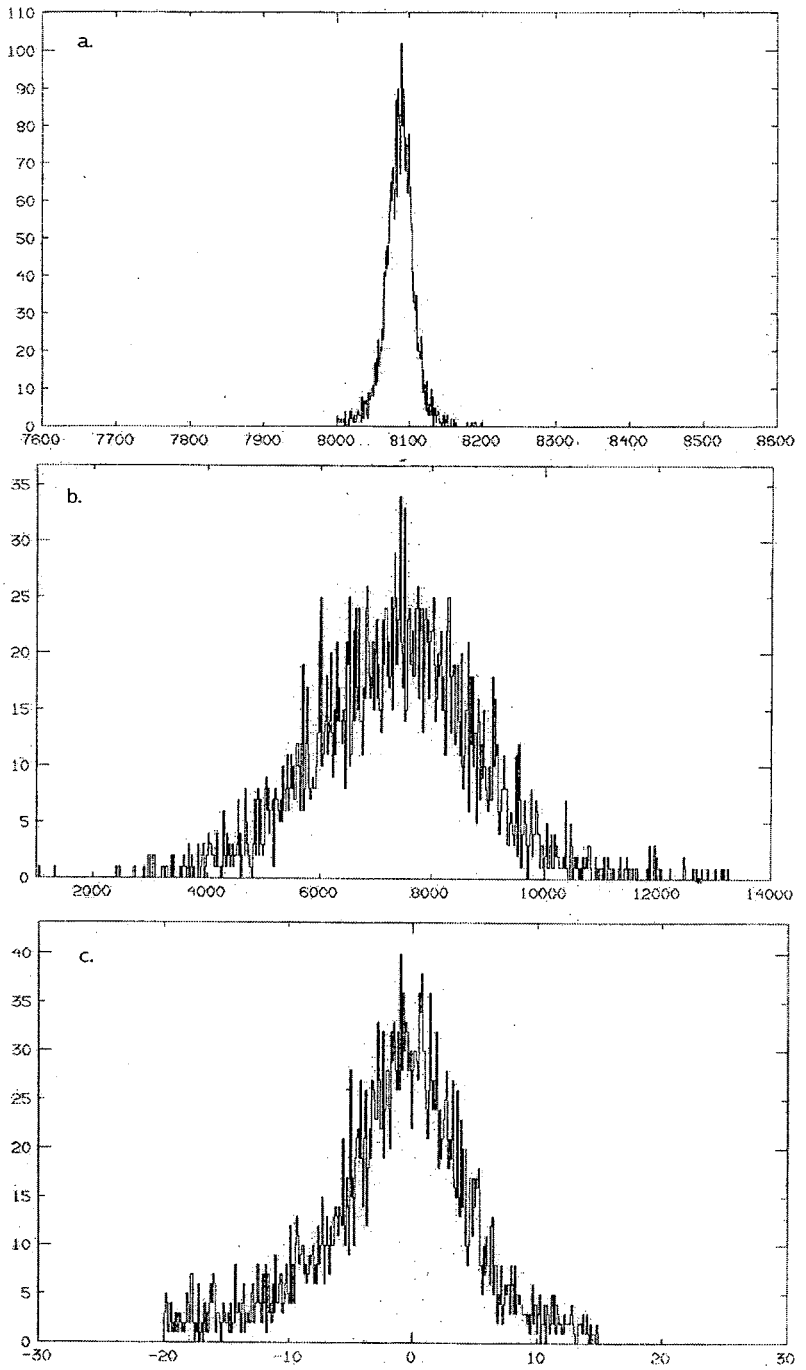

Figure 4.14: Correlated alpha decay spectrum (a.), evaporation residue spectrum (b.), and difference in position distribution (c.) for the 215.3 MeV ^{208}Pb(^{48}Ca,2n)^{254}No experiment. Energies for windows (a.) and (b.) are in keV. The difference in position distribution (c.) is in units of detector pixels.

At each excitation energy, the total number of correlations was determined from the correlation search. Then, the data were sorted according to the correlation time between the evaporation residue implantation and the alpha decay. For some of the excitation energies, only a small number of correlations ($5 \leq$ number of correlations ≤ 25) were found. In that case, the decay curve was made using a part of the MLDS program that makes input files based on only a small number of events. For the rest of the experiments (number of correlations ≤ 5), no decay curve was made. The summaries of the decay curves is found in Table 4.12. From these decay curves and those formed by the MLDS program, 2 and 3 component fits were made corresponding to the decay of ^{255}No , ^{254}No and a long-lived component. From the alpha decay spectra seen from the data, the presence of ^{255}No and ^{254}No was not questioned and therefore their half-lives were fixed when performing the MLDS fits. The initial activities were all allowed to vary in the MLDS program. The number of counts was calculated by integrating the resulting decay curves made with the half-lives and initial activities of MLDS over the time windows used in the correlation search. Various files that corresponded to a majority of the activity of ^{255}No and ^{254}No were also examined with MLDS to find the corresponding experimental half-life. An experimental half-life of $169\ ^{+13}_{-12}$ seconds was found for ^{255}No and an experimental half-life of 47.5 ± 0.4 seconds was found for ^{254}No. The summary of the MLDS fits to the data for ^{255}No and ^{254}No can be found in Table 4.13.

Table 4.12: Decay tables for correlations searches of evaporation residues and ^{255}No and ^{254}No decay. Times are in seconds and denote the start of each time bin. Counts corresponds to the number of correlations in the time bin that satisfied the correlation search parameters.

Experiment (MeV)									
	209.0		211.3	211.5	213.8	215.3	216.3	218.8	221.4
Time	Counts	Time	Counts	Counts	Counts	Counts	Counts	Counts	Counts
0	267	0	23	1576	23	901	47	14	11
50	141	20	14	1162	21	698	32	11	10
100	85	40	7	849	10	563	25	4	5
150	43	60	4	639	5	390	19	7	5
200	27	80	7	457	10	301	16	4	2
250	10	100	3	386	10	223	11	4	4
300	19	120	0	289	2	158	9	2	2
350	13	140	1	241	2	104	5	6	2
400	6	160	3	165	0	78	2	1	1
450	7	180	2	131	1	52	3	1	0
500	8	200	3	96	1	39	1	0	0
550	5	220	1	77	0	33	6	1	0
600	3	240	3	66	0	29	1	0	0
650	3	260	1	57	1	20	3	0	0
700	1	280	0	48	1	20	3	0	0
750	3	300	0	36	0	14	1	0	0
800	1	320	1	43	2	7	1	0	0
850	3	340	1	24	1	7	1	0	1
900	2	360	0	26	0	6	1	0	0
950	5	380	0	20	0	4	0	1	0
1000	0	400	1	20	0	1	1	0	0
1050	0	420	1	13	1	1	2	0	1
1100	0	440	1	21	0	1	0	0	0
1150	0	460	0	11	1	3	2	0	0
1200	0	480	0	19	0	4	1	1	0
1250	1								
1300	0								
1350	2								
1400	0								
1450	0								
1500	0								
1550	0								
1600	1								
1650	2								
1700	3								
1750	0								

Table 4.13: MLDS results to the decay curves found in Table 4.12 (^{255}No $t_{½}$ = 3.1 ± 0.2 min, ^{254}No $t_{½}$ = 55 ± 3 s). Based on the work of [Lei1999], the half-life of ^{254}No was fixed at 47 s. The half-lives of ^{255}No and ^{254}No were fixed to eliminate the influence of random events.

Beam Energy	Isotope	Half-life	Initial Activity	Number of Counts
204.0 MeV	^{255}No			$1.0^{+2.3}_{-0.8}$
206.5 MeV	^{254}No	47 s	$0.05^{+0.05}_{-0.04}$ s^{-1}	3^{+4}_{-3}
	^{255}No	186 s	$0.029^{+0.016}_{-0.012}$ s^{-1}	8^{+4}_{-3}
207.8 MeV	^{254}No	47 s	$0.11^{+0.09}_{-0.07}$ s^{-1}	7^{+6}_{-5}
	^{255}No	186 s	$0.09^{+0.03}_{-0.02}$ s^{-1}	25^{+7}_{-6}
208.8 MeV	^{254}No	47 s	$0.13^{+0.08}_{-0.07}$ s^{-1}	9^{+5}_{-4}
	^{255}No	186 s	$0.07^{+0.03}_{-0.02}$ s^{-1}	15^{+6}_{-5}
209.0 MeV	^{254}No	47 s	6.8 ± 0.4 s^{-1}	460 ± 30
	^{255}No	186 s	$0.68^{+0.09}_{-0.08}$ s^{-1}	180 ± 20
211.3 MeV	^{254}No	47 s	$0.95^{+0.15}_{-0.14}$ s^{-1}	65 ± 10
211.5 MeV	^{254}No	47 s	89.2 ± 1.4 s^{-1}	6040 ± 90
213.8 MeV	^{254}No	47 s	$1.25^{+0.17}_{-0.16}$ s^{-1}	85^{+11}_{-10}
215.3 MeV	^{254}No	47 s	53.7 ± 1.1 s^{-1}	3640 ± 70
216.3 MeV	^{254}No	47 s	2.5 ± 0.2 s^{-1}	170^{+16}_{-15}
218.8 MeV	^{254}No	47 s	$0.79^{+0.14}_{-0.12}$ s^{-1}	54^{+9}_{-8}
221.4 MeV	^{254}No	47 s	$0.62^{+0.12}_{-0.11}$ s^{-1}	42^{+8}_{-7}

Using the number of counts from the MLDS fits, half-lives based on the activity, decay branching ratios (^{255}No α 61.4 ± 2.5%, ^{254}No α 90 ± 4%), the data from Table 4.11 and a 45 ± 10% BGS efficiency, the cross sections were calculated using Equations 3.10 – 3.13. The excitation energies, isotopes and production cross sections are listed in Table 4.14. The production cross sections were then compared to the results of the HIVAP code with the Reisdorf and Schädel parameters and to the results of previous experimental work done in Germany [Gäg1989] and Russia [Oga2000c]. The previous work on the ^{208}Pb(^{48}Ca,xn) reaction is quite similar to the experimental results obtained in this thesis. No serious deviations exist. There does seem to be a slight cross section enhancement at lower excitation energies in the German work, but overall, the cross sections are quite similar. However, unlike the comparisons of hot fusion cross sections and predictions of the HIVAP code in which the code often closely predicted experimental results, the HIVAP code with the Reisdorf and Schädel parameters does not accurately reflect what is seen experimentally for ^{255}No and is over predictive for ^{254}No. This is not totally unexpected as the Reisdorf and Schädel parameters were made as a result of fits to hot fusion reactions, not cold fusion reactions. The comparison of these results can be seen in Figure 4.15 for ^{255}No and Figure 4.16 for ^{254}No.

Table 4.14: Production cross sections for ^{255}No and ^{254}No.

Excitation Energy (MeV)	Isotope	Production Cross Section (nb)
12.2	^{255}No	$0.3\ ^{+0.6}_{-0.2}$
14.2	^{254}No	$0.6\ ^{+0.8}_{-0.6}$
	^{255}No	$2.3\ ^{+1.3}_{-1.0}$
15.2	^{254}No	$1.7\ ^{+1.5}_{-1.3}$
	^{255}No	9 ± 3
16.1	^{254}No	40 ± 20
	^{255}No	$100\ ^{+50}_{-40}$
16.3	^{254}No	58 ± 15
	^{255}No	33 ± 9
18.1	^{254}No	900 ± 300
18.3	^{254}No	530 ± 130
20.2	^{254}No	$3500\ ^{+1000}_{-900}$
21.4	^{254}No	1900 ± 500
22.2	^{254}No	2300 ± 600
24.2	^{254}No	1700 ± 500
26.3	^{254}No	530 ± 160

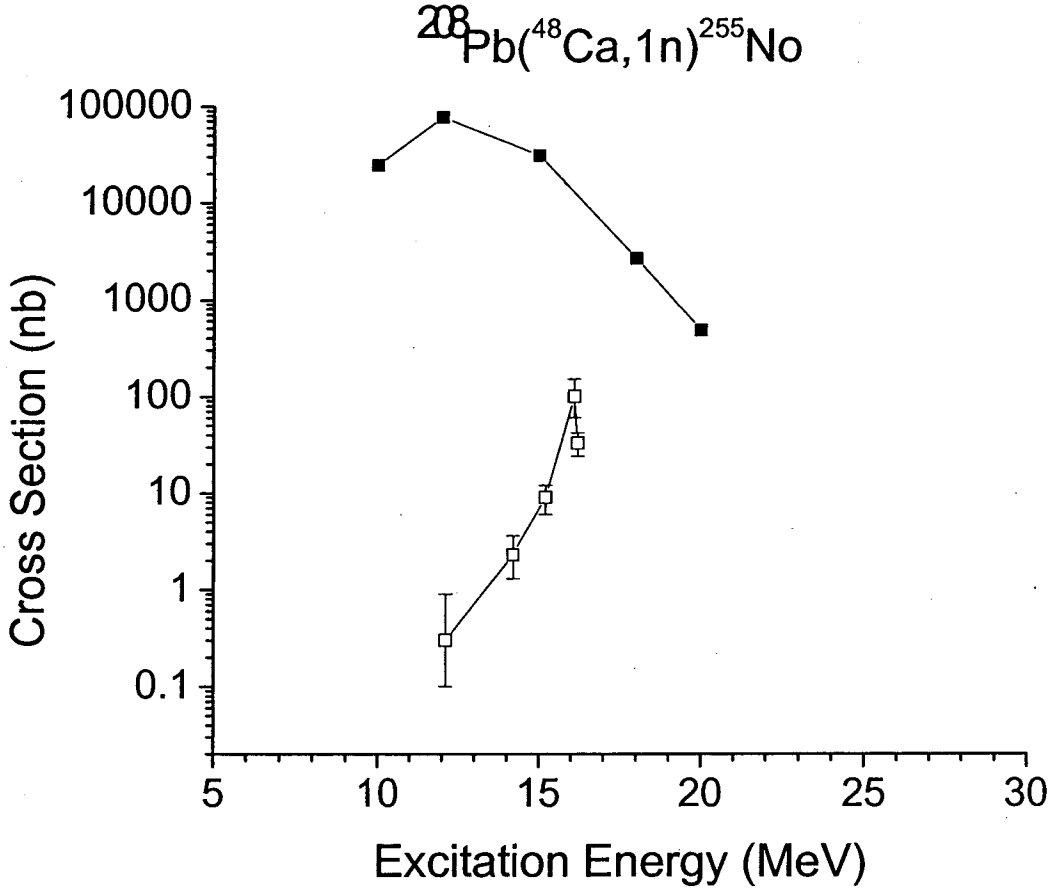

Figure 4.15: Predictions of the HIVAP code using the Reisdorf and Schädel parameters (solid symbols ■) and the experimental production cross sections (open symbols □) for the $^{208}Pb(^{48}Ca,1n)^{255}No$ reaction.

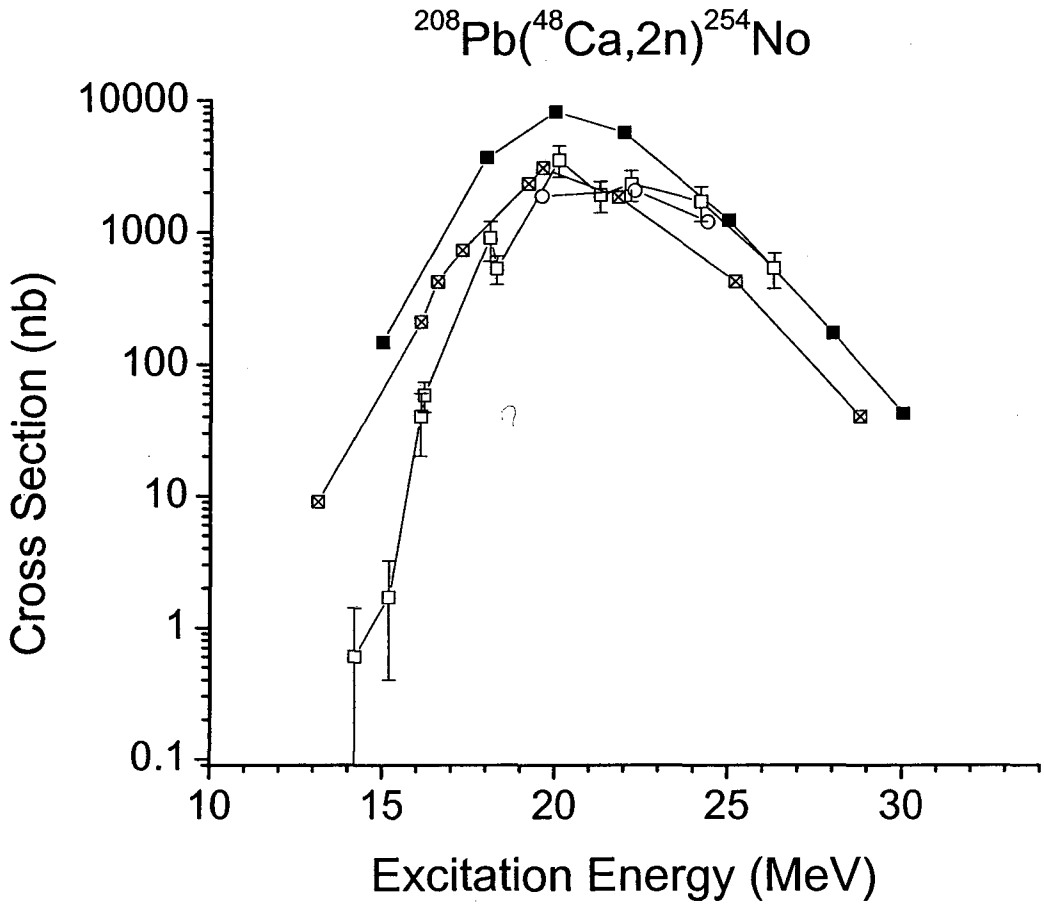

Figure 4.16: Predictions of the HIVAP code using the Reisdorf and Schädel parameters (solid symbols ■), the experimental production cross sections (open symbols □), previous results of Gäggeler, et al. [Gäg1989] (open symbols with an ×), and previous results of Oganessian, et al. [Oga2000c] (open circles o) for the ^{208}Pb(^{48}Ca,2n)^{254}No reaction.

4.4.2 ^{253}No and ^{252}No

Correlation searches were performed to look for evaporation residue alpha decay correlations as well as evaporation residue spontaneous fission correlations. The evaporation residue alpha decay correlation search performed was similar to the correlation search performed looking for ^{255}No and ^{254}No with the PPAC in place. The alpha energy window was altered to look for the alpha decay of ^{253}No (7.920 MeV – 8.201 MeV) and ^{252}No (8.37 MeV – 8.45 MeV). The evaporation residue energy window (1 – 14 MeV), the PPAC condition window (1000 – 2500), and the position difference window (-20 – 15 pixels) all remained the same. The time window between evaporation residue implantation and alpha decay was altered depending on the half-life of ^{253}No (0 – 1000 seconds) and ^{252}No (0 – 25 seconds). The evaporation residue spontaneous fission correlation search differed from the search for evaporation residue alpha decay correlations in two ways. First, the energy condition for a spontaneous fission correlation search is much larger and done in channels not energy. No fission calibration was performed before the experiment and therefore no reliable energy determination was made. Second, the position window was expanded to include a much larger section of the detector. Because of the large energy signal of a fission fragment, the code is unable to calculate an accurate position determination for fission fragment signals based on the position signals present in the data. For this evaporation residue spontaneous fission correlation search, the spontaneous fission energy window was set at 500-4000 channels and the difference in position window was set at ±250 pixels, or ±14.5 millimeters. A total of 195 evaporation residue ^{253}No alpha decays correlations, 6 evaporation residue ^{252}No alpha decay correlations, and 2 evaporation residue ^{252}No spontaneous fission

correlations were observed. A decay curve was made from the correlations observed in the ^{253}No data with 25 second time bins. Using MLDS and the relative decay information, half-lives and initial activities for ^{253}No and ^{252}No were determined. The decay curve and the results of the MLDS fits can be seen in Table 4.15.

Table 4.15: Decay curves and results of MLDS fits for the correlations from the ^{253}No and ^{252}No reactions at an excitation energy of 33.8 MeV. The time bins for the decay curve are in seconds and correspond to the beginning of the time window (^{253}No $t_{½} = 102 \pm 18$ s, ^{252}No $t_{½} = 2.30 \pm 0.22$ s).

Time Bin	Counts
0	35
25	24
50	22
75	23
100	21
125	8
150	13
175	13
200	6
225	7
250	6
275	2
300	0
325	3
350	3
375	3
400	1
425	1
450	0
475	1
500	1
525	0
550	0
575	0
600	1
625	0
650	0
675	1

Isotope	Half-Life	Initial Activity	Number of Counts
^{253}No	$88\ ^{+6}_{-5}$ s	1.55 ± 0.13 s^{-1}	$196\ ^{+17}_{-16}$
^{252}No	$3.0\ ^{+1.2}_{-0.9}$ s		6

Production cross sections were then calculated for the two reactions based on the results of the MLDS fits found in Table 4.15. The production cross section for the $^{208}Pb(^{48}Ca,3n)^{253}No$ reaction was found to be 53 ± 14 nb at an excitation energy of 33.8 MeV and the production cross section for the $^{208}Pb(^{48}Ca,4n)^{252}No$ was found to be $1.8\ ^{+1.1}_{-0.8}$ nb at an excitation energy of 33.8 MeV. These experimental results were then compared to the predictions of the HIVAP code using the Reisdorf and Schädel parameters. The prediction for the 3n-exit channel product, ^{253}No, was high by a factor of four while the prediction for the 4n-exit channel product, ^{252}No, was only high by a factor of two. These overestimations seem to get smaller as the excitation energies get higher showing that there might be a problem with the way the HIVAP parameters of Reisdorf and Schädel treat the entrance channel and its effects on the total fusion cross section. Figure 4.17 shows the comparison between the experimental data and the predictions of HIVAP for the $^{208}Pb(^{48}Ca,3n)^{253}No$ reaction and Figure 4.18 shows the comparison between the experimental data and the predictions of HIVAP for the $^{208}Pb(^{48}Ca,4n)^{252}No$ reaction.

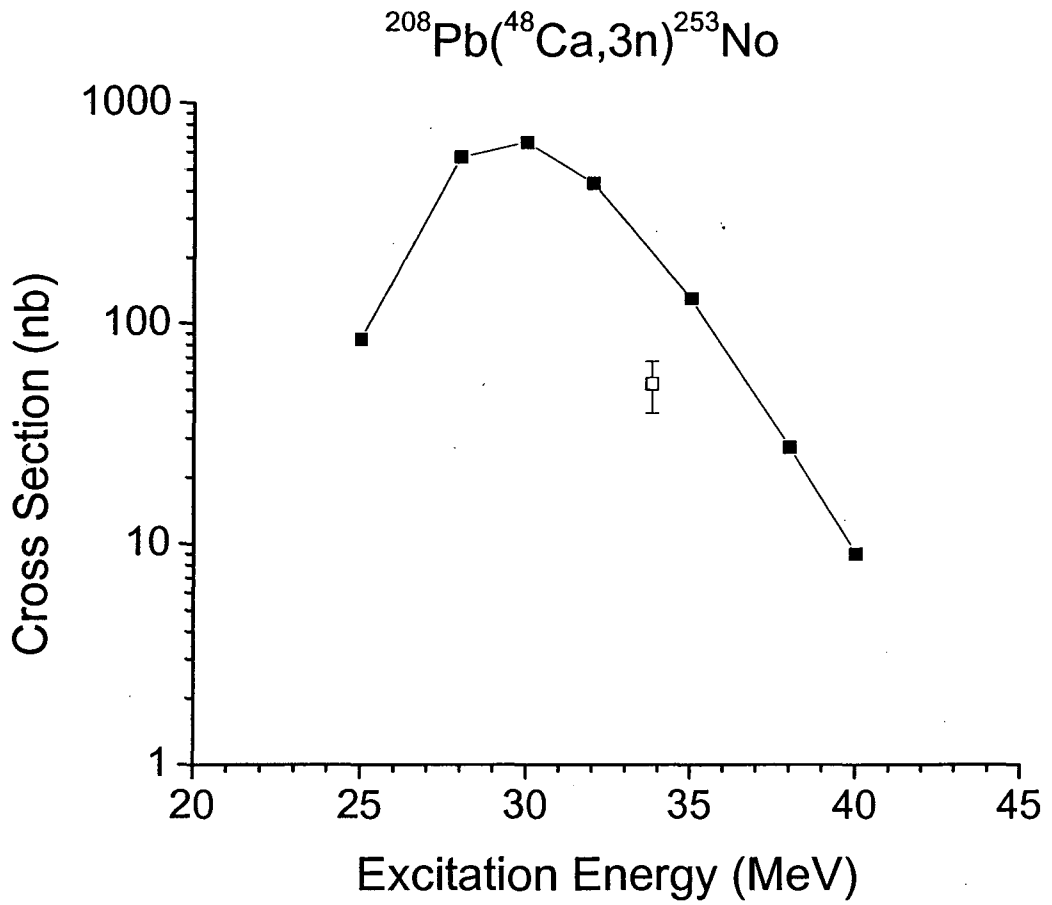

Figure 4.17: Predictions of the HIVAP code using the Reisdorf and Schädel parameters (solid symbols ■) and the experimental production cross sections (open symbols □) for the ^{208}Pb(^{48}Ca,3n)^{253}No reaction.

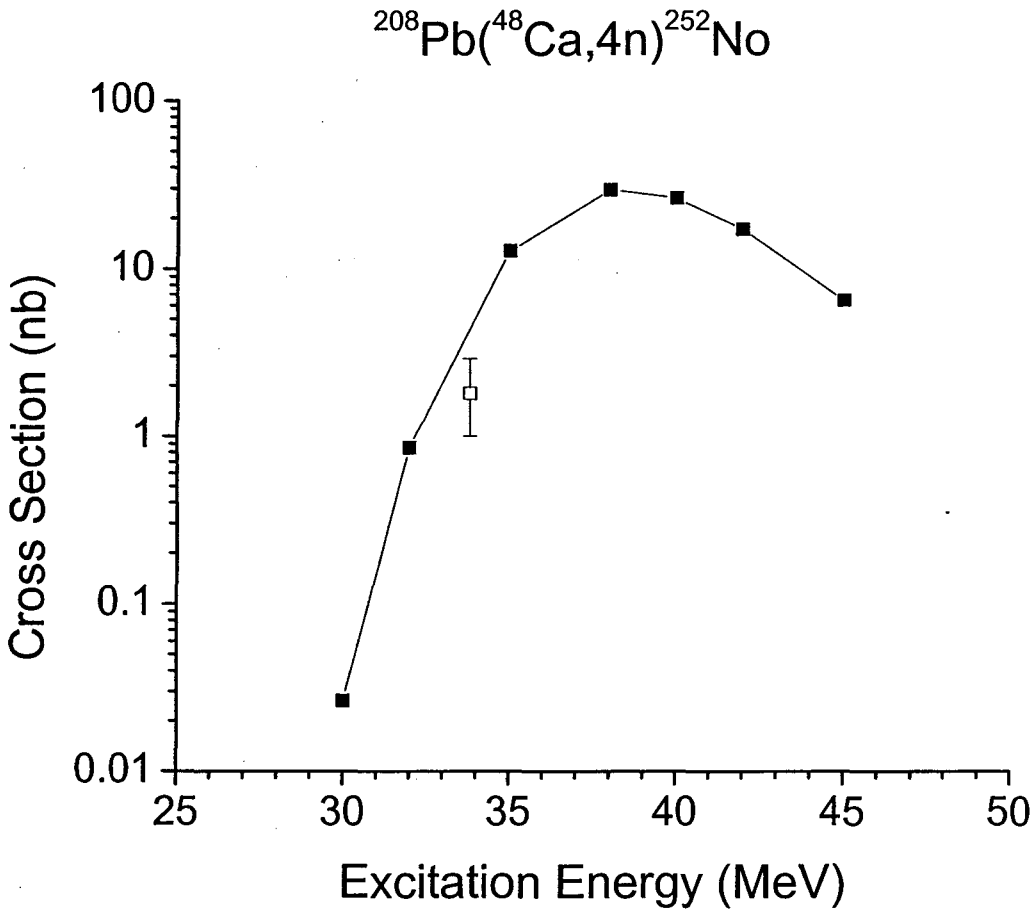

Figure 4.18: Predictions of the HIVAP code using the Reisdorf and Schädel parameters (solid symbols ■) and the experimental production cross sections (open symbols □) for the ^{208}Pb(^{48}Ca,4n)^{252}No reaction.

4.5 $^{208}Pb + ^{50}Ti$

^{257}Rf (E_α = 8.774(8), 9.013(8) MeV, $t_{1/2}$ = 4.7 ± 0.3s) and ^{256}Rf (SF, $t_{1/2}$ = 6.7 ± 0.2 ms) were produced in the reaction of ^{208}Pb and ^{50}Ti. The reactions specifics for the $^{208}Pb(^{50}Ti,xn)^{258-x}Rf$ experiment are located in Table 4.16. The Coulomb barrier for this experiment was 239.4 MeV. The remaining experimental parameters were quite similar to previous experiments that used the BGS. The helium pressure in the BGS was held around 1.0 Torr. Approximately 90 ± 5% of the evaporation residues that made it to the focal plane detector were detected. The focal plane detector had a 50 ± 2% efficiency for detecting alpha decay and a 100 ± 2% efficiency for detecting spontaneous fission decay. The difference between the magnetic rigidities of the compound nuclei and the transfer products were similar to those obtained for the $^{208}Pb(^{48}Ca,xn)^{256-x}No$ reaction, and therefore the efficiency of the BGS was 45 ± 10%. A PPAC was used in the search for ^{257}Rf and ^{256}Rf to help discriminate between events that originated in the focal plane detector and those that occurred as a result of implantation in the focal plane detector. Calibrations for this experiment were performed by examining the decay products from the $^{148}Sm(^{50}Ti,xn)^{198-x}Po$ reaction: ^{197m}Po (E_α = 6.3834(24) MeV), ^{196}Po (E_α = 6.520(3) MeV), ^{195}Po (E_α = 6.609(5) MeV), ^{195m}Po (E_α = 6.699(5) MeV), and ^{194}Po (E_α = 6.843(3) MeV).

Table 4.16: Reaction specifics for the $^{208}Pb(^{50}Ti,xn)^{258-x}Rf$ experiment. CYC denotes cyclotron energies, COT denotes center of target energies, and E^* denotes excitation energies.

E_{CYC} (MeV)	E_{COT} (MeV)	E^* (MeV)	Current (eμA)	Dose ($\times 10^{16}$)	Rutherfords	Time (s)
230.0	226.0	12.9	2.78 ± 0.14	5.4 ± 0.3	19958400	37482
235.0	231.0	16.9	2.21 ± 0.11	1.27 ± 0.06	4471680	11030
237.0	233.1	18.6	1.39 ± 0.07	0.86 ± 0.04	2970880	11862
240.0	236.1	21.0	3.25 ± 0.16	2.16 ± 0.11	7297920	12776

4.5.1 ^{257}Rf

Correlation searches were performed at each of the four energies studied. The first correlation search focused on looking for correlations between evaporation residues and alpha decay from ^{257}Rf. The correlation search parameters were as follows: time window (0 – 45 seconds), evaporation residue energy window (1 – 14 MeV), alpha decay energy window (8.5 – 9.2 MeV), position window (±15 pixels, ±0.87 mm), and PPAC window (1000 – 2500). A total of 118 correlations were seen at the four different energies. No correlations were seen at the lowest energy of 226.0 MeV, 43 correlations were seen at 231.0 MeV, 29 correlations were seen at 233.1 MeV, and 46 correlations were seen 236.1 MeV. Because of the effectiveness of the BGS in separating out impurities, and because the decay region around ^{257}Rf was fairly clear, all of the correlations observed were assumed to have come from evaporation residue ^{257}Rf alpha decay correlations. A decay curve was made from the sum of the correlations from the four different experiments and an experimental half-life of $5.1\ ^{+0.5}_{-0.4}$ s (^{257}Rf $t_{½} = 4.7 \pm 0.3$ s) was determined using MLDS. Figure 4.19 shows the results of the correlation search for all of the experiments performed. The various decay energies of ^{257}Rf are clearly seen in the top graph (a.) of Figure 4.19 and the broad distribution of the evaporation residues is seen in the middle graph (b.). Finally, the position window (c.) is clearly shown in the bottom graph and illustrates that the correlations occur within a very small separation.

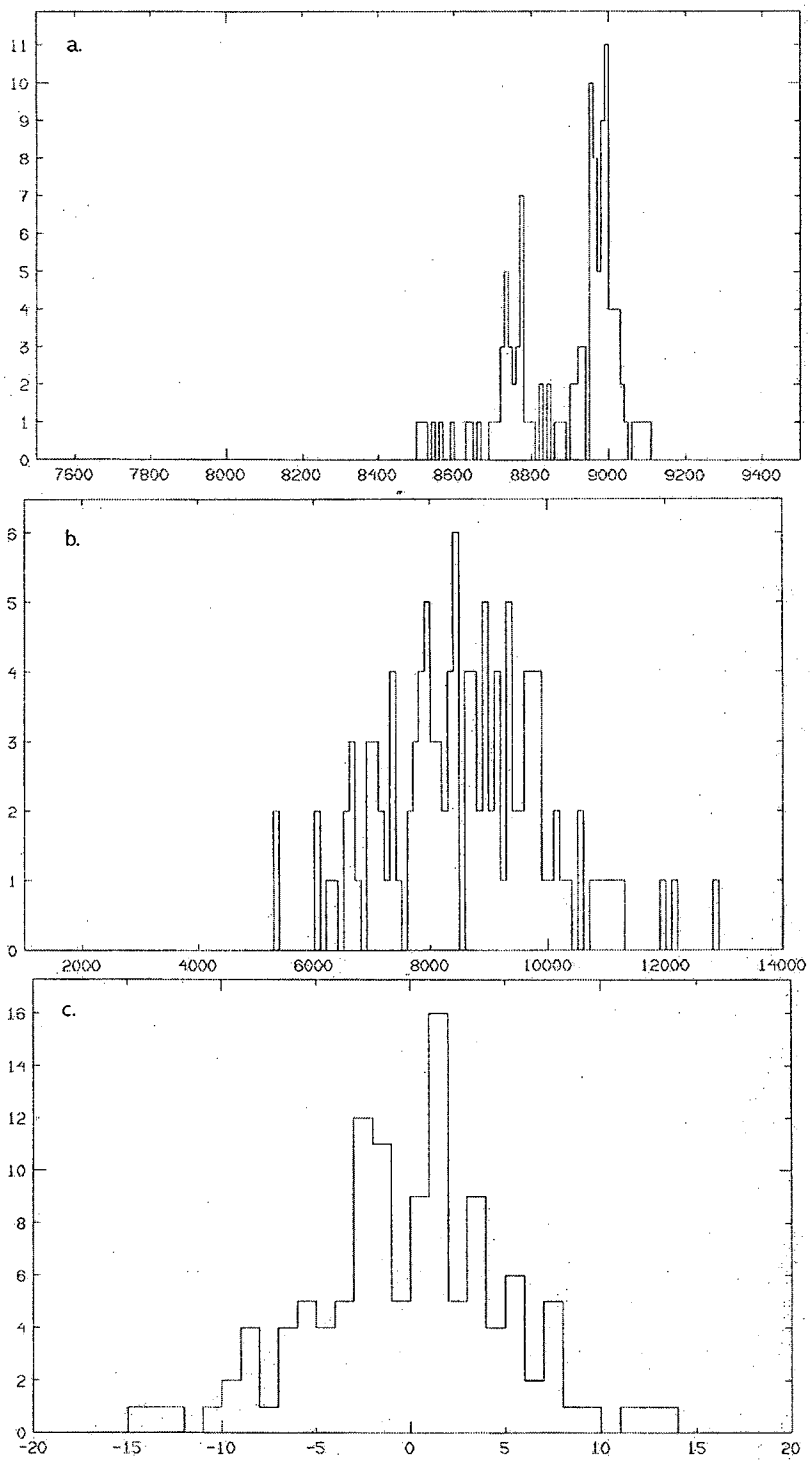

Figure 4.19: Correlated alpha decay spectrum (a.), evaporation residue spectrum (b.), and difference in position distribution (c.) for the sum of the four experiments performed in the $^{208}Pb(^{50}Ti,1n)^{257}Rf$ experiment. Energies for windows (a.) and (b.) are in keV. The difference in position distribution (c.) is in units of detector pixels.

A second correlation search was performed looking for alpha-alpha correlations from the decay of ^{257}Rf and ^{253}No. The correlation search parameters were as follows: time window (0 – 1000 seconds), mother alpha decay window (8.5 – 9.2 MeV), daughter alpha decay window (7.9 – 8.2 MeV), position window (±15 pixels, ±0.87 mm), and PPAC window (1000 – 2500). The time window and daughter alpha decay windows were chosen to look for the 1.7-minute, 8.01-MeV alpha activity of ^{253}No. A total of 30 alpha-alpha correlations were seen between ^{257}Rf and ^{253}No. No correlations were seen at 226.0 MeV, 13 correlations at 231.0 MeV, 7 correlations at 233.1 MeV, and 10 correlations at 236.1 MeV. These numbers are close to what would be expected from a 50 ± 2% detector efficiency and an 80 ± 5% alpha decay branch for ^{253}No. A decay curve was made from the sum of the alpha-alpha correlations and an experimental half-life of $81\ ^{+13}_{-12}$ s (^{253}No $t_{½}$ = 102 ± 18 s) was determined using MLDS. Figure 4.20 shows the results of the alpha-alpha correlation search performed. The top window (a.) illustrates the decays of the daughter isotope ^{253}No. The middle window shows the mother ^{257}Rf alpha decays that were correlated to the ^{253}No seen in the top window. The bottom window (c.) again illustrates the small distance between correlated events. The graphs clearly show the multiple decay energies present in the decay of ^{257}Rf and the single decay energy of ^{253}No.

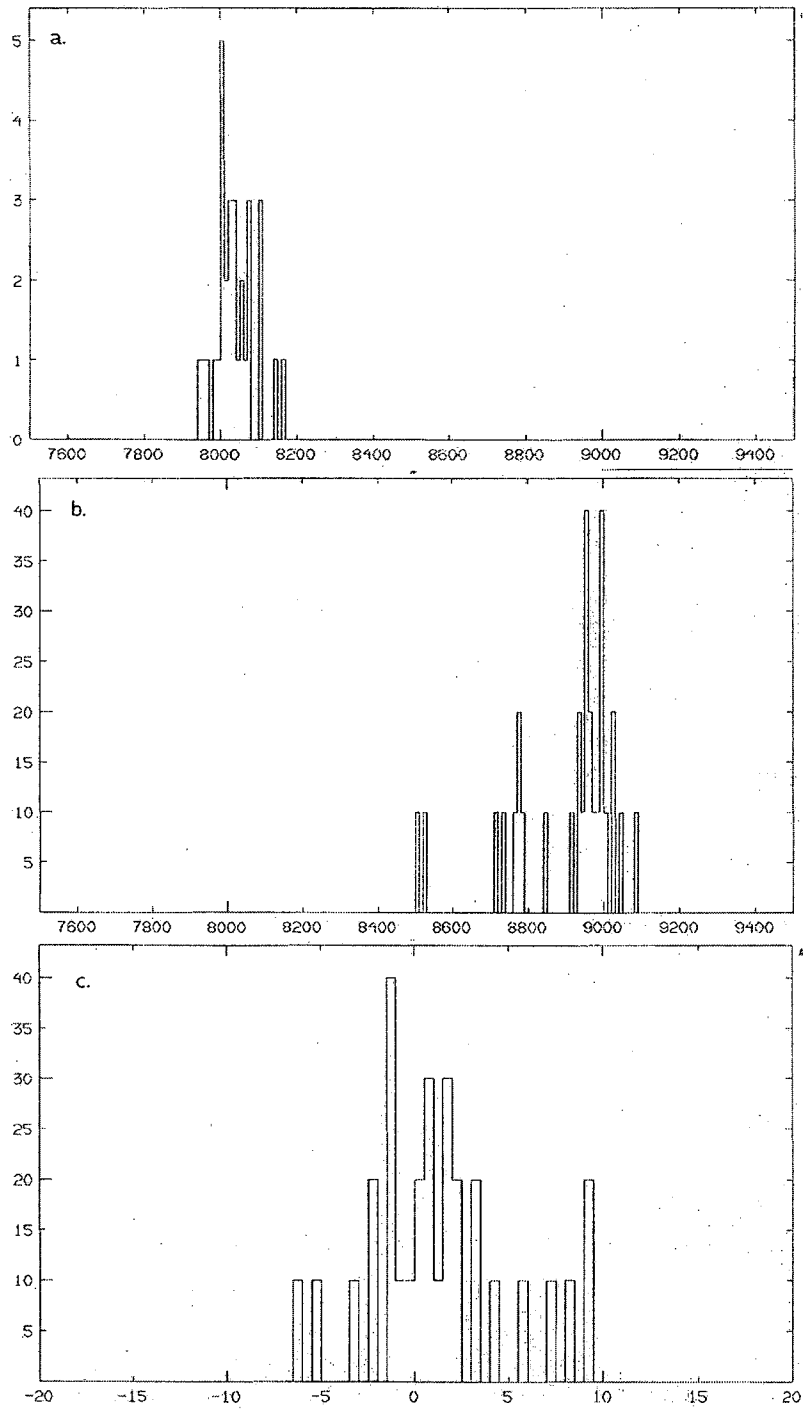

Figure 4.20: Correlated daughter alpha decay spectrum (a.), mother alpha decay spectrum (b.), and difference in position distribution (c.) for the sum of the four experiments performed in the ^{208}Pb(^{50}Ti,1n)^{257}Rf experiment. Energies for windows (a.) and (b.) are in keV. The difference in position distribution (c.) is in units of detector pixels.

Using the number of correlations found at each of the individual energies, a 79.6 ± 2.0% alpha decay branching ratio, and a 45 ± 10% BGS efficiency, the production cross sections were calculated for the $^{208}Pb(^{50}Ti,1n)^{257}Rf$ reaction at the four energies studied. The production cross sections obtained at the associated excitation energies were: ≤ 0.086 nb (12.9 MeV), 16 ± 4 nb (16.9 MeV), 16 ± 5 nb (18.6 MeV), and 10 ± 3 nb (21.0 MeV). The cross section at 12.9 MeV is a one event upper limit cross section as no correlations that matched the search parameters were found. These cross sections were compared with predictions from the HIVAP code using the Reisdorf and Schädel parameters. As was seen with the $^{208}Pb(^{48}Ca,1n)^{255}No$ reaction, the 1n-exit channel predictions of HIVAP greatly overestimate the production cross sections. The experimental cross sections were smaller than the predictions by a couple of orders of magnitude at the lower energies. It also appears that the HIVAP code incorrectly predicts the center of the excitation function, usually to lower excitation energies than what is seen experimentally. The experimental cross sections were also compared to previous experimental $^{208}Pb(^{50}Ti,1n)^{257}Rf$ results of Heßberger, et al. [Heβ1997]. These experimental cross sections are a lot closer in magnitude than the predictions of HIVAP. There still appears to be a difference in the center of the excitation function between the results of Heßberger and this thesis. It appears the maximum of the 1n-exit channel excitation function appears around 16 MeV for Heßberger whereas the maximum appears around 18-19 MeV for the results of this thesis. Figure 4.21 shows the comparison of the predictions from HIVAP and the experimental results for the $^{208}Pb(^{50}Ti,1n)^{257}Rf$ reaction.

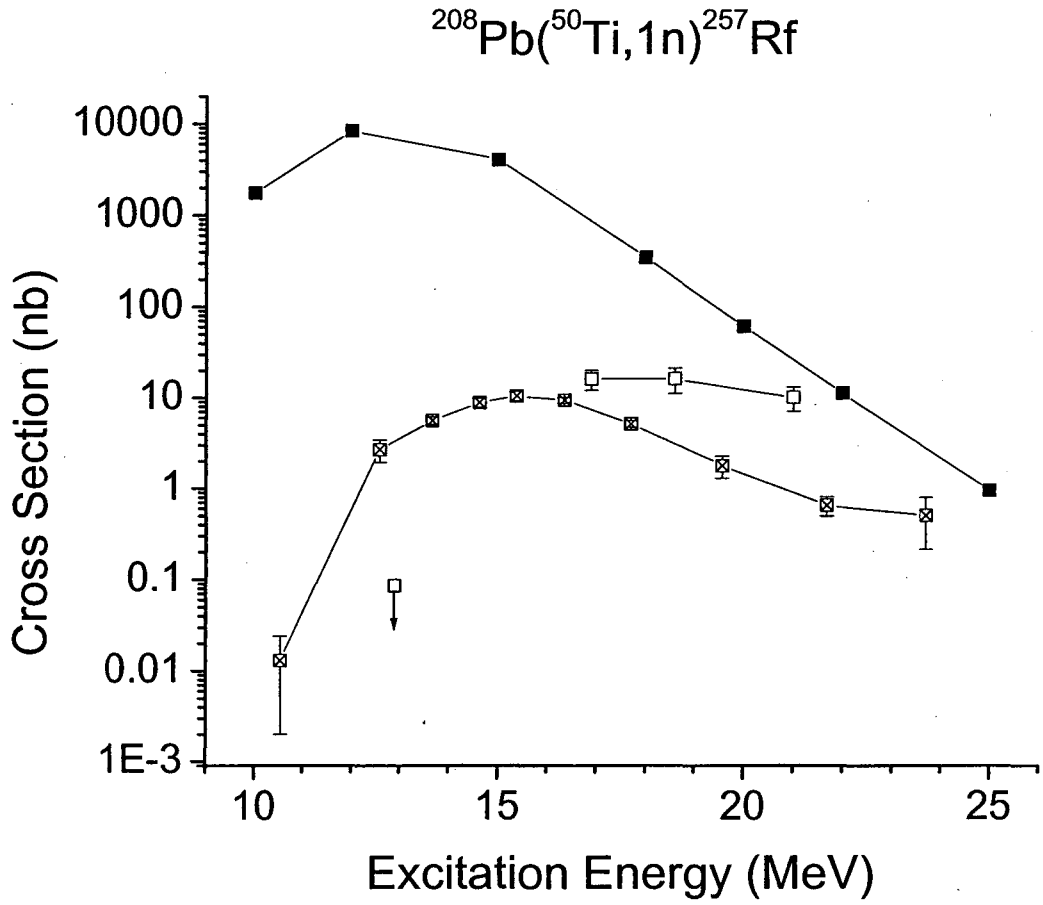

Figure 4.21: Predictions of the HIVAP code using the Reisdorf and Schädel parameters (solid symbols ■), the experimental production cross sections (open symbols □), and the previous results of Heßberger, et al. [Heβ1997] (open symbols with an ×) for the ^{208}Pb(^{50}Ti,1n)^{257}Rf reaction.

4.5.2 ^{256}Rf

Correlations searches were performed looking for the spontaneous fission decay of ^{256}Rf in the attempt to calculate cross sections for the 2n-exit channel from the ^{208}Pb(^{50}Ti,2n) reaction. Spontaneous fission correlation searches differ from evaporation residue alpha decay correlation searches in two ways. The first difference is that the position window is larger when searching for fission correlations. Fission products are more energetic than alpha decays and therefore are more likely to travel farther in the silicon detector. The large amount of energy deposited by the fission products also makes position determination more difficult. The focal plane detector was setup so that high energy fission products occurring near the top or bottom of a strip were likely to saturate the signal making accurate position determinations difficult. Therefore a larger position window is used when looking for evaporation residue spontaneous fission correlations. The second difference lies in the energy calibrations for the higher energy fissions. Spontaneous fission sources are not used in the calibration of the focal plane detector to eliminate the possibility of background fission activity in the detector. Without an appropriate energy calibration, the spontaneous fission energy window is in channel numbers and not keV. Aside from these two differences, the rest of the correlation search procedure was similar to those already performed.

When looking for the ^{256}Rf produced in the ^{208}Pb(^{50}Ti,2n) reaction, the following correlation search parameters were set. Time window (0 – 70 milliseconds), evaporation residue energy window (1 – 14 MeV), spontaneous fission energy window (1650 – 4000 channels), position window (±250 pixels, ±14.5 mm), and PPAC condition window (1000 – 2500). These correlation search parameters were used to find 4 evaporation

residue fission correlations at an excitation energy of 16.9 MeV, 5 evaporation residue fission correlations at an excitation energy of 18.6 MeV, and 77 evaporation residue fission correlations at an excitation energy of 21.0 MeV. The trend to higher numbers of correlations was consistent with the increase in excitation energy moving from an area where the 1n-exit channel was more prominent to an area where the 2n-exit channel was more prominent. A sum of all of the correlations between evaporation residues and spontaneous fissions is shown in Figure 4.22.

The specific times between evaporation residue implantation and spontaneous fission were taken for each energy and made into decay curves for input into the decay curve fitting program MLDS. Initial activities as well as half-lives and the total number of counts at each excitation energy were obtained from the MLDS program. An experimental half-life of $7.0\ ^{+0.7}_{-0.6}$ ms (^{256}Rf $t_{½} = 6.7 \pm 0.2$ ms) was obtained for ^{256}Rf.

Using the number of counts obtained from MLDS, a detection efficiency of $100 \pm 2\%$, a BGS efficiency of $45 \pm 10\%$, and a $98\ ^{+2}_{-7}\%$ spontaneous fission branching ratio, cross sections for the ^{208}Pb(^{50}Ti,2n)^{256}Rf reaction were obtained as follows: $0.6\ ^{+0.5}_{-0.3}$ nb (16.9 MeV), $1.1\ ^{+0.8}_{-0.5}$ nb (18.6 MeV), and 6.7 ± 1.8 nb (21.0 MeV). These cross sections are compared to the results of Heßberger, et al. [Heβ1997], and compare fairly well. With the energy spread used, it was again easy to see the energy differences on the low energy side of the excitation functions. This discrepancy can only be explained by a differing energy between the two machines used to create the ^{50}Ti beams used in these experiments. The 2n-exit channel results were also compared to the predictions of the HIVAP code using the input parameters of Reisdorf and Schädel and

appear to be just as different from the code as the rest of the cold fusion reactions already shown. The cross section comparison can be seen in Figure 4.23.

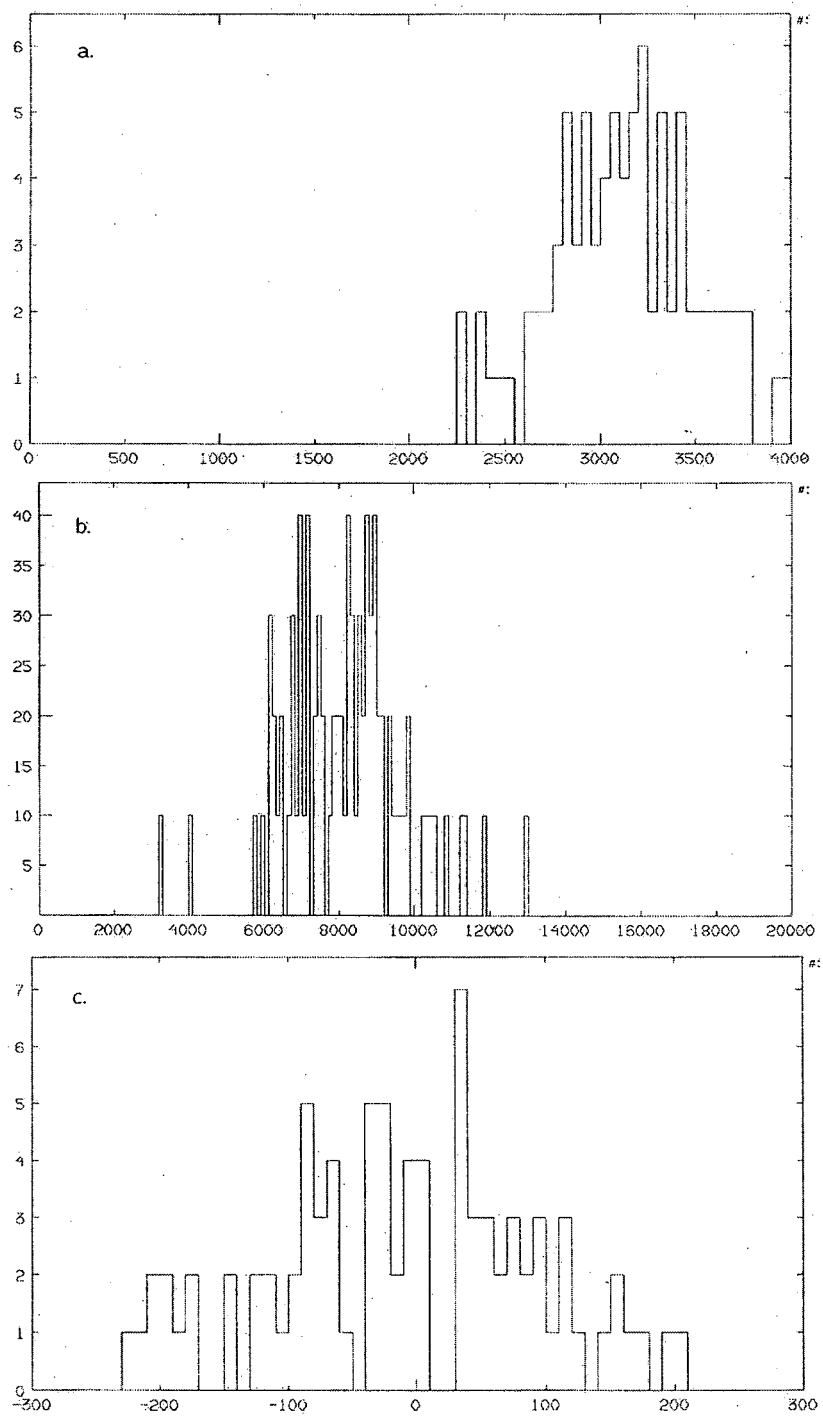

Figure 4.22: Correlated spontaneous fission decay spectrum (a.), evaporation residue spectrum (b.), and difference in position distribution (c.) for the sum of the three experiments performed in the $^{208}Pb(^{50}Ti,2n)^{256}Rf$ experiment. The top graph (a.) is in channels whereas the energy for window (b.) is in keV. The difference in position distribution (c.) is in units of detector pixels.

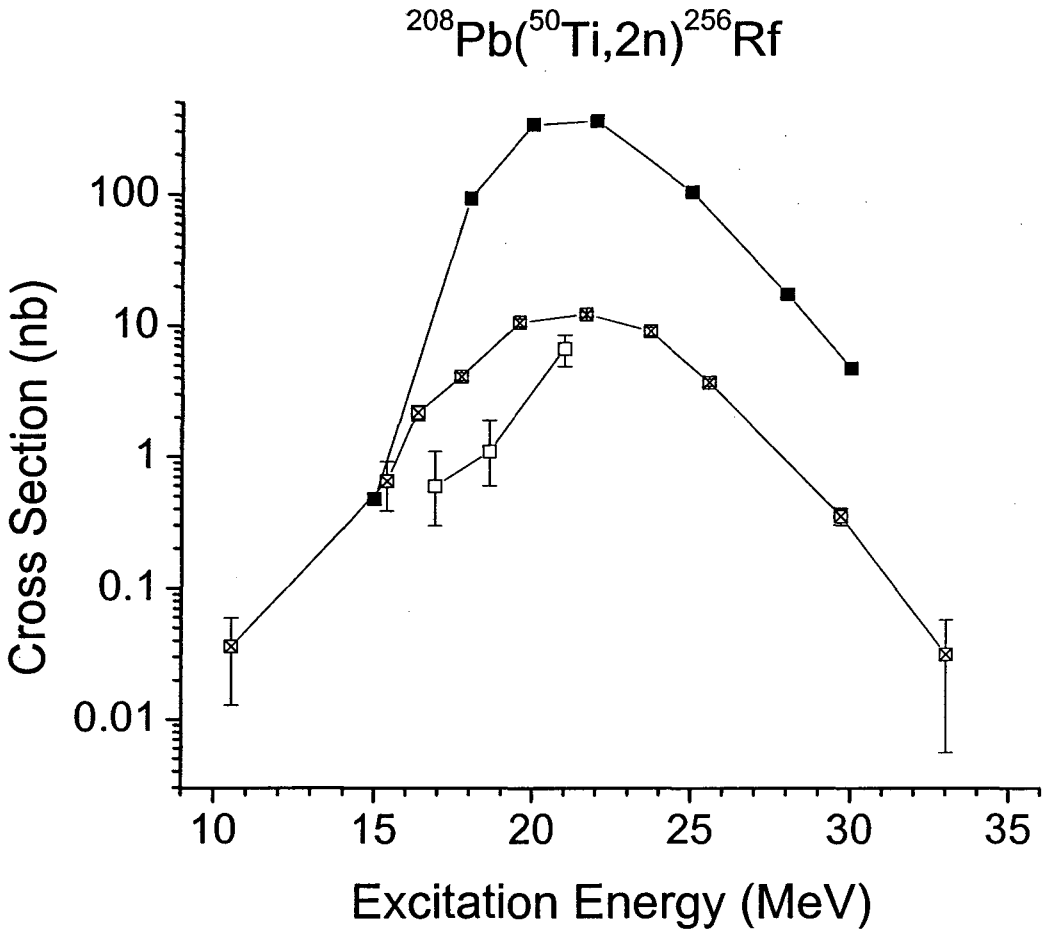

Figure 4.23: Predictions of the HIVAP code using the Reisdorf and Schädel parameters (solid symbols ■), the experimental production cross sections (open symbols □), and the previous results of Heßberger, et al. [Heβ1997] (open symbols with an ⊠) for the ^{208}Pb(^{50}Ti,2n)^{256}Rf reaction.

4.6 $^{208}Pb + {}^{51}V \rightarrow {}^{257}Db + 2n$

The $^{208}Pb(^{51}V,2n)^{257}Db$ reaction was examined in the attempt to study a possible production route of dubnium for chemical study. This reaction was chosen and would be compared with a similar reaction, $^{209}Bi(^{50}Ti,2n)^{257}Db$ discussed subsequently, which produced the same compound nucleus.

$^{51}V^{11+}$ at energy of 255.0 MeV from the cyclotron lost approximately 5 MeV in the carbon windows and half of the target leaving 250.0 MeV in the center of the target which corresponded to an excitation energy of 24.9 MeV. The Coulomb barrier was 250.7 MeV. The experiment lasted 38535 seconds delivering a total beam dose of $(2.90 \pm 0.14) \times 10^{16}$ particles for an average current of 1.33 ± 0.07 eμA. A total of 10375000 Rutherford events were collected during the experiment. The compound nucleus recoils travel through 1 Torr of helium in the gas-filled chamber and had a magnetic rigidity of 2.05 Tm whereas the transfer products of the reaction had a magnetic rigidity of 1.48 Tm giving a BGS efficiency of 45 ± 10%. No PPAC was used in this particular experiment, but because of the short half-life of ^{257}Db (E_α = 8.970(20) MeV, $t_{½} = 1.3\ ^{+0.5}_{-0.3}$ s), it wasn't a concern. The experiment was calibrated using the $^{154}Sm(^{51}V,xn)^{205-x}At$ reaction at an excitation energy of 75.8 MeV which would lead to the emission of between five and eight neutrons. The following activities were used in the calibration: ^{200}Po (E_α = 5.8619(18) MeV), ^{199m}Po (E_α = 6.059(3) MeV), ^{198}Po (E_α = 6.1820(22) MeV), ^{200m}At (E_α = 6.5374(23) MeV), ^{199}At (E_α = 6.643(3) MeV), ^{198}At (E_α = 6.754(4) MeV), and ^{198m}At (E_α = 6.856(4) MeV).

Once the data was collected, correlation searches were performed looking for both evaporation residue alpha decay correlations as well as alpha-alpha decay correlations. The alpha decay daughter of ^{257}Db is ^{253}Lr (E_α = 8.800(20) MeV, $t_{½}$ = 1.3 $^{+0.6}_{-0.3}$ s). With these decay half-lives and decay energies as a guide the following correlation parameters were set looking for the evaporation residue alpha decay correlations: time window (0 – 15 seconds), position window (±15 pixels, ±0.87 mm), evaporation residue energy window (2 – 14 MeV), alpha decay energy window (8.90 – 9.25 MeV). The following correlation parameters were set for the search for alpha-alpha correlations: time window (0 – 15 seconds), position window (±15 pixels, ±0.87 mm), mother alpha energy window (8.90 – 9.25 MeV), daughter alpha energy window (8.65 – 8.87 MeV).

A total of 10 evaporation residue alpha decay correlations were seen as well as 5 alpha-alpha correlations. The number of alpha-alpha correlations is expected considering the branching ratio for alpha decay for ^{253}Lr is 98 ± 2% and the detection efficiency for alpha decay in the focal plane detector was 50 ± 2%. From these efficiencies, five alpha-alpha decay correlations would be expected and were seen. Decay curves were made from the correlation data and analyzed using MLDS. Half-lives and initial activities were determined from the MLDS fits and used to calculated the cross sections. Experimental half-lives of 1.1 ± 0.2 s (^{257}Db $t_{½}$ = 1.3 $^{+0.5}_{-0.3}$ s) for ^{257}Db and 0.9 $^{+0.4}_{-0.3}$ s (^{254}Lr $t_{½}$ = 1.3 $^{+0.6}_{-0.3}$ s) for ^{253}Lr were determined.

Using the number of evaporation residue alpha decay correlations, a BGS efficiency of 45 ± 10%, a 95 ± 5% evaporation residue detection efficiency, and a 82 ± 11% alpha-decay branching ratio for ^{257}Db, a production cross section was

calculated for the one experimental energy. A production cross section of $1.4^{+0.7}_{-0.6}$ nb was calculated for an excitation energy of 24.9 MeV. As the experiment only considered one experimental energy, an assessment of the behavior of the excitation function was difficult. Nonetheless, this experimental point was compared with the predictions of the HIVAP code using the Reisdorf and Schädel parameters. Again, the HIVAP predictions are not similar to the cross sections seen experimentally. The comparison of the predictions with the experimental cross section can be seen in Figure 4.24.

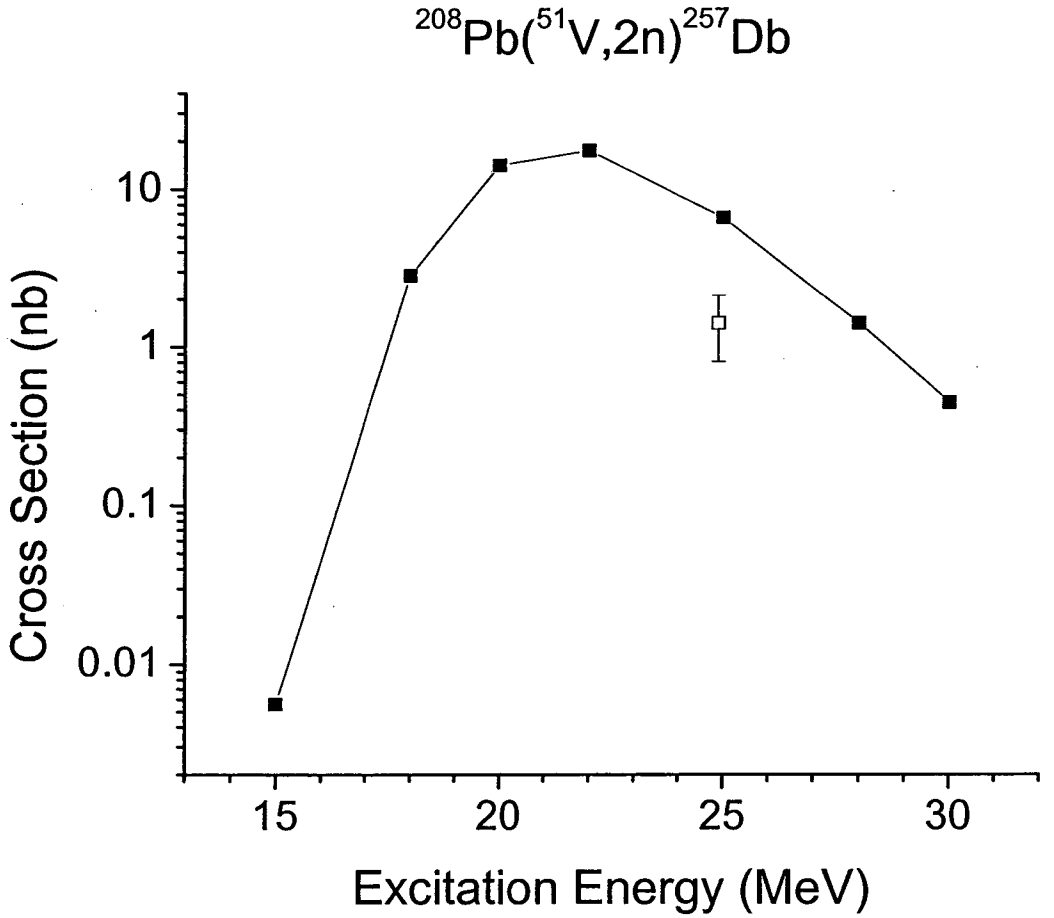

Figure 4.24: Predictions of the HIVAP code using the Reisdorf and Schädel parameters (solid symbols ■), the experimental production cross sections (open symbols □) for the $^{208}Pb(^{51}V,2n)^{257}Db$ reaction.

4.7 $^{209}Bi + ^{50}Ti$

The $^{209}Bi + ^{50}Ti$ reaction was examined as another possible production route for possible chemistry experiments with dubnium. The experiment was also examined to look at the effects of different target and projectile combinations forming the same compound nucleus. Two separate experiments were performed for this reaction at two different energies. The Coulomb barrier for this reaction was 253.2 MeV.

The first experiment was performed with $^{50}Ti^{12+}$ beams at an energy of 235 MeV, which then lost approximately 4 MeV as it passed through the carbon windows and half of the bismuth target leaving 231.2 MeV in the center of the target. This corresponded to a compound nucleus excitation energy of 15.0 MeV.

The experiment lasted 13413 seconds at an average beam current of 2.87 ± 0.15 eμA which corresponded to a total beam dose of $(2.00 \pm 0.10) \times 10^{16}$. A total of 6091472 Rutherford scattered beam events were recorded during the experiment. The magnetic rigidity of the compound nucleus recoils were 2.10 Tm whereas the magnetic rigidity of the transfer products was 1.48 Tm. This led to a BGS efficiency of $45 \pm 10\%$. No PPAC was used in this first experiment. About $90 \pm 5\%$ of the evaporation residues making it to the focal plane detector were actually detected. This first experiment had no calibration reaction.

The second experiment was run at a slightly higher energy. 237 MeV $^{50}Ti^{12+}$ lost approximately 3.5 MeV leaving 233.5 MeV at the center of the target which corresponded to a compound nucleus excitation energy of 16.9 MeV.

The second experiment lasted a total of 23510 seconds at an average beam current of 1.68 ± 0.09 eμA giving a total beam dose of $(2.05 \pm 0.11) \times 10^{16}$. A total of 6293120

Rutherford scattered beam events were recorded. The magnetic rigidities of the evaporation residues and transfer products in the BGS remained 2.10 Tm and 1.48 Tm respectively, leaving the BGS efficiency at 45 ± 10%. A PPAC detector was used in this second experiment to discriminate between events originating in the focal plane detector and those recorded as implantation events. Again, approximately 90 ± 5% of the evaporation residue events making it to the focal plane detector were actually detected.

The focal plane detector for the second experiment was calibrated using the $^{nat}Dy(^{50}Ti,xn)^{214-x}Ra$ reaction. The most prominent isotopes of natural dysprosium are ^{162}Dy, ^{163}Dy, and ^{164}Dy. At an excitation energy of approximately 55-60 MeV, the 4n- and 5n-exit channels were the preferred neutron evaporation channels. The focal plane detectors were calibrated using the following isotopes: ^{205}Rn (E_α = 6.262(3) MeV), ^{204}Rn (E_α = 6.4189(25) MeV), $^{208,209}Fr$ (E_α = 6.641(3) MeV, 6.646(5) MeV), $^{209,210}Ra$ (E_α = 7.008(5) MeV, 7.019(5) MeV), and ^{208}Ra (E_α = 7.133(5) MeV).

4.7.1 ^{258}Db and ^{257}Db

The ^{258}Db (E_α = 9.172(15) MeV, $t_{1/2} = 4.4\ ^{+0.9}_{-0.6}$ s) produced in this reaction was produced at excitation energies corresponding to the supposed maximum in the ^{209}Bi(^{50}Ti,1n) excitation function. Correlation searches were aimed at finding the evaporation residue alpha decay correlations of ^{258}Db as well as possible evaporation residue electron capture spontaneous fission correlations of ^{258}Rf (SF, $t_{1/2} = 12 \pm 2$ ms)

The first correlation search focused on looking for the evaporation residue alpha decay correlations for ^{258}Db at 231.2 MeV. In this particular experiment, no PPAC was used and no energy calibration was present making the search for decays somewhat difficult. Nonetheless, a broad energy window was used (~ 8 – 10 MeV), with the common position window and no positive correlations were seen. A possible correlation was seen, but without a proper energy calibration, a positive identification was impossible. A one event upper limit production cross section of 0.33 nb was calculated for ^{258}Db at an excitation energy of 15.0 MeV.

The second correlation search again looked for the evaporation residue alpha decay correlations of ^{258}Db, this time at 233.5 MeV. Identification of positive correlations was made easier by the use of the PPAC and a proper calibration. The following correlation search parameters were used: time window (0 – 45 seconds), position window (±15 pixels, ±0.87 mm), evaporation residue energy window (1-14 MeV), alpha decay energy window (8.8 – 9.5 MeV), and PPAC window (1000 – 2500). A total of 10 correlations was seen at 233.5 MeV. The experimental half-life of the activity was determined from an MLDS fit to the lifetimes of the 10 correlations to be $2.9\ ^{+1.0}_{-0.8}$ seconds. The possibility that some of the events could have resulted from

^{257}Db (E_α = 8.970(20) MeV, $t_{½}$ = 1.3 $^{+0.5}_{-0.3}$ s) was small. On one side, the excitation energy is more favorable to the 1n-exit channel versus the 2n-exit channel, and two, no correlations were seen at the most prominent energy for ^{257}Db at 8.970 MeV reducing the probability that decays at the other energies were possible. With a 50 ± 2% alpha decay detection efficiency and a 67 $^{+5}_{-9}$% alpha decay branching ratio, a production cross section of 3.1 $^{+1.5}_{-1.3}$ nb was calculated at an excitation energy of 16.9 MeV. Using an 82 ± 11% alpha decay branching ratio, a one event upper limit production cross section of 0.25 nb was calculated for the 2n-exit channel ^{257}Db.

The third correlation search focused on looking for spontaneous fissions in correlation with evaporation residues. The spontaneous fissions would arise from the decay of ^{258}Rf, the electron capture decay daughter of ^{258}Db. The following search parameters were used: time window (0 – 45 seconds), position window (±250 pixels, ±14.5 mm), evaporation residue energy window (1 – 14 MeV), spontaneous fission channel window (1650 – 4000), and PPAC window (1000 – 2500). A total of 8 evaporation residue spontaneous fission correlations were seen using these parameters. Taking into account a 50 ± 2% alpha detection efficiency, a 33 $^{+9}_{-5}$% electron capture branching ratio versus a 67 $^{+5}_{-9}$% alpha decay branching ratio, a 100 ± 2% spontaneous fission detection efficiency, and an 87 ± 11% spontaneous fission branching ratio in ^{258}Rf, we should have expected 8.7 spontaneous fissions. This results gives further support to claim that only the 1n-exit channel product, ^{258}Db was seen, and not ^{257}Db the 2n-exit channel product.

These production cross sections and upper limit cross sections were compared to previous experiments of Heßberger et al. [Heβ2001a]. The comparisons with the available experimental data are somewhat difficult because of the fact that an incomplete excitation function was measured. Therefore, having only a few experimental points makes comparison difficult. However, it does appear that an energy shift in the 1n-exit channel excitation function is indeed present as it has been in the experiments already discussed. The absence of correlations at 15.0 MeV excitation energy is questionable though and could be the result of faulty experimental equipment. Without additional data points however, a more accurate comparison can not be performed. The experimental points were also compared to the results of predictions by the HIVAP code using the Reisdorf and Schädel parameters. The HIVAP code predictions again predict cross sections that are higher than those seen experimentally at these low excitation energies. Figure 4.25 and Figure 4.26 shows the results of the ^{209}Bi(^{50}Ti,1n)^{258}Db and ^{209}Bi(^{50}Ti,2n)^{257}Db reactions along with other experimental results and the predictions of HIVAP.

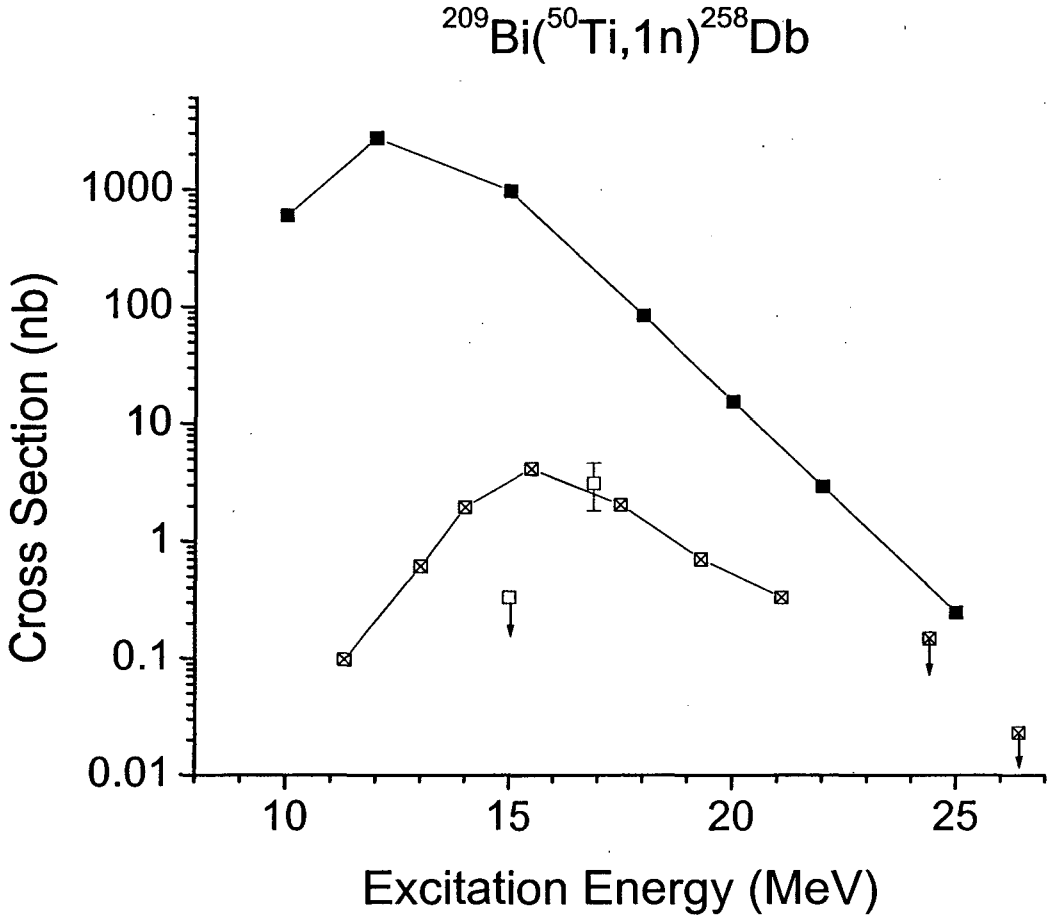

Figure 4.25: Predictions of the HIVAP code using the Reisdorf and Schädel parameters (solid symbols ■), the experimental production cross sections (open symbols □), and the previous results of Heßberger, et al. [Heβ2001a] (open symbols with an ×) for the ^{209}Bi(^{50}Ti,1n)^{258}Db reaction.

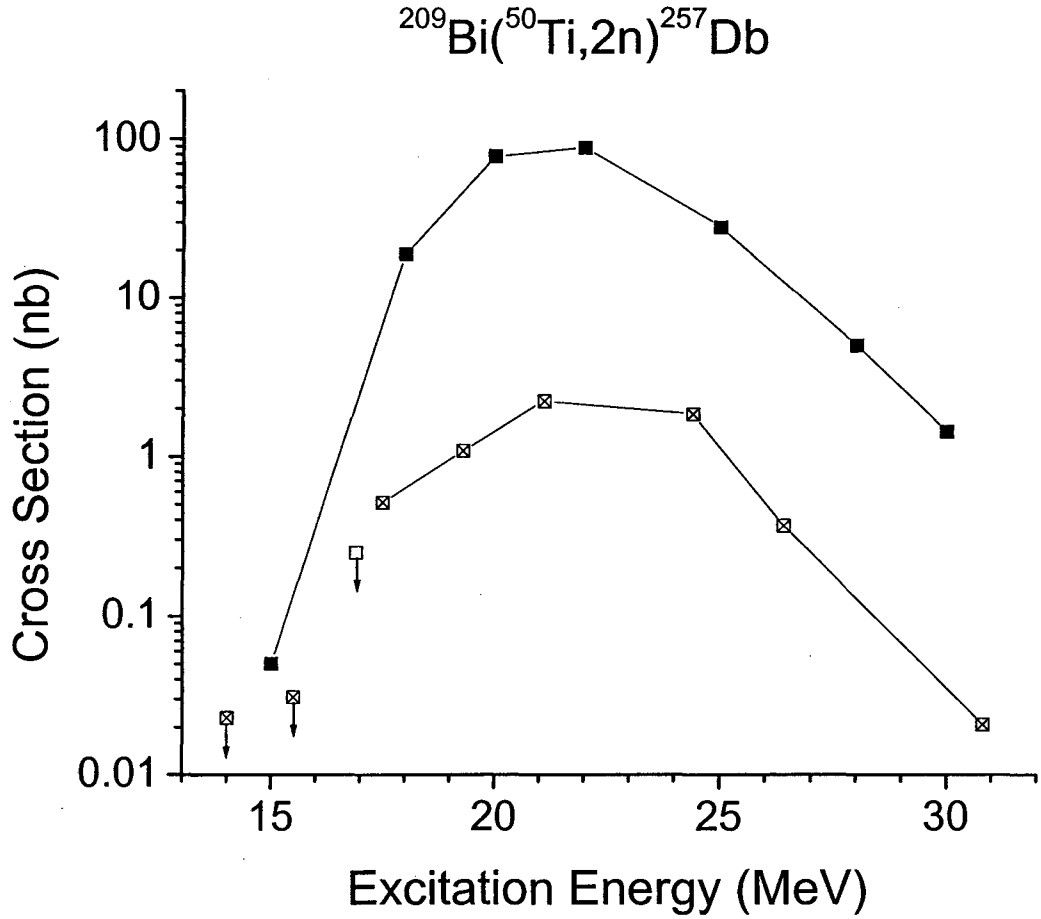

Figure 4.26: Predictions of the HIVAP code using the Reisdorf and Schädel parameters (solid symbols ■), the experimental production cross sections (open symbols □), and the previous results of Heßberger, et al. [Heβ2001a] (open symbols with an ×) for the ^{209}Bi(^{50}Ti,2n)^{257}Db reaction.

4.8 $^{209}Bi + {}^{51}V \rightarrow {}^{258}Sg + 2n$

^{258}Sg (SF, $t_{½} \approx 2.9$ ms) was produced in the reaction of ^{209}Bi and ^{51}V in the attempt to study the effect an odd number of protons in the target and projectile would have on production cross sections. Measurements had already been made on the even proton number reaction $^{208}Pb + {}^{50}Ti$. Adding a proton to both the target and projectile gave the vanadium on bismuth reaction. Studying the effects the odd protons have on the production cross sections would help determine future production routes to the heavy elements.

The reactions specifics for the $^{209}Bi(^{51}V,2n)^{258}Sg$ experiment are located in Table 4.17. The Coulomb barrier for this reaction was 253.2 MeV. The compound nuclei in these reactions had a magnetic rigidity of 2.06 Tm whereas the transfer products had a magnetic rigidity of 1.48 Tm. These rigidities corresponded to a BGS efficiency of 45 ± 10%. A PPAC was used in this experiment as in others to discriminate between evaporation residue implantations in the focal plane detector and fission events from ^{258}Sg. The event rate in the focal plane detector was small for this experiment, so it was assumed that 100 ± 2% of the evaporation residues that made it to the focal plane detector were detected. No spontaneous fission calibration had been performed prior to the experiment as long-lived spontaneous fission isotopes have a tendency to build up on the detector when performing calibration experiments.

Table 4.17: Reaction specifics for the $^{209}Bi(^{51}V,2n)^{258}Sg$ experiment. CYC denotes cyclotron energies, COT denotes center of target energies, and E^* denotes excitation energies.

E_{CYC} (MeV)	E_{COT} (MeV)	E^* (MeV)	Current (eμA)	Dose ($\times 10^{17}$)	Rutherfords	Time (s)
249.0	245.4	20.3	2.80 ± 0.14	1.37 ± 0.07	41446400	93943
252.0	248.4	22.7	2.68 ± 0.14	2.13 ± 0.11	62864000	152673
255.0	251.4	25.2	1.99 ± 0.10	2.26 ± 0.12	65129600	217916

Once all of the data had been collected, a detailed correlation search began looking for evaporation residue spontaneous fission correlations. Because the half-life of ^{258}Sg is approximately 2.9 milliseconds and decays primarily (~100%) through spontaneous fission [Heβ1997], the number of expected random correlations was extremely small (< 0.007 for each evaporation residue event). The following conditions were used to perform the correlation search: time window (0 – 50 milliseconds), position window (±250 pixels, ±14.5 mm), evaporation residue channel window (0 – 4000), spontaneous fission channel window (1650 – 4000), and PPAC window (1000 – 2500). Channel windows were used because no spontaneous fission energy calibration had been performed before the experiment. The window sizes were chosen based on previous experimental evidence for the appearance of fission events in the data.

A total of nine evaporation residue spontaneous fission correlation events were found at the three different energies. In the data, all of the correlations were seen with an evaporation residue event followed by a spontaneous fission as the next event. Table 4.18 contains a summary of the results of the correlation search for ^{258}Sg.

Table 4.18: Summary of evaporation residue spontaneous fission correlations from the $^{209}Bi(^{51}V,2n)^{258}Sg$ reaction. The energy "E" is listed as the center of target beam energy. "Strip" corresponds to the detector strip in which the event occurred. "dt" and "dp" correspond to the differences in time and position between the evaporation residue "EVR" and spontaneous fission "SF" events which are listed in channels.

E (MeV)	Date	Time	Strip	EVR (chan)	SF (chan)	dt (ms)	dp (mm)
245.4	10/15/01	08:35	14	3022	3111	6.005	7.1
248.4	10/13/01	11:12	3	2556	2940	4.019	3.4
	10/13/01	12:14	2	2363	3234	2.873	9.3
	10/13/01	21:56	12	2203	3113	7.053	6.7
	10/13/01	23:01	11	2479	2667	1.632	2.8
	10/14/01	12:27	17	2190	3585	2.582	9.9
251.4	10/10/01	07:03	8	2342	2541	4.779	1.2
	10/10/01	22:51	5	2422	3019	3.709	1.6
	10/11/01	05:40	4	2019	2980	2.924	9.8

The channels for the evaporation residues and spontaneous fissions listed in Table 4.18 are consistent with evaporation residue spontaneous fission correlations done previously (Section 4.5.2, Figure 4.22). The correlated evaporation residue channels corresponded to energies between 8 and 12 MeV, well within the range of evaporation residues seen in previous experiments.

The lifetimes of the correlation events was taken and fit using MLDS to establish an experimental half-life for ^{258}Sg ($t_{½} \approx 2.9$ ms). One previous experiment has listed a half-life for ^{258}Sg of $2.9\ ^{+1.3}_{-0.7}$ milliseconds [Heβ1997]. An experimental half-life of $2.7\ ^{+0.9}_{-0.7}$ milliseconds was obtained from the MLDS fit to the data.

Production cross sections were calculated from the number of correlations seen, a 100% fission detection efficiency and a 100 ± 5% spontaneous fission branching ratio to be $14\ ^{+32}_{-12}$ pb, $50\ ^{+30}_{-20}$ pb, and $26\ ^{+26}_{-15}$ pb corresponding to compound nucleus excitation energies of 20.3 MeV, 22.7 MeV, and 25.2 MeV. These experimental values were compared to experimental data from GSI [Heβ2001b] and the results of the HIVAP code using the Reisdorf and Schädel parameters. The production cross section comparison for the ^{209}Bi(^{51}V,2n)^{258}Sg reaction can be seen in Figure 4.27. The small number of correlations leads to large error bars and a difficulty in comparing the experimental results presented in Figure 4.27. The experimental results are however consistent in the fact that they are both smaller by more than an order of magnitude than the predictions of the HIVAP code.

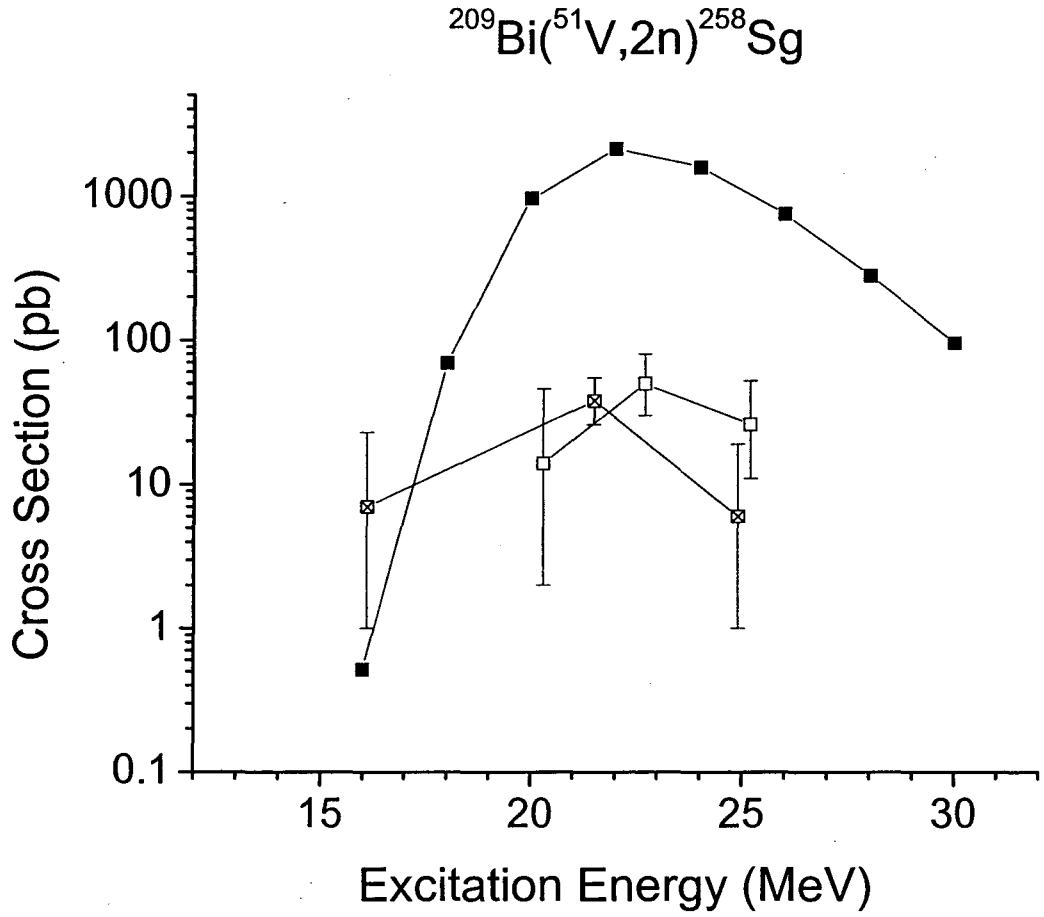

Figure 4.27: Predictions of the HIVAP code using the Reisdorf and Schädel parameters (solid symbols ■), the experimental production cross sections (open symbols □), and the previous results of Heßberger, et al. [Heβ2001b] (open symbols with an ×) for the $^{209}Bi(^{51}V,2n)^{258}Sg$ reaction.

Cross sections from this reaction of a projectile and target with an odd proton was smaller than the similar even proton projectile and target reaction $^{208}Pb(^{50}Ti,2n)^{256}Rf$ by almost a factor of 200. Obviously the odd projectile and targets have an effect on the production cross section reducing it by a factor of about 200, but how that effect manifests itself is still unknown.

5 Discussion

5.1 Cross sections

Tables 5.1 and 5.2 contain a summary of the experimental production cross sections of this thesis. Each reaction is listed with the beam energy at the center of the target, the excitation energy at the center of the target, and the production cross section. The hot fusion reaction summary is seen in Table 5.1 and the cold fusion reaction summary is found in Table 5.2.

Table 5.1: Summary of experimental hot fusion production cross sections. Cross sections without errors are upper limit cross sections only.

Reaction	Energy (MeV)	E^* Energy (MeV)	Cross Section
$^{248}Cm(^{15}N,3n)^{260}Lr$	75.9	35.2	2.3 ± 1.2 nb
$^{248}Cm(^{15}N,3n)^{260}Lr$	78.8	37.9	2.8 ± 1.4 nb
$^{248}Cm(^{15}N,4n)^{259}Lr$	75.9	35.2	$27\ ^{+17}_{-14}$ nb
$^{248}Cm(^{15}N,4n)^{259}Lr$	78.8	37.9	90 ± 40 nb
$^{238}U(^{18}O,4n)^{252}Fm$	82.4	37.7	29 ± 3 nb
$^{238}U(^{18}O,4n)^{252}Fm$	94.9	49.3	180 ± 20 nb
$^{238}U(^{18}O,4n)^{252}Fm$	99.3	53.4	47 ± 5 nb
$^{238}U(^{22}Ne,3n)^{257}No$	105.2	40.0	≤ 4.5 nb
$^{238}U(^{22}Ne,3n)^{257}No$	109.7	44.2	≤ 6.9 nb
$^{238}U(^{22}Ne,3n)^{257}No$	116.2	50.1	≤ 6.7 nb
$^{238}U(^{22}Ne,4n)^{256}No$	105.2	40.0	$23\ ^{+20}_{-16}$ nb
$^{238}U(^{22}Ne,4n)^{256}No$	109.7	44.2	$14\ ^{+21}_{-9}$ nb
$^{238}U(^{22}Ne,4n)^{256}No$	116.2	50.1	≤ 6.8 nb

Table 5.2: Summary of experimental cold fusion production cross sections. Cross sections without errors are upper limit cross sections only.

Reaction	Energy (MeV)	E^* Energy (MeV)	Cross Section
$^{208}Pb(^{48}Ca,1n)^{255}No$	204.0	12.2	$0.3\ ^{+0.6}_{-0.2}$ nb
$^{208}Pb(^{48}Ca,1n)^{255}No$	206.5	14.2	$2.3\ ^{+1.3}_{-1.0}$ nb
$^{208}Pb(^{48}Ca,1n)^{255}No$	207.8	15.2	9 ± 3 nb
$^{208}Pb(^{48}Ca,1n)^{255}No$	208.8	16.1	$100\ ^{+50}_{-40}$ nb
$^{208}Pb(^{48}Ca,1n)^{255}No$	209.0	16.3	33 ± 9 nb
$^{208}Pb(^{48}Ca,2n)^{254}No$	206.5	14.2	$0.6\ ^{+0.8}_{-0.6}$ nb
$^{208}Pb(^{48}Ca,2n)^{254}No$	207.8	15.2	$1.7\ ^{+1.5}_{-1.3}$ nb
$^{208}Pb(^{48}Ca,2n)^{254}No$	208.8	16.1	40 ± 20 nb
$^{208}Pb(^{48}Ca,2n)^{254}No$	209.0	16.3	58 ± 15 nb
$^{208}Pb(^{48}Ca,2n)^{254}No$	211.3	18.1	900 ± 300 nb
$^{208}Pb(^{48}Ca,2n)^{254}No$	211.5	18.3	530 ± 130 nb
$^{208}Pb(^{48}Ca,2n)^{254}No$	213.8	20.2	$3500\ ^{+1000}_{-900}$ nb
$^{208}Pb(^{48}Ca,2n)^{254}No$	215.3	21.4	1900 ± 500 nb
$^{208}Pb(^{48}Ca,2n)^{254}No$	216.3	22.2	2300 ± 600 nb
$^{208}Pb(^{48}Ca,2n)^{254}No$	218.8	24.2	1700 ± 500 nb
$^{208}Pb(^{48}Ca,2n)^{254}No$	221.4	26.3	530 ± 160 nb
$^{208}Pb(^{48}Ca,3n)^{253}No$	230.6	33.8	53 ± 14nb
$^{208}Pb(^{48}Ca,4n)^{252}No$	230.6	33.8	$1.8\ ^{+1.1}_{-0.8}$ nb
$^{208}Pb(^{50}Ti,1n)^{257}Rf$	226.0	12.9	≤ 0.086 nb
$^{208}Pb(^{50}Ti,1n)^{257}Rf$	231.0	16.9	16 ± 4 nb
$^{208}Pb(^{50}Ti,1n)^{257}Rf$	233.1	18.6	16 ± 5 nb
$^{208}Pb(^{50}Ti,1n)^{257}Rf$	236.1	21.0	10 ± 3 nb
$^{208}Pb(^{50}Ti,2n)^{256}Rf$	231.0	16.9	$0.6\ ^{+0.5}_{-0.3}$ nb
$^{208}Pb(^{50}Ti,2n)^{256}Rf$	233.1	18.6	$1.1\ ^{+0.8}_{-0.5}$ nb
$^{208}Pb(^{50}Ti,2n)^{256}Rf$	236.1	21.0	6.7 ± 1.8 nb
$^{208}Pb(^{51}V,2n)^{257}Db$	250.0	24.9	$1.4\ ^{+0.7}_{-0.6}$ nb
$^{209}Bi(^{50}Ti,1n)^{258}Db$	231.2	15.0	≤ 0.33 nb
$^{209}Bi(^{50}Ti,1n)^{258}Db$	233.5	16.9	$3.1\ ^{+1.5}_{-1.3}$ nb
$^{209}Bi(^{50}Ti,2n)^{257}Db$	233.5	16.9	≤ 0.25 nb
$^{209}Bi(^{51}V,2n)^{258}Sg$	245.4	20.3	$14\ ^{+32}_{-12}$ pb
$^{209}Bi(^{51}V,2n)^{258}Sg$	248.4	22.7	$50\ ^{+30}_{-20}$ pb
$^{209}Bi(^{51}V,2n)^{258}Sg$	251.4	25.2	$26\ ^{+26}_{-15}$ pb

Gaussian curves were used to develop a generalized set of systematics and to observe similarities and differences between experimental excitation functions observed at different institutions as well as obtain information about the shape of cold and hot fusion excitation functions. Gaussian curves were used as the shape of excitation functions near their centroid are Gaussian in shape. Using the computer program MathCAD, a simple Gaussian equation, Equation 5.1, was used to fit the experimental data from GSI for two reactions, ^{208}Pb + ^{50}Ti and ^{209}Bi + ^{50}Ti. These reactions were chosen as the cross sections for the 1n- and 2n-exit channels have been determined at more than 5 different excitation energies [Heβ1997, Heβ2001]. The Gaussian function used had the form:

$$g(e) = \frac{g_o}{\sqrt{2\pi\sigma}} \exp\left[\frac{-(e-m)^2}{2\sigma^2}\right] \tag{5.1}$$

where "g_o" is the area of the Gaussian function, "m" is the centroid of the Gaussian function, "σ" is the standard deviation and the energy, "e", is the excitation energy of the function.

The fit to the experimental data from GSI was performed by altering the Gaussian curve by adjusting the width (σ), centroid (m) and magnitude (g_o) until the curve agreed with the experimental data points. Figure 5.1 shows the results of the adjusting the Gaussian curves to the GSI experimental data. Table 5.3 contains the results of the fits to the experimental data.

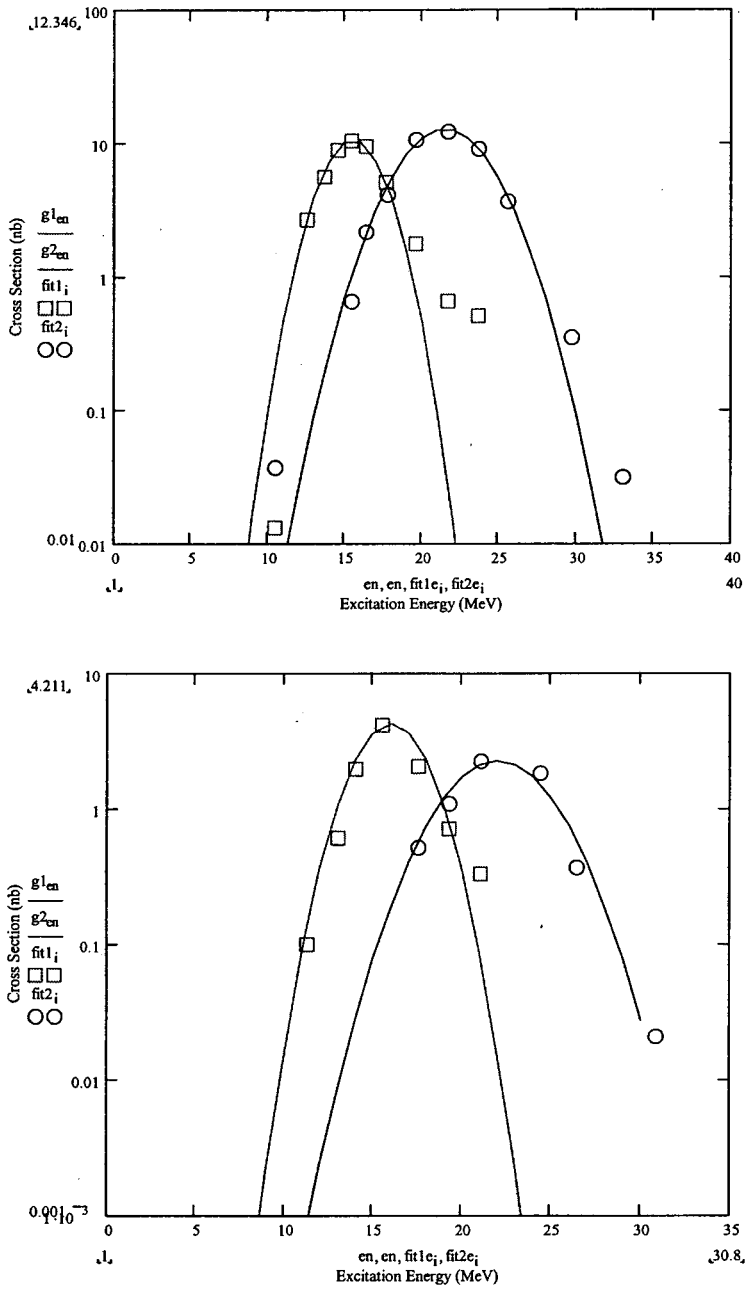

Figure 5.1: Gaussian curves (solid lines) and the experimental data for the $^{208}Pb(^{50}Ti,1n)^{257}Rf$ (top □), $^{208}Pb(^{50}Ti,2n)^{256}Rf$ (top o), $^{209}Bi(^{50}Ti,1n)^{258}Db$ (bottom □) and $^{209}Bi(^{50}Ti,2n)^{257}Db$ (bottom o) reactions [Heβ1997, Heβ2001].

Table 5.3: Results of fits of the Gaussian curves to the experimental data from GSI for the $^{208}Pb(^{50}Ti,xn)^{258-x}Rf$ and $^{209}Bi(^{50}Ti,xn)^{259-x}Db$ reactions. The standard deviation and centroid are labeled "σ" and "m" and the ratio of the areas is "g_o2/g_o1".

Projectile	Target	σ1	m1 (MeV)	σ2	m2 (MeV)	g_o2 / g_o1
^{208}Pb	^{50}Ti	1.8	15.5	2.7	21.5	1.8
^{209}Bi	^{50}Ti	1.8	16.0	2.7	22.0	0.79

Several important things can be seen from these Gaussian curves. The same standard deviations were used for the 1n- and 2n-exit channel excitation functions for the $^{208}Pb + {}^{50}Ti$ and $^{209}Bi + {}^{50}Ti$ reactions. The standard deviations from these fits correspond to FWHM for these excitation functions of 4.2 MeV for the 1n-exit channel and 6.4 MeV for the 2n-exit channel. A difference of 6 MeV in excitation energy for the two centroids was seen for the two experiments. Different areas were used to fit the different excitation functions and therefore different initial area ratios were used. Deviations were seen on the high excitation energy side of the excitation function as the decrease in the excitation function due to fission survivability is much less than the decrease in the excitation function due to the effects of the Coulomb barrier on the low excitation energy side of the excitation function.

The experimental results for the $^{208}Pb(^{50}Ti,xn)^{258-x}Rf$ and $^{209}Bi(^{50}Ti,xn)^{259-x}Db$ reactions from this thesis as well as the other experimental results were then fit to Gaussian curves using the similar centroids, centroid differences, and ratios of 2n to 1n initial areas. The actual initial areas were changed, but the ratios were kept similar. The centroids were altered to make the Gaussian curves appear to model the experimental data. Figure 5.2 shows the Gaussian curve results for the $^{208}Pb(^{50}Ti,xn)^{258-x}Rf$ and $^{209}Bi(^{50}Ti,xn)^{259-x}Db$ experimental results of this thesis. Figure 5.3 illustrates the results of the Gaussian curves to the $^{208}Pb(^{48}Ca,xn)^{256-x}No$ and $^{209}Bi(^{51}V,xn)^{260-x}Sg$ reactions. Finally, Figure 5.4 shows the results of the $^{208}Pb(^{51}V,xn)^{259-x}Db$ reaction. Table 5.4 summarizes the results of the Gaussian curve fits to the experimental data.

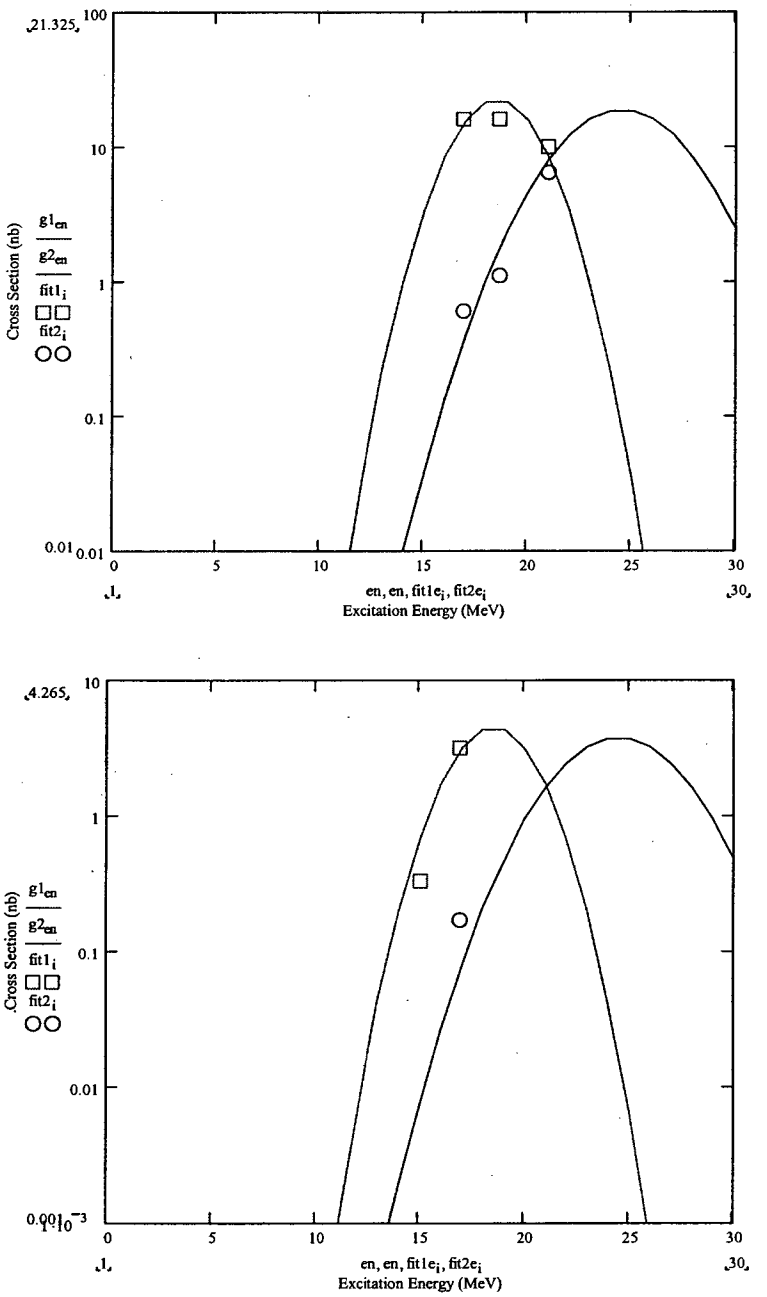

Figure 5.2: Gaussian curves (solid lines) and the experimental data from this thesis for the $^{208}Pb(^{50}Ti,1n)^{257}Rf$ (top □), $^{208}Pb(^{50}Ti,2n)^{256}Rf$ (top ○), $^{209}Bi(^{50}Ti,1n)^{258}Db$ (bottom □) and $^{209}Bi(^{50}Ti,2n)^{257}Db$ (bottom ○) reactions. The only data point in the $^{209}Bi(^{50}Ti,2n)^{257}Db$ reaction is an upper limit cross section only.

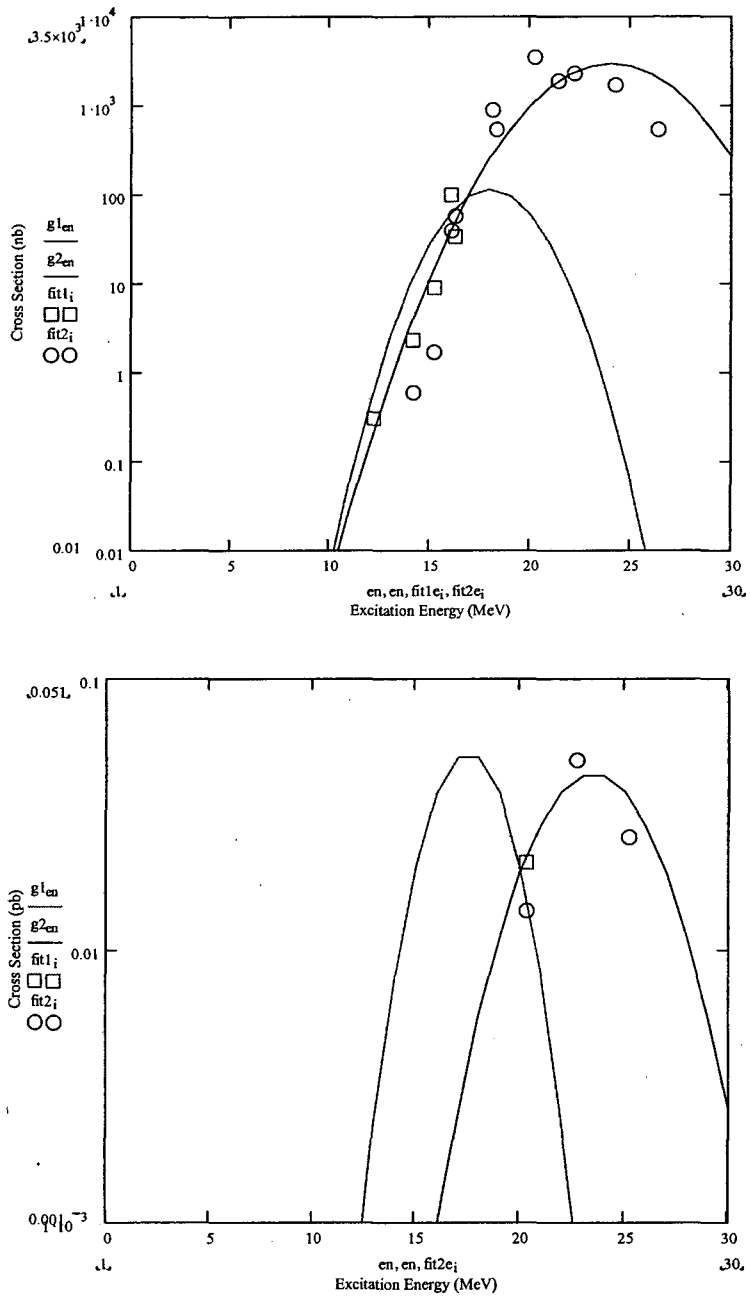

Figure 5.3: Gaussian curves (solid lines) and the experimental data from this thesis for the $^{208}Pb(^{48}Ca,1n)^{255}No$ (top □), $^{208}Pb(^{48}Ca,2n)^{254}No$ (top o), $^{209}Bi(^{51}V,1n)^{259}Sg$ (bottom □) and $^{209}Bi(^{51}V,2n)^{258}Sg$ (bottom o) reactions. The only data point in the $^{209}Bi(^{51}V,1n)^{259}Sg$ reaction is an upper limit cross section only.

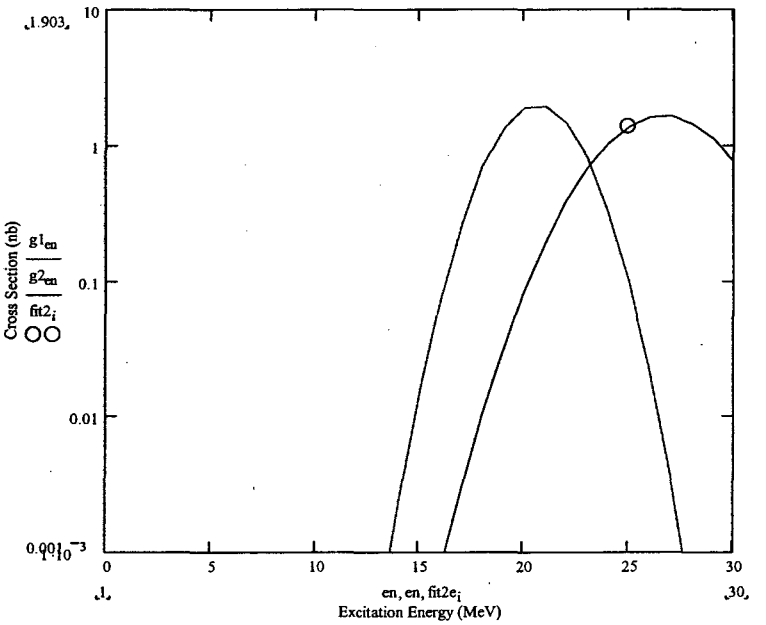

Figure 5.4: Gaussian curves (solid lines) and the experimental data from this thesis for the $^{208}Pb(^{51}V,2n)^{257}Db$ (o) reaction.

Table 5.4: Results of Gaussian fits to the experimental data from this thesis for the $^{208}Pb(^{50}Ti,xn)^{258-x}Rf$, $^{209}Bi(^{50}Ti,xn)^{259-x}Db$, $^{208}Pb(^{48}Ca,xn)^{256-x}No$, $^{209}Bi(^{51}V,xn)^{260-x}Sg$, and $^{208}Pb(^{51}V,xn)^{259-x}Db$ reactions. The standard deviation and centroid are labeled "σ" and "m" and the ratio of the areas is "g_o2/g_o1".

Projectile	Target	σ1	m1 (MeV)	σ2	x2 (MeV)	g_o2 / g_o1
^{208}Pb	^{50}Ti	1.8	18.5	2.7	24.5	1.25
^{209}Bi	^{50}Ti	1.8	18.5	2.7	24.5	1.25
^{208}Pb	^{48}Ca	1.8	18.0	2.7	24.0	40
^{209}Bi	^{51}V	1.8	17.5	2.7	23.5	1.25
^{208}Pb	^{51}V	1.8	18.0	2.7	24.0	1.25

In Figure 5.2, the Gaussian fits to the experimental data were quite good. The only observable discrepancy was the movement of the centroid to higher excitation energies on the order of 2.5 to 3 MeV. Otherwise, keeping the difference in centroid energy between the 1n- and 2n-exit channels constant and the standard deviations constant, the Gaussian fits seemed to predict and model the experimental results. The one point in the $^{209}Bi(^{50}Ti,xn)^{259-x}Db$ reaction for the 2n-exit channel was an upper limit showing that it was probable that no events were seen. The Gaussian fit to the $^{208}Pb(^{48}Ca,xn)^{256-x}No$ experimental data was not as good as other Gaussian fits were to the other experimental data. It was possible that the 2n-exit channel was so large that the 1n-exit channel was masked. Adding to this problem were the similar decay energies and half-lives of ^{255}No and ^{254}No, the 1n- and 2n-exit channel products. An increase in the ratio $g_0(2n)/g_0(1n)$ was also seen for this reaction which was unlike the other cold fusion reactions. Better fits were obtained with a smaller 2n standard deviation and a larger area ratio, but these fitting parameters were dissimilar to the rest of the cold fusion fit parameters. The fit to the $^{209}Bi(^{51}V,xn)^{260-x}Sg$ was performed using the same standard deviations as the other experiments, and the fact that no ^{259}Sg was seen in the experiment at the lowest experimental excitation energy, a guess in terms of the initial area ratio was taken to reflect what was seen experimentally. The parameters for the fit to the experimental $^{208}Pb(^{51}V,xn)^{259-x}Db$ data point is speculative as only one experimental point was obtained. With only one point, an infinite number of Gaussian fits are possible, and the one proposed is only speculative.

From the Gaussian fit results for the cold fusion reactions, it was seen that the widths of these excitation functions, the excitation energies of the centroids, and the

difference in excitation energy between the centroids were all consistent. A similar attempt was made to fit the experimental results of the hot fusion reactions using the fits to the cold fusion experiments as an initial guess.

Knowing that the excitation energy at the Coulomb barrier is higher for the hot fusion reactions than the cold fusion reactions, and the fact that the 4n-exit channel is favored over the 3n-exit channel led to an initial guess for the parameters used to fit the experimental results for the hot fusion reactions from this thesis. The standard deviations were slightly higher than those observed for the cold fusion reactions. Understandably the centroids were located at higher excitation energies, and the difference between the centroids for the 3n- and 4n-exit channels was larger than the differences seen in the cold fusion reactions. The $g_0(4n)/g_0(3n)$ ratio was also larger than the $g_0(2n)/g_0(1n)$ ratio observed in the cold fusion reactions. The results to the Gaussian fits can be seen in Figures 5.5 and 5.6, with the summary of the Gaussian fit parameters located in Table 5.5.

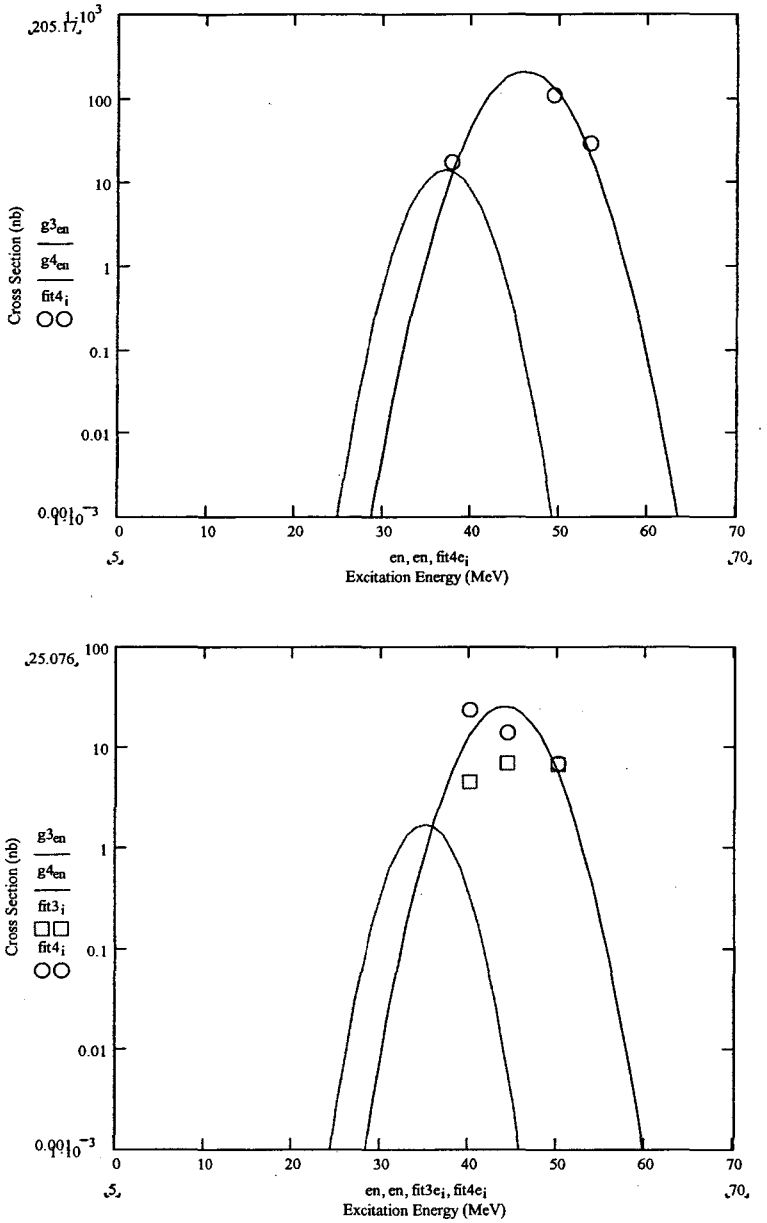

Figure 5.5: Gaussian curves (solid lines) and the experimental data from this thesis for the $^{238}U(^{18}O,4n)^{252}Fm$ (top o), $^{238}U(^{22}Ne,3n)^{257}No$ (bottom □) and $^{238}U(^{22}Ne,4n)^{256}No$ (bottom o) reactions. The data points in the $^{238}U(^{22}Ne,3n)^{257}No$ reaction are upper limit cross sections only.

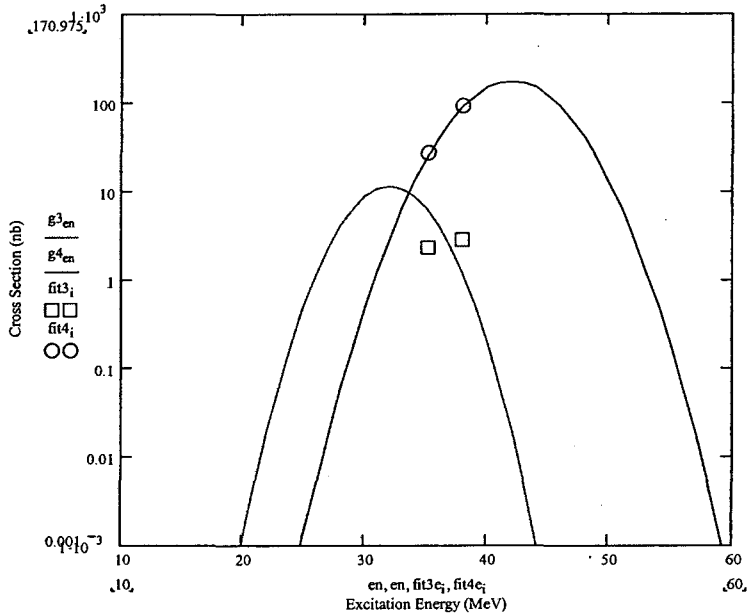

Figure 5.6: Gaussian curves (solid lines) and the experimental data from this thesis for the $^{248}Cm(^{15}N,3n)^{260}Lr$ (□) and $^{248}Cm(^{15}N,4n)^{259}Lr$ (○) reactions.

Table 5.5: Results of Gaussian fits to the experimental data from this thesis for the $^{238}U(^{18}O,xn)^{256-x}Fm$, $^{238}U(^{22}Ne,xn)^{260-x}No$, and $^{248}Cm(^{15}N,xn)^{263-x}Lr$ reactions. The standard deviation and centroid are labeled "σ" and "m" and the ratio of the initial areas is "g_o4/g_o3".

Projectile	Target	σ3	m3 (MeV)	σ4	m4 (MeV)	g_o4 / g_o3
^{238}U	^{18}O	2.8	37	3.5	46	18.75
^{238}U	^{22}Ne	2.8	37	3.5	46	18.75
^{248}Cm	^{15}N	2.8	32	3.5	42	18.75

These same Gaussian curves were fit to the data from Donets et al. [Don1966] for the $^{238}U(^{18}O,xn)^{256-x}Fm$ and $^{238}U(^{22}Ne,xn)^{260-x}No$ reactions and Eskola et al. [Esk1971] for the $^{248}Cm(^{15}N,xn)^{263-x}Lr$ reaction. The same standard deviations, similar centroids and similar centroid differences for the 3n- and 4n-exit channel excitation functions were found. The standard deviations from Table 5.5 correspond to FWHM values of 6.6 and 8.2 MeV for the 3n- and 4n-exit channel excitation functions. The results in Figure 5.5 are self-explanatory. The parameters for the Gaussian fits match the data very well and in the case of the $^{238}U(^{22}Ne,3n)^{257}No$ illustrates the fact that no ^{257}No should have been seen in the reactions as the cross sections for the 3n-exit channel in that reaction are extremely small at those energies. The Gaussian fit to the $^{248}Cm(^{15}N,xn)^{263-x}Lr$ experimental data is also good. The error bars on the cross sections for the 3n-exit channel are in line with the Gaussian fit.

Gaussian curves can be used to help model the shape of excitation functions for various hot and cold fusion reactions around their centroids. Information was obtained from these curves (Tables 5.4 and 5.5) that shows a possible systematic link between the 1n-, 2n-exit channels from the cold fusion reactions and 3n- and 4n- exit channels from the hot fusion reactions. Additional data points for the cold and hot fusion excitation functions mentioned in this thesis would help in the development of modeling the excitation functions with a Gaussian curve and in the understanding of the trends in the shapes of cold and hot fusion excitation functions.

5.2 Exit channel systematics

Cross sections produced in various reactions can be grouped according to projectile isospin (isospin = (number of neutrons – number of protons) ÷ 2) and then plotted as a function of the maximum experimental cross section of an excitation function for a given exit channel versus the atomic number of the isotope produced. These cross sections are grouped by projectile isospin as the isospins of the targets and resulting compound nuclei are nearly equal. Therefore, the only real difference in these reactions is the projectile isospin. In most of these plots, a decrease in production cross section is seen with an increase in the atomic number of the product. Comparing experimental cross sections to the trend seen systematically can show whether the various cross section values are consistent or not.

The experimental results for the 1n-exit channel reactions were compared to other 1n-exit channel production cross sections in Figure 5.7. For the 1n-exit channel it appears that all of the values were similar to what is seen systematically.

In a similar manner the experimental results for the 2n-exit channel were compared to similar reactions with isospins of 2.5, 3 and 4. The 2n-exit channel experimental results are also consistent with the systematics presented here. The energies studied experimentally included the maxima of the 2n-exit channel excitation functions and therefore give good agreement with the systematics. In one of the experiments only an upper limit value was obtained for the 2n-exit channel and therefore the corresponding data point in Figure 5.8 is not in good agreement with the systematics. Figure 5.8 shows the results of the comparison.

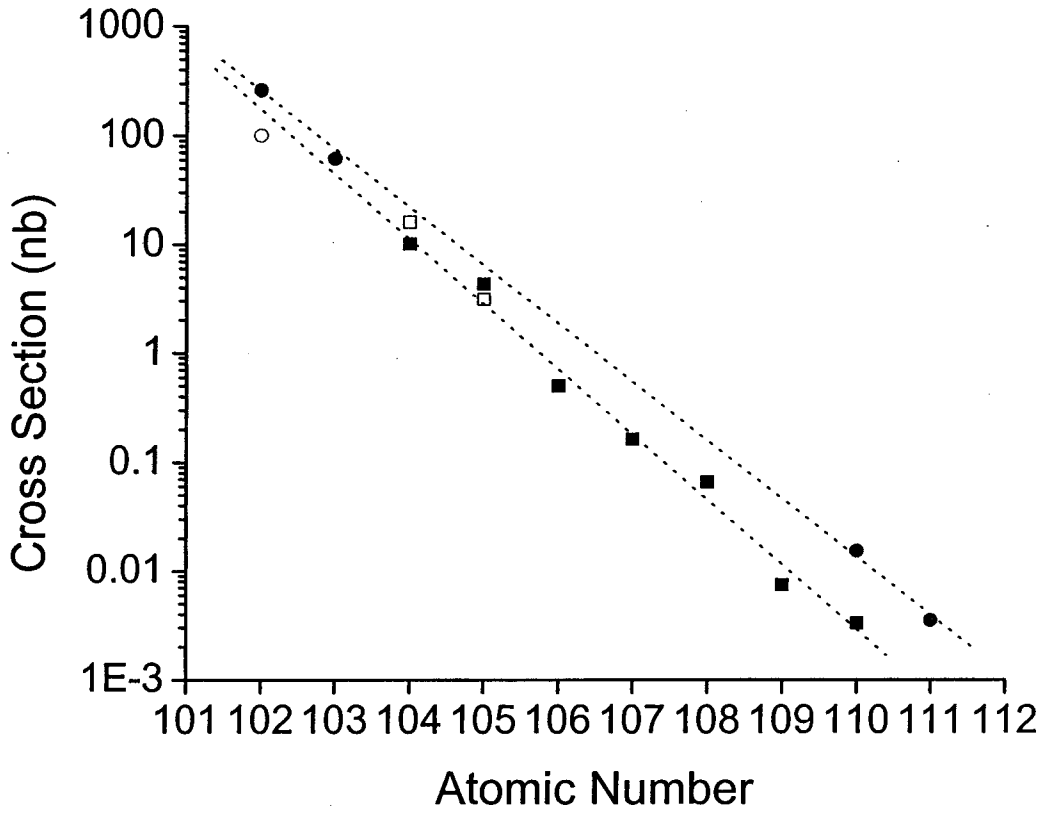

Figure 5.7: 1n-exit channel systematics (solid symbols ■) compared with experimental results (open symbols o). Square symbols (■) represent an isospin of 3 and circle symbols (●) an isospin of 4 [Gäg1989, Heβ1997, Heβ2001, Mün1985, Mün1989, Hof1998, Hof1997, Hof2001, Hof1995a]. The dotted lines are to guide the eye along cross sections from the same isospin.

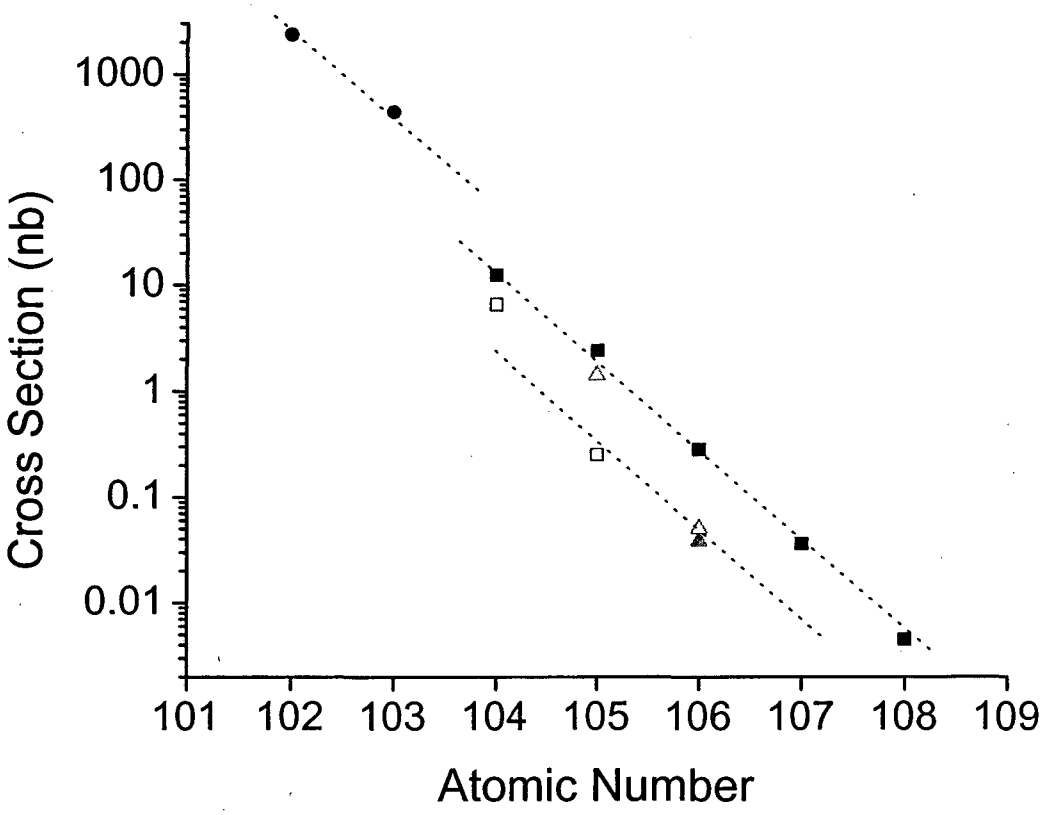

Figure 5.8: 2n-exit channel systematics (solid symbols ■) compared with experimental results (open symbols □). Triangle symbols (◣) represent an isospin of 2.5, square symbols (■) an isospin of 3, and circle symbols (●) an isospin of 4 [Gäg1989, Heβ1997, Heβ2001, Mün1985, Mün1989, Hof1998]. The dotted lines are to guide the eye along cross sections from the same isospin.

Finally, the experimental 4n-exit channel data were compared with systematics for the 4n-exit channel. No 3n-exit channel comparison was done as there is not enough experimental data present to make any systematic study. There are quite a few ways to produce elements heavier than einsteinium in hot fusion reactions as there is a variety of target and projectiles to work with. With the hot fusion reactions, a specific projectile was chosen to do the comparison with experimental data. A significant amount of experimental work has been done with ^{22}Ne projectiles and therefore these reactions were chosen to do the comparison for the 4n-exit channel. Figure 5.9 shows the comparison of the ^{22}Ne experimental work of this thesis (open symbol) compared with other ^{22}Ne experimental work making isotopes of the elements from fermium to bohrium (solid symbols). The experimental results of this thesis are consistent with the systematic trends.

The comparison of the experimental production cross sections with the systematics of the 1n-, 2n- and 4n-exit channel seems rather straight forward. In a majority of the cases, the data seem to correspond well with what has been seen previously and in a few cases, larger production cross sections might have been seen for a particular reaction if the excitation function had been studied in greater detail.

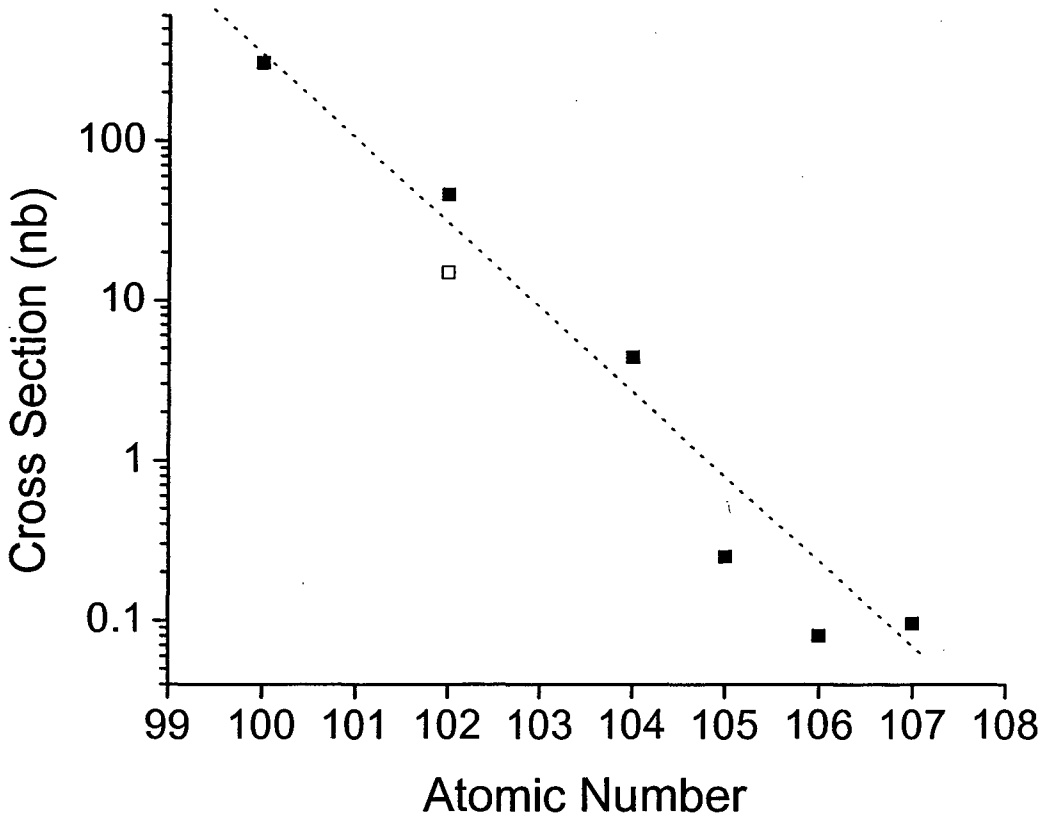

Figure 5.9 : 4n-exit channel systematics (solid symbols ■) compared with experimental results of this thesis (open symbols □) for hot fusion reactions with ^{22}Ne projectiles [Tür1999, Hof1998, Laz2000, Lan1988, Laz1994, Wil2000]. The dotted line is present to guide the eye.

5.3 HIVAP cross sections

The comparisons between the experimental cross sections of this thesis and the predictions of the HIVAP code with the Reisdorf and Schädel parameters were presented in Section 4. The Reisdorf and Schädel input parameters were satisfactory in predicting the cross sections for the 3n- and 4n-exit channel excitation functions from the hot fusion reactions, but were not statisfactory at predicting the 1n- and 2n-exit channel excitation functions for the cold fusion reactions.

The Reisdorf and Schädel input parameters for HIVAP were altered in the attempt to model the experimental results more accurately. These alterations were called the Patin parameters. A full list of the input parameters as they appear in the input file can be found in Appendix B. The aim was to alter as few of the parameters as possible. Only six of the Reisdorf and Schädel input parameters were changed: LEVELPAR, AF/AN, V0, Q2, SIGR0, and CUTOFF. LEVELPAR is the value of the radius parameter that is used when calculating the level density ratios for the de-excitation steps. LEVELPAR was altered to 1.16, the value used in the calculations of Töke and Swiatecki [Tök1981]. AF/AN is an integer that determines what designates the calculation to be used. In the Reisdorf and Schädel parameter set, AF/AN equals 1 meaning the level density ratio was calculated using Reisdorf [Rei1981]. The Patin parameters used an AF/AN value equal to 2 to designate using the level density calculations of Töke and Swiatecki [Tök1981]. The Töke/Swiatecki calculation better reflects what occurs experimentally in the cold fusion reactions. V0 equals the nuclear well potential for the target atom which was changed to reflect a smaller potential well depth of about 50 MeV rather than 70 MeV used in the Reisdorf and Schädel parameters. Q2 is the quadrupole moment of the target

atom in units of fm^2. A Q2 value of 0 was used to reflect that in the cold fusion reactions, the lead and bismuth targets are essentially spherical. The SIGR0 value is the percent fluctuation in R0 used to calculate the fusion barrier in the entrance channel used for determining the fusion cross section. CUTOFF is the integration limit in units of SIGR0. SIGR0 and CUTOFF influence the entrance channel fusion barrier and were altered depending on the specific reactions to reflect the wide differences between the predictions of the HIVAP code using the Reisdorf and Schädel parameters and the experimental data. The values of SIGR0 varied between 1.7 and 4.0 percent. The CUTOFF value was left at 4.0 or 5.0.

The input parameter values LEVELPAR, AF/AN, V0 and Q2 were left at their altered values when comparing the predictions of the Patin parameters to the experimental data. The values of SIGR0 and CUTOFF were varied to reflect the changes in the projectile and targets used in the reactions. The largest effect in the predictions of the HIVAP code came by as a result of the alterations to the entrance channel values of SIGR0 and CUTOFF. A small barrier fluctuation value was chosen for the $^{208}Pb(^{48}Ca,xn)$ reaction because of the spherical character of both the projectile and target. As the projectiles moved away from the sphericity of ^{48}Ca and the target was changed to ^{209}Bi, the barrier fluctuation value was increased. Figures 5.10, 5.11, 5.12 and 5.13 show a comparison between the predictions of HIVAP using the Patin parameters, the experimental data of this thesis, and experimental results obtained elsewhere.

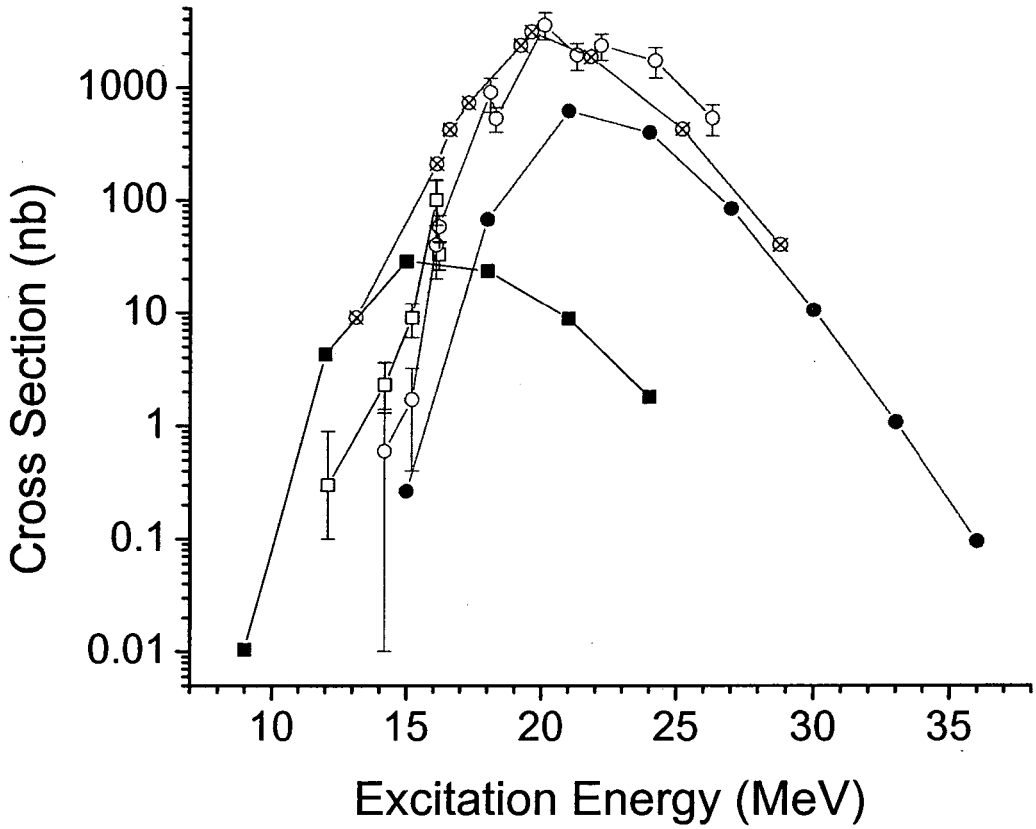

Figure 5.10: Predictions of the HIVAP code using the Patin parameters (solid symbols ■,●), the experimental production cross sections (open symbols □,○), and previous experimental results [Gäg1989] (open symbols with an ×) for the ^{208}Pb(^{48}Ca,1n)^{255}No (squares) and ^{208}Pb(^{48}Ca,2n)^{254}No (circles) reactions. A SIGR0 value of 1.7 and a CUTOFF value of 5.0 were used in the input parameter set.

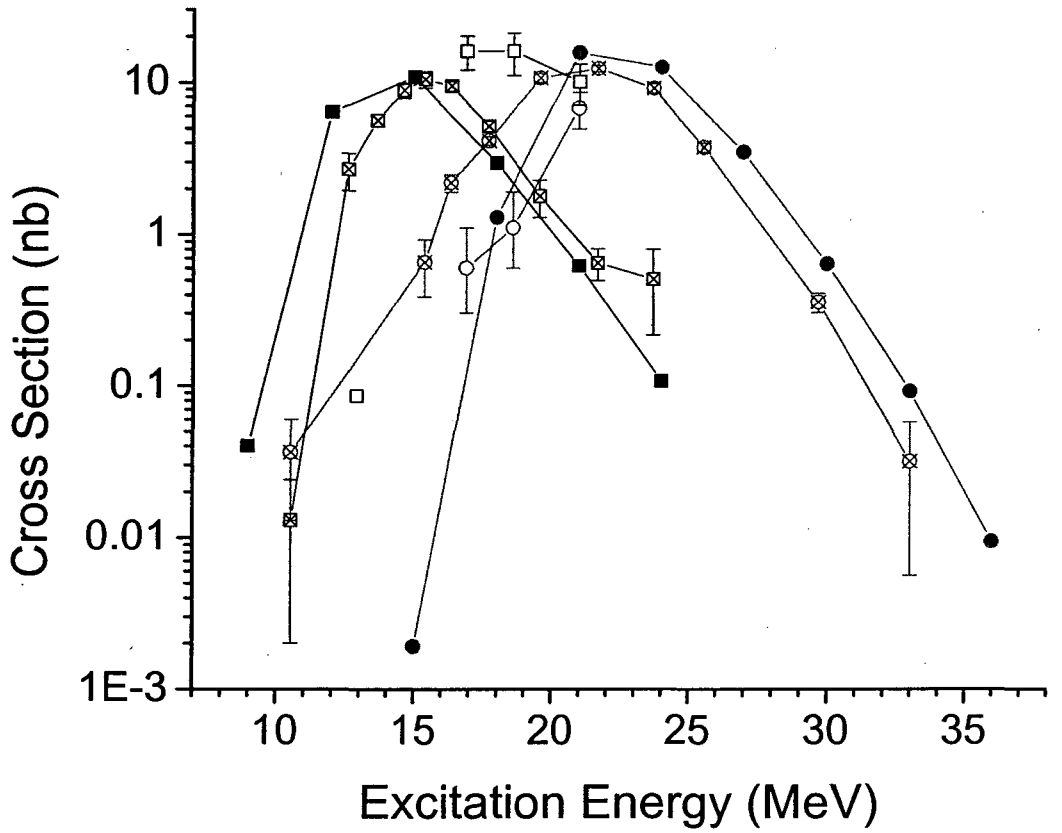

Figure 5.11: Predictions of the HIVAP code using the Patin parameters (solid symbols ■,●), the experimental production cross sections (open symbols □,○), and previous experimental results [Heβ1997] (open symbols with an ×) for the ^{208}Pb(^{50}Ti,1n)^{257}Rf (squares) and ^{208}Pb(^{50}Ti,2n)^{256}Rf (circles) reactions. A SIGR0 value of 2.6 and a CUTOFF value of 5.0 were used in the input parameter set.

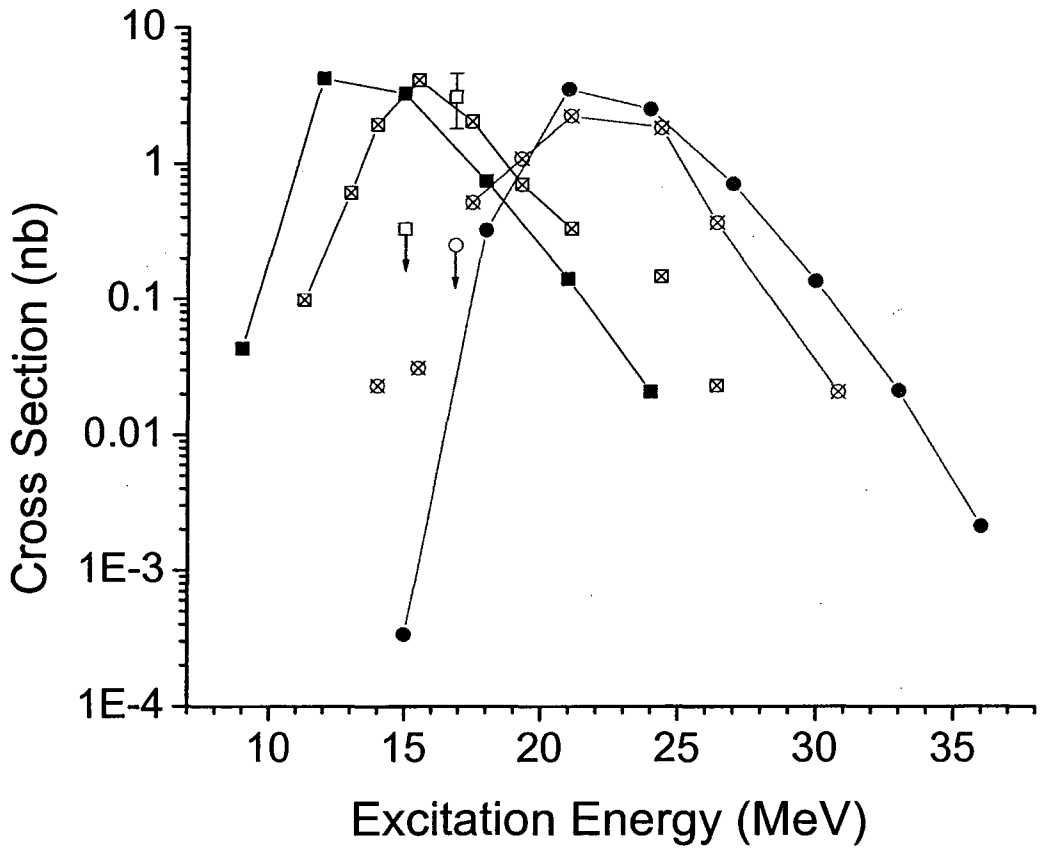

Figure 5.12: Predictions of the HIVAP code using the Patin parameters (solid symbols ■,●), the experimental production cross sections (open symbols □,○), and previous experimental results [Heβ2001a] (open symbols with an ×) for the ^{209}Bi(^{50}Ti,1n)^{258}Db (squares) and ^{209}Bi(^{50}Ti,2n)^{257}Db (circles) reactions. A SIGR0 value of 2.9 and a CUTOFF value of 5.0 were used in the input parameter set.

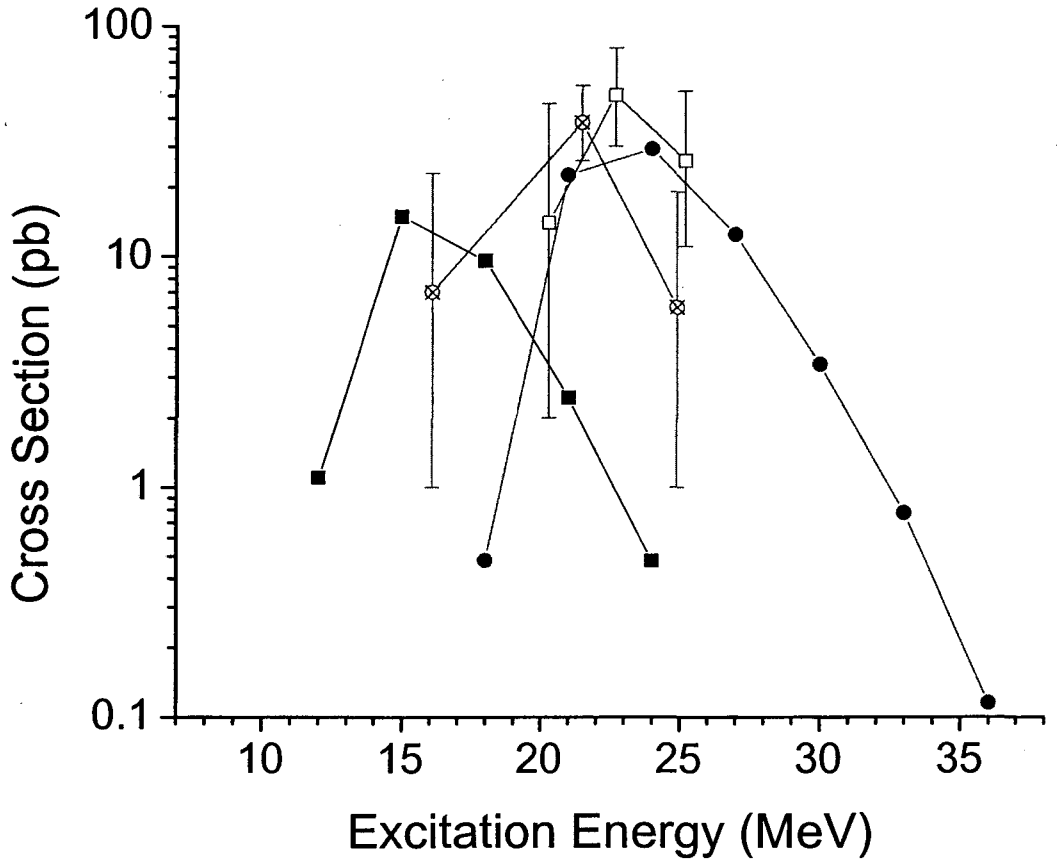

Figure 5.13: Predictions of the HIVAP code using the Patin parameters (solid symbols ■,●), the experimental production cross sections (open symbols □,○), and previous experimental results [Heβ2001b] (open symbols with an ×) for the ^{209}Bi(^{51}V,1n)^{259}Sg (squares) and ^{209}Bi(^{51}V,2n)^{258}Sg (circles) reactions. A SIGR0 value of 4.0 and a CUTOFF value of 4.0 were used in the input parameter set.

The alterations to the input parameters seem to have a dramatic effect on the predictions of the HIVAP code in comparison to the predictions of the HIVAP code using the Reisdorf and Schädel parameters. The Patin parameters more accurately reflect what is occurring in the cold fusion reactions. The Reisdorf and Schädel parameter set was tailored for hot fusion reactions with actinide targets and accurately predicts those particular production cross sections. Barrier fluctuations between different targets and projectiles aren't as important in the hot fusion reactions as they don't change as drastically from target to target, and projectile to projectile. In addition, the hot fusion reactions that were modeled by Reisdorf and Schädel occurred at energies well above the barrier where these fluctuations do not have as much influence on the production cross section. The Patin parameters are more accurate as a result of tailoring the input parameters to these specific cold fusion reactions. The differences in the percentage of fusion barrier fluctuation (SIGR0) were discovered through comparison of the HIVAP predictions using the altered parameters and the experimental data of this thesis. Very little barrier fluctuation was require to model the ^{208}Pb(^{48}Ca,xn) reaction whereas increasingly larger barrier fluctuation values were required for the ^{208}Pb(^{50}Ti,xn), ^{209}Bi(^{50}Ti,xn), and ^{209}Bi(^{51}V,xn) reactions. The following trend of increasing barrier fluctuation value SIGR0 was observed: ^{208}Pb(^{50}Ti,2n)^{256}Rf < ^{209}Bi(^{50}Ti,2n)^{257}Db < ^{208}Pb(^{51}V,2n)^{257}Db < ^{209}Bi(^{51}V,2n)^{258}Sg. An effective input parameter set has been found to predict the production cross sections of cold fusion reactions by allowing for small variations in the SIGR0 and CUTOFF parameters.

5.4 Odd particle effects

Using two different targets, ^{208}Pb and ^{209}Bi, and two different projectiles, ^{50}Ti and ^{51}V, four different reactions can occur. In this case, two of the reactions, ^{208}Pb(^{51}V,xn)$^{259-x}$Db and ^{209}Bi(^{50}Ti,xn)$^{259-x}$Db produce the same compound nucleus. By studying these four different reactions, insights can be obtained into the role of the odd proton in the target (^{209}Bi + ^{50}Ti), or in the projectile (^{208}Pb + ^{51}V), or in both (^{209}Bi + ^{51}V) when compared to the even proton projectile and target system (^{208}Pb + ^{50}Ti). Using the experimental results of this thesis and the predictions of HIVAP using the altered parameters from Section 5.3, it appears that the production cross sections can vary by a factor of 300 depending on where the odd proton is located.

As a standard, the cross sections for the 2n-exit channel were used from each of the four reactions. The maximum in the ^{208}Pb(^{50}Ti,2n)^{256}Rf reaction had a cross section of about 10 nb. When the odd proton was located in the projectile as in the ^{208}Pb(^{51}V,2n)^{257}Db reaction, the maximum cross section was about 2 nb. If the odd proton was located in the target as in the ^{209}Bi(^{50}Ti,2n)^{257}Db reaction, the maximum cross section was about 3 nb. In this case, a larger cross section was obtained in the reaction of the even Z projectile with the odd Z target. When both the target and projectile had an odd proton as in the ^{209}Bi(^{51}V,2n)^{258}Sg reaction, the maximum cross section decreased by a factor of more than 200 to 50 pb. These results were seen in both the experimental data as well as the predictions of the HIVAP code with both the Reisdorf and Schädel parameters and the Patin input parameters. These results were also seen in the predictions of the SPIT code. The specific ratios between the maxima were different, but the trend for the maximum of the 2n-exit channel cross sections was always the same:

$^{208}Pb(^{50}Ti,2n)^{256}Rf > ^{209}Bi(^{50}Ti,2n)^{257}Db > ^{208}Pb(^{51}V,2n)^{257}Db >> ^{209}Bi(^{51}V,2n)^{258}Sg$. ^{52}Cr, a projectile with the same number of neutrons as ^{50}Ti and ^{51}V, would according to these systematics have a smaller maximum 2n-exit channel cross section from the $^{208}Pb(^{52}Cr,2n)^{258}Sg$ and $^{209}Bi(^{52}Cr,2n)^{259}Bh$ reactions than either the $^{208}Pb(^{51}V,2n)^{257}Db$ and $^{209}Bi(^{51}V,2n)^{258}Sg$ reactions. Predictions using the HIVAP code with the Patin input parameters also predict a smaller 2n-exit channel maximum cross section. The SPIT code predicts similar 2n-exit channel maximum cross sections for all three of the reactions: $^{209}Bi(^{51}V,2n)^{258}Sg$, $^{208}Pb(^{52}Cr,2n)^{258}Sg$, and $^{209}Bi(^{52}Cr,2n)^{259}Bh$. It would be worthwhile to obtain experimental evidence to back up these predictions, especially if the cross sections are in the picobarn to tens of picobarns range.

The significant difference in the maximum cross section for the $^{209}Bi(^{51}V,2n)^{258}Sg$ reaction versus the $^{208}Pb(^{50}Ti,2n)^{256}Rf$, $^{209}Bi(^{50}Ti,2n)^{257}Db$, and $^{208}Pb(^{51}V,2n)^{257}Db$ reactions cannot be explained by large differences in Q-value, neutron separation energy differences, or by shell effects. Another explanation must exist. One possible explanation was obtained using the calculations of Blocki and Swiatecki [Blo1982, Swi2002]. For each reaction, the deformation energy of the optimized neck configuration of the combined system can be plotted versus the length between the projectile and target centers minus their radii. These plots can be seen in Figure 5.14. The curve for a particular reaction represents the additional barrier which must be overcome after the target and projectile reach a touching configuration. The difference between the deformation energy at the maximum of the curve (saddle point) and the deformation energy at the injection point (0-3 fm for all of these reactions) can then be placed in an exponential function to arrive at the probability of overcoming the barrier to compound

nucleus formation. These probabilities are plotted in Figure 5.15 for various injection point distances.

It is seen from these calculations that the difference in energy between the maximum of the curve and the injection point increases as Z increases, which leads to the decreased probability of forming the compound nucleus. The probability of compound nucleus formation also decreases as the distance of the injection point increases. If the injection point is held at a constant length, the target and projectile system have a larger barrier to surmount to reach the complete fusion of the compound nucleus, and will more likely slide down the barrier to fission. This is somewhat similar to what is seen experimentally. This explanation is only an attempt at explaining the large difference in the 2n-exit channel cross sections seen. It is not a complete explanation, but it does give some insight into what possibly might be occurring in these reactions.

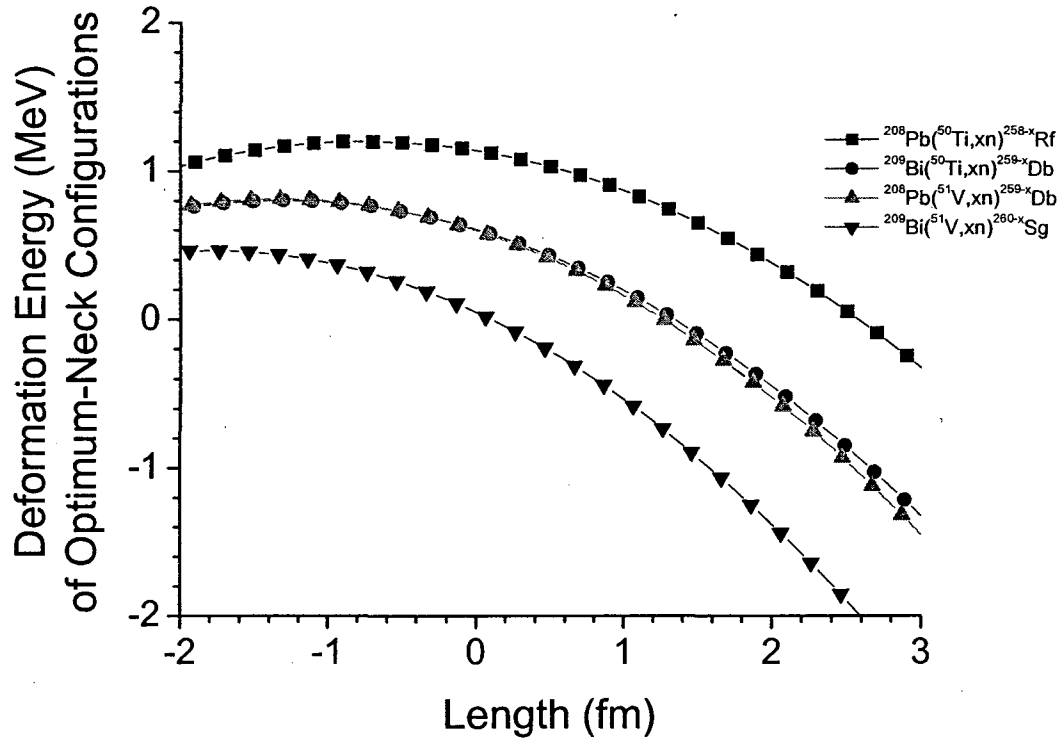

Figure 5.14: Plot of the deformation energy (MeV) of an optimum neck configuration versus length (fm) [Blo1982, Swi2002] for various cold fusion reactions.

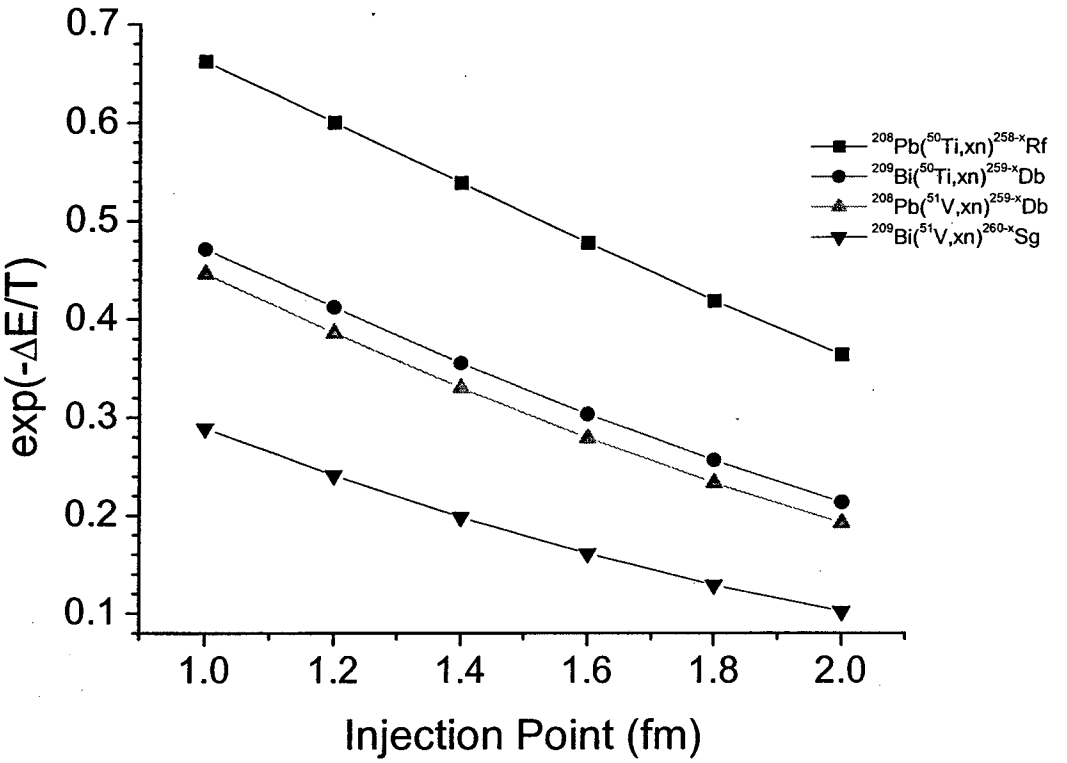

Figure 5.15: Plot of the probability of overcoming the barrier from Figure 5.14 versus the injection point length (fm). ΔE is the difference in deformation energy at the maximum of the curve and the injection point. The temperature T was calculated assuming an excitation energy of 20 MeV and a level density parameter a equal to A/8.5 MeV.

6 Conclusions and future research

6.1 Conclusions

The MG system is an effective system to study the production of isotopes with fairly significant cross sections (> 1 nb). Studies of heavier system become increasingly difficult as the cross sections become smaller. The catcher foil technique is useful when studying long-lived heavy element isotopes but not as effective when studying the short-lived isotopes of the heaviest elements. The BGS is extremely successful for the study of cold fusion reactions. The large difference between the magnetic rigidities of the evaporation residues and transfer products makes separation of cold fusion reaction products highly efficient. The BGS efficiency for hot fusion reactions using lighter beams is significantly lower and therefore reduces the usefulness of the BGS in the study of hot fusion reactions. Overall, as the study of hot fusion reactions continues, new techniques are needed to observe the short half-life neutron rich heavy element activities produced with heavy ion beams and actinide targets. The BGS should continue to be used to study the various effects in cold fusion reactions.

The non-observation of the 3n-exit channel in the hot fusion ^{238}U target reactions indicates that the 3n-exit channel is more difficult to observe than anticipated. One possible explanation is the sub-Coulomb barrier fusion required for these reactions to be successful. The sub-Coulomb barrier energies coupled with the 3-neutron evaporation steps at which depletion by fusion can occur leaves the 3n-exit channel as a difficult route for the production of the neutron-rich isotopes of the heaviest elements compared to the 4n-exit channel. As the 4n-exit channel is closer to the Coulomb barrier, the fusion cross

section is higher making the 4n-exit channel a more dominant route to heavy element production. Gaussian modeling confirmed that the fusion barrier has a significant role in the depression of the 3n-exit channel versus the 4n-exit channel in hot fusion reactions.

The observation of equally probable 1n- and 2n-exit channels in cold fusion reactions is no surprise. The same sub-Coulomb barrier hindrance observed in the 3n-exit channel in hot fusion reactions is reduced in cold fusion reactions because of a reduced chance for fission because of only one neutron evaporation step. The increase in the fusion cross section at higher energies is canceled out by the second evaporation step for the 2n-exit channel leaving both the 1n- and 2n-exit channels approximately equal. These results are consistent for all of the cold fusion experiments except the $^{208}Pb(^{48}Ca,xn)^{256-x}No$ reaction in which the 2n-exit channel is much larger than the 1n-exit channel. Possible explanations include the significant fusion cross section enhancement at lower excitation energies for the doubly magic projectile and target system.

The HIVAP code using the Reisdorf and Schädel parameters was accurate in predicting the hot fusion reaction cross sections. Modifications to the input parameters of the HIVAP code helped accurately predict the cold fusion production cross sections. It was observed that fusion barrier fluctuations could play an important role in the overall production cross section. These effects were not seen in the hot fusion reactions probably because hot fusion reaction targets are deformed and not spherical like the lead and bismuth targets. The HIVAP code has been shown to be an effective tool for predicting the production cross sections for various reaction mechanisms. It is, however, important to use HIVAP only to predict the cross sections of isotopes in regions where experiments

have already been performed, and input parameters have carefully been tailored. The HIVAP code is only effective when used to predict cross sections in a particular region of the Chart of Nuclides.

6.2 Future research

The observation that the 3n-exit channel is more difficult to see as the projectile Z increases could lead to the demise of future hot fusion reactions for the production of neutron-rich nuclei. The MG system should be used to study the $^{238}U(^{22}Ne,3n)^{257}No$ reaction in more detail in order to learn more about 3n-exit channel systematics. The BGS is not suited to the study of this particular experiment, because the efficiency of the BGS is to low to produce any significant results. Heavier beams would lead to better efficiencies in the BGS, but lower cross sections may negate the gain from the larger efficiency. The reactions of ^{238}U, ^{244}Pu, and ^{248}Cm targets with high intensity ^{48}Ca beams may help provide insight into the 3n-exit channel, but with production cross sections in the picobarn range, the possibility of a successful study is slim.

With efficiencies in the BGS around 45%, the continuing study of cold fusion reactions with ^{208}Pb and ^{209}Bi targets is promising. Additional work needs to be done to complete the 1n- and 2n- exit channel excitation functions for the $^{208}Pb(^{50}Ti,xn)^{258-x}Rf$, $^{209}Bi(^{50}Ti,xn)^{259-x}Db$, $^{208}Pb(^{51}V,xn)^{259-x}Db$, and $^{209}Bi(^{51}V,xn)^{260-x}Sg$ reactions. Once those are complete, detailed information can be accumulated from the shapes of the excitation functions using the Gaussian fits as well as the predictions of the HIVAP code using the Patin parameters. Studies should be continued by comparing those results with additional experiments with ^{52}Cr and ^{208}Pb and ^{209}Bi targets. These reactions would be useful not only for comparison with the already completed reactions with ^{50}Ti and ^{51}V (N=28) projectiles, but also for the study of the neutron-deficient isotopes of the heaviest elements. Once these experiments have been completed, a completely new set of experiments should be performed using the slightly heavier projectiles ^{54}Cr, ^{55}Mn, and

^{56}Fe (N = 30) with the ^{208}Pb and ^{209}Bi targets. These reactions would be important as similarities could be drawn between the results of these experiments and the results of the experiments with ^{50}Ti and ^{51}V projectiles that have already been studied. These reactions would also extend the study of the neutron-deficient heavy element isotopes.

All of these experiments are exciting and interesting scientifically and have one main goal, to study the different cross sections for reactions producing the heavy elements.

Appendix A: GOOSY data analysis code

```
X$ANAL:@PROCEDURE(P_BUFFER,P_EVENT)RETURNS(BIN FIXED(31));

/*
================================================================================
     COMMENTS
================================================================================

DESIGNED FOR TYPE 10_1 EVENTS/SUBEVENTS WITH SUBCRATE NUMBER USED TO LABEL
  DIFFERENT SUBEVENTS

EACH EVENT HAS AT LEAST ONE SUBEVENT; THE DATE IS FOUND IN THE SUBEVENT


================================================================================
     VARIABLE DECLARATIONS
================================================================================
*/

DCL P_BUFFER                POINTER;  /* to current buffer */
DCL P_EVENT                 POINTER;  /* to current event  */

/* DATA ELEMENTS FOR EL, YLT, YHT, YLB, YHB, BL, BH, PT */
DCL P_EL                   POINTER STATIC;
DCL P_EH                    POINTER STATIC;
DCL P_YLT                  POINTER STATIC;
DCL P_YHT                  POINTER STATIC;
DCL P_YLB                  POINTER STATIC;
DCL P_YHB                   POINTER STATIC;
DCL P_BL                   POINTER STATIC;
DCL P_BH                   POINTER STATIC;
DCL P_PT                    POINTER STATIC;
DCL P_SEL                  POINTER STATIC;
DCL P_SEH                   POINTER STATIC;
DCL P_SYLT                 POINTER STATIC;
DCL P_SYHT                 POINTER STATIC;
DCL P_SYLB                 POINTER STATIC;
DCL P_SYHB                  POINTER STATIC;
DCL P_SBL                  POINTER STATIC;
DCL P_SBH                  POINTER STATIC;
DCL P_SPT                   POINTER STATIC;
DCL P_CEL                  POINTER STATIC;
DCL P_CEH                   POINTER STATIC;
DCL P_CYLT                 POINTER STATIC;
DCL P_CYHT                 POINTER STATIC;
DCL P_CYLB                 POINTER STATIC;
DCL P_CYHB                  POINTER STATIC;
DCL P_CBL                  POINTER STATIC;
DCL P_CBH                  POINTER STATIC;
DCL P_CPT                   POINTER STATIC;

/* DATA ELEMENTS FOR CALIBRATION SLOPES AND INTERCEPTS */
DCL P_ELM                   POINTER STATIC;
DCL P_ELB                   POINTER STATIC;
DCL P_EHM                   POINTER STATIC;
DCL P_EHB                   POINTER STATIC;
DCL P_YLTM                 POINTER STATIC;
DCL P_YLTB                 POINTER STATIC;
DCL P_YLBM                 POINTER STATIC;
DCL P_YLBB                 POINTER STATIC;
DCL P_YHTM                 POINTER STATIC;
DCL P_YHTB                 POINTER STATIC;
DCL P_YHBM                 POINTER STATIC;
DCL P_YHBB                 POINTER STATIC;
```

```
/* DATA ELEMENTS FOR CALIBRATED POSITIONS AND ENERGIES */
DCL P_PKEV                  POINTER STATIC;
DCL P_PMEV                  POINTER STATIC;
DCL P_PLO                   POINTER STATIC;
DCL P_PHI                  POINTER STATIC;
DCL P_YELT                  POINTER STATIC;
DCL P_YEHT                 POINTER STATIC;
DCL P_YELB                 POINTER STATIC;
DCL P_YEHB                  POINTER STATIC;
DCL P_EKEV                 POINTER STATIC;
DCL P_EMEV                 POINTER STATIC;
DCL P_ELO                   POINTER STATIC;
DCL P_EHI                   POINTER STATIC;

/* DATA ELEMENTS FOR CORRELATIONS */
DCL P_E_EVR                POINTER STATIC;
DCL P_E_MOM                 POINTER STATIC;
DCL P_DTEA                  POINTER STATIC;
DCL P_E_DAU                POINTER STATIC;
DCL P_E_FISS               POINTER STATIC;
DCL P_E_EVRF                POINTER STATIC;
DCL P_E_PPAC                POINTER STATIC;

/* DATA ELEMENTS NAI AND RUTHERFORDS */
DCL P_NAIL                 POINTER STATIC;
DCL P_NAIH                  POINTER STATIC;
DCL P_RESLSW               POINTER STATIC;
DCL P_RESMSW               POINTER STATIC;
DCL P_RWSLSW               POINTER STATIC;
DCL P_RWSMSW                POINTER STATIC;
DCL P_RE                   POINTER STATIC;
DCL P_RW                   POINTER STATIC;

/* OTHER DATA ELEMENTS */
DCL P_IPAR                  POINTER STATIC;
DCL P_SLOPE                POINTER STATIC;
DCL P_PPAC                 POINTER STATIC;
DCL P_ERROR                 POINTER STATIC;

/***** SYSTEM VARIABLE STRUCTURES AND PROCEEDURES *****/
/***** ------ NOT REFERENCED IN DATA BASE ------- *****/

@INCLUDE $MACRO(DCL_PROC);
@INCLUDE $MACRO(S$MESS);
@INCLUDE $MACRO($MACRO);
@INCLUDE $MACRO(U$PRTCL);
@INCLUDE $MACRO(SA$VE10_1);
@INCLUDE $MACRO(SA$VES10_1);
@INCLUDE $MACRO(SA$BUFHE);
@INCLUDE $MACRO(U$RANDOM);

/***** SYSTEM VARIABLE STRUCTURES REFERENCED IN DATA BASE *****/

DCL P_SECAM     POINTER STATIC;
@INCLUDE $MACRO(SA$secam);
P_SA$SECAM = P_SECAM;

/*
DCL 1 S_ BASED(P_),
    2 L__LOW   BIN FIXED(31),
    2 L__HIGH  BIN FIXED(31),
    2 R_(1 REFER(L__LOW):1 REFER(L__HIGH))   BIN FLOAT(24);
*/

DCL 1 S_EL BASED(P_EL),
    2 L_EL_LOW   BIN FIXED(31),
    2 L_EL_HIGH  BIN FIXED(31),
    2 R_EL(1 REFER(L_EL_LOW):1 REFER(L_EL_HIGH))   BIN FLOAT(24);
```

```
DCL 1 S_EH BASED(P_EH),
    2 L_EH_LOW   BIN FIXED(31),
    2 L_EH_HIGH  BIN FIXED(31),
    2 R_EH(1 REFER(L_EH_LOW):1 REFER(L_EH_HIGH))   BIN FLOAT(24);
DCL 1 S_YLT BASED(P_YLT),
    2 L_YLT_LOW   BIN FIXED(31),
    2 L_YLT_HIGH  BIN FIXED(31),
    2 R_YLT(1 REFER(L_YLT_LOW):1 REFER(L_YLT_HIGH))   BIN FLOAT(24);
DCL 1 S_YHT BASED(P_YHT),
    2 L_YHT_LOW   BIN FIXED(31),
    2 L_YHT_HIGH  BIN FIXED(31),
    2 R_YHT(1 REFER(L_YHT_LOW):1 REFER(L_YHT_HIGH))   BIN FLOAT(24);
DCL 1 S_YLB BASED(P_YLB),
    2 L_YLB_LOW   BIN FIXED(31),
    2 L_YLB_HIGH  BIN FIXED(31),
    2 R_YLB(1 REFER(L_YLB_LOW):1 REFER(L_YLB_HIGH))   BIN FLOAT(24);
DCL 1 S_YHB BASED(P_YHB),
    2 L_YHB_LOW   BIN FIXED(31),
    2 L_YHB_HIGH  BIN FIXED(31),
    2 R_YHB(1 REFER(L_YHB_LOW):1 REFER(L_YHB_HIGH))   BIN FLOAT(24);
DCL 1 S_BL BASED(P_BL),
    2 L_BL_LOW   BIN FIXED(31),
    2 L_BL_HIGH  BIN FIXED(31),
    2 R_BL(1 REFER(L_BL_LOW):1 REFER(L_BL_HIGH))   BIN FLOAT(24);
DCL 1 S_BH BASED(P_BH),
    2 L_BH_LOW   BIN FIXED(31),
    2 L_BH_HIGH  BIN FIXED(31),
    2 R_BH(1 REFER(L_BH_LOW):1 REFER(L_BH_HIGH))   BIN FLOAT(24);
DCL 1 S_PT BASED(P_PT),
    2 L_PT_LOW   BIN FIXED(31),
    2 L_PT_HIGH  BIN FIXED(31),
    2 R_PT(1 REFER(L_PT_LOW):1 REFER(L_PT_HIGH))   BIN FLOAT(24);
DCL 1 S_CEL BASED(P_CEL),
    2 L_CEL_LOW   BIN FIXED(31),
    2 L_CEL_HIGH  BIN FIXED(31),
    2 R_CEL(1 REFER(L_CEL_LOW):1 REFER(L_CEL_HIGH))   BIN FLOAT(24);
DCL 1 S_CEH BASED(P_CEH),
    2 L_CEH_LOW   BIN FIXED(31),
    2 L_CEH_HIGH  BIN FIXED(31),
    2 R_CEH(1 REFER(L_CEH_LOW):1 REFER(L_CEH_HIGH))   BIN FLOAT(24);
DCL 1 S_CYLT BASED(P_CYLT),
    2 L_CYLT_LOW   BIN FIXED(31),
    2 L_CYLT_HIGH  BIN FIXED(31),
    2 R_CYLT(1 REFER(L_CYLT_LOW):1 REFER(L_CYLT_HIGH))   BIN FLOAT(24);
DCL 1 S_CYHT BASED(P_CYHT),
    2 L_CYHT_LOW   BIN FIXED(31),
    2 L_CYHT_HIGH  BIN FIXED(31),
    2 R_CYHT(1 REFER(L_CYHT_LOW):1 REFER(L_CYHT_HIGH))   BIN FLOAT(24);
DCL 1 S_CYLB BASED(P_CYLB),
    2 L_CYLB_LOW   BIN FIXED(31),
    2 L_CYLB_HIGH  BIN FIXED(31),
    2 R_CYLB(1 REFER(L_CYLB_LOW):1 REFER(L_CYLB_HIGH))   BIN FLOAT(24);
DCL 1 S_CYHB BASED(P_CYHB),
    2 L_CYHB_LOW   BIN FIXED(31),
    2 L_CYHB_HIGH  BIN FIXED(31),
    2 R_CYHB(1 REFER(L_CYHB_LOW):1 REFER(L_CYHB_HIGH))   BIN FLOAT(24);
DCL 1 S_CBL BASED(P_CBL),
    2 L_CBL_LOW   BIN FIXED(31),
    2 L_CBL_HIGH  BIN FIXED(31),
    2 R_CBL(1 REFER(L_CBL_LOW):1 REFER(L_CBL_HIGH))   BIN FLOAT(24);
DCL 1 S_CBH BASED(P_CBH),
    2 L_CBH_LOW   BIN FIXED(31),
    2 L_CBH_HIGH  BIN FIXED(31),
    2 R_CBH(1 REFER(L_CBH_LOW):1 REFER(L_CBH_HIGH))   BIN FLOAT(24);
DCL 1 S_CPT BASED(P_CPT),
    2 L_CPT_LOW   BIN FIXED(31),
    2 L_CPT_HIGH  BIN FIXED(31),
    2 R_CPT(1 REFER(L_CPT_LOW):1 REFER(L_CPT_HIGH))   BIN FLOAT(24);
DCL 1 S_SEL BASED(P_SEL),
```

```
    2 L_SEL_LOW   BIN FIXED(31),
    2 L_SEL_HIGH  BIN FIXED(31),
    2 R_SEL(1 REFER(L_SEL_LOW):1 REFER(L_SEL_HIGH))   BIN FLOAT(24);
DCL 1 S_SEH BASED(P_SEH),
    2 L_SEH_LOW   BIN FIXED(31),
    2 L_SEH_HIGH  BIN FIXED(31),
    2 R_SEH(1 REFER(L_SEH_LOW):1 REFER(L_SEH_HIGH))   BIN FLOAT(24);
DCL 1 S_SYLT BASED(P_SYLT),
    2 L_SYLT_LOW   BIN FIXED(31),
    2 L_SYLT_HIGH  BIN FIXED(31),
    2 R_SYLT(1 REFER(L_SYLT_LOW):1 REFER(L_SYLT_HIGH))   BIN FLOAT(24);
DCL 1 S_SYHT BASED(P_SYHT),
    2 L_SYHT_LOW   BIN FIXED(31),
    2 L_SYHT_HIGH  BIN FIXED(31),
    2 R_SYHT(1 REFER(L_SYHT_LOW):1 REFER(L_SYHT_HIGH))   BIN FLOAT(24);
DCL 1 S_SYLB BASED(P_SYLB),
    2 L_SYLB_LOW   BIN FIXED(31),
    2 L_SYLB_HIGH  BIN FIXED(31),
    2 R_SYLB(1 REFER(L_SYLB_LOW):1 REFER(L_SYLB_HIGH))   BIN FLOAT(24);
DCL 1 S_SYHB BASED(P_SYHB),
    2 L_SYHB_LOW   BIN FIXED(31),
    2 L_SYHB_HIGH  BIN FIXED(31),
    2 R_SYHB(1 REFER(L_SYHB_LOW):1 REFER(L_SYHB_HIGH))   BIN FLOAT(24);
DCL 1 S_SBL BASED(P_SBL),
    2 L_SBL_LOW   BIN FIXED(31),
    2 L_SBL_HIGH  BIN FIXED(31),
    2 R_SBL(1 REFER(L_SBL_LOW):1 REFER(L_SBL_HIGH))   BIN FLOAT(24);
DCL 1 S_SBH BASED(P_SBH),
    2 L_SBH_LOW   BIN FIXED(31),
    2 L_SBH_HIGH  BIN FIXED(31),
    2 R_SBH(1 REFER(L_SBH_LOW):1 REFER(L_SBH_HIGH))   BIN FLOAT(24);
DCL 1 S_SPT BASED(P_CPT),
    2 L_SPT_LOW   BIN FIXED(31),
    2 L_SPT_HIGH  BIN FIXED(31),
    2 R_SPT(1 REFER(L_SPT_LOW):1 REFER(L_SPT_HIGH))   BIN FLOAT(24);
DCL 1 S_ELM BASED(P_ELM),
    2 L_ELM_LOW   BIN FIXED(31),
    2 L_ELM_HIGH  BIN FIXED(31),
    2 R_ELM(1 REFER(L_ELM_LOW):1 REFER(L_ELM_HIGH))   BIN FLOAT(24);
DCL 1 S_ELB BASED(P_ELB),
    2 L_ELB_LOW   BIN FIXED(31),
    2 L_ELB_HIGH  BIN FIXED(31),
    2 R_ELB(1 REFER(L_ELB_LOW):1 REFER(L_ELB_HIGH))   BIN FLOAT(24);
DCL 1 S_EHM BASED(P_EHM),
    2 L_EHM_LOW   BIN FIXED(31),
    2 L_EHM_HIGH  BIN FIXED(31),
    2 R_EHM(1 REFER(L_EHM_LOW):1 REFER(L_EHM_HIGH))   BIN FLOAT(24);
DCL 1 S_EHB BASED(P_EHB),
    2 L_EHB_LOW   BIN FIXED(31),
    2 L_EHB_HIGH  BIN FIXED(31),
    2 R_EHB(1 REFER(L_EHB_LOW):1 REFER(L_EHB_HIGH))   BIN FLOAT(24);
DCL 1 S_YLTM BASED(P_YLTM),
    2 L_YLTM_LOW   BIN FIXED(31),
    2 L_YLTM_HIGH  BIN FIXED(31),
    2 R_YLTM(1 REFER(L_YLTM_LOW):1 REFER(L_YLTM_HIGH))   BIN FLOAT(24);
DCL 1 S_YLTB BASED(P_YLTB),
    2 L_YLTB_LOW   BIN FIXED(31),
    2 L_YLTB_HIGH  BIN FIXED(31),
    2 R_YLTB(1 REFER(L_YLTB_LOW):1 REFER(L_YLTB_HIGH))   BIN FLOAT(24);
DCL 1 S_YLBM BASED(P_YLBM),
    2 L_YLBM_LOW   BIN FIXED(31),
    2 L_YLBM_HIGH  BIN FIXED(31),
    2 R_YLBM(1 REFER(L_YLBM_LOW):1 REFER(L_YLBM_HIGH))   BIN FLOAT(24);
DCL 1 S_YLBB BASED(P_YLBB),
    2 L_YLBB_LOW   BIN FIXED(31),
    2 L_YLBB_HIGH  BIN FIXED(31),
    2 R_YLBB(1 REFER(L_YLBB_LOW):1 REFER(L_YLBB_HIGH))   BIN FLOAT(24);
DCL 1 S_YHTM BASED(P_YHTM),
    2 L_YHTM_LOW   BIN FIXED(31),
```

```
     2 L_YHTM_HIGH  BIN FIXED(31),
     2 R_YHTM(1 REFER(L_YHTM_LOW):1 REFER(L_YHTM_HIGH))   BIN FLOAT(24);
DCL  1 S_YHTB BASED(P_YHTB),
     2 L_YHTB_LOW   BIN FIXED(31),
     2 L_YHTB_HIGH  BIN FIXED(31),
     2 R_YHTB(1 REFER(L_YHTB_LOW):1 REFER(L_YHTB_HIGH))   BIN FLOAT(24);
DCL  1 S_YHBM BASED(P_YHBM),
     2 L_YHBM_LOW   BIN FIXED(31),
     2 L_YHBM_HIGH  BIN FIXED(31),
     2 R_YHBM(1 REFER(L_YHBM_LOW):1 REFER(L_YHBM_HIGH))   BIN FLOAT(24);
DCL  1 S_YHBB BASED(P_YHBB),
     2 L_YHBB_LOW   BIN FIXED(31),
     2 L_YHBB_HIGH  BIN FIXED(31),
     2 R_YHBB(1 REFER(L_YHBB_LOW):1 REFER(L_YHBB_HIGH))   BIN FLOAT(24);
DCL  1 S_PKEV BASED(P_PKEV),
     2 L_PKEV_LOW   BIN FIXED(31),
     2 L_PKEV_HIGH  BIN FIXED(31),
     2 R_PKEV(1 REFER(L_PKEV_LOW):1 REFER(L_PKEV_HIGH))   BIN FLOAT(24);
DCL  1 S_PMEV BASED(P_PMEV),
     2 L_PMEV_LOW   BIN FIXED(31),
     2 L_PMEV_HIGH  BIN FIXED(31),
     2 R_PMEV(1 REFER(L_PMEV_LOW):1 REFER(L_PMEV_HIGH))   BIN FLOAT(24);
DCL  1 S_PLO BASED(P_PLO),
     2 L_PLO_LOW   BIN FIXED(31),
     2 L_PLO_HIGH  BIN FIXED(31),
     2 R_PLO(1 REFER(L_PLO_LOW):1 REFER(L_PLO_HIGH))   BIN FLOAT(24);
DCL  1 S_PHI BASED(P_PHI),
     2 L_PHI_LOW   BIN FIXED(31),
     2 L_PHI_HIGH  BIN FIXED(31),
     2 R_PHI(1 REFER(L_PHI_LOW):1 REFER(L_PHI_HIGH))   BIN FLOAT(24);
DCL  1 S_YELT BASED(P_YELT),
     2 L_YELT_LOW   BIN FIXED(31),
     2 L_YELT_HIGH  BIN FIXED(31),
     2 R_YELT(1 REFER(L_YELT_LOW):1 REFER(L_YELT_HIGH))   BIN FLOAT(24);
DCL  1 S_YEHT BASED(P_YEHT),
     2 L_YEHT_LOW   BIN FIXED(31),
     2 L_YEHT_HIGH  BIN FIXED(31),
     2 R_YEHT(1 REFER(L_YEHT_LOW):1 REFER(L_YEHT_HIGH))   BIN FLOAT(24);
DCL  1 S_YELB BASED(P_YELB),
     2 L_YELB_LOW   BIN FIXED(31),
     2 L_YELB_HIGH  BIN FIXED(31),
     2 R_YELB(1 REFER(L_YELB_LOW):1 REFER(L_YELB_HIGH))   BIN FLOAT(24);
DCL  1 S_YEHB BASED(P_YEHB),
     2 L_YEHB_LOW   BIN FIXED(31),
     2 L_YEHB_HIGH  BIN FIXED(31),
     2 R_YEHB(1 REFER(L_YEHB_LOW):1 REFER(L_YEHB_HIGH))   BIN FLOAT(24);
DCL  1 S_EKEV BASED(P_EKEV),
     2 L_EKEV_LOW   BIN FIXED(31),
     2 L_EKEV_HIGH  BIN FIXED(31),
     2 R_EKEV(1 REFER(L_EKEV_LOW):1 REFER(L_EKEV_HIGH))   BIN FLOAT(24);
DCL  1 S_EMEV BASED(P_EMEV),
     2 L_EMEV_LOW   BIN FIXED(31),
     2 L_EMEV_HIGH  BIN FIXED(31),
     2 R_EMEV(1 REFER(L_EMEV_LOW):1 REFER(L_EMEV_HIGH))   BIN FLOAT(24);
DCL  1 S_ELO BASED(P_ELO),
     2 L_ELO_LOW   BIN FIXED(31),
     2 L_ELO_HIGH  BIN FIXED(31),
     2 R_ELO(1 REFER(L_ELO_LOW):1 REFER(L_ELO_HIGH))   BIN FLOAT(24);
DCL  1 S_EHI BASED(P_EHI),
     2 L_EHI_LOW   BIN FIXED(31),
     2 L_EHI_HIGH  BIN FIXED(31),
     2 R_EHI(1 REFER(L_EHI_LOW):1 REFER(L_EHI_HIGH))   BIN FLOAT(24);
DCL  1 S_E_EVR BASED(P_E_EVR),
     2 L_E_EVR_LOW   BIN FIXED(31),
     2 L_E_EVR_HIGH  BIN FIXED(31),
     2 R_E_EVR(1 REFER(L_E_EVR_LOW):1 REFER(L_E_EVR_HIGH))   BIN FLOAT(24);
DCL  1 S_E_MOM BASED(P_E_MOM),
     2 L_E_MOM_LOW   BIN FIXED(31),
     2 L_E_MOM_HIGH  BIN FIXED(31),
```

```
    2 R_E_MOM(1 REFER(L_E_MOM_LOW):1 REFER(L_E_MOM_HIGH))   BIN FLOAT(24);
DCL 1 S_DTEA BASED(P_DTEA),
    2 L_DTEA_LOW   BIN FIXED(31),
    2 L_DTEA_HIGH  BIN FIXED(31),
    2 R_DTEA(1 REFER(L_DTEA_LOW):1 REFER(L_DTEA_HIGH))   BIN FLOAT(24);
DCL 1 S_E_DAU BASED(P_E_DAU),
    2 L_E_DAU_LOW   BIN FIXED(31),
    2 L_E_DAU_HIGH  BIN FIXED(31),
    2 R_E_DAU(1 REFER(L_E_DAU_LOW):1 REFER(L_E_DAU_HIGH))   BIN FLOAT(24);
DCL 1 S_E_FISS BASED(P_E_FISS),
    2 L_E_FISS_LOW   BIN FIXED(31),
    2 L_E_FISS_HIGH  BIN FIXED(31),
    2 R_E_FISS(1 REFER(L_E_FISS_LOW):1 REFER(L_E_FISS_HIGH))   BIN FLOAT(24);
DCL 1 S_E_EVRF BASED(P_E_EVRF),
    2 L_E_EVRF_LOW   BIN FIXED(31),
    2 L_E_EVRF_HIGH  BIN FIXED(31),
    2 R_E_EVRF(1 REFER(L_E_EVRF_LOW):1 REFER(L_E_EVRF_HIGH))   BIN FLOAT(24);
DCL 1 S_E_PPAC BASED(P_E_PPAC),
    2 L_E_PPAC_LOW   BIN FIXED(31),
    2 L_E_PPAC_HIGH  BIN FIXED(31),
    2 R_E_PPAC(1 REFER(L_E_PPAC_LOW):1 REFER(L_E_PPAC_HIGH))   BIN FLOAT(24);
DCL 1 S_NAIL BASED(P_NAIL),
    2 L_NAIL_LOW   BIN FIXED(31),
    2 L_NAIL_HIGH  BIN FIXED(31),
    2 R_NAIL(1 REFER(L_NAIL_LOW):1 REFER(L_NAIL_HIGH))   BIN FLOAT(24);
DCL 1 S_NAIH BASED(P_NAIH),
    2 L_NAIH_LOW   BIN FIXED(31),
    2 L_NAIH_HIGH  BIN FIXED(31),
    2 R_NAIH(1 REFER(L_NAIH_LOW):1 REFER(L_NAIH_HIGH))   BIN FLOAT(24);
DCL 1 S_RESLSW BASED(P_RESLSW),
    2 L_RESLSW_LOW   BIN FIXED(31),
    2 L_RESLSW_HIGH  BIN FIXED(31),
    2 R_RESLSW(1 REFER(L_RESLSW_LOW):1 REFER(L_RESLSW_HIGH))   BIN FLOAT(24);
DCL 1 S_RESMSW BASED(P_RESMSW),
    2 L_RESMSW_LOW   BIN FIXED(31),
    2 L_RESMSW_HIGH  BIN FIXED(31),
    2 R_RESMSW(1 REFER(L_RESMSW_LOW):1 REFER(L_RESMSW_HIGH))   BIN FLOAT(24);
DCL 1 S_RWSLSW BASED(P_RWSLSW),
    2 L_RWSLSW_LOW   BIN FIXED(31),
    2 L_RWSLSW_HIGH  BIN FIXED(31),
    2 R_RWSLSW(1 REFER(L_RWSLSW_LOW):1 REFER(L_RWSLSW_HIGH))   BIN FLOAT(24);
DCL 1 S_RWSMSW BASED(P_RWSMSW),
    2 L_RWSMSW_LOW   BIN FIXED(31),
    2 L_RWSMSW_HIGH  BIN FIXED(31),
    2 R_RWSMSW(1 REFER(L_RWSMSW_LOW):1 REFER(L_RWSMSW_HIGH))   BIN FLOAT(24);
DCL 1 S_RE BASED(P_RE),
    2 L_RE_LOW   BIN FIXED(31),
    2 L_RE_HIGH  BIN FIXED(31),
    2 R_RE(1 REFER(L_RE_LOW):1 REFER(L_RE_HIGH))   BIN FLOAT(24);
DCL 1 S_RW BASED(P_RW),
    2 L_RW_LOW   BIN FIXED(31),
    2 L_RW_HIGH  BIN FIXED(31),
    2 R_RW(1 REFER(L_RW_LOW):1 REFER(L_RW_HIGH))   BIN FLOAT(24);
DCL 1 S_IPAR BASED(P_IPAR),
    2 L_IPAR_LOW   BIN FIXED(31),
    2 L_IPAR_HIGH  BIN FIXED(31),
    2 R_IPAR(1 REFER(L_IPAR_LOW):1 REFER(L_IPAR_HIGH))   BIN FLOAT(24);
DCL 1 S_SLOPE BASED(P_SLOPE),
    2 L_SLOPE_LOW   BIN FIXED(31),
    2 L_SLOPE_HIGH  BIN FIXED(31),
    2 R_SLOPE(1 REFER(L_SLOPE_LOW):1 REFER(L_SLOPE_HIGH))   BIN FLOAT(24);
DCL 1 S_PPAC BASED(P_PPAC),
    2 L_PPAC_LOW   BIN FIXED(31),
    2 L_PPAC_HIGH  BIN FIXED(31),
    2 R_PPAC(1 REFER(L_PPAC_LOW):1 REFER(L_PPAC_HIGH))   BIN FLOAT(24);
DCL 1 S_ERROR BASED(P_ERROR),
    2 L_ERROR_LOW   BIN FIXED(31),
    2 L_ERROR_HIGH  BIN FIXED(31),
    2 R_ERROR(1 REFER(L_ERROR_LOW):1 REFER(L_ERROR_HIGH))   BIN FLOAT(24);
```

```
/***** LOCAL PROCEDURE VARIABLES *****/

DCL (P_NEXT_EVENT,P_NEXT_SUBEVENT) POINTER;

DCL I                    BIN FIXED(31);
DCL J                   BIN FIXED(31);
DCL K                   BIN FIXED(31);
DCL L_INCR               BIN FIXED(31) INIT(1);
DCL B_PAUSE              BIT(1) ALIGNED STATIC;
DCL R_PRN               BIN FLOAT(24) STATIC INIT(1);
DCL R_MAX               BIN FLOAT(24) STATIC INIT(1);
DCL USLSW                BIN FLOAT(53) STATIC;
DCL USMSW               BIN FLOAT(53) STATIC;
DCL USSSW                BIN FLOAT(53) STATIC;
DCL MSLSW               BIN FLOAT(53) STATIC;
DCL MSMSW               BIN FLOAT(53) STATIC;
DCL SLSW                BIN FLOAT(53) STATIC;
DCL SMSW                BIN FLOAT(53) STATIC;
DCL MLSW                BIN FLOAT(53) STATIC;
DCL MMSW                BIN FLOAT(53) STATIC;
DCL TIMEUS              BIN FLOAT(53) STATIC INIT(0.);
DCL TIMEMS              BIN FLOAT(53) STATIC INIT(0.);
DCL TIMESEC              BIN FLOAT(53) STATIC INIT(0.);
DCL TIME                BIN FLOAT(53) STATIC INIT(0.);
DCL TIMEMIN              BIN FLOAT(53) STATIC INIT(0.);
DCL B_RE                BIT(1) ALIGNED STATIC;
DCL B_RW                BIT(1) ALIGNED STATIC;
DCL B_TIME               BIT(1);
DCL N1000               BIN FLOAT(53) INIT(1000.0000000);
DCL N216                BIN FLOAT(53) INIT(65536.000000);
DCL N224                 BIN FLOAT(53) INIT(16777216.000);
DCL N232                BIN FLOAT(53) INIT(4294967296.0);
DCL C_TIME               CHAR(128) VARYING;
DCL R_EPUNCH             BIN FLOAT(24);
DCL R_SPUNCH             BIN FLOAT(24);
DCL B_MOTHER            BIT(1) ALIGNED STATIC;
DCL B_DAUGHTER          BIT(1) ALIGNED STATIC;
DCL B_EVAP              BIT(1) ALIGNED STATIC;
DCL B_EVAPF              BIT(1) ALIGNED STATIC;
DCL B_FISSION            BIT(1) ALIGNED STATIC;
DCL B_PPAC              BIT(1) ALIGNED STATIC;
DCL B_EVR               BIT(1) ALIGNED STATIC;
DCL B_MOM               BIT(1) ALIGNED STATIC;
DCL B_DAU                BIT(1) ALIGNED STATIC;
DCL B_FISS               BIT(1) ALIGNED STATIC;
DCL B_EVRF               BIT(1) ALIGNED STATIC;
DCL B_PUNCH(8)           BIT(1) ALIGNED STATIC;
DCL B_PUNCHTHROUGH       BIT(1) ALIGNED STATIC;
DCL C                    BIN FIXED(31);
DCL N                    BIN FIXED(31);
DCL Q                    BIN FIXED(31) INIT(0);
DCL R                    BIN FIXED(31) INIT(0);
DCL U                    BIN FIXED(31) INIT(0);
DCL I_EVCT              BIN FIXED(31) STATIC INIT(0);
DCL T_EA                 BIN FLOAT(24) STATIC;
DCL T_EA_MAX            BIN FLOAT(24) STATIC;
DCL T_EA_MIN            BIN FLOAT(24) STATIC;
DCL T_AA                BIN FLOAT(24) STATIC;
DCL T_AA_MAX            BIN FLOAT(24) STATIC;
DCL T_AA_MIN             BIN FLOAT(24) STATIC;
DCL T_EF                 BIN FLOAT(24) STATIC;
DCL T_EF_MAX             BIN FLOAT(24) STATIC;
DCL T_EF_MIN             BIN FLOAT(24) STATIC;
DCL C_EVAP              CHAR(128) VARYING;
DCL P_DIFF_EA           BIN FLOAT(24) STATIC;
DCL P_DIFF_AA           BIN FLOAT(24) STATIC;
DCL P_DIFF_EF            BIN FLOAT(24) STATIC;
DCL E_RATIO              BIN FLOAT(24) STATIC;
```

```
DCL LOGT_EA             BIN FLOAT(24) STATIC;
DCL R_DT                  BIN FLOAT(24);

/*
================================================================================
================================================================================

     INTERACTIVE PARAMETERS USED IN THIS CODE
     ----------------------------------------

PARAMETER      DESCRIPTION                   VALUES USED
---------       -----------                  -----------
R_IPAR(1)      DO CORRELATIONS?              1=YES,0=NO
R_IPAR(2)       PRINT CORRELATIONS           1=YES,0=NO
R_IPAR(3)       NUMBER OF CORRELATIONS          VARIABLE
R_IPAR(4)      CLEAR BUFFERS/EVENT COUNTERS  1=YES,0=NO
R_IPAR(5)       POSITION GATE ALPHAS LOW        VARIABLE
R_IPAR(6)      POSITION GATE ALPHAS HIGH     VARIABLE
R_IPAR(7)      POSITION GATE FISSIONS LOW    VARIABLE
R_IPAR(8)      POSITION GATE FISSIONS HIGH   VARIABLE
R_IPAR(9)
R_IPAR(10)     TIME EVAP-MAX                 VARIABLE
R_IPAR(11)     TIME EVAP-MIN                 VARIABLE
R_IPAR(12)     TIME ALPHA-MAX                VARIABLE
R_IPAR(13)      TIME ALPHA-MIN                      VARIABLE
R_IPAR(14)     TIME EVAP-FISS MAX            VARIABLE
R_IPAR(15)     TIME EVAP-FISS MIN            VARIABLE
R_IPAR(16)
R_IPAR(17)      LIST EVENTS QUESTION            VARIABLE
R_IPAR(18)      STRIP LISTER                    1-32
R_IPAR(19)      MINIMUM EVENT NUMBER            VARIABLE
R_IPAR(20)      MAXIMUM NUMBER OF EVENTS        VARIABLE
R_IPAR(21)
R_IPAR(22)
R_IPAR(23)      PRINT TIMES?                  1=YES,0=NO
R_IPAR(24)     PRINT TIME LOW RANGE          VARIABLE
R_IPAR(25)      PRINT TIME HIGH RANGE         VARIABLE
R_IPAR(26)      PRINT EVENTS VICTOR?             1=YES,0=NO
R_IPAR(27)
R_IPAR(28)
R_IPAR(29)
R_IPAR(30)      CORRELATED EVENT COUNTER         1=YES,0=NO

================================================================================
*/

/*
================================================================================
     X$ANAL - MAIN BODY OF PROCEEDURE STARTS HERE
================================================================================
*/

@DCL_MSG(XIO_NOOUTPUT);
@ON_ANY_W(U_CLEANUP);
STS$VALUE=1;

P_SA$BUFHE = P_BUFFER;                        /* SET POINTER TO BUFFER HEADER */
P_SA$VE10_1 = P_EVENT;                        /* SET POINTER TO EVENT HEADER  */

P_NEXT_EVENT    = ADDR(LA$VE10_1_NEXT);
P_NEXT_SUBEVENT = ADDR(IA$VE10_1(1));

R_ERROR(1) = 0.;

DO WHILE (P_NEXT_SUBEVENT ^= P_NEXT_EVENT);  /* LOOP OVER SUBEVENTS IN EVENT */

   P_SA$VES10_1 = P_NEXT_SUBEVENT;            /* SET POINTER TO SUBEVENT HDR  */
   P_NEXT_SUBEVENT = ADDR(LA$VES10_1_NEXT);
```

```
   I_EVCT=I_EVCT+1;
   R_ERROR(1) = 0.5;
   R_ERROR(2) = 0.5;
   R_ERROR(1) = 1.;      CALL UNPACK_RAW;     /** RA$SECAM PROC **/
   R_ERROR(1) = 2.;      CALL TIMES;          /** TIME ORGANIZATION **/
   R_ERROR(1) = 3.;      CALL CALIBRATION;    /** CALIBRATION **/
   R_ERROR(1) = 4.;      CALL POSITION;       /** POSITION DETERMINATION **/
   R_ERROR(1) = 5.;      CALL SINGLES;        /** SINGLES SPECTRA **/
   R_ERROR(1) = 6.;      CALL BUFFER;         /** CORRELATION ROUTINE **/
   R_ERROR(1) = 7.;      CALL EVENTLIST;
   R_ERROR(1) = -0.5;
   R_ERROR(2) = -0.5;
END;

/*
================================================================================
     PROCEDURE FOR UNPACKING RAW DATA INTO RA$SECAM AND MAKING RAW SPECTRA
     SPECTRA-(S)
================================================================================
*/

UNPACK_RAW : PROCEDURE;

DCL SE_INDEX            BIN FIXED(31);

/** INITIALIZE RA$SECAM **/ R_ERROR(2) = 1.;
DO I = 1 TO 353;
   RA$SECAM(I)=0.;
END;
R_ERROR(2) = 11.;
R_ERROR(2) = 12.;
R_ERROR(2) = 13.;
R_NAIL(1) = 0.;
R_NAIH(1) = 0.;
R_RESLSW(1) = 0.;
R_RESMSW(1) = 0.;
R_RWSLSW(1) = 0.;
R_RWSMSW(1) = 0.;
R_RE(1) = 0.;
R_RE(1) = 0.;
DO I = 1 TO 32;
   R_EL(I) = 0.;
   R_EH(I) = 0.;
   R_YLT(I) = 0.;
   R_YHT(I) = 0.;
   R_YLB(I) = 0.;
   R_YHB(I) = 0.;
END;
DO I = 1 TO 16;
   R_BL(I) = 0.;
   R_BH(I) = 0.;
END;
DO I = 1 TO 8;
   R_PT(I) = 0.;
END;
R_PPAC(1) = 0.;

R_ERROR(2) = 2.;
IF (I_EVCT >= R_IPAR(19)) & (I_EVCT <= R_IPAR(20)) & (R_IPAR(26) = 1) THEN DO;
   @CALL U$PRTCL(
   'Buf:'||      TRIM(CHAR(LA$BUFHE_buf))||
   ', evts:'||   TRIM(CHAR(LA$BUFHE_evt))||
   ', EV len:'||TRIM(CHAR(LA$ve10_1_dlen))||
   ', t/s:'||    TRIM(CHAR(IA$ve10_1_type))||
   '/'||         TRIM(CHAR(IA$ve10_1_subtype))||
   ', #:'||      TRIM(CHAR(LA$ve10_1_count))||
   ' SE len:'|| TRIM(CHAR(LA$ves10_1_dlen))||
   ', t/s:'||    TRIM(CHAR(IA$ves10_1_type))||
   '/'||         TRIM(CHAR(IA$ves10_1_subtype))||
```

```
   ', id:'||    TRIM(CHAR(IA$ves10_1_procid))
   ,U$M_prtterm);
END;

/** LOAD RA$SECAM **/ R_ERROR(2) = 3.;
DO I = 1 TO (LA$VES10_1_DLEN - 2) BY 2;
   SE_INDEX = FIXED(IA$VES10_1(I),31);
   IF (SE_INDEX > 0 & SE_INDEX <= 354) THEN DO;
      RA$SECAM(SE_INDEX) = POSINT(IA$VES10_1(I+1),1,16);
      IF (R_IPAR(26) = 1) & (I_EVCT >= R_IPAR(19)) & (I_EVCT <= R_IPAR(20)) THEN DO;
         @CALL U$PRTCL(
         '# '||TRIM(CHAR(IA$ves10_1(I)))||
         ' value '||TRIM(CHAR(IA$ves10_1(I+1)))
         ,U$M_prtterm);
      END;
   END;
END;


/** CREATE RAW SPECTRA **/ R_ERROR(2) = 4.;
DO I = 1 TO 352;
   IF RA$SECAM(I) > 0 & RA$SECAM(I) < 4095 THEN
$ACCU1(L,DB,$SPECTRUM,S,I,L_INCR,1,RA$SECAM(I));
END;

/** CREATE DATA ELEMENT VALUES **/
R_ERROR(2) = 5.;
R_ERROR(2) = 6.;

/* EL,EH,YLT,YHT,YLB,YHB */ R_ERROR(2) = 7.;
DO I = 1 TO 32;
   IF RA$SECAM(I+31) > 0 & RA$SECAM(I+31) <= 4096 THEN R_EL(I) = RA$SECAM(I+31);
   IF RA$SECAM(I+63) > 0 & RA$SECAM(I+63) <= 4096 THEN R_EH(I) = RA$SECAM(I+63);
   IF RA$SECAM(I+95) > 0 & RA$SECAM(I+95) <= 4096 THEN R_YLT(I) = RA$SECAM(I+95);
   IF RA$SECAM(I+127) > 0 & RA$SECAM(I+127) <= 4096 THEN R_YHT(I) = RA$SECAM(I+127);
   IF RA$SECAM(I+159) > 0 & RA$SECAM(I+159) <= 4096 THEN R_YLB(I) = RA$SECAM(I+159);
   IF RA$SECAM(I+191) > 0 & RA$SECAM(I+191) <= 4096 THEN R_YHB(I) = RA$SECAM(I+191);
END;

/* BACKWARDS & PUNCHTHROUGHS */ R_ERROR(2) = 8.;
DO I = 1 TO 16;
   IF RA$SECAM(I+223) > 0 & RA$SECAM(I+223) <= 4096 THEN R_BL(I) = RA$SECAM(I+223);
   IF RA$SECAM(I+239) > 0 & RA$SECAM(I+239) <= 4096 THEN R_BH(I) = RA$SECAM(I+239);
END;
DO I = 1 TO 8;
   IF RA$SECAM(I+271) > 0 & RA$SECAM(I+271) <= 4096 THEN R_PT(I) = RA$SECAM(I+271);
END;

/* PPAC */ R_ERROR(2) = 9.;
IF RA$SECAM(260) > 0 & RA$SECAM(260) <= 4096 THEN R_PPAC(1) = RA$SECAM(260);

/* SODIUM IODIDE */
IF RA$SECAM(268) > 0 & RA$SECAM(268) <= 4096 THEN R_NAIL(1) = RA$SECAM(268);
IF RA$SECAM(269) > 0 & RA$SECAM(269) <= 4096 THEN R_NAIH(1) = RA$SECAM(269);

/* RUTHERFORDS */
IF RA$SECAM(25) > 0 & RA$SECAM(25) <= 4096 THEN R_RESLSW(1) = RA$SECAM(25);
IF RA$SECAM(26) > 0 & RA$SECAM(26) <= 4096 THEN R_RESMSW(1) = RA$SECAM(26);
IF RA$SECAM(27) > 0 & RA$SECAM(27) <= 4096 THEN R_RWSLSW(1) = RA$SECAM(27);
IF RA$SECAM(28) > 0 & RA$SECAM(28) <= 4096 THEN R_RWSMSW(1) = RA$SECAM(28);
IF RA$SECAM(270) > 0 & RA$SECAM(270) <= 4096 THEN R_RE(1) = RA$SECAM(270);
IF RA$SECAM(271) > 0 & RA$SECAM(271) <= 4096 THEN R_RW(1) = RA$SECAM(271);

END UNPACK_RAW;

/*
================================================================================
     TIME ANALYSIS
     SPECTRA-(SEC,TIME,RE_RATE,RW_RATE,RUTH_RATE,CHOPMS,CHOPUS)
```

```
================================================================================
*/

TIMES : PROCEDURE;

/** ZERO PARAMETERS **/
USLSW = 0.;
USMSW = 0.;
USSSW = 0.;
MSLSW = 0.;
MSMSW = 0.;
SLSW = 0.;
SMSW = 0.;
MLSW = 0.;
MMSW = 0.;
TIMEUS = 0.;
TIMEMS = 0.;
TIMESEC = 0.;
TIMEMIN = 0.;
TIME = 0.;
B_RE = '0'B;
B_RW = '0'B;

/** DEFINE TIME VARIABLES **/
USLSW = RA$SECAM(3);
USMSW = RA$SECAM(4);
MSLSW = RA$SECAM(5);
MSMSW = RA$SECAM(6);
SLSW = RA$SECAM(7);
SMSW = RA$SECAM(8);
MLSW = RA$SECAM(9);
MMSW = RA$SECAM(10);
TIMESEC = SLSW;
TIMEMS = MSLSW + MSMSW*N216;
B_TIME = '1'B;
I = -1;
DO WHILE (B_TIME);
   I = I + 1;
   IF (TIMEMS > (I*N232)/N1000) & (TIMEMS < ((I+1)*N232)/N1000) THEN DO;
      USSSW = I;
      TIMEUS = USLSW + USMSW*N216 + USSSW*N232;
      B_TIME = '0'B;
   END;
   IF I > 50 THEN B_TIME = '0'B;
END;

R_ERROR(2) = 3.;
TIME = TIMEMS/(N1000);
TIMEMIN = TIMEMS/(60*N1000);

/** PRINT OUT TIMES **/ R_ERROR(2) = 4.;
IF (R_IPAR(23) = 1) THEN DO;
   IF TIMESEC > R_IPAR(24) & TIMESEC < R_IPAR(25) THEN DO;
      PUT STRING(C_TIME) EDIT(
      'Time',TIME,
      ' Min',TIMEMIN,
      ' Sec',TIMESEC,
      ' Millisec',TIMEMS,
      ' Microsec',TIMEUS)
      (A,F(13,6),A,F(13,6),A,F(6,0),A,F(11,0),A,F(14,0));
      @CALL U$PRTCL(C_TIME, U$M_PRTTERM);
   END;
END;

$ACCU(L,DB,$SPECTRUM,SEC,L_INCR,1,TIMESEC);
$ACCU(L,DB,$SPECTRUM,TIME,L_INCR,1,TIME);
$ACCU(L,DB,$SPECTRUM,TIMEMIN,L_INCR,1,TIMEMIN);

/** RUTHERFORD RATE SPECTRA **/ R_ERROR(2) = 5.;
```

```
$COND(WC,DB,$CONDITION,RE,B_RE,1,R_RE(1));
$COND(WC,DB,$CONDITION,RW,B_RW,1,R_RW(1));
IF B_RE THEN DO;
   $ACCU(L,DB,$SPECTRUM,RE_RATE,L_INCR,1,TIME);
   $ACCU(L,DB,$SPECTRUM,RUTH_RATE,L_INCR,1,TIME);
END;
IF B_RW THEN DO;
   $ACCU(L,DB,$SPECTRUM,RW_RATE,L_INCR,1,TIME);
   $ACCU(L,DB,$SPECTRUM,RUTH_RATE,L_INCR,1,TIME);
END;

END TIMES;

/*
================================================================================
     CALIBRATION ROUTINE AND SP, SUM, SUMP SPECTRA
     SPECTRA-(TMP,SP,SPSUM,PPAC,EVR_LOW)
================================================================================
*/

CALIBRATION : PROCEDURE;

/** ZERO PARAMETERS **/
B_PAUSE ='0'B;
B_PPAC = '0'B;
R_PRN = 0.;
DO I = 1 TO 32;
   R_EKEV(I) = 0.;
   R_EMEV(I) = 0.;
END;
R_ELO(1) = 0.;
R_EHI(1) = 0.;

/** TMP CREATION LINE AND PAUSE CONDITION **/
IF RA$SECAM(1) > 0 & RA$SECAM(1) < 30001 THEN DO;
   $ACCU(L,DB,$SPECTRUM,TMP,L_INCR,1,RA$SECAM(1));
   $COND(WC,DB,$CONDITION,PAUSE,B_PAUSE,1,RA$SECAM(1));
END;

/** SP SPECTRA CREATION **/
DO I = 1 TO 32;
   IF B_PAUSE THEN DO;
      IF R_EL(I) > 150 THEN DO;
         $ACCU1(L,DB,$SPECTRUM,SP,I,L_INCR,1,R_EL(I));
         $ACCU(L,DB,$SPECTRUM,SPSUM,L_INCR,1,R_EL(I));
      END;
   END;
END;

/** GENERATE RANDOM NUMBER **/
R_PRN=U$RANDOM(R_MAX);

/** FILL IN ARRAY WITH CALIBRATED DATA **/
DO I = 1 TO 32;
   IF R_EL(I) > 0 THEN DO;
      R_EKEV(I)=((R_EL(I)+R_PRN)*R_ELM(I))+R_ELB(I);
      R_EKEV(I)=R_EKEV(I) * (1.0 - R_SLOPE(I)*((R_YLT(I)/R_EL(I))-0.5));
      IF (R_EKEV(I) > 250) & (R_EKEV(I) > R_ELO(1)) THEN R_ELO(1) = R_EKEV(I);
   END;
END;
DO I = 1 TO 32;
   IF R_EH(I) > 0 THEN DO;
      R_EMEV(I)=R_EH(I);
      IF (R_EMEV(I) > 50) & (R_EMEV(I) > R_EHI(1)) THEN R_EHI(1) = R_EMEV(I);
   END;
END;

/** PPAC CONDITION SPECTRA **/
$COND(WC,DB,$CONDITION,PPAC,B_PPAC,1,R_PPAC(1));
```

```
IF B_PPAC THEN DO;
   $ACCU(L,DB,$SPECTRUM,PPAC,L_INCR,1,R_PPAC(1));
   IF R_ELO(1) > 5 THEN DO;
      $ACCU(L,DB,$SPECTRUM,EVR_LOW,L_INCR,1,R_ELO(1));
   END;
END;

END CALIBRATION;

/*
================================================================================
     POSITION DETERMINATION
     SPECTRA-(POS_T,POS_B)
================================================================================
*/

POSITION : PROCEDURE;

/** ZERO PARAMETERS **/
R_SEL(1) = 0.;
R_CEL(1) = 0.;
R_SEH(1) = 0.;
R_CEH(1) = 0.;
R_SYLT(1) = 0.;
R_CYLT(1) = 0.;
R_SYLB(1) = 0.;
R_CYLB(1) = 0.;
R_SYHT(1) = 0.;
R_CYHT(1) = 0.;
R_SYHB(1) = 0.;
R_CYHB(1) = 0.;
R_SBL(1) = 0.;
R_CBL(1) = 0.;
R_SBH(1) = 0.;
R_CBH(1) = 0.;
R_SPT(1) = 0.;
R_CPT(1) = 0.;
DO I = 1 TO 32;
   R_PKEV(I) = 0.;
   R_PMEV(I) = 0.;
   R_YELT(I) = 0.;
   R_YEHT(I) = 0.;
   R_YELB(I) = 0.;
   R_YEHB(I) = 0.;
END;
R_PLO(1) = 0.;
R_PHI(1) = 0.;

/** STRIP AND MAX CHANNEL ROUTINE **/
DO I = 1 TO 32;
   IF (R_EL(I) > 50) & (R_EL(I) > R_CEL(1)) THEN R_SEL(1) = I;
   IF (R_EL(I) > 50) & (R_EL(I) > R_CEL(1)) THEN R_CEL(1) = R_EL(I);
   IF (R_EH(I) > 50) & (R_EH(I) > R_CEH(1)) THEN R_SEH(1) = I;
   IF (R_EH(I) > 50) & (R_EH(I) > R_CEH(1)) THEN R_CEH(1) = R_EH(I);
   IF (R_YLT(I) > 50) & (R_YLT(I) > R_CYLT(1)) THEN R_SYLT(1) = I;
   IF (R_YLT(I) > 50) & (R_YLT(I) > R_CYLT(1)) THEN R_CYLT(1) = R_YLT(I);
   IF (R_YLB(I) > 50) & (R_YLB(I) > R_CYLB(1)) THEN R_SYLB(1) = I;
   IF (R_YLB(I) > 50) & (R_YLB(I) > R_CYLB(1)) THEN R_CYLB(1) = R_YLB(I);
   IF (R_YHT(I) > 50) & (R_YHT(I) > R_CYHT(1)) THEN R_SYHT(1) = I;
   IF (R_YHT(I) > 50) & (R_YHT(I) > R_CYHT(1)) THEN R_CYHT(1) = R_YHT(I);
   IF (R_YHB(I) > 50) & (R_YHB(I) > R_CYHB(1)) THEN R_SYHB(1) = I;
   IF (R_YHB(I) > 50) & (R_YHB(I) > R_CYHB(1)) THEN R_CYHB(1) = R_YHB(I);
END;

DO I = 1 TO 16;
   IF (R_BL(I) > 50) & (R_BL(I) > R_CBL(1)) THEN R_SBL(1) = I;
   IF (R_BL(I) > 50) & (R_BL(I) > R_CBL(1)) THEN R_CBL(1) = R_BL(I);
   IF (R_BH(I) > 50) & (R_BH(I) > R_CBH(1)) THEN R_SBH(1) = I;
```

```
   IF (R_BH(I) > 50) & (R_BH(I) > R_CBH(1)) THEN R_CBH(1) = R_BH(I);
END;

DO I = 1 TO 8;
   IF (R_PT(I) > 50) & (R_PT(I) > R_CPT(1)) THEN R_SPT(1) = I;
   IF (R_PT(I) > 50) & (R_PT(I) > R_CPT(1)) THEN R_CPT(1) = R_PT(I);
END;

/** POSITION LOW **/
IF R_CEL(1) > 0 THEN DO;
   R_PLO(1) = (R_CYLT(1)-R_CYLB(1))/(R_CEL(1)) * 500;
   $ACCU(L,DB,$SPECTRUM,PLO,L_INCR,1,R_PLO(1));
END;

/** POSITION HIGH **/
IF R_CEH(1) > 0 THEN DO;
   R_PHI(1) = (R_CYHT(1)-R_CYHB(1))/(R_CEH(1)) * 500;
   $ACCU(L,DB,$SPECTRUM,PHI,L_INCR,1,R_PHI(1));
END;

END POSITION;

/*
================================================================================
     SINGLES SPECTRA CREATION
     SPECTRA-(E_KEV,SUM,E_MEV,SUMMEV,EP_KEV,SUMP,EA_KEV,SUMA
              RUTHEAST,RUTHWEST,EVR_HIGH)
================================================================================
*/

SINGLES : PROCEDURE;

/** ZERO PARAMETERS **/

DO I = 1 TO 32;
   IF R_EL(I) > 50 & R_EL(I) < 4095 THEN
$ACCU1(L,DB,$SPECTRUM,EKEV,I,L_INCR,1,R_EKEV(I));
END;

IF R_ELO(1) > 5 THEN $ACCU(L,DB,$SPECTRUM,SUML,L_INCR,1,R_ELO(1));

DO I = 1 TO 32;
   IF R_EH(I) > 50 & R_EH(I) < 4095 THEN
$ACCU1(L,DB,$SPECTRUM,EMEV,I,L_INCR,1,R_EMEV(I));
END;

IF R_EHI(1) > 5 THEN $ACCU(L,DB,$SPECTRUM,SUMH,L_INCR,1,R_EHI(1));

IF B_PAUSE THEN DO;
   DO I = 1 TO 32;
      IF R_EL(I) > 50 & R_EL(I) < 4095 THEN
$ACCU1(L,DB,$SPECTRUM,EPKEV,I,L_INCR,1,R_EKEV(I));
   END;
   IF R_ELO(1) > 5 THEN $ACCU(L,DB,$SPECTRUM,SUMLP,L_INCR,1,R_ELO(1));
   DO I = 1 TO 32;
      IF R_EH(I) > 50 & R_EH(I) < 4095 THEN
$ACCU1(L,DB,$SPECTRUM,EPMEV,I,L_INCR,1,R_EMEV(I));
   END;
   IF R_EHI(1) > 5 THEN $ACCU(L,DB,$SPECTRUM,SUMHP,L_INCR,1,R_EHI(1));
END;

IF ^B_PPAC THEN DO;
   DO I = 1 TO 32;
      IF R_EL(I) > 50 & R_EL(I) < 4095 THEN
$ACCU1(L,DB,$SPECTRUM,EAKEV,I,L_INCR,1,R_EKEV(I));
   END;
   IF R_ELO(1) > 5 THEN $ACCU(L,DB,$SPECTRUM,SUMLA,L_INCR,1,R_ELO(1));
   DO I = 1 TO 32;
```

```
      IF R_EH(I) > 50 & R_EH(I) < 4095 THEN
$ACCU1(L,DB,$SPECTRUM,EAMEV,I,L_INCR,1,R_EMEV(I));
   END;
   IF R_EHI(1) > 5 THEN $ACCU(L,DB,$SPECTRUM,SUMHA,L_INCR,1,R_EHI(1));
END;

$ACCU(L,DB,$SPECTRUM,RUTHEAST,L_INCR,1,R_RE(1));
$ACCU(L,DB,$SPECTRUM,RUTHWEST,L_INCR,1,R_RW(1));

END SINGLES;

/*
================================================================================
     BUFFER ROUTINE
     SPECTRA-(DT_EA,DP_EA,E_EVAP,E_MOTHER,P_EVAP,P_MOTHER
              DT_AA,DP_AA,E_EVAPALPHA,E_DAUGHTER,P_EVAPALPHA,P_DAUGHTER,E_RATIO
              DT_EF,DP_EF,E_EVAPF,E_FISSION,P_EVAPF,P_FISSION)
================================================================================
*/

BUFFER : PROCEDURE;

/** ZERO PARAMETERS **/
T_EA_MAX = 0.;
T_EA_MIN = 0.;
T_AA_MAX = 0.;
T_AA_MIN = 0.;
T_EF_MAX = 0.;
T_EF_MIN = 0.;

B_MOTHER = '0'B;
B_DAUGHTER = '0'B;
B_FISSION = '0'B;
B_EVAP = '0'B;
B_EVAPF = '0'B;

B_MOM = '0'B;
B_DAU = '0'B;
B_EVR = '0'B;
B_EVRF = '0'B;
B_FISS = '0'B;
DO I = 1 TO 8;
   B_PUNCH(I) = '0'B;
END;
B_PUNCHTHROUGH = '0'B;

T_EA = 0.;
T_AA = 0.;
T_EF = 0.;
LOGT_EA = 0.;

P_DIFF_EA = 0.;
P_DIFF_AA = 0.;
P_DIFF_EF = 0.;

R_E_EVR(1) = 0.;
R_E_MOM(1) = 0.;
R_DTEA(1) = 0.;
R_E_DAU(1) = 0.;
R_E_FISS(1) = 0.;
R_E_EVRF(1) = 0.;

R_EPUNCH = 0.;
R_SPUNCH = 0.;

/** PPAC ISSUE **/
IF R_PPAC(1) < 100 & R_PPAC(1) > 0 THEN R_PPAC(1) = 0;

/** SET CONDITIONS **/
```

```
$COND(WC,DB,$CONDITION,E_EVR,B_EVR,1,R_CEL(1));
$COND(WC,DB,$CONDITION,E_MOM,B_MOM,1,R_CEL(1));
$COND(WC,DB,$CONDITION,E_DAU,B_DAU,1,R_CEL(1));
$COND(WC,DB,$CONDITION,E_FISS,B_FISS,1,R_CEH(1));
$COND(WC,DB,$CONDITION,E_EVRF,B_EVRF,1,R_CEL(1));
DO I = 1 TO 8;
   IF R_PT(I) > R_EPUNCH THEN DO;
      R_EPUNCH = R_PT(I);
      R_SPUNCH = I;
   END;
   $COND1(WC,DB,$CONDITION,PUNCH,I,B_PUNCH(I),1,R_PT(I));
END;
IF B_PUNCH(1) | B_PUNCH(2) | B_PUNCH(3) | B_PUNCH(4) | B_PUNCH(5) |
   B_PUNCH(6) | B_PUNCH(7) | B_PUNCH(8) THEN B_PUNCHTHROUGH = '1'B;
IF ^B_PUNCHTHROUGH THEN DO;
   $ACCU(L,DB,$SPECTRUM,SUMAPT,L_INCR,1,R_ELO(1));
END;
IF B_PUNCHTHROUGH THEN DO;
   $ACCU(L,DB,$SPECTRUM,SUMPT,L_INCR,1,R_ELO(1));
END;

/** SET TIMING MAXIMUMS AND MINIMUMS **/
T_EA_MAX = R_IPAR(10);
T_EA_MIN = R_IPAR(11);
T_AA_MAX = R_IPAR(12);
T_AA_MIN = R_IPAR(13);
T_EF_MAX = R_IPAR(14);
T_EF_MIN = R_IPAR(15);

/** DECLARE BUFFERS **/
DCL 1 EDATA(4000) STATIC,
    2 T                BIN FLOAT(53),
    2 E               BIN FLOAT(24),
    2 S                BIN FLOAT(24),
    2 P                BIN FLOAT(24),
    2 EV              BIN FLOAT(24),
    2 TMP             BIN FLOAT(24),
    2 PPAC             BIN FLOAT(24);
DCL (ECOUNTER,ELAST)   BIN FIXED(31) STATIC INIT(0);

DCL 1 MDATA(4000) STATIC,
    2 T                BIN FLOAT(53),
    2 E               BIN FLOAT(24),
    2 S                BIN FLOAT(24),
    2 P                BIN FLOAT(24),
    2 EV               BIN FLOAT(24),
    2 TMP             BIN FLOAT(24),
    2 PPAC             BIN FLOAT(24);
DCL (MCOUNTER,MLAST)   BIN FIXED(31) STATIC INIT(0);

DCL 1 DDATA(4000) STATIC,
    2 T                BIN FLOAT(53),
    2 E               BIN FLOAT(24),
    2 S                BIN FLOAT(24),
    2 P                BIN FLOAT(24),
    2 EV              BIN FLOAT(24),
    2 TMP             BIN FLOAT(24),
    2 PPAC             BIN FLOAT(24);
DCL (DCOUNTER,DLAST)   BIN FIXED(31) STATIC INIT(0);

DCL 1 EFDATA(4000) STATIC,
    2 T                BIN FLOAT(53),
    2 E               BIN FLOAT(24),
    2 S                BIN FLOAT(24),
    2 P                BIN FLOAT(24),
    2 EV              BIN FLOAT(24),
    2 TMP             BIN FLOAT(24),
    2 PPAC             BIN FLOAT(24);
DCL (EFCOUNTER,EFLAST) BIN FIXED(31) STATIC INIT(0);
```

```
DCL 1 FDATA(4000) STATIC,
    2 T                 BIN FLOAT(53),
    2 E                BIN FLOAT(24),
    2 S                 BIN FLOAT(24),
    2 P                 BIN FLOAT(24),
    2 EV                BIN FLOAT(24),
    2 TMP              BIN FLOAT(24),
    2 PPAC              BIN FLOAT(24);
DCL (FCOUNTER,FLAST)   BIN FIXED(31) STATIC INIT(0);

/** CLEAR THE EVENT COUNTERS AND CLEAR THE BUFFERS **/
IF R_IPAR(4) = 1 THEN DO;
   ECOUNTER = 0.;
   ELAST = 0.;
   MCOUNTER = 0.;
   MLAST = 0.;
   DCOUNTER = 0.;
   DLAST = 0.;
   EFCOUNTER = 0.;
   EFLAST = 0.;
   FCOUNTER = 0.;
   FLAST = 0.;
   Q = 0.;
   R = 0.;
   U = 0.;
   C = 0.;
   N = 0.;
   I_EVCT = 0.;
   DO I = 1 TO 4000;
      EDATA(I).T=0.;
      EDATA(I).E=0.;
      EDATA(I).S=0.;
      EDATA(I).P=0.;
      EDATA(I).EV=0.;
      EDATA(I).TMP=0.;
      EDATA(I).PPAC=0.;
      MDATA(I).T=0.;
      MDATA(I).E=0.;
      MDATA(I).S=0.;
      MDATA(I).P=0.;
      MDATA(I).EV=0.;
      MDATA(I).TMP=0.;
      MDATA(I).PPAC=0.;
      DDATA(I).T=0.;
      DDATA(I).E=0.;
      DDATA(I).S=0.;
      DDATA(I).P=0.;
      DDATA(I).EV=0.;
      DDATA(I).TMP=0.;
      DDATA(I).PPAC=0.;
      EFDATA(I).T=0.;
      EFDATA(I).E=0.;
      EFDATA(I).S=0.;
      EFDATA(I).P=0.;
      EFDATA(I).EV=0.;
      EFDATA(I).TMP=0.;
      EFDATA(I).PPAC=0.;
      FDATA(I).T=0.;
      FDATA(I).E=0.;
      FDATA(I).S=0.;
      FDATA(I).P=0.;
      FDATA(I).EV=0.;
      FDATA(I).TMP=0.;
      FDATA(I).PPAC=0.;
   END;
   R_IPAR(4) = 0;
END;
```

```
/** CHECK IF EVENT IS ALPHA OR EVR **/
IF B_EVR & (R_IPAR(1) = 1) & (B_PPAC) & (ABS(R_PLO(1)) > 0) THEN B_EVAP='1'B;
IF B_MOM & (R_IPAR(1) = 1) & (^B_PPAC) & (ABS(R_PLO(1)) > 0) THEN B_MOTHER='1'B;
IF B_DAU & (R_IPAR(1) = 1) & (^B_PPAC) & (ABS(R_PLO(1)) > 0) THEN B_DAUGHTER='1'B;
IF B_FISS & (R_IPAR(1) = 1) & (^B_PPAC) & (ABS(R_PHI(1)) > 0) THEN B_FISSION='1'B;
IF B_EVRF & (R_IPAR(1) = 1) & (B_PPAC) & (ABS(R_PLO(1)) > 0) THEN B_EVAPF='1'B;

/** STORAGE OF EVR **/
IF B_EVAP THEN DO;
   I = R_SEL(1);
   IF (R_IPAR(30) = 1) THEN $ACCU1(L,DB,$SPECTRUM,CT_EVR,I,L_INCR,1,R_ELO(1));
   ELAST = ELAST + 1;
   IF ELAST > 4000 THEN ELAST = 1;
   EDATA(ELAST).T = TIMEMS;
   EDATA(ELAST).E = R_ELO(1);
   EDATA(ELAST).S = R_SEL(1);
   EDATA(ELAST).P = R_PLO(1);
   EDATA(ELAST).EV = I_EVCT;
   EDATA(ELAST).TMP = RA$SECAM(1);
   EDATA(ELAST).PPAC = R_PPAC(1);
   IF ECOUNTER < 4000 THEN ECOUNTER = ECOUNTER + 1;
END;

/** STORAGE OF EVR FISSION **/
IF B_EVAPF THEN DO;
   I = R_SEL(1);
   IF (R_IPAR(30) = 1) THEN $ACCU1(L,DB,$SPECTRUM,CT_EVRF,I,L_INCR,1,R_ELO(1));
   EFLAST = EFLAST + 1;
   IF EFLAST > 4000 THEN EFLAST = 1;
   EFDATA(EFLAST).T = TIMEMS;
   EFDATA(EFLAST).E = R_ELO(1);
   EFDATA(EFLAST).S = R_SEL(1);
   EFDATA(EFLAST).P = R_PLO(1);
   EFDATA(EFLAST).EV = I_EVCT;
   EFDATA(EFLAST).TMP = RA$SECAM(1);
   EFDATA(EFLAST).PPAC = R_PPAC(1);
   IF EFCOUNTER < 4000 THEN EFCOUNTER = EFCOUNTER + 1;
END;

/** CHECK IF ALPHA CORELATED WITH EVAP RESIDUE **/
IF B_MOTHER THEN DO;
   I = R_SEL(1);
   IF (R_IPAR(30) = 1) THEN $ACCU1(L,DB,$SPECTRUM,CT_MOM,I,L_INCR,1,R_ELO(1));
   Q=1;
   MLAST = MLAST + 1;
   IF MLAST > 4000 THEN MLAST = 1;
   MDATA(MLAST).T = TIMEMS;
   MDATA(MLAST).E = R_ELO(1);
   MDATA(MLAST).S = R_SEL(1);
   MDATA(MLAST).P = R_PLO(1);
   MDATA(MLAST).EV = I_EVCT;
   MDATA(MLAST).TMP = RA$SECAM(1);
   MDATA(MLAST).PPAC = R_PPAC(1);
   IF MCOUNTER < 4000 THEN MCOUNTER = MCOUNTER + 1;
   C = ECOUNTER;
   N = ELAST;
   LOOKUPREA: DO WHILE (C > 0);
      T_EA = TIMEMS - EDATA(N).T;
      IF (T_EA >= T_EA_MAX) THEN LEAVE LOOKUPREA;
      IF R_SEL(1) = 0 THEN LEAVE LOOKUPREA;
      P_DIFF_EA = EDATA(N).P-R_PLO(1);
      IF (T_EA > T_EA_MIN) &
         (T_EA < T_EA_MAX) &
         R_ELO(1) > 200. &
         (EDATA(N).S = MDATA(MLAST).S) &
         (P_DIFF_EA > R_IPAR(5)) &
         (P_DIFF_EA < R_IPAR(6)) THEN DO;
         LOGT_EA = LOG10(T_EA);
         IF R_IPAR(2) = 1 THEN DO;
```

```
            PUT STRING(C_EVAP) EDIT(
            'EM-Evap ',
            ' St',EDATA(N).S,
            ' Pos', EDATA(N).P,
            ' Time', EDATA(N).T,
            ' E_Evap',EDATA(N).E,
            ' Ev_Evap',EDATA(N).EV,
            ' Dp',P_DIFF_EA,
            ' Dt',T_EA)
            (A,A,F(3),A,F(10),A,F(10),A,F(6),A,F(8),A,F(12,3),A,F(8));
            @CALL U$PRTCL(C_EVAP, U$M_PRTTERM);
            PUT STRING(C_EVAP) EDIT(
            '   Moth ',
            ' St', R_SEL(1),
            ' Pos', R_PLO(1),
            ' Time', TIMEMS,
            ' E_Moth', R_ELO(1),
            ' Ev_Moth', I_EVCT)
            (A,A,F(3),A,F(10),A,F(10),A,F(6),A,F(8));
            @CALL U$PRTCL(C_EVAP, U$M_PRTTERM);
         END;
         $ACCU(L,DB,$SPECTRUM,DT_EA,L_INCR,1,T_EA);
         $ACCU(L,DB,$SPECTRUM,LOGDT_EA,L_INCR,1,LOGT_EA);
         $ACCU(L,DB,$SPECTRUM,E_EVAP,L_INCR,1,EDATA(N).E);
         $ACCU(L,DB,$SPECTRUM,E_MOTHER,L_INCR,1,R_ELO(1));
         $ACCU(L,DB,$SPECTRUM,P_MOTHER,L_INCR,1,R_PLO(1));
         $ACCU(L,DB,$SPECTRUM,P_EVAP,L_INCR,1,EDATA(N).P);
         $ACCU(L,DB,$SPECTRUM,DP_EA,L_INCR,1,P_DIFF_EA);
         $ACCU(L,DB,$SPECTRUM,RATE_EA,L_INCR,1,TIMESEC);
         R_E_EVR(1) = EDATA(N).E;
         R_E_MOM(1) = R_ELO(1);
         R_E_PPAC(1) = EDATA(N).PPAC;
         R_DTEA(1) = T_EA;
         Q=Q+1;
         IF Q > R_IPAR(3) THEN LEAVE LOOKUPREA;
      END;
      N = N - 1;
      IF N <= 0 THEN N = 4000;
      C = C - 1;
   END LOOKUPREA;
END;

/** CHECK IF ALPHA CORRELATED TO ALPHA **/
IF B_DAUGHTER THEN DO;
   I = R_SEL(1);
   IF (R_IPAR(30) = 1) THEN $ACCU1(L,DB,$SPECTRUM,CT_DAU,I,L_INCR,1,R_ELO(1));
   R=1;
   DLAST = DLAST + 1;
   IF DLAST > 4000 THEN DLAST = 1;
   DDATA(DLAST).T = TIMEMS;
   DDATA(DLAST).E = R_ELO(1);
   DDATA(DLAST).S = R_SEL(1);
   DDATA(DLAST).P = R_PLO(1);
   DDATA(DLAST).EV = I_EVCT;
   DDATA(DLAST).TMP = RA$SECAM(1);
   DDATA(DLAST).PPAC = R_PPAC(1);
   IF DCOUNTER < 4000 THEN DCOUNTER = DCOUNTER + 1;
   C = MCOUNTER;
   N = MLAST;
   LOOKUPALAL: DO WHILE (C > 0);
      T_AA = TIMEMS - MDATA(N).T;
      IF (T_AA >= T_AA_MAX) THEN LEAVE LOOKUPALAL;
      IF R_SEL(1) = 0 THEN LEAVE LOOKUPALAL;
      P_DIFF_AA = MDATA(N).P-R_PLO(1);
      IF (T_AA > T_AA_MIN) &
         (T_AA < T_AA_MAX) &
         R_ELO(1) > 200. &
         (MDATA(N).S = DDATA(DLAST).S) &
         (P_DIFF_AA > R_IPAR(5)) &
```

```
         (P_DIFF_AA < R_IPAR(6)) THEN DO;
         IF R_IPAR(2) = 1 THEN DO;
            PUT STRING(C_EVAP) EDIT(
            'MD-Moth ',
            ' St',MDATA(N).S,
            ' Pos', MDATA(N).P,
            ' Time', MDATA(N).T,
            ' E_Moth',MDATA(N).E,
            ' Ev_Moth',MDATA(N).EV,
            ' Dp',P_DIFF_AA,
            ' Dt',T_AA)
            (A,A,F(3),A,F(10),A,F(10),A,F(6),A,F(8),A,F(12,3),A,F(8));
            @CALL U$PRTCL(C_EVAP, U$M_PRTTERM);
            PUT STRING(C_EVAP) EDIT(
            '   Daug ',
            ' St', R_SEL(1),
            ' Pos', R_PLO(1),
            ' Time', TIMEMS,
            ' E_Daug', R_ELO(1),
            ' Ev_Daug', I_EVCT)
            (A,A,F(3),A,F(10),A,F(10),A,F(6),A,F(8));
            @CALL U$PRTCL(C_EVAP, U$M_PRTTERM);
         END;
         E_RATIO = (R_ELO(1) / MDATA(N).E) * 1000.;
         $ACCU(L,DB,$SPECTRUM,E_RATIO,L_INCR,1,E_RATIO);
         $ACCU(L,DB,$SPECTRUM,DT_AA,L_INCR,1,T_AA);
         $ACCU(L,DB,$SPECTRUM,E_EVAPALPHA,L_INCR,1,MDATA(N).E);
         $ACCU(L,DB,$SPECTRUM,E_DAUGHTER,L_INCR,1,R_ELO(1));
         $ACCU(L,DB,$SPECTRUM,DP_AA,L_INCR,1,P_DIFF_AA);
         $ACCU(L,DB,$SPECTRUM,P_DAUGHTER,L_INCR,1,R_PLO(1));
         $ACCU(L,DB,$SPECTRUM,P_EVAPALPHA,L_INCR,1,MDATA(N).P);
         R_E_MOM(1) = MDATA(N).E;
         R_E_DAU(1) = R_ELO(1);
         R=R+1;
         IF R > R_IPAR(3) THEN LEAVE LOOKUPALAL;
      END;
      N = N - 1;
      IF N <= 0 THEN N = 4000;
      C = C - 1;
   END LOOKUPALAL;
END;

/** CHECK IF FISSION CORELATED WITH EVAP RESIDUE **/
IF B_FISSION THEN DO;
   I = R_SEH(1);
   IF (R_IPAR(30) = 1) THEN $ACCU1(L,DB,$SPECTRUM,CT_FISS,I,L_INCR,1,R_EHI(1));
   U=1;
   FLAST = FLAST + 1;
   IF FLAST > 4000 THEN FLAST = 1;
   FDATA(FLAST).T = TIMEMS;
   FDATA(FLAST).E = R_EHI(1);
   FDATA(FLAST).S = R_SEH(1);
   FDATA(FLAST).P = R_PHI(1);
   FDATA(FLAST).EV = I_EVCT;
   FDATA(FLAST).TMP = RA$SECAM(1);
   FDATA(FLAST).PPAC = R_PPAC(1);
   IF FCOUNTER < 4000 THEN FCOUNTER = FCOUNTER + 1;
   C = EFCOUNTER;
   N = EFLAST;
   LOOKUPEF: DO WHILE (C > 0);
      T_EF = TIMEMS - EFDATA(N).T;
      IF (T_EF >= T_EF_MAX) THEN LEAVE LOOKUPEF;
      IF R_SEH(1) = 0 THEN LEAVE LOOKUPEF;
      P_DIFF_EF = EFDATA(N).P-FDATA(FLAST).P;
      IF (T_EF > T_EF_MIN) &
         (T_EF < T_EF_MAX) &
         (EFDATA(N).S = FDATA(FLAST).S) &
         (P_DIFF_EF > R_IPAR(7)) &
         (P_DIFF_EF < R_IPAR(8)) THEN DO;
```

```
         IF R_IPAR(2) = 1 THEN DO;
            PUT STRING(C_EVAP) EDIT(
            'EF-Evap ',
            ' St',EFDATA(N).S,
            ' Pos', EFDATA(N).P,
            ' Time', EFDATA(N).T,
            ' E_Evap',EFDATA(N).E,
            ' Ev_Evap',EFDATA(N).EV,
            ' Dp',P_DIFF_EF,
            ' Dt',T_EF)
            (A,A,F(3),A,F(10,3),A,F(10),A,F(6),A,F(8),A,F(12,3),A,F(9,3));
            @CALL U$PRTCL(C_EVAP, U$M_PRTTERM);
            PUT STRING(C_EVAP) EDIT(
            '   Fiss ',
            ' St', R_SEH(1),
            ' Pos', R_PHI(1),
            ' Time', TIMEMS,
            ' E_Fiss', R_EHI(1),
            ' Ev_Fiss', I_EVCT)
            (A,A,F(3),A,F(10,3),A,F(10),A,F(6),A,F(8));
            @CALL U$PRTCL(C_EVAP, U$M_PRTTERM);
         END;
         $ACCU(L,DB,$SPECTRUM,DT_EF,L_INCR,1,T_EF);
         $ACCU(L,DB,$SPECTRUM,E_EVAPF,L_INCR,1,EFDATA(N).E);
         $ACCU(L,DB,$SPECTRUM,E_FISSION,L_INCR,1,R_EHI(1));
         $ACCU(L,DB,$SPECTRUM,P_FISSION,L_INCR,1,R_PHI(1));
         $ACCU(L,DB,$SPECTRUM,P_EVAPF,L_INCR,1,EFDATA(N).P);
         $ACCU(L,DB,$SPECTRUM,DP_EF,L_INCR,1,P_DIFF_EF);
         $ACCU(L,DB,$SPECTRUM,RATE_EF,L_INCR,1,TIMESEC);
         R_E_EVRF(1) = EFDATA(N).E;
         R_E_FISS(1) = R_EHI(1);
         U=U+1;
         IF U > R_IPAR(3) THEN LEAVE LOOKUPEF;
      END;
      N = N - 1;
      IF N <= 0 THEN N = 4000;
      C = C - 1;
   END LOOKUPEF;
END;

END BUFFER;

/*
================================================================================
     EVENT LISTING PROCEDURE
================================================================================
*/

EVENTLIST : PROCEDURE;


IF R_IPAR(17) > 10 THEN R_SEL(1) = 50;

IF (R_IPAR(17) = 1) THEN DO;
   IF I_EVCT > R_IPAR(19) & I_EVCT < (R_IPAR(19)+R_IPAR(20)) THEN DO;
      IF (R_SEH(1) = R_IPAR(18)) | (R_SEL(1) = R_IPAR(18)) THEN DO;
         PUT STRING(C_EVAP) EDIT(
         'Ev',I_EVCT,
         ' StL',R_SEL(1),
         ' StH',R_SEH(1),
         ' TIMEMS',TIME,
         ' P_Lo',R_PLO(1),
         ' E_Lo',R_ELO(1),
         ' P_Hi',R_PHI(1),
         ' E_Hi',R_EHI(1))
         (A,F(8),A,F(3),A,F(3),A,F(10,3),A,F(8,2),A,F(10,3),A,F(8,2),A,F(5));
         @CALL U$PRTCL(C_EVAP, U$M_PRTTERM);
      END;
   END;
```

```
END;

IF (R_IPAR(17) = 2) THEN DO;
   IF I_EVCT < R_IPAR(19) & I_EVCT > (R_IPAR(19)-R_IPAR(20)) THEN DO;
      PUT STRING(C_EVAP) EDIT(
      'Ev',I_EVCT,
      ' St',R_SEL(1),
      ' Time',TIME,
      ' PPAC',R_PPAC(1),
      ' P_Lo',R_PLO(1),
      ' E_Lo',R_ELO(1),
      ' P_Hi',R_PHI(1),
      ' E_Hi',R_EHI(1))
      (A,F(7,0),A,F(3,0),A,F(10,3),A,F(5,0),A,F(6,0),A,F(10,3),A,F(6,0),A,F(10,3));
      @CALL U$PRTCL(C_EVAP, U$M_PRTTERM);
   END;
END;

IF (R_IPAR(17) = 3) & (R_PPAC(1) = 0) & (R_SEL(1) > 3) THEN DO;
   IF (R_ELO(1) > R_IPAR(19)) & (R_ELO(1) < R_IPAR(20)) | ((R_EHI(1) > 1850) & (R_EHI(1)
< 2760)) THEN DO;
      PUT STRING(C_EVAP) EDIT(
      'Ev',I_EVCT,
      ' St',R_SEL(1),
      ' Time',TIME,
      ' P_Lo',R_PLO(1),
      ' E_Lo',R_ELO(1),
      ' P_Hi',R_PHI(1),
      ' E_Hi',R_EHI(1))
      (A,F(8,0),A,F(4,0),A,F(11,3),A,F(7,0),A,F(11,3),A,F(7,0),A,F(6,0));
      @CALL U$PRTCL(C_EVAP, U$M_PRTTERM);
   END;
END;

IF (R_IPAR(17) = 4) THEN DO;
   IF (I_EVCT >= R_IPAR(19)) & (I_EVCT <= R_IPAR(20)) THEN DO;
      I = R_IPAR(18);
      PUT STRING(C_EVAP) EDIT(
          I_EVCT,
          TIMEMS,
          R_PPAC(1),
          R_SEL(1),
          R_EL(I),
          R_PLO(1),
          R_SEH(1),
          R_EH(I),
          R_PHI(1),
          R_YHT(I),
          R_YHB(I),
          R_YEHT(I),
          R_YEHB(I))
          (F(6),F(13),F(5),F(3),F(5),F(9,2),F(3),F(5),F(9,2),F(5),F(5),F(5),F(5));
      @CALL U$PRTCL(C_EVAP, U$M_PRTTERM);
   END;
END;

IF (R_IPAR(17) = 5) THEN DO;
   IF (I_EVCT >= R_IPAR(19)) & (I_EVCT <= R_IPAR(20)) THEN DO;
      PUT STRING(C_EVAP) EDIT(
          I_EVCT,
          TIMEUS,
          R_PPAC(1),
          R_SEL(1),
          R_SYLT(1),
          R_SYLB(1),
          R_CEL(1),
          R_CYLT(1),
          R_CYLB(1),
          R_PLO(1),
```

```
            R_SEH(1),
            R_SYHT(1),
            R_SYHB(1),
            R_CEH(1),
            R_CYHT(1),
            R_CYHB(1),
            R_PHI(1))

(F(6),F(13),F(5),F(5),F(5),F(5),F(5),F(5),F(5),F(8),F(5),F(5),F(5),F(5),F(5),F(5),F(8));
        @CALL U$PRTCL(C_EVAP, U$M_PRTTERM);
    END;
END;

IF (R_IPAR(17) = 6) & (I_EVCT >= R_IPAR(19)) & (I_EVCT <= R_IPAR(20)) THEN DO;
    DO I = 1 TO 32;
        PUT STRING(C_EVAP) EDIT(
            I,
            R_EL(I),
            R_YLT(I),
            R_YLB(I),
            R_EH(I),
            R_YHT(I),
            R_YHB(I))
            (F(6),F(6),F(6),F(6),F(6),F(6),F(6));
        @CALL U$PRTCL(C_EVAP, U$M_PRTTERM);
    END;
END;

END EVENTLIST;

/*
================================================================================
*/

@RET(STS$VALUE);

/*
================================================================================
     ENTRY CALLED DURING STARTUP OR BY COMMAND 'INITIALIZE ANALYSIS'
================================================================================
*/

$XANAL:ENTRY RETURNS(BIN FIXED(31));
@INCLUDE $MACRO($SECDEF);

/***** LOCATE DATA ELEMENTS *****/

$LOC(DE,DB,DATA,EVENT,W);      IF ^STS$SUCCESS THEN @RET(STS$VALUE); P_SECAM =
P$_DB_DATA_EVENT;

$LOC(DE,DB,DATA,EL,W);         IF ^STS$SUCCESS THEN @RET(STS$VALUE); P_EL = P$_DB_DATA_EL;
$LOC(DE,DB,DATA,EH,W);         IF ^STS$SUCCESS THEN @RET(STS$VALUE); P_EH = P$_DB_DATA_EH;
$LOC(DE,DB,DATA,YLT,W);               IF ^STS$SUCCESS THEN @RET(STS$VALUE); P_YLT =
P$_DB_DATA_YLT;
$LOC(DE,DB,DATA,YHT,W);               IF ^STS$SUCCESS THEN @RET(STS$VALUE); P_YHT =
P$_DB_DATA_YHT;
$LOC(DE,DB,DATA,YLB,W);               IF ^STS$SUCCESS THEN @RET(STS$VALUE); P_YLB =
P$_DB_DATA_YLB;
$LOC(DE,DB,DATA,YHB,W);               IF ^STS$SUCCESS THEN @RET(STS$VALUE); P_YHB =
P$_DB_DATA_YHB;
$LOC(DE,DB,DATA,BL,W);         IF ^STS$SUCCESS THEN @RET(STS$VALUE); P_BL = P$_DB_DATA_BL;
$LOC(DE,DB,DATA,BH,W);         IF ^STS$SUCCESS THEN @RET(STS$VALUE); P_BH = P$_DB_DATA_BH;
$LOC(DE,DB,DATA,PT,W);         IF ^STS$SUCCESS THEN @RET(STS$VALUE); P_PT = P$_DB_DATA_PT;
$LOC(DE,DB,DATA,CEL,W);               IF ^STS$SUCCESS THEN @RET(STS$VALUE); P_CEL =
P$_DB_DATA_CEL;
$LOC(DE,DB,DATA,CEH,W);               IF ^STS$SUCCESS THEN @RET(STS$VALUE); P_CEH =
P$_DB_DATA_CEH;
$LOC(DE,DB,DATA,CYLT,W);       IF ^STS$SUCCESS THEN @RET(STS$VALUE); P_CYLT =
P$_DB_DATA_CYLT;
```

```
$LOC(DE,DB,DATA,CYHT,W);      IF ^STS$SUCCESS THEN @RET(STS$VALUE); P_CYHT =
P$_DB_DATA_CYHT;
$LOC(DE,DB,DATA,CYLB,W);      IF ^STS$SUCCESS THEN @RET(STS$VALUE); P_CYLB =
P$_DB_DATA_CYLB;
$LOC(DE,DB,DATA,CYHB,W);      IF ^STS$SUCCESS THEN @RET(STS$VALUE); P_CYHB =
P$_DB_DATA_CYHB;
$LOC(DE,DB,DATA,CBL,W);              IF ^STS$SUCCESS THEN @RET(STS$VALUE); P_CBL =
P$_DB_DATA_CBL;
$LOC(DE,DB,DATA,CBH,W);              IF ^STS$SUCCESS THEN @RET(STS$VALUE); P_CBH =
P$_DB_DATA_CBH;
$LOC(DE,DB,DATA,CPT,W);              IF ^STS$SUCCESS THEN @RET(STS$VALUE); P_CPT =
P$_DB_DATA_CPT;
$LOC(DE,DB,DATA,SEL,W);              IF ^STS$SUCCESS THEN @RET(STS$VALUE); P_SEL =
P$_DB_DATA_SEL;
$LOC(DE,DB,DATA,SEH,W);              IF ^STS$SUCCESS THEN @RET(STS$VALUE); P_SEH =
P$_DB_DATA_SEH;
$LOC(DE,DB,DATA,SYLT,W);      IF ^STS$SUCCESS THEN @RET(STS$VALUE); P_SYLT =
P$_DB_DATA_SYLT;
$LOC(DE,DB,DATA,SYHT,W);      IF ^STS$SUCCESS THEN @RET(STS$VALUE); P_SYHT =
P$_DB_DATA_SYHT;
$LOC(DE,DB,DATA,SYLB,W);      IF ^STS$SUCCESS THEN @RET(STS$VALUE); P_SYLB =
P$_DB_DATA_SYLB;
$LOC(DE,DB,DATA,SYHB,W);      IF ^STS$SUCCESS THEN @RET(STS$VALUE); P_SYHB =
P$_DB_DATA_SYHB;
$LOC(DE,DB,DATA,SBL,W);              IF ^STS$SUCCESS THEN @RET(STS$VALUE); P_SBL =
P$_DB_DATA_SBL;
$LOC(DE,DB,DATA,SBH,W);              IF ^STS$SUCCESS THEN @RET(STS$VALUE); P_SBH =
P$_DB_DATA_SBH;
$LOC(DE,DB,DATA,SPT,W);              IF ^STS$SUCCESS THEN @RET(STS$VALUE); P_SPT =
P$_DB_DATA_SPT;

$LOC(DE,DB,DATA,ELM,W);              IF ^STS$SUCCESS THEN @RET(STS$VALUE); P_ELM =
P$_DB_DATA_ELM;
$LOC(DE,DB,DATA,ELB,W);              IF ^STS$SUCCESS THEN @RET(STS$VALUE); P_ELB =
P$_DB_DATA_ELB;
$LOC(DE,DB,DATA,EHM,W);              IF ^STS$SUCCESS THEN @RET(STS$VALUE); P_EHM =
P$_DB_DATA_EHM;
$LOC(DE,DB,DATA,EHB,W);              IF ^STS$SUCCESS THEN @RET(STS$VALUE); P_EHB =
P$_DB_DATA_EHB;
$LOC(DE,DB,DATA,YLTM,W);      IF ^STS$SUCCESS THEN @RET(STS$VALUE); P_YLTM =
P$_DB_DATA_YLTM;
$LOC(DE,DB,DATA,YLTB,W);      IF ^STS$SUCCESS THEN @RET(STS$VALUE); P_YLTB =
P$_DB_DATA_YLTB;
$LOC(DE,DB,DATA,YLBM,W);      IF ^STS$SUCCESS THEN @RET(STS$VALUE); P_YLBM =
P$_DB_DATA_YLBM;
$LOC(DE,DB,DATA,YLBB,W);      IF ^STS$SUCCESS THEN @RET(STS$VALUE); P_YLBB =
P$_DB_DATA_YLBB;
$LOC(DE,DB,DATA,YHTM,W);      IF ^STS$SUCCESS THEN @RET(STS$VALUE); P_YHTM =
P$_DB_DATA_YHTM;
$LOC(DE,DB,DATA,YHTB,W);      IF ^STS$SUCCESS THEN @RET(STS$VALUE); P_YHTB =
P$_DB_DATA_YHTB;
$LOC(DE,DB,DATA,YHBM,W);      IF ^STS$SUCCESS THEN @RET(STS$VALUE); P_YHBM =
P$_DB_DATA_YHBM;
$LOC(DE,DB,DATA,YHBB,W);      IF ^STS$SUCCESS THEN @RET(STS$VALUE); P_YHBB =
P$_DB_DATA_YHBB;

$LOC(DE,DB,DATA,PKEV,W);      IF ^STS$SUCCESS THEN @RET(STS$VALUE); P_PKEV =
P$_DB_DATA_PKEV;
$LOC(DE,DB,DATA,PMEV,W);      IF ^STS$SUCCESS THEN @RET(STS$VALUE); P_PMEV =
P$_DB_DATA_PMEV;
$LOC(DE,DB,DATA,PLO,W);              IF ^STS$SUCCESS THEN @RET(STS$VALUE); P_PLO =
P$_DB_DATA_EHM;
$LOC(DE,DB,DATA,PHI,W);              IF ^STS$SUCCESS THEN @RET(STS$VALUE); P_PHI =
P$_DB_DATA_EHB;
$LOC(DE,DB,DATA,YELT,W);      IF ^STS$SUCCESS THEN @RET(STS$VALUE); P_YELT =
P$_DB_DATA_YELT;
$LOC(DE,DB,DATA,YEHT,W);      IF ^STS$SUCCESS THEN @RET(STS$VALUE); P_YEHT =
P$_DB_DATA_YEHT;
```

```
$LOC(DE,DB,DATA,YELB,W);      IF ^STS$SUCCESS THEN @RET(STS$VALUE); P_YELB =
P$_DB_DATA_YELB;
$LOC(DE,DB,DATA,YEHB,W);      IF ^STS$SUCCESS THEN @RET(STS$VALUE); P_YEHB =
P$_DB_DATA_YEHB;
$LOC(DE,DB,DATA,EKEV,W);      IF ^STS$SUCCESS THEN @RET(STS$VALUE); P_EKEV =
P$_DB_DATA_EKEV;
$LOC(DE,DB,DATA,EMEV,W);      IF ^STS$SUCCESS THEN @RET(STS$VALUE); P_EMEV =
P$_DB_DATA_EMEV;
$LOC(DE,DB,DATA,ELO,W);             IF ^STS$SUCCESS THEN @RET(STS$VALUE); P_ELO =
P$_DB_DATA_ELO;
$LOC(DE,DB,DATA,EHI,W);             IF ^STS$SUCCESS THEN @RET(STS$VALUE); P_EHI =
P$_DB_DATA_EHI;

$LOC(DE,DB,DATA,E_EVR,W);     IF ^STS$SUCCESS THEN @RET(STS$VALUE); P_E_EVR =
P$_DB_DATA_E_EVR;
$LOC(DE,DB,DATA,E_MOM,W);     IF ^STS$SUCCESS THEN @RET(STS$VALUE); P_E_MOM =
P$_DB_DATA_E_MOM;
$LOC(DE,DB,DATA,DTEA,W);      IF ^STS$SUCCESS THEN @RET(STS$VALUE); P_DTEA =
P$_DB_DATA_DTEA;
$LOC(DE,DB,DATA,E_DAU,W);     IF ^STS$SUCCESS THEN @RET(STS$VALUE); P_E_DAU =
P$_DB_DATA_E_DAU;
$LOC(DE,DB,DATA,E_EVRF,W);    IF ^STS$SUCCESS THEN @RET(STS$VALUE); P_E_EVRF =
P$_DB_DATA_E_EVRF;
$LOC(DE,DB,DATA,E_FISS,W);    IF ^STS$SUCCESS THEN @RET(STS$VALUE); P_E_FISS =
P$_DB_DATA_E_FISS;
$LOC(DE,DB,DATA,E_PPAC,W);    IF ^STS$SUCCESS THEN @RET(STS$VALUE); P_E_PPAC =
P$_DB_DATA_E_PPAC;

$LOC(DE,DB,DATA,NAIL,W);      IF ^STS$SUCCESS THEN @RET(STS$VALUE); P_NAIL =
P$_DB_DATA_NAIL;
$LOC(DE,DB,DATA,NAIH,W);      IF ^STS$SUCCESS THEN @RET(STS$VALUE); P_NAIH =
P$_DB_DATA_NAIH;
$LOC(DE,DB,DATA,RESLSW,W);    IF ^STS$SUCCESS THEN @RET(STS$VALUE); P_RESLSW =
P$_DB_DATA_RESLSW;
$LOC(DE,DB,DATA,RESMSW,W);    IF ^STS$SUCCESS THEN @RET(STS$VALUE); P_RESMSW =
P$_DB_DATA_RESMSW;
$LOC(DE,DB,DATA,RWSLSW,W);    IF ^STS$SUCCESS THEN @RET(STS$VALUE); P_RWSLSW =
P$_DB_DATA_RWSLSW;
$LOC(DE,DB,DATA,RWSMSW,W);    IF ^STS$SUCCESS THEN @RET(STS$VALUE); P_RWSMSW =
P$_DB_DATA_RWSMSW;
$LOC(DE,DB,DATA,RE,W);        IF ^STS$SUCCESS THEN @RET(STS$VALUE); P_RE = P$_DB_DATA_RE;
$LOC(DE,DB,DATA,RW,W);        IF ^STS$SUCCESS THEN @RET(STS$VALUE); P_RW = P$_DB_DATA_RW;

$LOC(DE,DB,DATA,IPAR,W);      IF ^STS$SUCCESS THEN @RET(STS$VALUE); P_IPAR =
P$_DB_DATA_IPAR;
$LOC(DE,DB,DATA,SLOPE,W);     IF ^STS$SUCCESS THEN @RET(STS$VALUE); P_SLOPE =
P$_DB_DATA_SLOPE;
$LOC(DE,DB,DATA,PPAC,W);      IF ^STS$SUCCESS THEN @RET(STS$VALUE); P_PPAC =
P$_DB_DATA_PPAC;
$LOC(DE,DB,DATA,ERROR,W);     IF ^STS$SUCCESS THEN @RET(STS$VALUE); P_ERROR =
P$_DB_DATA_ERROR;

/***** LOCATE CONDITIONS *****/

$LOC(COND,DB,$CONDITION,RE,W,WC);           IF ^STS$SUCCESS THEN @RET(STS$VALUE);
$LOC(COND,DB,$CONDITION,RW,W,WC);           IF ^STS$SUCCESS THEN @RET(STS$VALUE);
$LOC(COND,DB,$CONDITION,PAUSE,W,WC);        IF ^STS$SUCCESS THEN @RET(STS$VALUE);
$LOC(COND,DB,$CONDITION,PPAC,W,WC);         IF ^STS$SUCCESS THEN @RET(STS$VALUE);
$LOC(COND,DB,$CONDITION,E_EVR,W,WC);        IF ^STS$SUCCESS THEN @RET(STS$VALUE);
$LOC(COND,DB,$CONDITION,E_MOM,W,WC);        IF ^STS$SUCCESS THEN @RET(STS$VALUE);
$LOC(COND,DB,$CONDITION,E_DAU,W,WC);        IF ^STS$SUCCESS THEN @RET(STS$VALUE);
$LOC(COND,DB,$CONDITION,E_FISS,W,WC);       IF ^STS$SUCCESS THEN @RET(STS$VALUE);
$LOC(COND,DB,$CONDITION,E_EVRF,W,WC);       IF ^STS$SUCCESS THEN @RET(STS$VALUE);
$LOC1(COND,DB,$CONDITION,PUNCH,1,8,W,WC);   IF ^STS$SUCCESS THEN @RET(STS$VALUE);

/***** LOCATE SPECTRA *****/

$LOC1(SPEC,DB,$SPECTRUM,S,1,352,W,L);       IF ^STS$SUCCESS THEN @RET(STS$VALUE);
$LOC(SPEC,DB,$SPECTRUM,SEC,W,L);            IF ^STS$SUCCESS THEN @RET(STS$VALUE);
```

```
$LOC(SPEC,DB,$SPECTRUM,TIME,W,L);            IF ^STS$SUCCESS THEN @RET(STS$VALUE);
$LOC(SPEC,DB,$SPECTRUM,TIMEMIN,W,L);         IF ^STS$SUCCESS THEN @RET(STS$VALUE);
$LOC(SPEC,DB,$SPECTRUM,RE_RATE,W,L);         IF ^STS$SUCCESS THEN @RET(STS$VALUE);
$LOC(SPEC,DB,$SPECTRUM,RW_RATE,W,L);         IF ^STS$SUCCESS THEN @RET(STS$VALUE);
$LOC(SPEC,DB,$SPECTRUM,RUTH_RATE,W,L);              IF ^STS$SUCCESS THEN @RET(STS$VALUE);
$LOC(SPEC,DB,$SPECTRUM,TMP,W,L);             IF ^STS$SUCCESS THEN @RET(STS$VALUE);
$LOC1(SPEC,DB,$SPECTRUM,SP,1,32,W,L);        IF ^STS$SUCCESS THEN @RET(STS$VALUE);
$LOC(SPEC,DB,$SPECTRUM,SPSUM,W,L);           IF ^STS$SUCCESS THEN @RET(STS$VALUE);
$LOC(SPEC,DB,$SPECTRUM,PPAC,W,L);            IF ^STS$SUCCESS THEN @RET(STS$VALUE);
$LOC(SPEC,DB,$SPECTRUM,EVR_LOW,W,L);         IF ^STS$SUCCESS THEN @RET(STS$VALUE);
$LOC(SPEC,DB,$SPECTRUM,PLO,W,L);             IF ^STS$SUCCESS THEN @RET(STS$VALUE);
$LOC1(SPEC,DB,$SPECTRUM,PKEV,1,32,W,L);             IF ^STS$SUCCESS THEN @RET(STS$VALUE);
$LOC(SPEC,DB,$SPECTRUM,PHI,W,L);             IF ^STS$SUCCESS THEN @RET(STS$VALUE);
$LOC1(SPEC,DB,$SPECTRUM,PMEV,1,32,W,L);             IF ^STS$SUCCESS THEN @RET(STS$VALUE);
$LOC1(SPEC,DB,$SPECTRUM,EKEV,1,32,W,L);             IF ^STS$SUCCESS THEN @RET(STS$VALUE);
$LOC(SPEC,DB,$SPECTRUM,SUML,W,L);            IF ^STS$SUCCESS THEN @RET(STS$VALUE);
$LOC1(SPEC,DB,$SPECTRUM,EMEV,1,32,W,L);             IF ^STS$SUCCESS THEN @RET(STS$VALUE);
$LOC(SPEC,DB,$SPECTRUM,SUMH,W,L);            IF ^STS$SUCCESS THEN @RET(STS$VALUE);
$LOC1(SPEC,DB,$SPECTRUM,EPKEV,1,32,W,L);     IF ^STS$SUCCESS THEN @RET(STS$VALUE);
$LOC(SPEC,DB,$SPECTRUM,SUMLP,W,L);           IF ^STS$SUCCESS THEN @RET(STS$VALUE);
$LOC1(SPEC,DB,$SPECTRUM,EPMEV,1,32,W,L);     IF ^STS$SUCCESS THEN @RET(STS$VALUE);
$LOC(SPEC,DB,$SPECTRUM,SUMHP,W,L);           IF ^STS$SUCCESS THEN @RET(STS$VALUE);
$LOC1(SPEC,DB,$SPECTRUM,EAKEV,1,32,W,L);     IF ^STS$SUCCESS THEN @RET(STS$VALUE);
$LOC(SPEC,DB,$SPECTRUM,SUMLA,W,L);           IF ^STS$SUCCESS THEN @RET(STS$VALUE);
$LOC1(SPEC,DB,$SPECTRUM,EAMEV,1,32,W,L);     IF ^STS$SUCCESS THEN @RET(STS$VALUE);
$LOC(SPEC,DB,$SPECTRUM,SUMHA,W,L);           IF ^STS$SUCCESS THEN @RET(STS$VALUE);
$LOC(SPEC,DB,$SPECTRUM,RUTHEAST,W,L);        IF ^STS$SUCCESS THEN @RET(STS$VALUE);
$LOC(SPEC,DB,$SPECTRUM,RUTHWEST,W,L);        IF ^STS$SUCCESS THEN @RET(STS$VALUE);
$LOC(SPEC,DB,$SPECTRUM,SUMAPT,W,L);          IF ^STS$SUCCESS THEN @RET(STS$VALUE);
$LOC(SPEC,DB,$SPECTRUM,SUMPT,W,L);           IF ^STS$SUCCESS THEN @RET(STS$VALUE);
$LOC(SPEC,DB,$SPECTRUM,DT_EA,W,L);           IF ^STS$SUCCESS THEN @RET(STS$VALUE);
$LOC(SPEC,DB,$SPECTRUM,LOGDT_EA,W,L);        IF ^STS$SUCCESS THEN @RET(STS$VALUE);
$LOC(SPEC,DB,$SPECTRUM,E_EVAP,W,L);          IF ^STS$SUCCESS THEN @RET(STS$VALUE);
$LOC(SPEC,DB,$SPECTRUM,E_MOTHER,W,L);        IF ^STS$SUCCESS THEN @RET(STS$VALUE);
$LOC(SPEC,DB,$SPECTRUM,P_MOTHER,W,L);        IF ^STS$SUCCESS THEN @RET(STS$VALUE);
$LOC(SPEC,DB,$SPECTRUM,P_EVAP,W,L);          IF ^STS$SUCCESS THEN @RET(STS$VALUE);
$LOC(SPEC,DB,$SPECTRUM,DP_EA,W,L);           IF ^STS$SUCCESS THEN @RET(STS$VALUE);
$LOC(SPEC,DB,$SPECTRUM,RATE_EA,W,L);         IF ^STS$SUCCESS THEN @RET(STS$VALUE);
$LOC(SPEC,DB,$SPECTRUM,E_RATIO,W,L);         IF ^STS$SUCCESS THEN @RET(STS$VALUE);
$LOC(SPEC,DB,$SPECTRUM,DT_AA,W,L);           IF ^STS$SUCCESS THEN @RET(STS$VALUE);
$LOC(SPEC,DB,$SPECTRUM,E_EVAPALPHA,W,L);     IF ^STS$SUCCESS THEN @RET(STS$VALUE);
$LOC(SPEC,DB,$SPECTRUM,E_DAUGHTER,W,L);             IF ^STS$SUCCESS THEN @RET(STS$VALUE);
$LOC(SPEC,DB,$SPECTRUM,DP_AA,W,L);           IF ^STS$SUCCESS THEN @RET(STS$VALUE);
$LOC(SPEC,DB,$SPECTRUM,P_EVAPALPHA,W,L);     IF ^STS$SUCCESS THEN @RET(STS$VALUE);
$LOC(SPEC,DB,$SPECTRUM,P_DAUGHTER,W,L);             IF ^STS$SUCCESS THEN @RET(STS$VALUE);
$LOC(SPEC,DB,$SPECTRUM,DP_EF,W,L);           IF ^STS$SUCCESS THEN @RET(STS$VALUE);
$LOC(SPEC,DB,$SPECTRUM,E_EVAPF,W,L);         IF ^STS$SUCCESS THEN @RET(STS$VALUE);
$LOC(SPEC,DB,$SPECTRUM,E_FISSION,W,L);              IF ^STS$SUCCESS THEN @RET(STS$VALUE);
$LOC(SPEC,DB,$SPECTRUM,P_EVAPF,W,L);         IF ^STS$SUCCESS THEN @RET(STS$VALUE);
$LOC(SPEC,DB,$SPECTRUM,P_FISSION,W,L);              IF ^STS$SUCCESS THEN @RET(STS$VALUE);
$LOC(SPEC,DB,$SPECTRUM,DT_EF,W,L);           IF ^STS$SUCCESS THEN @RET(STS$VALUE);
$LOC(SPEC,DB,$SPECTRUM,RATE_EF,W,L);         IF ^STS$SUCCESS THEN @RET(STS$VALUE);
$LOC1(SPEC,DB,$SPECTRUM,CT_EVR,1,32,W,L);    IF ^STS$SUCCESS THEN @RET(STS$VALUE);
$LOC1(SPEC,DB,$SPECTRUM,CT_MOM,1,32,W,L);    IF ^STS$SUCCESS THEN @RET(STS$VALUE);
$LOC1(SPEC,DB,$SPECTRUM,CT_DAU,1,32,W,L);    IF ^STS$SUCCESS THEN @RET(STS$VALUE);
$LOC1(SPEC,DB,$SPECTRUM,CT_EVRF,1,32,W,L);   IF ^STS$SUCCESS THEN @RET(STS$VALUE);
$LOC1(SPEC,DB,$SPECTRUM,CT_FISS,1,32,W,L);   IF ^STS$SUCCESS THEN @RET(STS$VALUE);

STS$VALUE=1;
@RET(STS$VALUE);

/*
=============================================================================
     PROCEDURE CALLED IN CASE OF AN ERROR
=============================================================================
*/
U_CLEANUP:PROCEDURE;
END U_CLEANUP;
```

```
/*
================================================================================
*/

END X$ANAL;
/*
================================================================================
     END OF PROCEDURE X$ANAL
================================================================================
*/
```

Appendix B: Patin parameters input file listing all of the HIVAP input parameters.

```
  Ti-50 + Bi-209          Patin Parameters
-------------------------------------------------------------------------
  APROJ = 50 ZPROJ = 22 ATARG = 209 ZTARG = 83
  SHELL(GS) = 2 SHELF(SADDLE) = 2  PAIR= 4  MC = 0  MP = 0
  IBF = 1
  FISROT PARAMETERS = 0
  NOFISSION = 0 NONEUTRONS = 0 NOPROTONS = 0 NOALPHAS = 0 NOGAMMAS = 0
  DISC = 0  GAMMAS(IGAM) = 1
-------------------------------------------------------------------------
  NEUTRONS = 4  PROTONS = 1
  MASSES LOG UNIT = 9
  NUMB = 0  IOVER = 1  INERT = 0  INERF = 0  FINERT = 1
  LIMITS = 1
  PRINT = 5  LOGUN = 0  ICOR = 1
  NUMISO = 0 LBDM = 5
  IRAST = 0  WKB = 1  ITRANS = 0  JFJI = 1
-------------------------------------------------------------------------
 ANG.MOM. LOSS  NEUTRONS 1  PROTONS 1  ALPHAS 3
-------------------------------------------------------------------------
 IF IGAM NOT ZERO
  EG1WU = 0.01 EG2WU = 10
  EG1MIN = 1 EG1MAX = 20
  EG2MIN = 1 EG2MAX = 4
  JFACT = 1
-------------------------------------------------------------------------
 IF  IGAM NOT ZERO
  CGIANT = 0.0  EGIANT = 80  WGIANT =  5  STRIPE = 0  IOPTG = 0
-------------------------------------------------------------------------
  LEVELPAR = 1.16  AF/AN = 2
  BARFAC = 1.0
  EDAMP = 18.0  BAR0 =  0.0
  SHELL0 = 0.0  DELT= 11.0  QVALUE = 0.0
-------------------------------------------------------------------------
 ONLY IF LDBM=(5)
  LDBM = 1 PREEX = 1 AX = 0 ENH = 0 BETA0 = 0 EDCOLL = 0 UCRIT = 5
-------------------------------------------------------------------------
 ONLY IF LIMITS NOT ZERO
  CUT = 0.1E-6 FRACT2 = 0.1E-6
  ABSMIN = 0 PRCN = 0 SIGLOW = 0 DEL1 = 0 NOLEP = 0 NOLJI = 0 NOLJF =0
-------------------------------------------------------------------------
 IF INERT NOT ZERO (LOWER PART YRAST LINE)
  ENERGY       SPIN           ENERGY       SPIN     ENERGY    SPIN
-------------------------------------------------------------------------
  E = 6 IEXC = 1 IFUS = 11 LIMBAR = 0
  JLOWER = 0 JUPPER = 0 NEWFIS = 0 TSTROT = 0 JFIS = 0 EN = 0
  V0 = 48  R0 = 1.12 D = 0.75 Q2 = 0 CRED = 1.0
  NOCURV = 0  NOPROX = 0  IOPT = 0  ITEST = 0
  SIGR0 = 2.9  CUTOFF = 5.0  XTH = 0.7  APUSH = 18.0  FPUSH = 0.75
-------------------------------------------------------------------------
-1 0 0 0 0 0 0 0 0 0 0 0 0
```

References

[Alo1970] J. Alonso, computer code JORPLE, Lawrence Berkeley National Laboratory , Berkeley, CA, 1970.

[Alo1974] J. Alonso, *Gmelin Handbuch der Anorganischen Chemie*, **7b**, 28 (1974).

[Arm1985] P. Armbruster, Ann. Rev. Nucl. Sci. **35**, 135 (1985).

[Aum1974] D. C. Aumann and G. Müllen, Nucl. Instru. Meth. **115**, 75 (1974).

[Bas1977] R. Bass, Phys. Rev. Lett. **39**, 265 (1977).

[Bet1972] H. D. Betz, Rev. Mod. Phys. **44**, 465 (1972).

[Blo1982] J. Blocki and W. J. Swiatecki, Lawrence Berkeley National Laboratory Report LBL-12811, 1982.

[Bon1974] J. P. Bondorf, M. I. Sobel, and D. Sperber, Phys. Rep. **15**, 83 (1974).

[Cho1956a] G. R. Choppin, B.G. Harvey and S. G. Thompson, J. Inorg. Nucl. Chem. **2**, 66 (1956).

[Cho1956b] G. R. Choppin and R. J. Silva, J. Inorg. Nucl. Chem. **3**, 153 (1956).

[Chu1999] S. Y. F. Chu, L. P. Ekström, and R. B. Firestone, WWW Table of Radioactive Isotopes, http://nucleardata.nuclear.lu.se/nucleardata/toi/ (1999).

[Coh1974] S. Cohen, F. Plasil and W. J. Swiatecki, Ann. Phys. **82**, 557 (1974).

[Don1966] E. D. Donets, V. A. Shchegolev, and V. A. Ermakov, Sov. J. Nucl. Phys. **2**, 723 (1966).

[Dre1999] R. Dressler, Ph.D. Thesis, Universität Bern, Switzerland, 1999.

[Esk1971] K. Eskola, P. Eskola, M. Nurmia, and A. Ghiorso, Phys. Rev. **C 4**, 632 (1971).

[Ess1987] H. G. Essel, H. Grein, T. Kroll, W. Kynast, M. Richter, H. Sohlbach, W. Spreng, K. Winkelmann, W. F. J. Müller, IEEE Trans. Nucl. Sci. **34**, 907 (1987).

[Ess2000] H. G. Essel and N. Kurz, IEEE Trans. Nucl. Sci. **47**, 337 (2000).

[Fie1957] P. R. Fields, A. M. Friedman, J. Milsted, H. Atterling, W. Forsling, L. W. Holm, and B. Åström, Phys. Rev. **107**, 1460 (1957).

[Fle1958] G. N. Flerov, S. M. Polikanov, A. S. Karamian, A. S. Pasivk, D. M. Parfanovich, N. I. Tarantin, V. A. Karnaukhov, V. A. Druin, V. V. Volkov, A. M. Semchinova, Y. T. Oganessian, V. I. Khalizev, and G. I. Khlebnikov, Sov. Phys. Dokl. **3**, 546 (1958).

[Fle1976] G. N. Flerov, Y. T. Oganessian, A. A. Pleve, N. V. Pronin, and Y. P. Tretyakov, Nucl. Phys. **A 267**, 359 (1976).

[Gäg1989] H. W. Gäggeler, D. T. Jost, A. Türler, P. Armbruster, W. Brüchle, H. Folger, F. P. Heßberger, S. Hofmann, G. Münzenberg, V. Ninov, W. Reisdorf, M. Schädel, K. Sümmerer, J. V. Kratz, U. Scherer, and M. E. Leino, Nucl. Phys. **A 502**, 561c (1989).

[Ghi1950] A. Ghiorso, R. A. James, L. O. Morgan, and G. T. Seaborg, Phys. Rev. **78**, 472 (1950).

[Ghi1955a] A. Ghiorso, S. G. Thompson, G. H. Higgins, G. T. Seaborg, M. H. Studier, P. R. Fields, S. M. Fried, H. Diamond, J. F. Mech, G. L. Pyle, J. R. Huizenga, A. Hirsch, W. M. Manning, C. I. Browne, H. L. Smith, and R. W. Spence, Phys. Rev. **99**, 1048 (1955).

[Ghi1955b] A. Ghiorso, B. G. Harvey, G. R. Choppin, S. G. Thompson, and G. T. Seaborg, Phys. Rev. **98**, 1518 (1955).

[Ghi1958] A. Ghiorso, T. Sikkeland, J. R. Watson, and G. T. Seaborg, Phys. Rev. Lett. **1**, 18 (1958).

[Ghi1961] A. Ghiorso, T. Sikkeland, A. E. Larsh, and R. M. Latimer, Phys Rev. Lett. **6**, 473 (1961).

[Ghi1967a] A. Ghiorso, T. Sikkeland, and M. J. Nurmia, Phys. Rev. Lett. **18**, 401 (1967).

[Ghi1967b] A. Ghiorso and T. Sikkeland, Phys. Today **20**, 25 (1967).

[Ghi1969] A. Ghiorso, M. Nurmia, J. Harris, K. Eskola, and P. Eskola, Phys. Rev. Lett. **22**, 1317 (1969).

[Ghi1970] A. Ghiorso, M. Nurmia, K .Eskola, J. Harris, and P. Eskola, Phys. Rev. Lett. **24**, 1498 (1970).

[Ghi1974] A. Ghiorso, J. M. Nitschke, J. R. Alonso, C. T. Alonso, M. Nurmia, G. T. Seaborg, E. K. Hulet, and R. W. Lougheed, Phys. Rev. Lett. **33**, 1490 (1974).

[Ghi1988] A. Ghiorso, S. Yashita, M. E. Leino, L. Frank, J. Kalnins, P. Armbruster, J. –P. Dufour, and P. K. Lemmertz, Nucl. Instru. Meth. **A 269**, 192 (1988).

[Gre1991] K. E. Gregorich, Nucl. Instr. Meth. In Phys. Res. **A 302**, 135 (1991).

[Gre1994] K. E. Gregorich, M. R. Lane, M. F. Mohar, D. M. Lee, C. D. Kacher, E. R. Sylwester, and D. C. Hoffman, Phys. Rev. Lett. **72**, 1423 (1994).

[Gro1967] J. R. Grover and J. Gilat, Phys. Rev. **157**, 802 (1967).

[Hay1988] G. R. Haynes, J. D. Leyba, and D. C. Hoffman, (unpublished), 1988.

[Heβ1997] F. P. Heßberger, S. Hofmann, V. Ninov, P. Armbruster, H. Folger, G. Münzenberg, H. –J. Schött, A. G. Popeko, A. N. Yeremin, A. N. Andreyev, and S. Saro, Z. Phys. **A 359**, 415 (1997).

[Heβ2001a] F. P. Heßberger, S. Hofmann, D. Ackermann, V. Ninov, M. Leino, G. Münzenberg, S. Saro, A. Lavrentev, A. G. Popeko, A. N. Yeremin, and Ch. Stodel, Eur. Phys. J. **A 12**, 57 (2001).

[Heβ2001b] F. P. Heßberger, Private communication (2001).

[Hff1980] D. C. Hoffman, D. M. Lee, A. Ghiorso, M. J. Nurmia, and K. Aleklett, Phys. Rev. **C 22**, 1581 (1980).

[Hff1998] D. C. Hoffman, *Actinides and the Environment*, eds. P. A. Stone, A. Gonis, and A. A. Borovoi. (Kluwer Academic Publishers, Norwell 1998).

[Hff1999] D. C. Hoffman and D. M. Lee, J. Chem. Ed. **76**, 331 (1999).

[Hff2000] D. C. Hoffman, A. Ghiorso, and G. T. Seaborg, *The Transuranium People.* (Imperial College Press, London 2000).

[Hil1953] D. L. Hill and J. A. Wheeler, Phys. Rev. **89**, 1102 (1953).

[Hof1995a] S. Hofmann, V. Ninov, F. P. Heßberger, P. Armbruster, H. Folger, G. Münzenberg, H. –J. Schött, A. G. Popeko, A. V. Yeremin, A. N. Andreyev, S. Saro, R. Janik, and M. Leino, Z. Phys. **A 350**, 277 (1995).

[Hof1995b] S. Hofmann, V. Ninov, F. P. Heßberger, P. Armbruster, H. Folger, G. Münzenberg, H. –J. Schött, A. G. Popeko, A. V. Yeremin, A. N. Andreyev, S. Saro, R. Janik, and M. Leino, Z. Phys. **A 350**, 281 (1995).

[Hof1996] S. Hofmann, V. Ninov, F. P. Heßberger, P. Armbruster, H. Folger, G. Münzenberg, H. –J. Schött, A. G. Popeko, A. V. Yeremin, S. Saro, R. Janik, and M. Leino, Z. Phys. **A 354**, 229 (1996).

[Hof1997] S. Hofmann, F. P. Heßberger, V. Ninov, P. Armbruster, G. Münzenberg, C. Stodel, A. G. Popeko, A. V. Yeremin, S. Saro, and M. Leino, Z. Phys. **A 358**, 377 (1997).

[Hof1998] S. Hofmann, Rep. Prog. Phys. **61**, 639 (1998).

[Hof2000] S. Hofmann and G. Münzenberg, Rev. Mod. Phys. **72**, 733 (2000).

[Hof2001] S. Hoffman, F. P. Heßberger, D. Ackermann, G. Münzenberg, S. Antalic, P. Cagarda, B. Kindler, J. Kojouharova, M. Leino, B. Lommel, R. Mann, A. G. Popeko, S. Reshitko, S. Saro, J. Uusitalo, and A. V. Yeremin, Eur. Phys. J. **A** (to be published), 2001.

[Ilj1982] A. S. Iljinov, Y. T. Oganessian, and E. A. Cherepanov, Sov. J. Nucl. Phys. **36**, 69 (1982).

[Iup1997] IUPAC, Pure Appl. Chem. **69**, 2471 (1997).

[Kra1992] J. V. Kratz, M. K. Gober, H. P. Zimmermann, M. Schädel, W. Brüchle, E. Schimpf, K. E. Gregorich, A. Türler, N. J. Hannick, K. R. Czerwinski, B. Kadkhodayan, D. M. Lee, M. J. Nurmia, D. C. Hoffman, H. Gäggeler, D. Jost, J. Kovacs, U. W. Scherer, and A. Weber, Phys. Rev **C 45**, 1064 (1992).

[Lan1998] M. R. Lane, K. E. Gregorich, D. M. Lee, B. Wierczinski, C. A. McGrath, M. B. Hendricks, D. A. Shaughnessy, D. A. Strellis, E. R. Sylwester, P. A. Wilk, and D. C. Hoffman, Phys. Rev. **C 58**, 3413 (1998).

[Laz1994] Y. A. Lazarev, Y. V. Lobanov, Y. T. Oganessian, V. K. Utyonkov, F. S. Abdullin, G. V. Buklanov, B. N. Gikal, S. Iliev, A. N. Mezentsev, A. N. Polyakov, I. M. Sedykh, I. V. Shirokovsky, V. G. Subbotin, A. M. Sukhov, Y. S. Tsyganov, V. E. Zhuchko, R. W. Lougheed, K. J. Moody, J. F. Wild, E. K. Hulet, and J. H. McQuaid, Phys. Rev. Lett. **73**, 624 (1994).

[Laz1996] Y. A. Lazarev, Y. V. Lobanov, Y. T. Oganessian, V. K. Utyonkov, F. S. Abdullin, A. N. Polyakov, J. Rigol, I. V. Shirokovsky, Y. S. Tsyganov, S. Iliev, V. G. Subbotin, A. M. Sukhov, G. V. Buklanov, B. N. Gikal, V. B. Kutner, A. N. Mezentsev, K. Subotic, J. F. Wild, R. W. Lougheed, and K. J. Moody, Phys. Rev. **C 54**, 620 (1996).

[Laz2000] Y. A. Lazarev, Y. V. Lobanov, Y. T. Oganessian, V. K. Utyonkov, F. S. Abdullin, A. N. Polyakov, J. Rigol, I. V. Shirokovsky, Y. S. Tsyganov, S. Iliev, V. G. Subbotin, A. M. Sukhov, G. V. Buklanov, A. N. Mezentsev, K. Subotic, K. J. Moody, N. J. Stoyer, J. F. Wild, and R. W. Lougheed, Phys. Rev. **C 62**, 064307 (2000).

[Lei1999] M. Leino, H. Kankaanpää, R. –D. Herzberg, A. J. Chewter, F. P. Heßberger, Y. Le Coz, F. Becker, P. A. Butler, J. F. C. Cocks, O. Dorvaux, K. Eskola, J. Gerl, P. T. Greenlees, K. Helariutta, M. Houry, G. D. Jones, P. Jones, R. Julin, S. Juutinen, H. Kettunen, T. L. Khoo, A. Kleinböhl, W. Korten, P. Kuusiniemi, R. Lucas, M Muikku, P. Nieminen, R. D. Page, P. Rahkila, P. Reiter, A. Savelius, C. Schlegel, C. Theisen, W. H. Trzaska, and H. –J. Wollersheim, Eur. Phys. J. **A 6**, 63 (1999).

[Lir1976] S. Liran and N. Zeldes, At. Data. Nucl. Data. Tabl. **17**, 431 (1976).

[Lir2001] S. Liran, A. Marinov, and N. Zeldes, At. Data. Nucl. Data. Tabl. (to be published), 2001.

[Mal1968] J. Maly, J. Sikkeland, R. Silva, and A. Ghiorso, Science **160**, 1114 (1968).

[McM1940] E. McMillian and P. H. Abelson, Phys. Rev. **57**, 1185 (1940).

[Moo1983] K. J. Moody, Ph.D. Thesis, University of California-Berkeley, 1983.

[Moo1990] K. J. Moody, R. W. Lougheed, R. J. Dougan, E. K. Hulet, J. F. Wild, K. Sümmerer, R. L. Hahn, J. van Aarle, and G. R. Bethune, Phys. Rev. **C 41**, 152 (1990).

[Moo2001] K. J. Moody, Private communication, December 17th, 2001.

[Mül1975] G. Müllen and D. C. Aumann, Nucl. Instru. Meth. **128**, 425 (1975).

[Mün1979] G. Münzenberg, W. Faust, S. Hofmann, P. Armbruster, K. Guttner, and H. Ewald, Nucl. Instru. Meth. **161**, 65 (1979).

[Mün1981] G. Münzenberg, S. Hofmann, F. P. Heßberger, W. Reisdorf, K. –H. Schmidt, J. H. R. Schneider, P. Armbruster, C. –C. Sahm, and B. Thuma, Z. Phys. **A 300**, 107 (1981).

[Mün1982] G. Münzenberg, P. Armbruster, F. P. Heßberger, S. Hofmann, K. Poppensieker, W. Reisdorf, J. H. R. Schneider, W. F. W. Schneider, K. – H. Schmidt, C. –C. Sahm, and D. Vermeulen, Z. Phys. **A 309**, 89 (1982).

[Mün1984a] G. Münzenberg, P. Armbruster, H. Folger, F. P. Heßberger, S. Hofmann, J. Keller, K. Poppensieker, A. B. Quint, W. Reisdorf, K. –H. Schmidt, H. –J. Schött, M. E. Leino, and R. Hingmann, Z. Phys. **A 317**, 235 (1984).

[Mün1984b] G. Münzenberg, W. Reisdorf, S. Hofmann, Y. K. Agarwal, F. P. Heßberger, K. Poppensieker, J. H. R. Schneider, W. F. W. Schneider, K. –

H. Schmidt, H. –J. Schött, P. Armbruster, C. –C. Sahm, and D. Vermeulen, Z. Phys. **A 315**, 145 (1984).

[Mün1985] G. Münzenberg, S. Hofmann, H. Folger, F. P. Heßberger, J. Keller, K. Poppensieker, A. B. Quint, W. Reisdorf, K. –H. Schmidt, H. –J. Schött, P. Armbruster, M. E. Leino, and R. Hingmann, Z. Phys. **A 322**, 227 (1985).

[Mün1987] G. Münzenberg, P. Armbruster, G. Bethes, H. Folger, F. P. Heßberger, S. Hofmann, J. Keller, K. Poppensieker, A. B. Quint, W. Reisdorf, K. –H. Schmidt, H. –J. Schött, K. Sümmerer, I. Zychor, M. E. Leino, R. Hingmann, U. Gollerthan, and E. Hanelt, Z. Phys. **A 328**, 49 (1987).

[Mün1989] G. Münzenberg, P. Armbruster, S. Hofmann, F. P. Heßberger, H. Folger, J. Keller, V. Ninov, K. Poppensieker, A. B. Quint, W. Reisdorf, K. –H. Schmidt, J. R. H. Schneider, H. –J. Schött, K. Sümmerer, I. Zychor, M. E. Leino, D. Ackermann, U. Gollerthan, E. Hanelt, W. Morawek, D. Vermeulen, Y. Fujita, and T. Schwab, Z. Phys. **A 333**, 163 (1989).

[Mün2001] G. Münzenberg, Nucl. Phys. **A 690**, 175c (2001).

[Mye1966] W. D. Myers and W. J. Swiatecki, Ark. Fys. **36**, 343 (1966).

[Nin1999] V. Ninov and K. E. Gregorich, ENAM98, ed. B. M. Scherrill, D. J. Morrissey, and C. N. Davids. (AIP, Woodbury 1999).

[Nit1981] J. M. Nitschke, M. Fowler, A. Ghiorso, R. E. Leber, M. E. Leino, M. J. Nurmia, L. P. Sommerville, K. E. Williams, E. K. Hulet, J. H. Landrum, R. W. Lougheed, J. F. Wild, C. E. Bemis, R. J. Silva, and P. Eskola, Nucl. Phys. **A 352**, 138 (1981).

[Oga1975] Y. T. Oganessian, A. S. Iljinov, A. G. Demin and S. P. Tretyakova, Nucl. Phys. **A 239**, 353 (1975).

[Oga1981] Y. T. Oganessian and Y. A. Lazarev, Pure Appl. Chem. **53**, 925 (1981).

[Oga1994] Y. T. Oganessian, J. Alloy. Comp. **213/214**, 50 (1994).

[Oga1999a] Y. T. Oganessian, V. K. Utyonkov, Y. V. Lobanov, F. S. Abdullin, A. N. Polyakov, I. V. Shirokovsky, Y. S. Tsyganov, G .G. Gulbekian, S. L. Bogomolov, B. N. Gikal, A. N. Mezentsev, S. Iliev, V. G. Subbotin, A. M. Sukhov, G. V. Buklanov, K. Subotic, M. G. Itkis, K. J. Moody, J. F. Wild, N. J .Stoyer, M. A. Stoyer, and R. W. Lougheed, Phys. Rev. Lett. **83**, 3154 (1999).

[Oga1999b] Y. T. Oganessian, A. V. Yeremin, G. G. Gulbekian, S. l. Bogomolov, V. I. Chepigin, B. N. Gikal, V. A. Gorshkov, M. G. Itkis, A. P. Kabachenko, V. B. Kutner, A. Y. Lavrentev, O. N. Malyshev, A. G. Popeko, J. Rohac, R. N. Sagaidak, S. Hofmann, G. Münzenberg, M. Veselsky, S. Saro, N. Iwasa, and K. Morita, Eur. Phys. J. **A 5**, 63 (1999).

[Oga2000a] Y. T. Oganessian, V. K. Utyonkov, Y. V. Lobanov, F. S. Abdullin, A. N. Polyakov, I. V. Shirokovsky, Y. S. Tsyganov, G .G. Gulbekian, S. L. Bogomolov, B. N. Gikal, A. N. Mezentsev, S. Iliev, V. G. Subbotin, A. M. Sukhov, G. V. Buklanov, K. Subotic, M. G. Itkis, O. V. Ivanov, K. J. Moody, J. F. Wild, N. J. Stoyer, M. A. Stoyer, and R. W. Lougheed, Phys. Rev. **C 62**, 041604R (2000).

[Oga2000b] Y. T. Oganessian, V. K. Utyonkov, Y. V. Lobanov, F. S. Abdullin, A. N. Polyakov, I. V. Shirokovsky, Y. S. Tsyganov, G .G. Gulbekian, S. L.

Bogomolov, B. N. Gikal, A. N. Mezentsev, S. Iliev, V. G. Subbotin, A. M. Sukhov, G. V. Buklanov, K. Subotic, M. G. Itkis, O. V. Ivanov, Y. E. Karelin, A. N. Tatarinov, K. J. Moody, J. F. Wild, N. J. Stoyer, M. A. Stoyer, C. A. Laue, and R. W. Lougheed, Phys. Rev. **C 63**, 011301R (2000).

[Oga2000c] Y. T. Oganessian, V. K. Utyonkov, Y. V. Lobanov, F. S. Abdullin, A. N. Polyakov, I. V. Shirokovsky, Y. S. Tsyganov, S. Iliev, V. G. Subbotin, A. M. Sukhov, G. V. Buklanov, A. N. Mezentsev, K. Subotic, O.V. Ivanov, K. J. Moody, J. F. Wild, N. J. Stoyer, M. A. Stoyer, and R. W. Lougheed, Proc. 4th Inter. Conf. On Dynam. Asp. Nucl. Fiss. (Singapore 2000), p 334.

[Oga2001a] Y. T. Oganessian, M. G. Itkis, A. G. Popeko, V. K. Utyonkov, and A. V. Yeremin, Nucl. Phys. **A 682**, 108c (2001).

[Oga2001b] Y. T. Oganessian, Nucl. Phys. **A 685**, 17c (2001).

[Pat1989] Z. Patyk, J. Skalski, and A. Sobiczewski, Nucl. Phys. **A 502**, 591c (1989).

[Pat1991] Z. Patyk, and A. Sobiczewski, Nucl. Phys. **A 533**, 132 (1991).

[Rat1991] W. Rathbun, Lawrence Berkeley National Laboratory Report LBL-29734, 1991.

[Rei1981] W. Reisdorf, Z. Phys. **A 300**, 227 (1981).

[Rei1990] W. Reisdorf (unpublished), 1990.

[Rei1992] W. Reisdorf and M. Schädel, Z. Phys. **A 343**, 47 (1992).

[Sch1984] K. H. Schmidt, C. –C. Sahm, K. Pielenz, and H. –G. Clerc, Z. Phys. **A 316**, 19 (1984).

[Shä1997] M. Schädel, W. Brüchle, R. Dressler, B. Eichler, H. W. Gäggeler, R. Günther, K. E. Gregorich, D. C. Hoffman, S. Hübener, D. T. Jost, J. V. Kratz, W. Paulus, D. Schumann, S. Timokhin, N. Trautmann, A. Türler, G. Wirth, and A. Yakushev, Nature **388**, 55 (1997).

[Sea1945] G. T. Seaborg, Chem. Eng. News **23**, 2190 (1945).

[Sea1946] G. T. Seaborg, A. C. Wahl, and J. W. Kennedy, Phys. Rev. **69**, 367 (1946).

[Sea1990] G. T. Seaborg and W. D. Loveland, *The Elements Beyond Uranium*. (John Wiley & Sons, New York, 1990).

[Seg1977] E. Segre, *Nuclei and Particles, An Introduction to Nuclear and Subnuclear Physics*, 2nd Ed. (W. A. Benjamin, Inc., London, 1977).

[Sha2000] D. A. Shaughnessy, Ph.D. Thesis, University of California-Berkeley, 2000.

[Shi1986] N. Shinohara, S. Usada, S. Ichikawa, T. Suzuki, M. Magara, H. Okashita, H. Yoshikawa, T. Horiguchi, Y. Iwata, S. Shibata, and I. Fujiwara, Phys. Rev. **C 34**, 909 (1986).

[Sik1966] T. Sikkeland, Ark. Fys. **36**, 539 (1966).

[Sik1968a] T. Sikkeland, A. Ghiorso, and M. Nurmia, Phys. Rev. **172**, 1232 (1968).

[Sik1968b] T. Sikkeland, J. Maly, and D. F. Lebeck, Phys. Rev. **169**, 1000 (1968).

[Smi1956] H. L. Smith and D. C. Hoffman, J. Inorg. Nucl. Chem. **3**, 243 (1956).

[Swi1982] W. J. Swiatecki, Nucl. Phys. **A 376**, 275 (1982).

[Swi2002] W. J. Swiatecki, Private communication, April-May, 2002.

[Tho1950a] S. G. Thompson, A. Ghiorso, and G. T. Seaborg, Phys. Rev. **77**, 838 (1950).

[Tho1950b] S. G. Thompson, K. Street, A. Ghiorso, and G. T. Seaborg, Phys. Rev. **78**, 298 (1950).

[Tök1981] J. Töke and W. J. Swiatecki, Nucl. Phys. **A 372**, 141 (1981).

[Tür1999] A. Türler, Private communication (1999).

[Tür2001] A. Türler, Ch. E. Düllmann, H. W. Gäggeler, U. W. Kirbach, A. B. Yakushev, M. Schädel, W. Brüchle, R. Dressler, K. Eberhardt, B. Eichler, R. Eichler, T. N. Ginter, I. Glaus, K. E. Gregorich, D. C. Hoffman, E. Jäger, D. T. Jost, D. M. Lee, H. Nitsche, J. B. Patin, V. Pershina, D. Piguet, Z. Qin, B. Schausten, E. Schimpf, H. –J. Schött, S. Soverna, R. Sudowe, P. Thörle, S. N. Timokhin, N. Trautmann, A. Vahle, G. Wirth, and P. Zielinski, Phys. Rev. Lett. (to be published), 2001.

[Ver1984] D. Vermeulen, H. –G. Clerc, C. –C. Sahm, K. –H. Schmidt, J. G. Keller, G. Münzenberg, and W. Reisdorf, Z. Phys. **A 318**, 157 (1984).

[Wil1988] J. F. Wild, G. R. Haynes, J. D. Leyba, and D. C. Hoffman (unpublished), 1988.

[Wil2000] P. A. Wilk, K. E. Gregorich, A. Türler, C. A. Laue, R. Eichler, V. Ninov, J. L. Adams, U. W. Kirbach, M. R. Lane, D. M. Lee, J. B. Patin, D. A. Shaughnessy, D. A. Strellis, H. Nitsche, and D. C. Hoffman, Phys. Rev. Lett. **85** 2697 (2000).

[Zva1969] I. Zvara, Y. T. Chuburkov, R. Tsaletka, and M. R. Shalayevsky, Radiokhimiya **11**, 2154 (1969); Sov. Radiochem. **11**, 161 (1969).

[Zva1970] I. Zvara, V. Z. Belov, Y. S. Korotkin, M. R. Shalayevsky, V. A. Shchegolev, M. Hussonois, and B. A. Zager, JINR P12-5120, Dubna, 1970.

Ernest Orlando Lawrence Berkeley National Laboratory
One Cyclotron Road | Berkeley, California 94720

Prepared for the U.S. Department of Energy under Contract No. DE-AC03-76SF00098